Retrospective Theses and Dissertations

Iowa State University Capstones, Theses and Dissertations

1981

Application of Kalman filtering in computer relaying of power systems

Adly Ageeb Girgis
Iowa State University

INFORMATION TO USERS

This was produced from a copy of a document sent to us for microfilming. While the most advanced technological means to photograph and reproduce this document have been used, the quality is heavily dependent upon the quality of the material submitted.

The following explanation of techniques is provided to help you understand markings or notations which may appear on this reproduction.

1. The sign or "target" for pages apparently lacking from the document photographed is "Missing Page(s)". If it was possible to obtain the missing page(s) or section, they are spliced into the film along with adjacent pages. This may have necessitated cutting through an image and duplicating adjacent pages to assure you of complete continuity.

2. When an image on the film is obliterated with a round black mark it is an indication that the film inspector noticed either blurred copy because of movement during exposure, or duplicate copy. Unless we meant to delete copyrighted materials that should not have been filmed, you will find a good image of the page in the adjacent frame. If copyrighted materials were deleted you will find a target note listing the pages in the adjacent frame.

3. When a map, drawing or chart, etc., is part of the material being photographed the photographer has followed a definite method in "sectioning" the material. It is customary to begin filming at the upper left hand corner of a large sheet and to continue from left to right in equal sections with small overlaps. If necessary, sectioning is continued again—beginning below the first row and continuing on until complete.

4. For any illustrations that cannot be reproduced satisfactorily by xerography, photographic prints can be purchased at additional cost and tipped into your xerographic copy. Requests can be made to our Dissertations Customer Services Department.

5. Some pages in any document may have indistinct print. In all cases we have filmed the best available copy.

8122515

GIRGIS, ADLY AGEEB

APPLICATION OF KALMAN FILTERING IN COMPUTER RELAYING OF POWER SYSTEMS

Iowa State University   PH.D.   1981

University
Microfilms
International 300 N. Zeeb Road, Ann Arbor, MI 48106

PLEASE NOTE:

In all cases this material has been filmed in the best possible way from the available copy.
Problems encountered with this document have been identified here with a check mark __√__.

1.   Glossy photographs or pages _____

2.   Colored illustrations, paper or print _____

3.   Photographs with dark background _____

4.   Illustrations are poor copy _____

5.   Pages with black marks, not original copy _____

6.   Print shows through as there is text on both sides of page _____

7.   Indistinct, broken or small print on several pages _____

8.   Print exceeds margin requirements _____

9.   Tightly bound copy with print lost in spine _____

10.   Computer printout pages with indistinct print __✓__

11.   Page(s) _____ lacking when material received, and not available from school or author.

12.   Page(s) _____ seem to be missing in numbering only as text follows.

13.   Two pages numbered _____. Text follows.

14.   Curling and wrinkled pages _____

15.   Other_____

Application of Kalman filtering in

computer relaying of power systems

by

Adly Ageeb Girgis

A Dissertation Submitted to the

Graduate Faculty in Partial Fulfillment of

The Requirements for the Degree of

DOCTOR OF PHILOSOPHY

Major: Electrical Engineering

Approved:

Signature was redacted for privacy.

In Charge of Major Work

Signature was redacted for privacy.

For the Major Department

Signature was redacted for privacy.

For the Graduate College

Iowa State University
Ames, Iowa

1981

TABLE OF CONTENTS

I. INTRODUCTION

With the rapid growth in electrical power demand, new and challenging problems have been presented to the electrical power engineer. Growth in demand has required the use of larger generation units, higher voltages, and longer transmission lines, which in turn have required the solution of new technical problems concerned with power system stability, protection, and operation. To overcome these problems, great effort is being made to develop new schemes for the control and protection of power systems.

In searching for new techniques, much attention has been given to the application of digital computers in the power system protection field. The idea of using a computer to process signals and locate a fault in a short period of time is very attractive and the possibilities are very promising. Computers are already used extensively in power system control functions, and applications in the protection task are seen in the not too far distant future.

A. The Use of Computers in Power System Control and Protection

The use of computers in the power system field falls into the two categories of off-line and on-line applications. Off-line processing is a well established art. Large main-frame computers are being used to perform load flow studies, stability investigations, and design functions. The on-line application of computers for control and instrumentation tasks has grown rapidly in the last decade with the availability of low cost minicomputers and well proven control techniques. Application

of small process control computers in power systems is a relatively new
development. An example of such an application is the computer based
control and data acquisition system. These computer based systems are
handling many sophisticated power system operations problems, including
state estimation, generation control, economic dispatch of generation,
and many other control functions. Small computers are also being used in
many supervisory control systems. Earlier process control computers were
minicomputers, while the modern ones tend to be microcomputers.

The use of digital computers for protection of power system equip-
ment, i.e., computer relaying, is an idea of quite recent origin. A
great deal of research is going on in this field. Although there are
some indications of what the future of these systems will be, as yet
there are no completed commercially available protection systems offering
relays based on digital computers. New ideas are being presented
regularly in the technical literature. It can be asserted with confi-
dence that the ideas being developed in this field, and to be pre-
sented in the following chapter, will be incorporated in the protection
systems of the future.

B. Expected Benefits of a Digital Protection System

Considering the extensive research going on in the field of digital
computer relaying, it is worth considering the benefits that are ex-
pected to follow from the adaptation of digital relaying techniques.
Although early workers in the field considered the use of a single
computer (a minicomputer) for all the relaying functions within a sub-
station, the present view is that the proper approach to this problem is

to use a number of microcomputers dedicated to the individual relaying tasks (1-3). These microcomputers are to have data exchange facilities among themselves. Some form of networking the microcomputers is definitely being considered. Through this networking concept, it is expected that the main advantage of a single computer system, shared data among relays, can be realized without the atte nt drawbacks of a central relaying computer.

The most important perceived benefits of a gital relaying system, as reported by different research groups (1-3), can be summarized as follows.

1. Economics

In the final analysis, this will be the most important consideration to the power companies. The cost of digital hardware has been steadily decreasing. The cost of conventional relaying has increased steadily during the same period. For example, a relaying task that required a $100,000 minicomputer in 1970 can now (1981) be handled by a $10,000 microcomputer. Contrast this with the cost of a typical transmission line protection system which has approximately doubled in the same period. Furthermore, the digital computer, being a programmable device, can be used to perform multiple functions. To the extent that this can be done without jeopardizing the security of the individual tasks, the economic comparison becomes even more favorable to the digital technology.

2. Performance

It is expected that in all cases the performance of a digital relay

will be at least equal to that of its conventional counterpart. Certain features come more naturally to a digital relay, for example, memory action, complex shaping of operational characteristics, etc., which lead to a better digital relay than the corresponding conventional relay.

3. Reliability

One of the most significant advantages of a digital relay, perceived in the earliest technical papers, is the fact that the digital computer is continuously active. Consequently, a very high order of self-diagnosis is going on continuously within a digital relay. Additional diagnostic features, such as the monitoring of many of its peripherals, can be easily programmed. Therefore, it is expected that most of the accidental failures within a digital relay system can be detected immediately, and appropriate corrective actions can be taken. Although some diagnostic functions are usually available in a conventional relay, this feature can be utilized in a digital relay with a high degree of sophistication.

4. Flexibility

The computer is theoretically capable of doing almost anything within the limits and understanding of the human programmer. The physical characteristics of available solid state or electromechanical sensing elements are no longer a constraint. Also, a given fixed hardware package can perform a variety of different functions by programming changes only. New complete functions can be added to existing hardware in the field.

5. Adaptive capability

A computer can continuously monitor power-system status and can

actually modify its settings or logic according to system conditions.
This is particularly attractive since many misoperations of conventional
relays have been attributed to failure of a relay setting to remain valid
as operating conditions change.

6. Mathematical ability

Computers can implement new, sophisticated, mathematically-oriented
relaying methods which would be impossible to obtain otherwise, and
which can easily be modified in the field.

7. Adaptability to overall system control

Computers dedicated to relaying can readily communicate with exist-
ing or planned substation and system control computers. They can even
share a data-base available from other systems through a common memory
facility or by a communications channel. In a similar fashion, they can
provide increased operator interface through displays, CRTs, loggers,
and direct interface to supervisory control and data acquisition (SCADA)
systems.

8. Compatibility with new transducers

The utility industry has been looking at a new generation of ac data
transducers for EHV applications to replace conventional current trans-
formers and potential devices. These transducers generally measure the
ac quantity and convert it directly to digital form at EHV potential,
then transmit the data to ground level via an insulated optical path.
The only sensible way to make relaying decisions from this already
digitized data is to process it digitally in a computer.

C. Limitations and Drawbacks of Computer Relaying

Computers do not have magic ability to inherently overcome familiar power-system oriented relaying problems. For example, computer relaying would suffer from the same overreach errors as would a conventional relay operating in the same situation. However, the programmer has at his disposal a much broader range of tools for recognizing and dealing with these phenomena than does a conventional relay designer.

The incredible speed with which a modern computer executes its instructions does not guarantee that it will produce a fast relaying decision. This does not mean that computers are slower, but thought and effort are required to program a computer relay to operate faster than a conventional relay. Some of the mathematical analysis methods recently proposed may help in this regard.

II. DIGITAL PROTECTION SCHEMES

A. The Centralization of Digital Protection Schemes

The introduction of on-line computers in power systems protection was highlighted after the U.S. northeast failure in 1965. Proposals for computer-based protection schemes have followed the general philosophy of centralization to maintain full utilization of computer hardware (4). At Iowa State University in 1968, J. D. Grimes (5) showed that a mini-computer could handle differential protection of five transmission lines in a substation. One of the first complete central schemes was proposed by Rockefeller (6) in which 129 substation ac voltages and currents would be sampled at 0.5 msec intervals and processed to provide protection facilities for the complete substation.

Several research groups have pursued this idea of a centralized computer protection scheme while others have concentrated on the particular aspects of fault detection, classification, and location. Mantey (7) investigated the requirement for area and localized computer-based control and protection schemes. Walker, Ott, Ogden, and Tudor (8) discussed the application of a substation computer for various tasks including protection and suggested the use of interface hardware for detecting high frequency transients. Similarly, Hope, Bell, and Jura (9,10) suggested a hardware fault detector based on the recognition of waveform patterns from a normal sine wave. Mann and Morrison (11,12), in line with Rockefeller, proposed a complete software scheme using a comparison of sampled data from current and previous cycles for the detection of abnormalities before any fault calculations are performed. Poncelet (13) discussed

further matters of software and system organization for a substation protection scheme. The idea of using a computer for backup protection requirements was also considered by a number of groups. Edgley, Poon, and Law (14,15) and Cheetham (16) suggested several computer backup protection schemes.

Of all computer relaying topics, transmission line relaying has attracted more researchers than any other subject. This is so for several reasons. Transmission line protection is computationally more complex, and thus is a significant test of a computer's capability; furthermore, the high cost of conventional transmission line relaying makes this a worthwhile problem to tackle. The problem is basically detection, classification, and location of the fault in the shortest possible time.

The trend towards centralization was different from the traditional aim of limiting the extent of maloperation due to a protection equipment failure. Now, the microprocessor technology has seemed to still all debate, with decentralized parallel processors being the only solution considered for high speed fault protection.

B. Measurement of the Parameters of an Assumed Waveform

This has been one of the most popular approaches. The fault waveforms are assumed to be very simple, such as a sinusoid or a sinusoid with an exponentially decaying dc offset, and the component parameters are derived from a minimum number of samples.

Mann (17) assumed the fault current waveform to be a sinusoid with an exponential offset. An expression was derived for the relay-to-fault

impedance modulus $|Z_{rf}|$ in terms of the samples of voltage v(t) and current i(t) and a factor K which is a function of the fault inception angle δ and time t after the fault occurrence. The impedance expression used by Mann is

$$|Z_{rf}| = \frac{v(t)}{i(t)} K(\delta,t) \qquad (2.1)$$

The technique used one set of samples, and thus it was susceptible to noise. Also, in order to determine the fault inception angle δ, accurate detection of the voltage zero-crossing and fault incidence were required which again were affected by noise in the relay signals. A simple off-line simulation study gave an error of 40 percent in the calculated impedance.

Mantey (7) assumed the fault current and voltage waveforms to be sinusoidal and used the expressions for the complex fault impedance Z_{rf} in the form

$$Z_{rf} = \frac{V_m}{I_m} \lfloor \theta \qquad (2.2)$$

where V_m and I_m are the maximum values of voltage and current respectively and θ is the phase angle by which the current lags the voltage. A special interface was described (18) which samples the instantaneous voltage and current at specific times after current zero-crossing, making the quantities I_m, $V_m \cos \theta$, and $V_m \sin \theta$ available for a host computer. It was reported that the technique has the minimal processing time, but the effect of noise was not investigated, and this would be a problem in view of the small number of samples involved.

Mann and Morrison (11,12) developed an algorithm based on the characterization of a pure sinusoidal waveform from synchronous data samples. In their algorithm, the equation for the instantaneous value of the fundamental sinusoid ($v = V_m \sin(\omega t + \theta)$) is differentiated. The result and the original equation can then be solved to yield the peak magnitude and phase in terms of the value and slope of the waveform at an arbitrary sampling instant.

$$V_m^{\,2} = v_k^{\,2} + v_k^{\prime\,2} \qquad , \qquad I_m^{\,2} = i_k^{\,2} + i_k^{\prime\,2} \qquad\qquad (2.3)$$

$$\theta_v = \text{ARCTAN}\,(v_k/v_k^{\prime}) \quad , \quad \theta_i = \text{ARCTAN}\,(i_k/i_k^{\prime}) \qquad\qquad (2.4)$$

The slope is approximated by the difference between two samples straddling the central sample point

$$v_k^{\prime} = \frac{1}{h\omega}\,(v_{k+1} - v_{k-1}) \quad , \quad i_k^{\prime} = \frac{1}{h\omega}\,(i_{k+1} - i_{k-1}) \qquad\qquad (2.5)$$

where h is the sampling interval in seconds. The technique relies on the removal of dc offset by matching the current transformer secondary burden to the system. Tests were conducted using theoretical, experimental, and actual fault data, and errors of ± 10 percent in impedance modulus and ± 15 percent in impedance angle were reported. Some digital smoothing was proposed to reduce the effect of noise.

Gilcrest, Rockefeller, and Udren (19) tested the feasibility of a similar three-phase scheme but used the first and second derivatives. The result is

$$|z_{rf}|^2 = \frac{V_m^2}{I_m^2} = \frac{(v_k')^2 + (v_k'')^2}{(i_k')^2 + (i_k'')^2} \tag{2.6}$$

$$\theta = \tan^{-1}\left(\frac{i'}{i''}\right) - \tan^{-1}\left(\frac{v'}{v''}\right) \tag{2.7}$$

where

$$v_k'' = \frac{1}{(h\omega)^2}(v_{k+1} - 2v_k + v_{k-1}) \tag{2.8}$$

The use of derivatives reduced the effect of the dc exponential and other low frequencies, but the accentuation of high frequencies was recognized and analog filtering and digital smoothing techniques were used in an attempt to alleviate the problem.

This technique was implemented by Westinghouse in their joint project with Pacific Gas & Electric, designated as PRODAR 70 (19,20). The PRODAR 70 system was installed on a 230KV, 38-mile transmission line at PG&E's Tesla substation in 1971. In 1974 the PRODAR 70 system was subjected to a series of eight staged faults on the protected line. The operating time of PRODAR 70 was reported to be 20-23 milliseconds.

Sinusoidal conditions were again assumed by Gilbert and Shovlin (21) to directly calculate apparent resistance and apparent reactance to a fault. Their algorithm was based on fitting data to 60 Hz sinusoidal quantities (voltage and current) using three consecutive samples. Equations for the apparent resistance and the apparent reactance were given as

$$R_{rf} = \frac{2v_{n-1}i_{n-1} - v_n i_{n-2} - v_{n-2}i_n}{2(i_{n-1}^2 - i_{n-2}i_n)} \tag{2.9}$$

$$X_{rf} = \frac{v_{n-1} i_n - v_n i_{n-1}}{i_{n-1}^2 - i_{n-2} i_n} \sin (\Delta) \qquad (2.10)$$

where Δ is the angular displacement between samples. The equations respond quickly to changes in the incoming data, but are highly suscep- tible to high frequency transients. This technique was implemented by Pennsylvania Power & Light Co. as the first part of a three part computer relaying project.

Also, Makino and Miki (22) assumed that the voltage and current are pure sine waves at the fundamental system frequency. Incoming data were used to calculate peak values of voltage and current, as well as power flow, using the following equations.

$$V^2 = \frac{v_1^2 + v_2^2 - 2 v_1 v_2 \cos (\omega \Delta t)}{(\sin \omega \Delta t)^2} \qquad (2.11)$$

$$I^2 = \frac{i_1^2 + i_2^2 - 2 i_1 i_2 \cos (\omega \Delta t)}{(\sin \omega \Delta t)^2} \qquad (2.12)$$

$$VI \cos \theta = \frac{v_1 i_1 + v_2 i_2 - (v_2 i_1 + v_1 i_2) \cos \omega \Delta t}{(\sin \omega \Delta t)^2} \qquad (2.13)$$

These equations will exhibit errors in proportion to individual sample errors due to the two-sample window. Digital filters were proposed to attenuate dc offsets and harmonics of third and higher order. This algorithm can be shown to be mathematically equivalent to the sinusoidal curve fit algorithm suggested by Gilbert and Shovlin with the data window reduced to two samples.

C. Lumped-Parameter R-L Model

In this approach, the lumped-parameter, resistance R_{rf} and induc-tance L_{rf}, model of the transmission line is used. The voltage v and currents i_x and i_y are generated for different types of fault and assumed to be related by the expression

$$v = R_{rf} i_x + L_{rf} \frac{di_y}{dt} \qquad (2.14)$$

where i_x and i_y are instantaneous currents linearly related to the currents in the three phases. Two unknowns R_{rf} and L_{rf} require deter-mination in equation (2.14).

McInnes and Morrison (23) investigated a solution in which equation (2.14) is integrated over two intervals giving the two simultaneous equations

$$\int_{t_1}^{t_2} vdt = R_{rf} \int_{t_1}^{t_2} i_x dt + L_{rf} (i_y(t_2) - i_y(t_1)) \qquad (2.15)$$

$$\int_{t_3}^{t_4} vdt = R_{rf} \int_{t_3}^{t_4} i_x dt + L_{rf} (i_y(t_4) - i_y(t_3)) \qquad (2.16)$$

from which R_{rf} and L_{rf} may be found. A total integration time of one quarter of a power frequency cycle was adopted. Tests using simulated and actual data revealed errors of 12 percent in reactance and 6 degrees in impedance angle. The algorithm recognizes the dc offset of the fault current, but neglects the shunt capacitance.

Poncelet (13) suggested to write equation (2.14) in the form

$$\varepsilon(t) = R_{rf} \, i_x + L_{rf} \, \frac{di_y}{dt} - v(t) \tag{2.17}$$

where $\varepsilon(t)$ is an error function. Values of R_{rf} and L_{rf} were found to minimize the mean square error E_m given by

$$E_m = \frac{1}{t_2 - t_1} \int_{t_1}^{t_2} \varepsilon^2(t) \, dt \tag{2.18}$$

considered over a particular period or periods. In one method (13) the mean square error was considered over one period and minimized directly in relation to R_{rf} and L_{rf} giving the equations

$$\int_{t_1}^{t_2} v \, i_x \, dt = R_{rf} \int_{t_1}^{t_2} i_x^2 \, dt + L_{rf} \int_{t_1}^{t_2} i_x \, \frac{di_y}{dt} \, dt \tag{2.19}$$

$$\int_{t_1}^{t_2} v \, \frac{di_y}{dt} \, dt = R_{rf} \int_{t_1}^{t_2} i_x \, \frac{di_y}{dt} \, dt + L_{rf} \int_{t_1}^{t_2} \left(\frac{di_y}{dt}\right)^2 \, dt \tag{2.20}$$

which may be solved for R_{rf} and L_{rf}. One problem in the method is the determination of the derivative of i_y.

Ranjbar and Cory (24) investigated the same technique by selecting overlapping limits of integration chosen to eliminate specific low order harmonics. For example, to eliminate harmonics of order K, m, and n, the authors gave

$$L_{rf} \left(\Sigma \int di_y\right) + R_{rf} \left(\Sigma \int i_x \, dt\right) = \Sigma \int v \, dt \tag{2.21}$$

where

$$\Sigma \int v \, dt = \int_0^{2\pi/K} v \, dt + \int_{\pi/m}^{2\pi/K+\pi/m} v \, dt$$

$$+ \int_{\pi/n}^{2\pi/K+\pi/n} v \, dt + \int_{\pi/m+\pi/n}^{2\pi/K+\pi/m+\pi/n} v \, dt \qquad (2.22)$$

The quantities $\Sigma \int di_y$ and $\Sigma \int i_x dt$ were calculated similarly. Ability to properly process dc offsets is retained and errors due to low order harmonics are thus minimized. The technique requires a sampling rate to be an integral multiple of the highest order harmonic to be eliminated, and also an integral multiple of double the value of the remaining harmonic order.

An extension of the differential equation approach was suggested by Sanderson and Wright (25) in the protection of a series capacitor compensated line.

The solution of the line differential equation approach was also implemented in the General Electric Co. – Philadelphia Electric Co. computer relaying joint project. The investigators (26,27) selected two successive sets of voltage and current samples and replaced the derivative in equation (2.14) by corresponding finite differences. In a field test (26) on a 500 KV, 72-mile transmission line, an operating time of 10-23 ms was reported. In a discussion on the project, it was shown that the algorithm might be ill conditioned for some types of faults (double line to ground). Again an analog low-pass filter was necessary to attenuate high frequency components.

Smolinski (28) suggested an algorithm for digital impedance calculation using a single PI section transmission line model. The

algorithm assumed the fault resistance to be sufficiently small so that the far-end line capacitance can be neglected. The model equation was given as

$$v = R_{rf} i + L_{rf} \frac{di}{dt} - R_{rf} C \frac{dv}{dt} - L_{rf} C \frac{d^2 v}{dt^2} \qquad (2.23)$$

By selecting four successive sets of voltage and current samples and replacing the derivatives in equation (2.23) by corresponding finite differences, the resistance and the inductance to the fault location can be obtained. The algorithm considers the effect of the line capacitance and Smolinsky claimed it does not require filtering, but the computational burden on the computer increases severely.

Suda and Furuse (29) proposed a technique to solve the line partial differential equations to be used for distance protection of cables or long transmission lines. The technique assumes zero initial conditions and zero voltage at the fault location. The algorithm is based on approximate voltage and current polynomial expansions with distance (x), which were derived by integrating the partial differential equations for a distributed parameter line. Using up to the second order term in x, the distributed parameter model equation was given as

$$v = \left(Ri + L \frac{di}{dt} \right) x - \left(RC \frac{dv}{dt} + LC \frac{d^2 v}{dt^2} \right) \frac{x^2}{2} \qquad (2.24)$$

The algorithm was tested on a 90-mile, single-phase simulated transmission line. The time derivative values were computed using a 5-point approximation procedure. Using a sampling frequency of 1920 Hz and a low pass

filter of 600 Hz cutoff frequency, an error of 10 percent after 12 ms was reported.

D. Correlation or Matched Filter Techniques

With the correlation technique it is assumed that the relaying signals contain the power frequency component plus white noise. Then the theory of matched filtering may be applied. Laycock and McLaren (30,31) correlated the signal and noise with a known sinusoidal reference to get the correlation function $\phi(\tau)$ as a function of τ. The value of τ at which $\phi(\tau)$ was maximum indicated the phase, while the maximum of $\phi(\tau)$ gave the magnitude. The correlation was performed over one complete cycle for each value of τ.

Hope, Malik, and Dash (32) proposed to correlate the voltage and current signals to determine the power of the line. The self correlation of the current signal was used to obtain the square of the magnitude of the current in the line. The impedance was then computed by taking the ratio of the power and the square of the current. An alternative algorithm using the self correlation of the voltage signal to determine the line admittance was also discussed. The authors reported an operating time of 16 ms and 5 percent error.

Malik, Hope, and Dash (33) extended the algorithm for differential protection by correlating the currents at the two ends of the protected equipment. Their algorithm was based on the fact that correlating two signals in phase results in a positive value and yields a negative value if they are 180 degrees out of phase.

E. Fourier and Walsh Transform Techniques

This class of techniques assumes the measured waveform to consist of a 60 Hz fundamental waveform plus an infinite sum of certain harmonics. An orthogonal pair of base functions (sinusoids or square waves) are correlated with the data samples to extract the components of the base function in the waveform.

Ramamoorty (34) proposed that the desired fundamental voltage or current can be extracted from the fault transients by correlating one cycle of data samples with the stored samples of reference fundamental sine and cosine waves. The general expressions for the sine and cosine components of voltage at sample k are

$$V_s = \frac{1}{N} [2 \sum_{\ell=1}^{N-1} v_{k-N+\ell} \sin\left(\frac{2\pi}{N}\ell\right)] \qquad (2.25)$$

$$V_c = \frac{1}{N} [v_{k-N} + v_k + 2 \sum_{\ell=1}^{N-1} v_{k-N+\ell} \cos\left(\frac{2\pi}{N}\ell\right)] \qquad (2.26)$$

where the v_i are the voltage samples and N is the number of samples per cycle. Similar expressions are evaluated for current components I_s and I_c. Implicit in Fourier analysis is filtering of the data; the output responds slowly, smoothly, and accurately to badly distorted waveforms. The operating time is more than one cycle.

In a compromise between speed of response and sharpness of filtering, Phadke, Hlibka, and Ibrahim (35) suggested a half-cycle Fourier transform algorithm. Of course, accuracy of results is more seriously affected by off-normal frequency components; dc offsets present a particular problem.

The authors of the algorithm remedy the latter by assuming that the fault waveform contains a dc offset of unknown magnitude but a known time constant. The suggested implementation finds the magnitude of the offset and subtracts it from the fault waveform prior to the Fourier analysis itself.

Horton (36) suggested an algorithm based on the Walsh function, which is closely related to the full-cycle Fourier transform. The orthogonal functions which are correlated with the fault waveform, however, are not 60 Hz sine and cosine waves, but odd and even square waves. Real time computation is simplified since the reference square waves assume values of ±1 only. However, some of this benefit is mitigated by the need to extract several harmonics of the square wave components along with the fundamental so that the desired sinusoidal 60 Hz components can be reconstructed.

As for the full-cycle Fourier analysis, the trend of results is heavily damped. Accuracy is good after one cycle even for distorted waveforms.

F. Least-Squares Fitting Techniques

The Fourier transform can be shown to be a means of fitting a fundamental sinusoid to the fault data samples with the minimum possible mean square error. Other algorithms have been proposed which perform a similar fit, but to a sinusoid having an exponentially-decaying dc transient and/or harmonic distortion.

Luckett, Munday, and Murray (37) claimed to have performed a

least-squares fit to the general fault waveform

$$K_i e^{-\lambda t} + \sum_{m=1}^{N} (K_{2m} \sin m\omega t + K_{2m+1} \cos m\omega t)$$

where the solution for the K coefficients was found by a least-squares fit of the form which minimizes the mean-square error between the assumed and actual waveforms.

Sachdev and Baribeau (38) suggested a least-squares fitting algorithm which solves simultaneous equations to obtain parameters of the fault waveform from a series of voltage or current samples. Seven parameters describing a fundamental component, a dc offset with unknown time constant, and a third harmonic component were identified. The concept of pseudoinverse was used to provide the least-squared-error solution of the unknowns from m independent equations. The computations were reduced by finding only the two fundamental wave parameters. Also, many of the computations were performed a priori and incorporated in the program.

G. Measurement of High Frequency Traveling Wave Phenomena

In this approach, utilization is made of the ringing phenomena caused by the traveling wavefronts due to the system fault disturbance.

Dommel and Michels (39) described the mathematical foundations for a traveling wave discriminant (TWD) relay. They devised a traveling wave discriminant function

$$D = (v - ZI)^2 + \frac{1}{\omega^2} \left(\frac{dv}{dt} - Z \frac{dI}{dt}\right)^2$$

where v and I are the initial changes in voltage and current. It was shown that D is invariant with respect to the fault location and the initiation angle at which the fault occurs. If D exceeds certain threshold level, a fault is declared. Boeing Co. and Bonneville Power Administration are conducting further development of this technique to reduce the operating time and improve its accuracy (39).

Takagi and Associates (40-43) described a new traveling wave current carrier differential (CCD) relay. They assumed a lossless transmission line and obtained a function based on the deviation in current and voltage at the ends of the protected line. If this function exceeds specific threshold value, an internal fault exists. The relay requires a data communication link between the ends of the protected line. The suggested relay is affected by mutual coupling, line losses, and frequency dependence of line parameters.

Other research groups are conducting research on the traveling wave relays to achieve ultra high speed relaying. Vitins (44) described a technique based on a combined evaluation of the voltage and current deviations generated by the fault occurrence. Specific functions were developed and compared with threshold levels to indicate a fault or no-fault condition.

III. OBJECTIVES AND KALMAN-FILTERING THEORY

A. Overview of the Problem and Objectives

Most of the techniques developed so far are based on unjustified waveform equations or optimistic assumptions which, in turn, introduce uncertainty in the computer relaying decisions. Therefore, the primary objective of this research was to investigate optimal estimation of the fundamental frequency components using Kalman-filtering techniques for computer relaying purposes. To achieve this goal, the nature of the non-fundamental components had to be determined. The research presented here is divided into four major parts.

(1) The non-fundamental components in the current and voltage waveforms are designated as noise signals. An overall characterization of the noise is developed based on the frequency of occurrence of different types of faults and the probability of fault location.

(2) Kalman filter models are developed for optimal estimation of the fundamental-frequency components. The effect of the sampling rate, sensitivity to changes in model parameters, and rate of convergence are examined.

(3) A full scheme for digital distance protection using Kalman filtering is developed and tested for all types of faults. The full scheme consists of fault detection, fault type classification, apparent impedance computation, and fault location calculation.

(4) Finally, the Kalman-filtering-based digital distance relay is compared with four other algorithms. Three of these algorithms were implemented in computer relaying projects by large industrial firms in the United States and the fourth algorithm was recently published (28).

B. Kalman Filtering Theory

The Kalman filter has been extensively used in many applications and is explained in many references. The equations and presentations of the Kalman filter here are taken largely from unpublished notes by Brown (45) and from Gelb (46).

The Kalman filter is a recursive optimal estimator. The mathematical model for the filter is based on the state space concept. What is presented here are only the equations necessary to implement the filter, and no attempt is made to explain the theory behind their development. For more details, refer to Brown (45) and Gelb (46).

In the formulation of a Kalman filter, knowledge of the a priori statistics of initial conditions, the process noise model, and the measurement noise model are required. To begin with, a mathematical model of the system is assumed to be of the form

$$x_{k+1} = \phi_k x_k + w_k \qquad (3.1)$$

This is the state model for the process to be estimated where

x_k is the n x 1 process state vector at time t_k

ϕ_k is the n x n state transition matrix

w_k is an $n \times 1$ vector uncorrelated sequence with known co-variance structure.

The observation (measurement) of the process is assumed to occur at discrete points in time in accordance with the relationship

$$z_k = H_k x_k + v_k \qquad (3.2)$$

where

z_k is the $m \times 1$ vector measurement at t_k

H_k is the $m \times n$ matrix giving the ideal (noiseless) connection between the measurement and the states

v_k is the $m \times 1$ measurement error assumed to be an uncorrelated sequence with known covariance structure.

The covariance matrices for the w_k and v_k vectors are given by

$$\overline{w_k w_i^T} = \begin{cases} Q_k, & i = k \\ 0, & i \neq k \end{cases} \qquad (3.3)$$

$$\overline{v_k v_i^T} = \begin{cases} R_k, & i = k \\ 0, & i \neq k \end{cases} \qquad (3.4)$$

$$\overline{w_k v_i^T} = 0, \quad \text{for all } k \text{ and } i$$

Having an a priori estimate $\hat{x}_k^-$ and its error covariance P_k^-, the recursive Kalman filter equations are as follows.

(1) Compute the Kalman gain K_k:

$$K_k = P_k^- H_k^T (H_k P_k^- H_k^T + R_k)^{-1} \qquad (3.5)$$

(2) Update estimate with measurement z_k:

$$\hat{x}_k = \hat{x}_k^- + K_k (z_k - H_k \hat{x}_k^-)$$ (3.6)

(3) Compute rror covariance for updated estimate:

$$P_k = (I - K_k H_k) P_k^-$$ (3.7)

(4) Project the estimate and error covariance

$$\hat{x}_{k+1} = \phi_k \hat{x}_k$$ (3.8)

$$P_{k+1}^- = \phi_k P_k \phi_k^T + Q_k$$ (3.9)

As stated above, to have an optimal estimator, a knowledge of the initial estimation error (noise) covariance P_o^-, an a priori estimate $\hat{x}_o^-$, and a model for the system and measurement are needed.

Developing the required model raised the following questions. (1) What is the autocorrelation function and variance of the noise signal, (2) is it a stationary random process, and (3) what would be the best model to achieve the highest accuracy and fastest response? To answer these questions, a bank of data of transient waveforms associated with actual power-system faults would be desirable. An actual data bank was not available, though, so a data bank of waveforms was generated by digital simulation.

IV. DIGITAL SIMULATION OF POWER SYSTEMS

Fault conditions in a power system always give rise to a very complex transient phenomena in the relaying signals. There is, therefore, a necessity for testing techniques which faithfully reproduce the type of waveforms which will be experienced by protection schemes in practical situations.

For many years, digital computer methods have been employed for the calculation of transient phenomena in power-system networks caused by switching operations.

The computational techniques used may be broadly classified into frequency-domain methods based on the Fourier transform and time-domain methods using a traveling wave approach. The use of such methods has intended to concentrate on the calculations of voltage transients for the purposes of attaining economical system-insulation levels.

Extensive use has been made of psuedo-steady-state models in which a synchronous machine is represented by an appropriate voltage and reactance, and each line is represented by an equivalent π or T circuit. Such models have proven to be adequate for the design of slow-speed relays. The new technology in high-speed relaying in general and computer relaying in particular has established a need for accurate determination of fault-transient waveforms during the first half cycle after the fault occurrence.

Frequency-domain simulation for transient analysis has been extensively studied by many authors (47-51), but only tested on simple

special problems with known boundary conditions. Ametani (51), Johns and Aggarwal (52), and Johns and El-Kateb (53) developed a technique to solve power-system transients due to faults at infinite bus-bars to avoid the boundary condition problems.

In this chapter, a frequency-domain digital simulation of a typical power system is developed to obtain the nature of transient-induced noise signals. It was felt that reasonable assumptions that simplify the problem without jeopardizing the nature of the noise signals, are essential. These assumptions and the solution of the associated problems will be discussed during the course of this work.

A. System Configuration Studied

There are many sources that contribute to the transient-induced noise signals. These sources may be classified as significant and non-significant sources.

The transducers, especially the current transformers (CT), are known to saturate, thereby producing noise components in the current signals. The CT saturation phenomenon is difficult to assess as it depends substantially upon the design of the CTs, CT selection criteria, and prevailing short circuit levels on the power system. Saturation, if it occurs, would be significant for near faults which are well within the first zone of an impedance relay. Also, CT saturation is less likely to occur within a half cycle to one cycle duration after the occurrence of a fault. The design of current transducers has been a topic of extensive research to meet protection requirements. Recently (54) a digital current transducer was introduced in power systems for metering and

protection purposes. Therefore, CT saturation effects are not con-
sidered to be significant.

Coupling capacitor voltage transformers (CCVT) are also likely to
produce significant noise signals for near faults. Once again, since
these faults are well within the first zone, the CCVT error contribu-
tions to the noise signal for near faults are not considered to be
significant.

Also it has been shown (55,56) that line loading, untransposition,
and structure of power systems have minor effects on the nature of the
non-fundamental transient components. Therefore, for the purpose of
this study, a digital frequency-domain simulation of a simple power
system configuration is developed to acquire data for various faults
and obtain the noise characteristics.
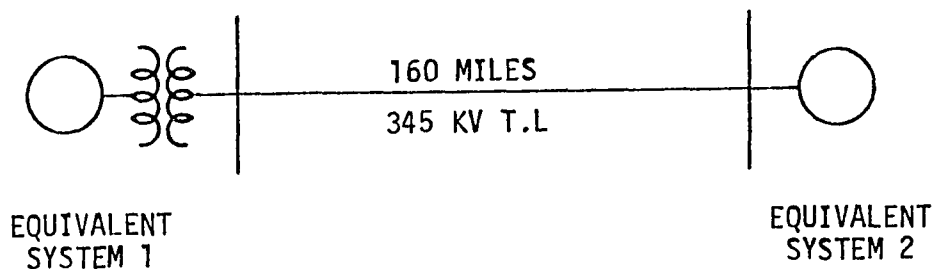
Figure 4.1. Power system model

The basic configuration studied and shown in Figure 4.1 corresponds
to a 345 KV, 160-mile transmission line connected to a 400 MVA generating
station at the sending end and an equivalent of a large interconnected
system at the receiving end. All different types of faults were applied
at different locations on the line, and voltage and current waveforms

at the sending end were obtained. The transmission line geometric configuration, as well as generator and transformer data, are given in Appendix A.

B. Frequency Domain Simulation of a Transmission Line

The determination of the fault-induced transients in a power system involves the solution of the partial differential equations of transmission lines

$$- \frac{\partial v(x,t)}{\partial x} = R\,i\,(x,t) + L\,\frac{\partial i(x,t)}{\partial t} \tag{4.1}$$

$$- \frac{\partial i(x,t)}{\partial x} = C\,\frac{\partial v(x,t)}{\partial t} \tag{4.2}$$

simultaneously and satisfying the boundary conditions of the line. In equations (4.1) and (4.2) R,L, and C are respectively the resistance, inductance, and capacitance matrices per unit length and v(x,t) and i(x,t) represent the voltage and current vectors in the a,b,c frame as functions of time, t, and distance, x. Applying the Laplace transform with zero initial conditions (57) to equations (4.1) and (4.2) leads to

$$- \frac{dV(x,s)}{dx} = Z(s) \cdot I(x,s) \tag{4.3}$$

$$- \frac{dI(x,s)}{dx} = Y(s) \cdot V(x,s) \tag{4.4}$$

Therefore,

$$\frac{d^2V(x,s)}{dx^2} = Z(s)\,Y(s)\,V(x,s) \tag{4.5}$$

$$\frac{d^2 I(x,s)}{dx^2} = Y(s)\, Z(s)\, I(x,s) \tag{4.6}$$

where

$$Z(s) = (R + sL)$$
$$Y(s) = sC \tag{4.7}$$

Assuming that the line is completely transposed, $Z(s)$ and $Y(s)$ take a particular form (58,59), in which all the diagonal elements are equal and all the off diagonal elements are also equal. Although transmission lines are often untransposed, transposition is a reasonable simplification and a usual assumption in analysis. The matrix product $Z(s)\, Y(s)$ is then diagonalizable by a modal decomposition matrix which is independent of the entries of the matrices. The symmetrical component transformation is a well known form of modal decomposition (58,59).

Therefore,

$$V_{abc}(x,s) = A V_{012}(x,s) \tag{4.8}$$

$$I_{abc}(x,s) = A I_{012}(x,s) \tag{4.9}$$

where

$$A = \begin{bmatrix} 1 & 1 & 1 \\ 1 & a^2 & a \\ 1 & a & a^2 \end{bmatrix} \quad ; \quad a = 1\underline{/120^\circ}$$

Thus, the transmission line symmetrical-components equation in the complex frequency domain may be represented by the two port form of equation (4.10).

$$
\begin{bmatrix}
VS_0(s) \\
VS_1(s) \\
VS_2(s) \\
IS_0(s) \\
IS_1(s) \\
IS_2(s)
\end{bmatrix}
=
\begin{bmatrix}
A_0(s) & & & B_0(s) & & \\
& A_1(s) & & & B_1(s) & \\
& & A_2(s) & & & B_2(s) \\
C_0(s) & & & A_0(s) & & \\
& C_1(s) & & & A_1(s) & \\
& & C_2(s) & & & A_2(s)
\end{bmatrix}
\begin{bmatrix}
VR_0(s) \\
VR_1(s) \\
VR_2(s) \\
IR_0(s) \\
IR_1(s) \\
IR_2(s)
\end{bmatrix}
\qquad (4.10)
$$

where

VS_j is the sending-end voltage $(x = 0)$ $\quad ; \; j=0,1,2$

IS_j is the sending-end current $\quad ; \; j=0,1,2$

VR_j is the voltage at the fault location $(x = X)$ $\quad ; \; j=0,1,2$

IR_j is the line current at the fault location $\quad ; \; j=0,1,2$

$A_j = 1/2 \, (\exp(x\gamma_j(s))) + \exp(-x\gamma_j(s))$ $\quad ; \; j=0,1,2$

$B_j = 1/2 \, (\exp(x\gamma_j(s))) - \exp(-x\gamma_j(s)) \cdot \dfrac{Z_j(s)}{Y_j(s)}$ $\quad ; \; j=0,1,2$

$C_j = 1/2 \, (\exp x\gamma_j(s)) - \exp(-x\gamma_j(s)) \cdot \dfrac{Y_j(s)}{Z_j(s)}$ $\quad ; \; j=0,1,2$

$\gamma_j(s) = \sqrt{Z_j(s) \cdot Y_j(s)}$ $\quad ; \; j=0,1,2$

0 indicates zero sequence

1 indicates positive sequence

2 indicates negative sequence

C. Simulation of Transformers and Generators

The simulation used in the course of this work makes use of a technique developed by Laughton (60) and by Chen and Dillon (58) which represents the transformer by a two-port matrix. Each submatrix reflects the structure and the type of the transformer. For a wye-wye transformer the symmetrical components are related by equation (4.12)

$$
\begin{bmatrix} VS_{012}(s) \\ \\ IS_{012}(s) \end{bmatrix} \quad \begin{bmatrix} U & \vdots & -Z_T(s) \\ - & - & - \\ 0 & \vdots & U \end{bmatrix} \begin{bmatrix} VG_{012}(s) \\ \\ IG_{012}(s) \end{bmatrix} \tag{4.12}
$$

Representing the synchronous generators by the symmetrical components and the operational impedance concept lead to

$$
ZG_{012}(s) = \begin{bmatrix} ZG_0(s) & & \\ & ZG_1(s) & \\ & & ZG_2(s) \end{bmatrix} \tag{4.13}
$$

The zero, positive, and negative sequence operational impedances of the generator are related to the subtransient parameters. It should be noted that this model gives reasonably accurate results during the first half cycle after the fault occurrence.

D. Fault Simulation

The basis of this method hinges on representing the voltage at the fault point by the sum of two voltages $\bar{V}_{fs}$, $\bar{V}_{ff}$ (53). The first of

these voltages, $\bar{V}_{fs}$, is sinusoidal and equal to the steady state voltage at the point of fault before the disturbance. $\bar{V}_{ff}$ is a suddenly applied voltage, which, when added to $\bar{V}_{fs}$, represents the post-fault voltage. A solution may thus be obtained by performing two separate calculations in which the desired voltages and currents are evaluated when $\bar{V}_{fs}$ is applied to the energized system and the superimposed voltage $\bar{V}_{ff}$ is applied to the line with all source voltage set at zero. The method is essentially one of superposition, and it should be noted that the steady-state voltage vector can be evaluated from a knowledge of the prefault voltage and currents at the terminating bus-bars. In fact, $\bar{V}_{fs}$ is only needed so far as it enables the value of $\bar{V}_{ff}$ to be evaluated.

It is interesting to note that the superimposed voltage technique has been used for a long time in steady state fault analysis and has been proven to be accurate. In the 1970s, the technique was developed to simulate faults on infinite bus-bars. Johns and El-Kateb (53) assumed that the superimposed voltage on the unfaulted phases is zero. This assumption is reasonable if an infinite bus is assumed.

In the scope of this work the superimposed voltage is obtained for each sequence component, based on the boundary conditions of each fault at the fault location.

E. Combination of Network Elements

It is necessary to combine the equations representing the generator, transformer, and transmission line so that by applying the appropriate set of superimposed voltages at the fault location the variation of both

currents and voltages can be determined.

From the previous sections, all the equations of the different sequence components are decoupled. Therefore, the equations for each sequence component will be written separately.
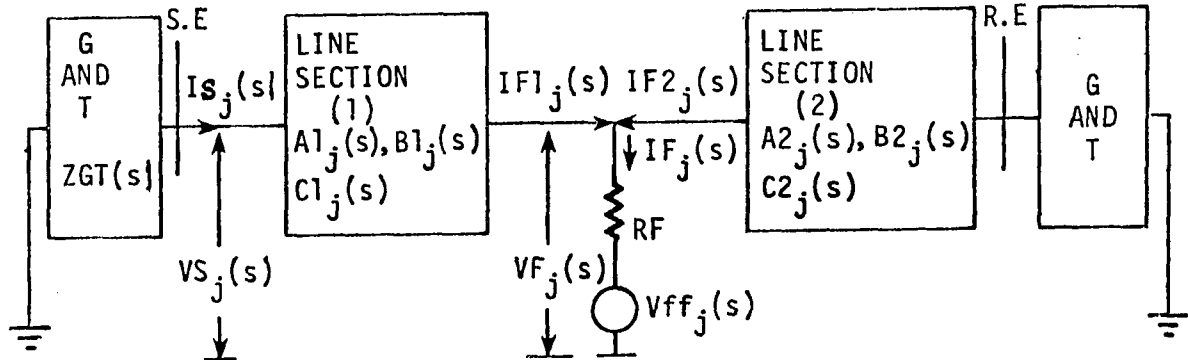

Figure 4.2. Sequence networks in the complex frequency domain

Using the transmission line equation (4.10) in the complex frequency domain and referring to Figure 4.2 then yields

$$VS_j(s) = A1_j(s)\ VF_j(s) + B1_j(s)\ IF1_j(s) \tag{4.14}$$

$$IS_j(s) = C1_j(s)\ VF_j(s) + A1_j(s)\ IF1_j(s) \tag{4.15}$$

Using the generator and transformer equations (4.12) and (4.13) then yields

$$VS_j(s) = -ZGT(s)\ IS_j(s) \tag{4.16}$$

From equations (4.14), (4.15) and (4.16) we have

$$IF1_j(s) = -TE1_j(s)\ VF_j(s) \tag{4.17}$$

where

$$TE1_j(s) = [A1_j(s) + ZGT_j(s) \, C1_j(s)]/$$

$$[B1_j(s) + ZGT_j(s) \, A1_j(s)] \qquad (4.18)$$

Similar equations were obtained for the other section of the line (between the fault location and the receiving end), thus

$$IF2_j(s) = -TE2_j(s) \, VF_j(s) \qquad (4.19)$$

Using (4.18), (4.19), and Figure 4.2

$$IF_j(s) = IF1_j(s) + IF2_j(s) = -VF_j(s)/TV_j(s) \qquad (4.20)$$

where

$$TV_j(s) = 1/[TE1_j(s) + TE2_j(s)] \qquad (4.21)$$

Finally

$$VF_j(s) = Vff_j(s) + RF \cdot IF_j(s) \qquad (4.22)$$

From (4.20) and (4.22)

$$VF_j(s) = VFF_j(s) \, TV_j(s)/[TV_j(s) + R_F] \qquad (4.23)$$

using the above relations and the boundary condition for each type of fault, the sequence voltages and currents at the sending end were obtained in the complex frequency domain. Using the modal transformation matrix A, the three phase quantities are obtained also in the complex frequency domain.

F. Transform Method of Solution

As stated in the previous sections, the voltages and currents at the relay location can be obtained at discrete points in the complex

frequency domain. To get the time solution, the problem is the numerical evaluation of the inverse Laplace transform integral.

The inverse Laplace transform integral is defined as

$$f(t) = \frac{1}{2\pi j} \int_{\alpha-j\infty}^{\alpha+j\infty} F(s) e^{st} ds \qquad (4.24)$$

where the path of integration is chosen to the right of all the poles of $F(s)$. The choice of convergence factor (α) assumes great importance in numerical calculations. It is now a matter of establishing a satisfactory numerical approximation to the integral transform.

G. Method of Computation

The voltages and currents at the sending end of the line may be computed numerically in the s domain along $s = \alpha + j\omega$. Theoretically the time function can be obtained by integrating from $-\infty$ to $+\infty$. As the process is carried out numerically, the integration has to be truncated in a limited range from $-\Omega$ to $+\Omega$. Truncating the range of integration gives rise to Gibb's oscillation due to the rectangular window in the frequency domain (47). These oscillations may be suppressed by the so-called sigma factor. The idea is to take the value of the time function at any given instant as being the average value associated with a period of π/Ω seconds centered on the time instant of interest. The derivation of the sigma factor is given by Day et al. (47) and leads to an elegant mathematical result. It works out that the required objective is simply achieved by multiplying $F(s)$ by the (sigma) factor

$$\sigma(\omega) = \frac{\sin\ (\omega\pi/\Omega)}{\omega\pi/\Omega} \tag{4.25}$$

prior to the inversion process. Therefore, $f(t)$ may be obtained as

$$f(t) = \frac{1}{2\pi} \int_{-\Omega}^{\Omega} F(\alpha + j\omega)\sigma(\omega)\ \exp\ ((\alpha + j\omega)t)\ d\omega$$

$$= \frac{e^{\alpha t}}{2\pi} \int_{-\Omega}^{\Omega} F(\alpha + j\omega)\sigma(\omega)\ e^{j\omega t}\ d\omega \tag{4.26}$$

Having taken the discrete samples at $s = \alpha \pm j\frac{\Delta\omega}{2}$, $\alpha + j\frac{3}{2}\Delta\omega$, etc. as indicated in Figure 4.3. Application of the midpoint rule of numerical
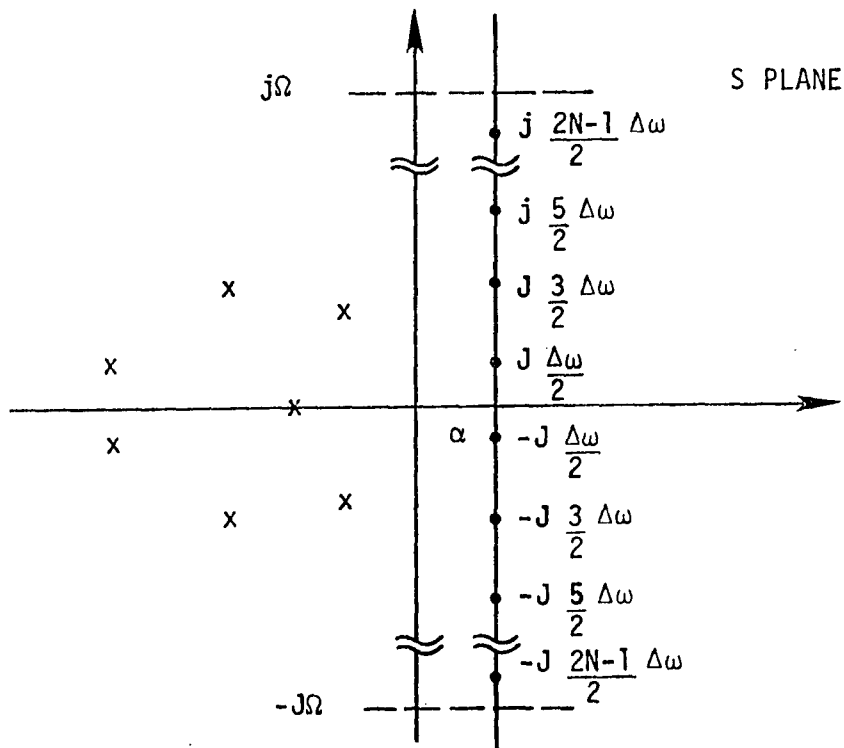
Figure 4.3. Discrete samples in the frequency domain

integration then gives the following approximation to the value f(t) at a selected time instant t_m

$$f(t_m) = \frac{1}{2\pi} \sum_{K=-N}^{N} F(\alpha + j \frac{2k-1}{2} \Delta\omega) \frac{\sin (\pi\left(\frac{2k-1}{2}\right) \Delta\omega)}{(\pi\left(\frac{2k-1}{2}\right) \Delta\omega)}$$

$$\exp ((\alpha + j \frac{2k-1}{2} \Delta\omega) t_m) \Delta\omega \qquad (4.27)$$

Considering the fact that f(t) is a real function, then

$$F(\alpha + j\omega) = F^*(\alpha - j\omega)$$

Therefore,

$$f(m\Delta t) = \frac{e^{\alpha m \Delta t}}{\pi} \text{ Real} \sum_{k=1}^{N} F(\alpha + j \frac{2k-1}{2} \Delta\omega) \cdot$$

$$\frac{\sin (\pi\left(\frac{2k-1}{2}\right) \Delta\omega)}{\pi\left(\frac{2k-1}{2}\right) \Delta\omega} e^{j \frac{2k-1}{2} \Delta\omega m \Delta t} \Delta\omega \qquad (4.28)$$

So,

$$f(m\Delta t) = \frac{e^{\alpha m \Delta t}}{\pi} \text{ Real} \{e^{j \frac{2\pi m}{N}} \sum_{k=1}^{N} F_k e^{j \frac{2\pi m}{N} (k-1)} \} \qquad (4.29)$$

where

$$F_k = F(\alpha + j \frac{2k-1}{2} \Delta\omega) \frac{\sin \left(\frac{2k-1}{2} \cdot \pi\Delta\omega\right)}{\frac{2k-1}{2} \cdot \pi\Delta\omega} \cdot \Delta\omega \qquad (4.30)$$

The special form of equation (4.29) allows the use of the FFT algorithm to reduce the computation time. A decimation-in-time algorithm (61,62)

is used to evaluate

$$f_1 (m\Delta t) = \sum_{k=1}^{N} F_k \, e^{j \frac{2\pi m}{N} (k-1)} \tag{4.31}$$

Then

$$f(m\Delta t) = \frac{e^{\alpha m \Delta t}}{\pi} \, \text{Real} \, \{e^{j \frac{2\pi m}{N}} f_1 (m\Delta t)\} \tag{4.32}$$

To use the FFT N is chosen to be 2^M, where M is an integer number.

H. Choice of Integration Parameters α, $\Delta\omega$, and Ω

To perform the numerical integration, it is necessary to assign values to the convergence parameter α, the step length $\Delta\omega$, and the range Ω. These three parameters are not only interrelated in a complex way but their choice depends on the time over which a solution is required. One way to obtain working rules is through mathematical experimentation, and for this to be effective, the experiment should be more severe than anything likely to be experienced in practice. In testing the choice of these parameters on known functions, namely the unit step, cosinusoidal and sinusoidal functions, it was noticed that large values of Ω result in small rise time for the first two functions. Therefore, higher values of Ω are generally recommended.

As it is assumed that F(s) has no singularities in the right half s plane, α may be chosen arbitrarily small so far as the Laplace transform is concerned. However, such arbitrariness will generally lead to un-satisfactory results in the discrete manipulation of the Laplace

transform. The reason is not difficult to see. Consider, for example, the case where α is chosen very small. The path of integration will be almost coincidental with the imaginary axis and, consequently, poles lying on or near the imaginary axis will have a very disturbing influence on the profile of the integrand. This profile will appear extremely peaked in the vicinity of such singularities and, in principle, very fine steps would need to be taken in the numerical integration process in order to adequately detect the nature of the singularity involved.

The effect of increasing α is to displace the integration contour away from the immediate vicinity of possible singularities of $F(s)$. This softens the profile of the integrand, thereby justifying larger steps in the numerical integration process.

The above argument seems to suggest that it would be advantageous to choose a large value of α. This led Day et al. (47-50) to choose a value of α of 10^3 to 10^4. But Day et al. (48) investigated the switching problem with observation time of microseconds and Ω of 10^6, which makes the choice of α reasonable for this special problem. Ametani (51) followed the same conclusion to solve power systems transient problems, but this is not correct either. The reason is this. While the integration profile may be very smooth, it would be unreasonable to accept the truncated contour as effectively approximating the infinite path from $-\infty$ to $+\infty$.

As a result of an extensive mathematical experimentation for this work, it has been established that α should neither be chosen "too"

large nor "too" small. A value of $\alpha = \Delta\omega$ gave eminently satisfactory results.

I. Choice of Time Duration τ

τ is the time duration of interest in the transient analysis. From the mathematical experimentation, it was noticed that the time function has a tendency to break up when $t_m \to \tau$. Also it was advisable to choose α and τ in such a way that $\alpha\tau$ is about unity. As a result of the mathematical experimentation and the above argument, the following choice gave satisfactory results:

$$\alpha = \Delta\omega = 7.5\pi$$

$$\tau = 8 \text{ cycles of the 60 Hz component}$$

$$N = 1024$$

A computer program was written to implement the principles discussed in the previous sections, and the waveforms of the currents and voltages at the relay location were obtained for the different types of faults at different locations.

V. RANDOM PROCESS DESCRIPTION OF THE FAULT-INDUCED NOISE SIGNALS

The noise signal in the current and voltage waveforms was obtained by subtracting the steady state fault time solution from the transient solution in the first two cycles after the occurrence of the fault. Prior to the fault occurrence, the system was assumed to be in normal loading conditions. Steady state fault calculation was performed using the three-component method (63) including the line capacitance.

A. Probability of Fault Location and Frequency of
Occurrence of Different Types of Faults

The magnitude of the noise is affected by many factors such as fault location, moment of inception, etc. Warrington (64) reported that over 95 percent of faults caused by flashovers occur within 30 degrees of the peak value of the voltage wave at the fault location. Swift (55) showed that the worst case condition in the current and voltage noise signal occurs where the fault is applied at a voltage peak. Therefore, all the transient-induced noise signals used in this study were produced when the voltage of the faulted phase was at its peak value.

It was assumed that the fault is equally probable at any location. This is based on assuming identical characteristics of the line insulators.

The frequency of occurrence of the different types of faults varies widely with such factors as relative insulation to ground and between phases, circuit configuration, the voltage class, method of grounding, quality of construction, etc. Thus, it is generally not easy to analytically generate an exact overall figure for the frequency of occurrence

of the different types of faults. But using the figures published in the literature, based on experience and/or observation on specific systems, a general trend of the frequency of occurrence was obtained. Van Zee and Felton (65) reported that 83 percent of line faults are single line to ground, 5 percent are double line to ground, and 11 percent are line to line faults. The report by Van Zee and Felton was based on the operation experience of a 500 KV system that has about 1,000 miles of transmission lines and 5 - 500/230 KV substations. Liew (66) reported that on the Ontario hydro 115 KV system, 83 percent of line faults are single line to ground and 17 percent are double line to ground. Also, it was reported by Warrington (64) about faults on a 275 KV system in Europe based on 12 years of observation. He found that 85 percent of line faults are single line to ground faults, 12 percent are double line to ground faults, and 3 percent may be line to line and/or three-phase faults.

To obtain an overall characterization of the noise signal, weighting factors were assigned to the different types of faults based on the general trend of the published figures. It is interesting to note that it was observed that the general nature of the noise did not change by changing the type of fault, but the magnitude was slightly affected. According to the above argument, a weighting factor of 0.85 was assigned to the single line to ground fault and a weighting factor of .05 to each of the other three types of faults. It will be shown later that the Kalman filter is relatively insensitive to changes in filter parameters.

B. Autocorrelation Function of the Noise Signal

As the transient noise signals are decaying transients, the time

reference was considered at the instant the fault occurs. As the noise

signal is non-stationary, the autocorrelation function was obtained as

$$\phi_{xx}(\tau) = E[x(0)x(\tau)] \tag{5.1}$$

considering M noise signals generated by M fault locations with the

probability of each to be 1/M then

$$\phi_{xx}(\tau) \cong \frac{1}{M} \sum_{j=1}^{M} x_j(0)x_j(\tau) \tag{5.2}$$

for each type of fault, where x denotes a current or a voltage noise

signal. Then the overall autocorrelation function may be obtained by

using the weighting factors for each type of fault as

$$\phi_{xx\,AV.}(\tau) = 0.85\ \phi_{xxAG}(\tau) + .05\ \phi_{xxBCG}(\tau)$$

$$+ .05\ \phi_{xxBC}(\tau) + .05\ \phi_{xxABC}(\tau) \tag{5.3}$$

This overall autocorrelation function was obtained for current and

voltage noise signals in the faulted phase, unfaulted phase, and zero

sequence. As the zero sequence component does not exist in the line to

line or the three-phase faults, according to the assumption of a com-

pletely transposed line, the zero sequence weighting factors considered

were .90 for the single line to ground and .10 for double line to

ground faults.

C. Variance of the Noise Signal

Similarly, the variance of the noise signal was obtained using the M sets of data for each fault as

$$VAR(\tau) \cong \frac{1}{M} \sum_{j=1}^{M} (x_j(\tau))^2 \qquad (5.4)$$

Similar to the autocorrelation function, an overall variance of the voltage and current noise signals were obtained using the weighting factor of each fault. As the variance of the noise signal has a tendency to decrease exponentially, an empirical exponential curve fit was obtained using a least-squares algorithm.

D. Frequency Spectrum of the Noise Signal

To complete the picture of the noise signals, the frequency spectrum of the noise signal was obtained. Figures 5.1 and 5.2 show a sample of a voltage and current noise signal in a faulted phase. As the noise signal is finite, the frequency spectrum was obtained numerically by a Fourier transform as follows:

$$F(j\omega) = \int_{-\infty}^{\infty} f(t)e^{-j\omega t} dt \qquad (5.5)$$

As

$$f(t) \begin{cases} \neq 0, & 0 < t < T \\ = 0, & \text{elsewhere} \end{cases} \qquad (5.6)$$

then

$$F(j\omega) = \int_{0}^{T} f(t)e^{-j\omega t} dt \qquad (5.7)$$
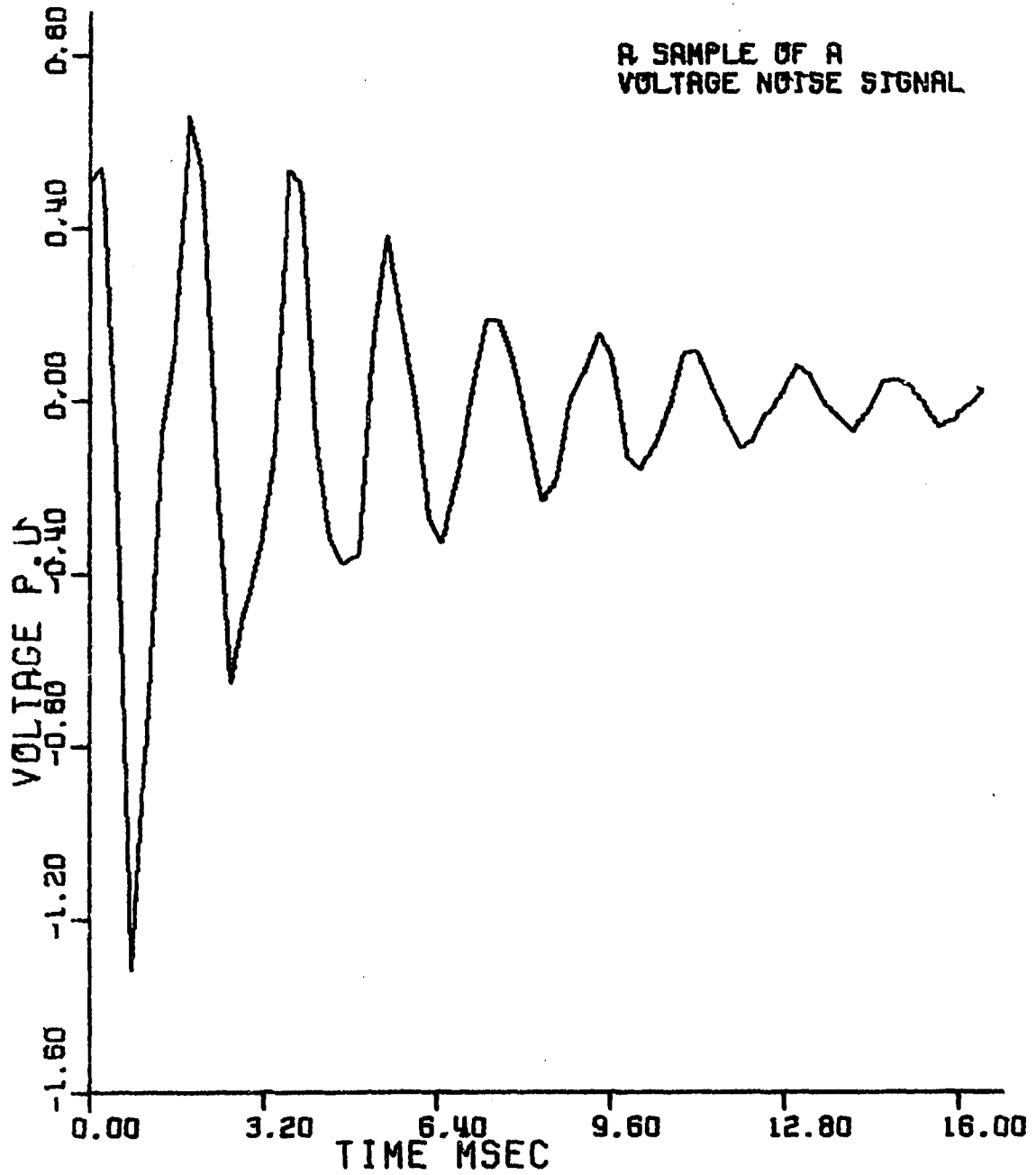
Figure 5.1.   A sample of a voltage noise signal
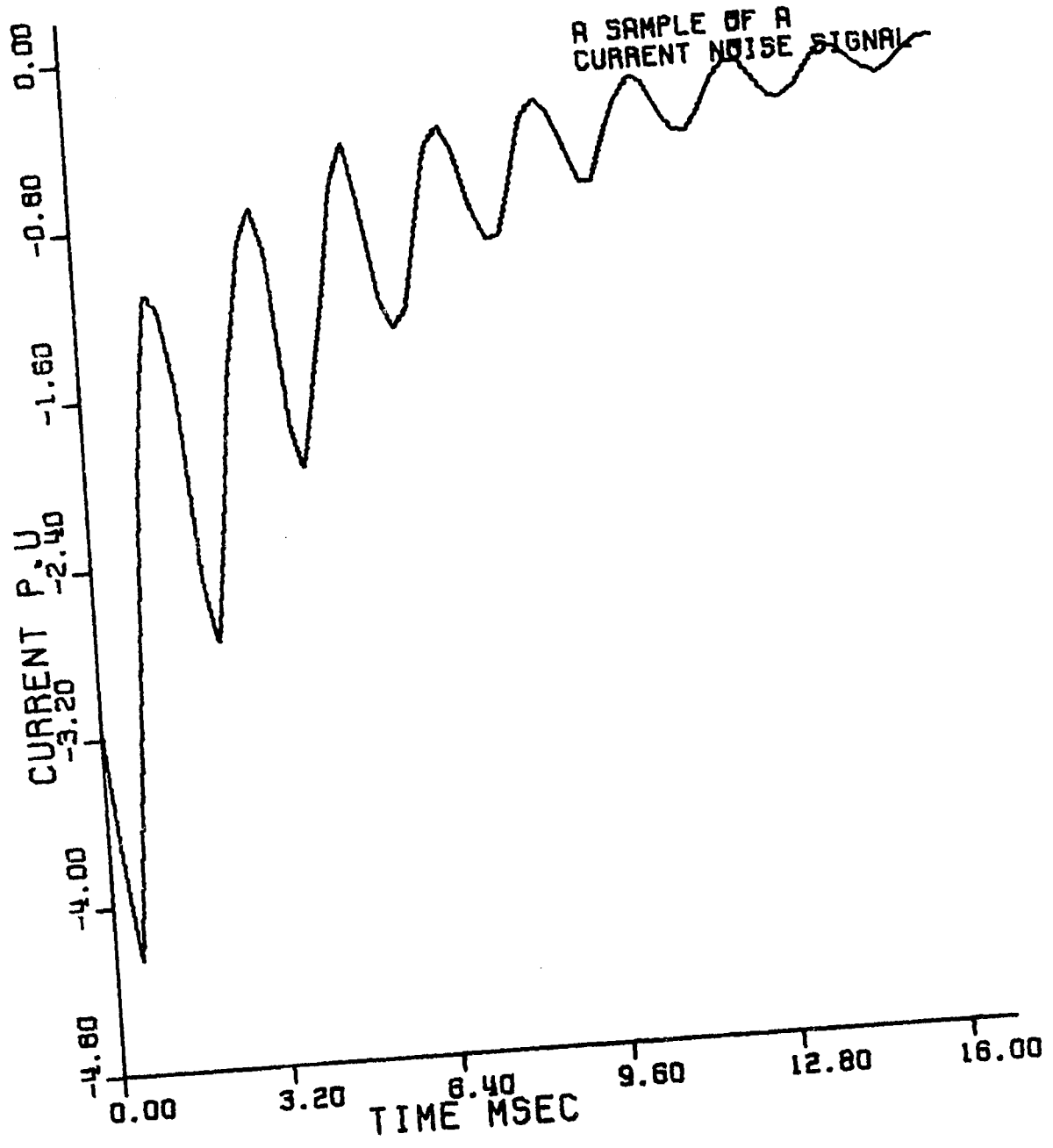
Figure 5.2. A sample of a current noise signal

Given samples of $f(t)$ at $\frac{\Delta t}{2}$, $\frac{3\Delta t}{2}$, ..., $\frac{2N+1}{2}\Delta t$, then

$$F(k\Delta\omega) = \sum_{i=0}^{N-1} f\left(\frac{2i+1}{2}\right)\Delta t \; e^{-jk\Delta\omega \frac{2i+1}{2}\Delta t} \; \Delta t \qquad (5.8)$$

$$= \left[\sum_{m=0}^{N-1} f_1(m\Delta t)e^{\frac{-j2\pi km}{N}}\right] e^{\frac{-jk\Delta\omega\Delta t}{2}} \; \Delta t \qquad (5.9)$$

The magnitude of $F(k\Delta\omega)$ is then given by

$$|F(k\Delta\omega)| = \Delta t \sum_{i=0}^{N-1} f_1(m\Delta t) \; W_N^{mk} \qquad (5.10)$$

where

Δt = the time between two consecutive samples

$W_N^{mk} = e^{-j2\pi km/N}$

The simple form of equation (5.10) allows the use of the fast Fourier transform algorithm. A Fortran computer program was written to obtain the frequency spectra of the current and voltage noise signals. Then, overall spectral functions were obtained using the weighting factors for each type of fault.

E. Modelling the Noise Signal

1. Voltage noise signal

Figure 5.3 shows the autocorrelation of the voltage noise signal in the faulted phase, unfaulted phase, and zero sequence voltage. Figures 5.4, 5.5, and 5.6 show the actual variance and the approximate exponential curve fit of the voltage noise signals in the faulted phase,

unfaulted phase, and zero sequence voltage. Figure 5.7 shows the frequency spectrum of the voltage noise signals. Examining the auto-correlation functions along with the frequency spectra suggested that the voltage noise be considered a white noise with an exponentially de-creasing variance.

Thus, the following variance structures were assumed

$$\text{Variance of voltage noise in the faulted phase} = K1_v e^{-t/T_1}$$

$$\text{Variance of voltage noise in the unfaulted phase} = K2_v e^{-t/T_1}$$

$$\text{Variance of zero sequence voltage noise} = K0_v e^{-t/T_1}$$

For the system under study, $K1_v$ was found to be 0.6, $K2_v$ was found to be equal to $K0_v$ = 0.1, and T_1 was found to be 0.0033 sec. It was also found that the above values are related to the parameters of the system under study. For example, the mean square of the change of the sending end voltage in the faulted phase was calculated to be 0.57, assuming equal probability for the fault location. Therefore, it was concluded that the initial variance of the voltage noise signal can be taken as the mean square of the change of the sending end voltage in the faulted phase and zero sequence voltage. The value of T_1 was found to be related to the parameters of the system under study. For practical applications, a reasonable value is given by equation (5.14)

$$T_1 = \frac{1}{2} \frac{L_1 \cdot \ell}{R_1 \cdot \ell + R_F} \tag{5.14}$$
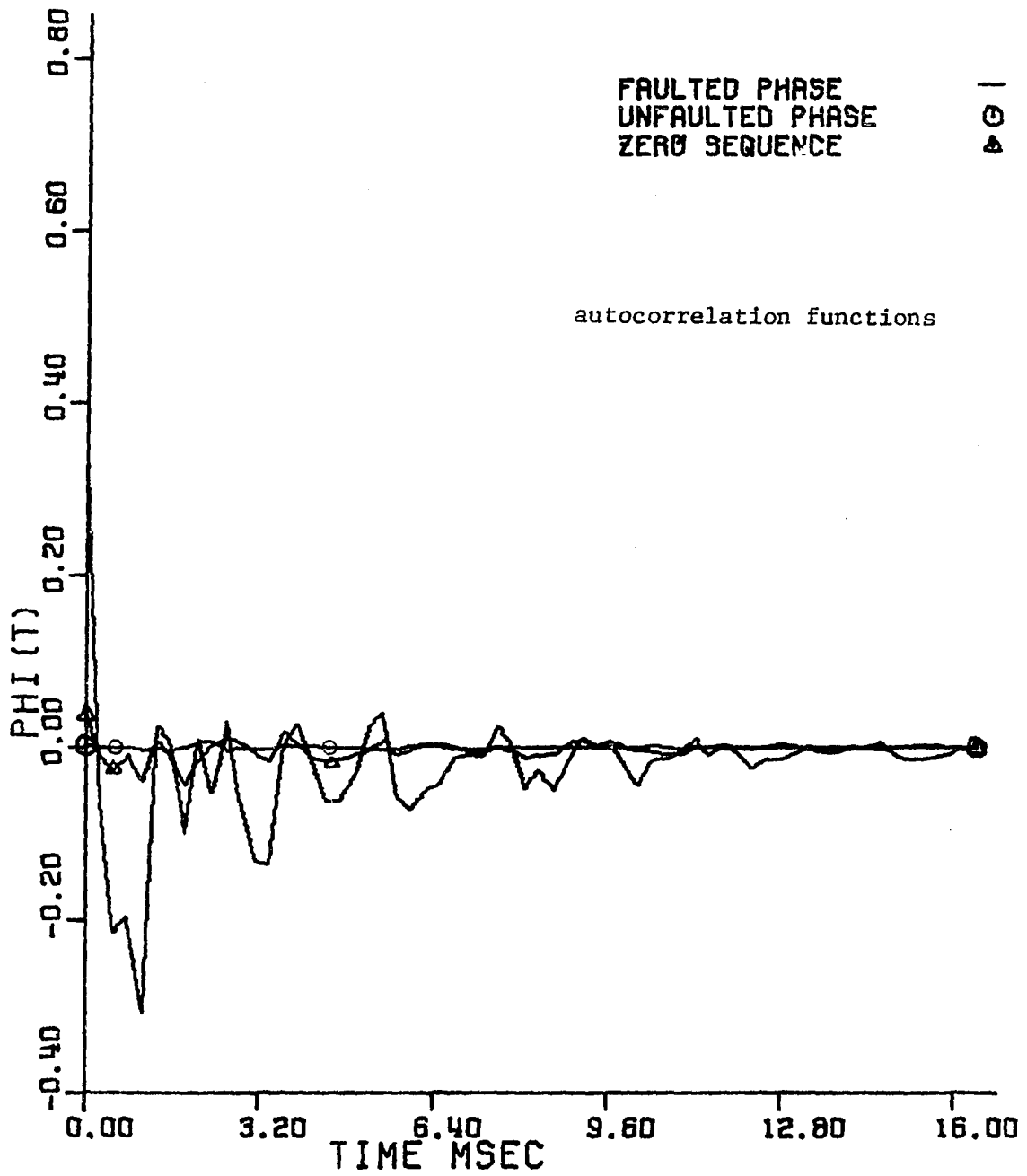
Figure 5.3. Autocorrelation functions of
voltage noise signals
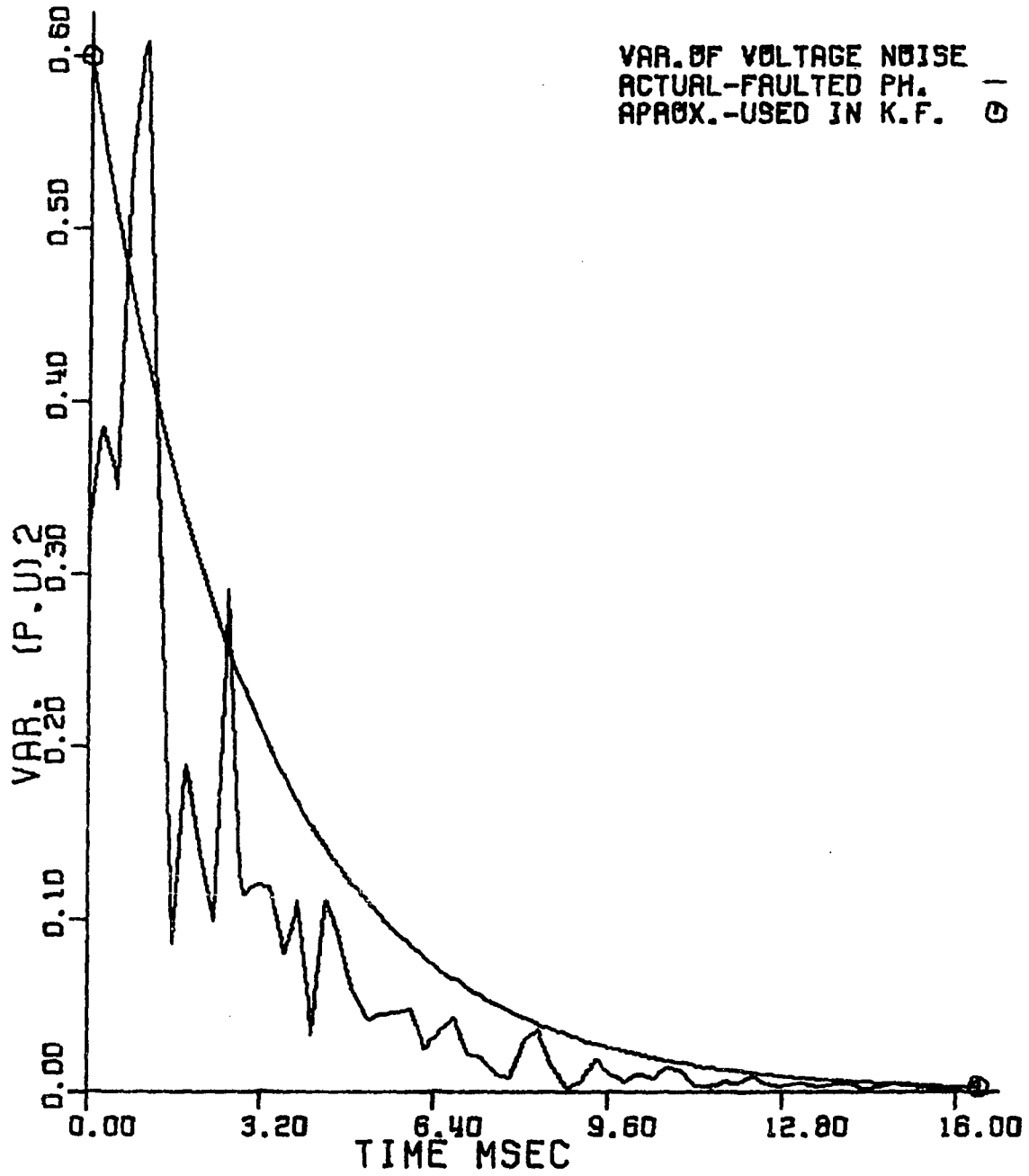
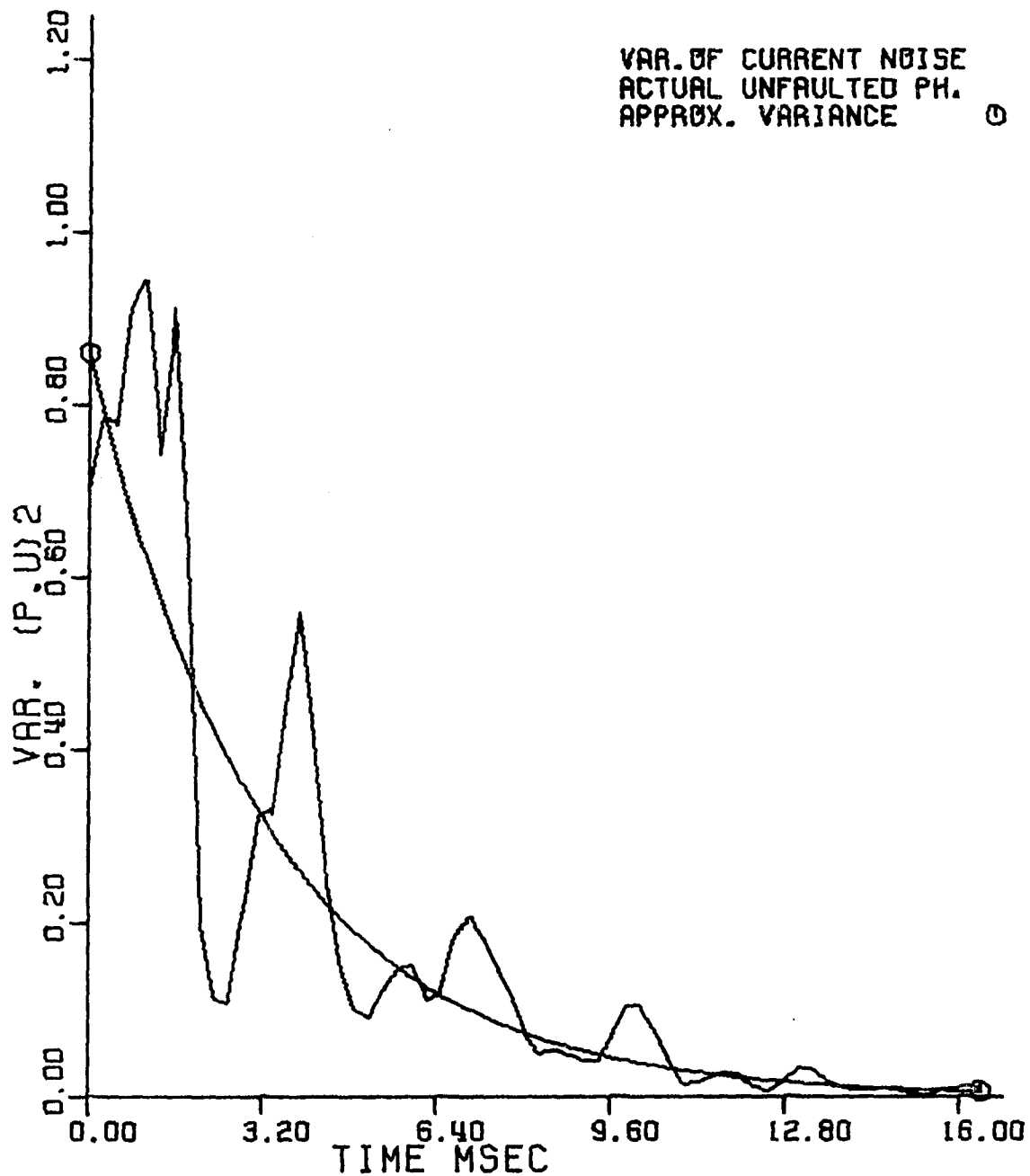Figure 5.4. Variance of voltage noise signal
in the faulted phase
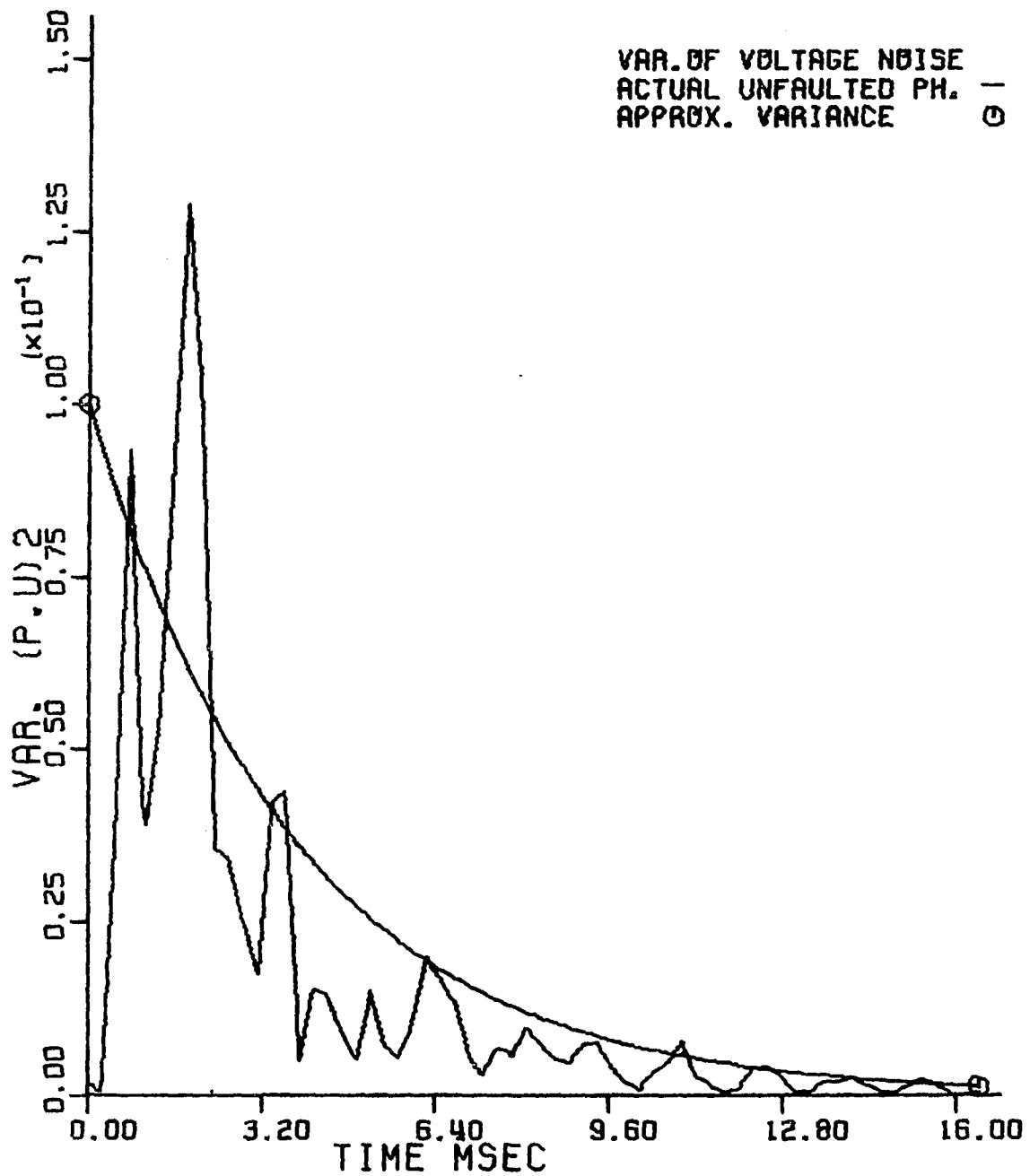
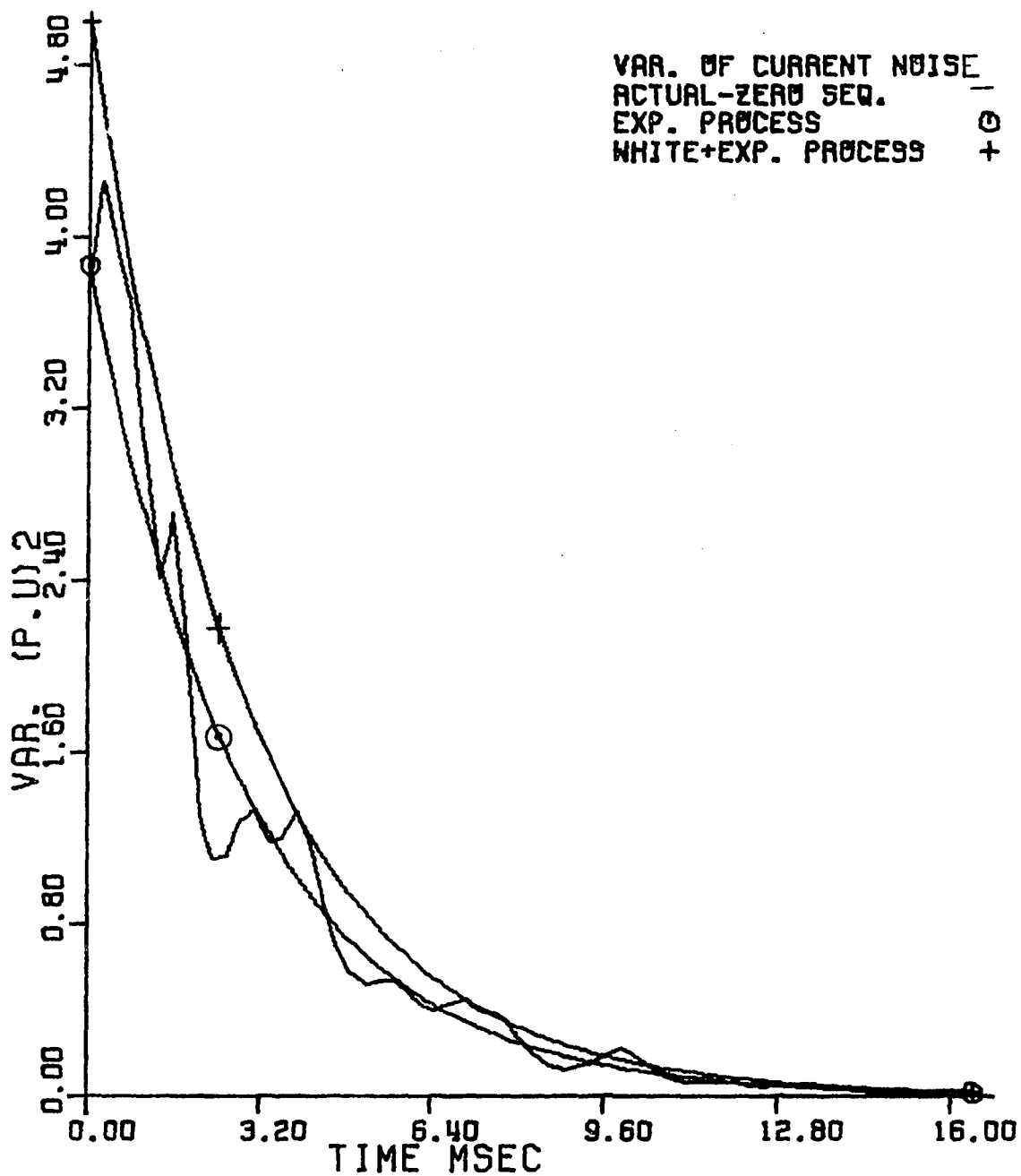Figure 5.5. Variance of voltage noise signal
in the unfaulted phase
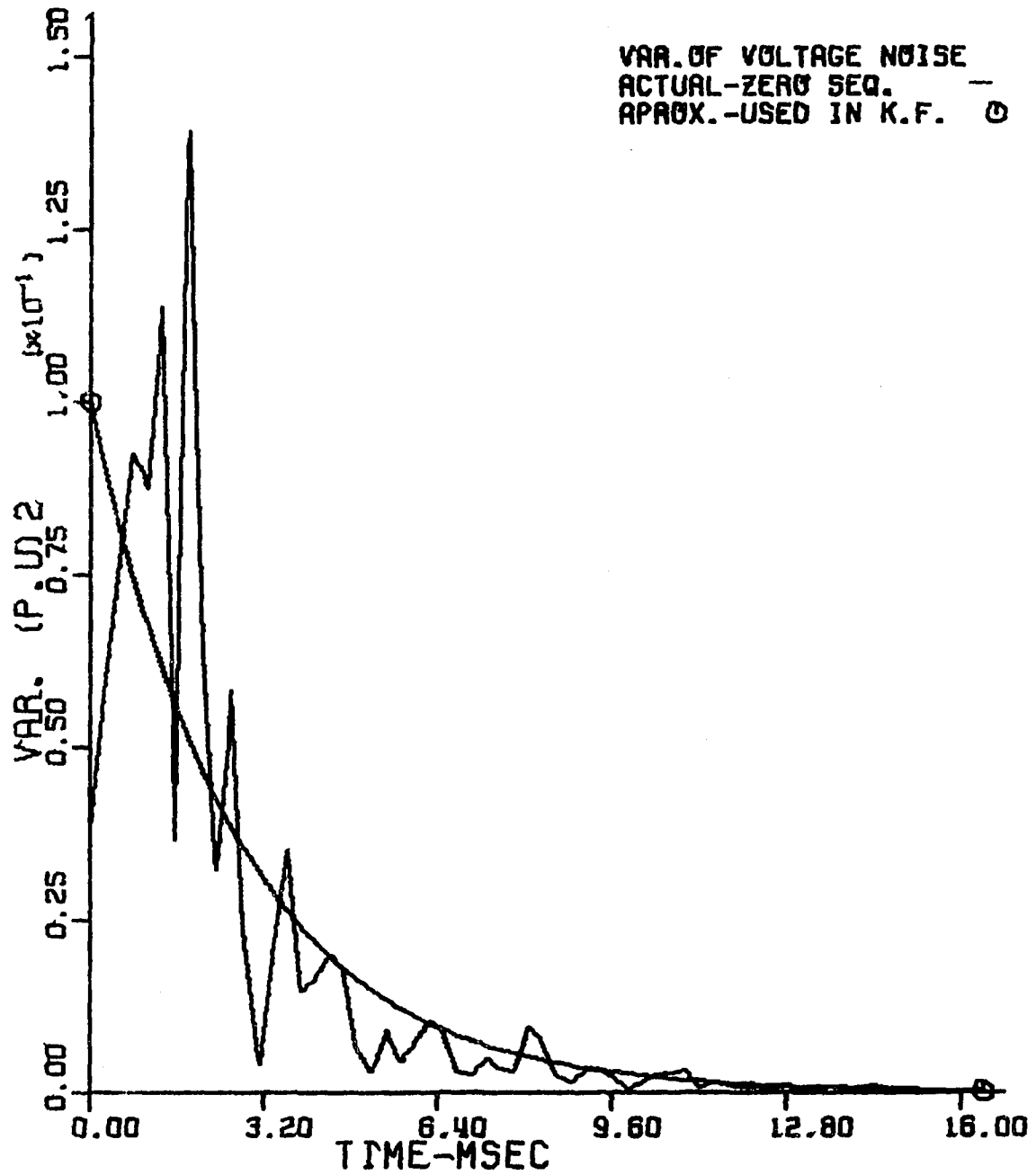
Figure 5.6. Variance of voltage noise signal
in the zero sequence voltage
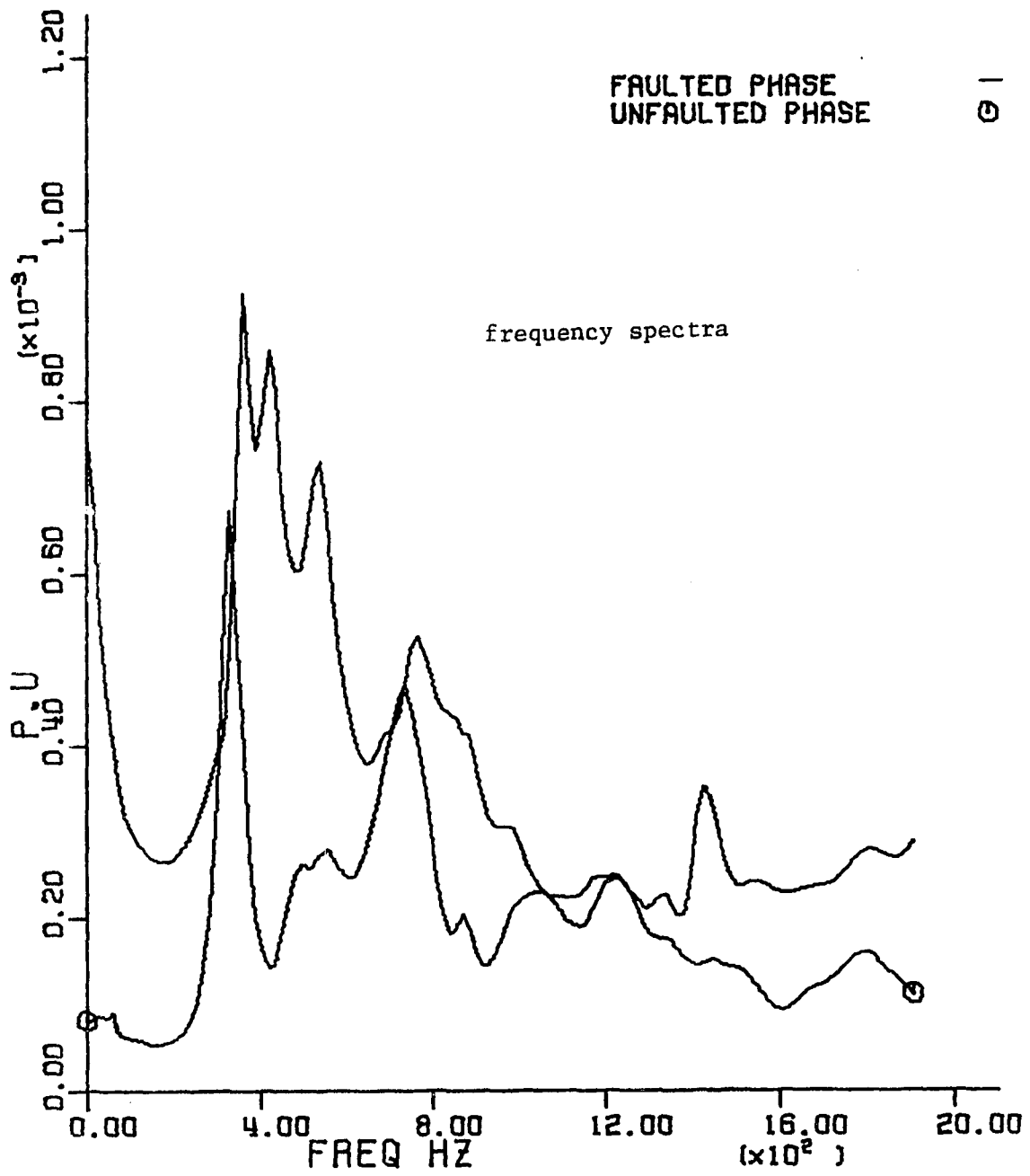
Figure 5.7. Frequency Spectra of voltage noise signals

where

L_1 is the positive sequence inductance per mile

R_1 is the positive sequence resistance per mile

R_F is the average expected fault resistance

ℓ is half the length of the line

2. Current noise signal

Figure 5.8 shows the autocorrelation functions of the current noise signals in the faulted phase, unfaulted phase, and zero sequence current. Figures 5.9, 5.10, and 5.11 show the actual variance and least-squares exponentially curve fit of the current noise signals in the faulted phase, unfaulted phase, and zero sequence current. Figure 4.12 shows the frequency spectra of the current noise signals. From the shown auto-correlation functions and the frequency spectra, an adequate representation of the current noise signal would appear to be a random exponential process plus a white noise sequence with a decreasing variance. This discrete representation of the exponential process is given by

$$x3_{k+1} = e^{-\beta \Delta t} \, x3_k + w_k \, , \quad k=0,1,2,\ldots,n \qquad (5.15)$$

Two parameters of the exponential part of the process, the initial variance, and the constant β, were obtained empirically from the expoentially decaying variance of Figures 5.9, 5.10, and 5.11 and the auto-correlation function of Figure 5.8. The value of the initial variance was found to be very nearly equal to the mean square of the sending end current assuming uniform probability for the fault location. The

parameter β was found to be the reciprocal of T_1 of equation (5.14).
The variance of w_k was found to be quite small. In the subsequent
analysis it was assumed to have a variance of .01.

The white noise part of the current noise was assumed to have an
exponentially decreasing variance with initial value equal to the
maximum difference between the actual variance and the least-squares
exponential variance of Figures 5.9, 5.10, and 5.11. The empirical
formulas for the variance of the white noise are given as

$$\text{Variance of white noise in the phase current} = KI \, e^{-k\Delta t/T_1}$$

$$\text{Variance of zero sequence white noise} = KO \, e^{-K\Delta t/T_1}$$

where KI and KO were found to be one-fourth of the mean square of the
sending end faulted-phase current and zero sequence current respectively,
assuming uniform probability for the fault location.
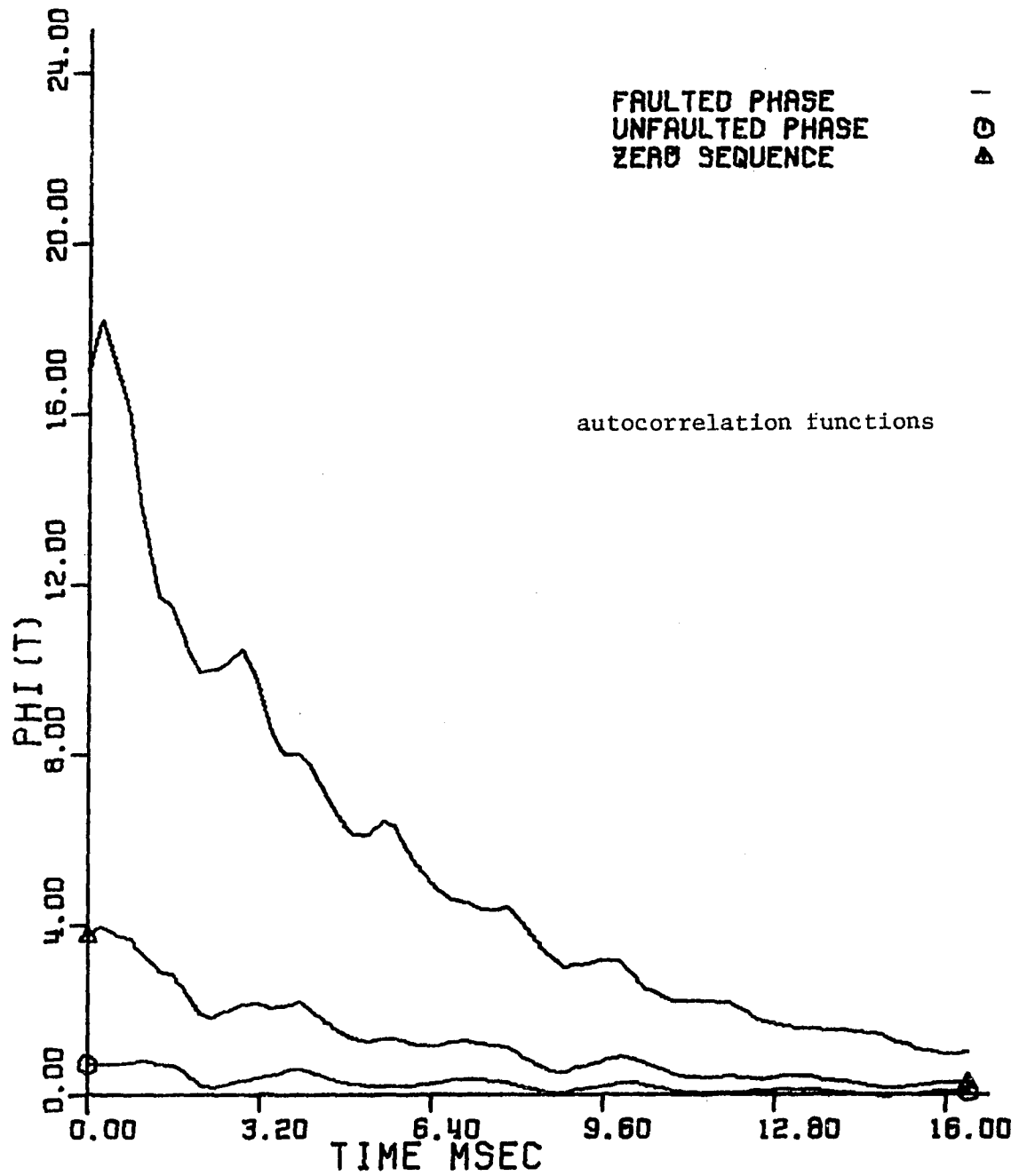
Figure 5.8. Autocorrelation functions of
current noise signals
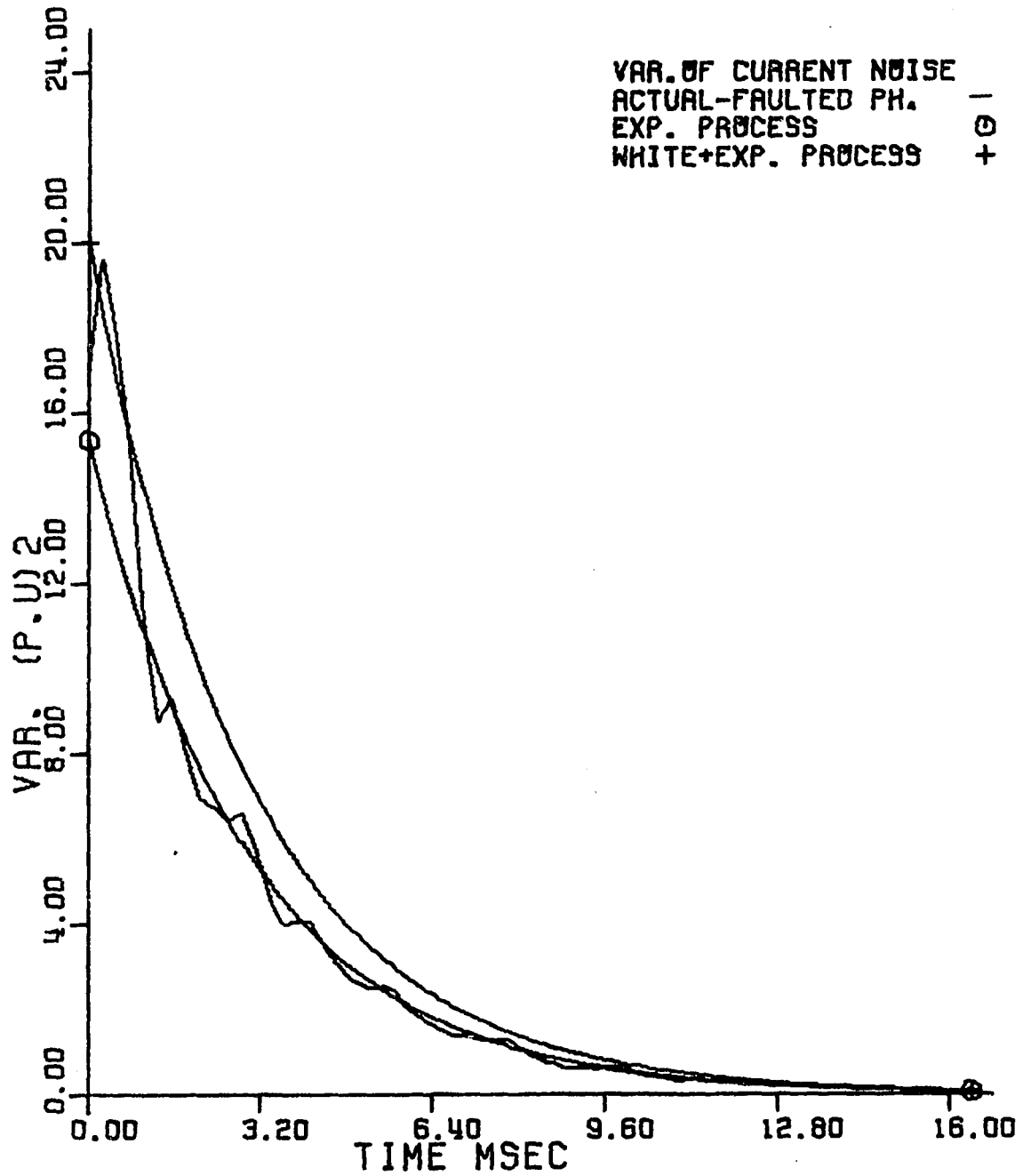
Figure 5.9. Variance of current noise signals
in the faulted phase

Figure 5.10. Variance of current noise signal
in the unfaulted phase

Figure 5.11. Variance of current noise signal
in the zero sequence
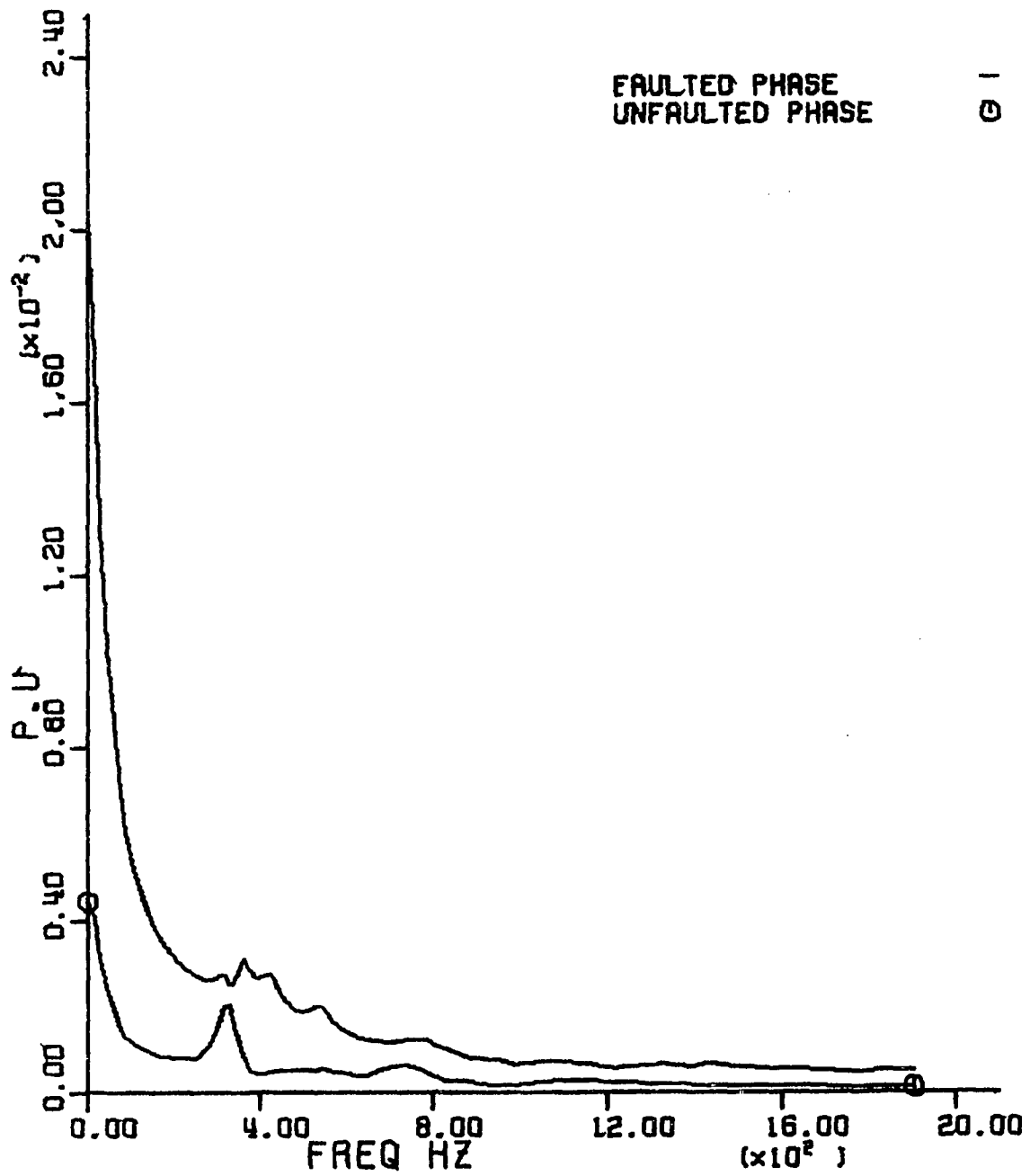
Figure 5.12. Frequency spectra of current noise signals

VI. KALMAN FILTER MODELS

A. State Model of the Phasor Components

The noise-free current or voltage signal can be expressed by the real or imaginary part of

$$S(t) = A \exp(j\omega_o t + \phi) \tag{6.1}$$

where A is the amplitude and ϕ is the phase angle at $t = 0$. Half of the faults on the transmission line are due to lightning (64) which may occur at any location and any instant depending on the weather conditions. Even flashover faults that mostly occur around the peak voltage at the fault location may be far or close to the relay location. Therefore, the probability distribution of the current or voltage phase at the relay location was assumed to be uniform. Considering the uniform distribution of the fault location, a Rayleigh distribution is a reasonable assumption for the signal amplitude.

It has been shown (67,68) that a phasor with a Rayleigh-distributed amplitude and a uniformly-distributed phase can be decomposed into two components x1 and x2, where both x1 and x2 are Gaussian with zero mean and the same variance. Consequently, the noise-free fault current or voltage is expressible as

$$S(t) = x1 \cos \omega_o t - x2 \sin \omega_o t \tag{5.2}$$

where x1 and x2 are statistically independent, zero-mean, Gaussian random variables. Then S(t) is a random process with random amplitude and phase, which is the model we wish for the signal components of the

fault currents or voltages. The problem then is to estimate x1 and x2

in the presence of the noise signals. The variance of x1 or x2 is

designated σ_v^2 for the voltage signals and σ_i^2 for the current signals.

B. Two-State Kalman Filter for Voltage Model

From the previous section and the Kalman filter equations of

section 3-A, the two-state Kalman filter as an optimal estimator can be

defined as:

1. State equations:

$$
\begin{bmatrix} x1_{k+1} \\ x2_{k+1} \end{bmatrix} = \begin{bmatrix} 1 & 0 \\ 0 & 1 \end{bmatrix} \begin{bmatrix} x1_k \\ x2_k \end{bmatrix}
\tag{6.3}
$$

2. Measurement equation:

$$
z_k = [\cos \omega_o k\Delta t - \sin \omega_o k\Delta t] \begin{bmatrix} x1_k \\ x2_k \end{bmatrix} + v_k
\tag{6.4}
$$

3. The initial covariance matrix:

$$
P_o^- = \begin{bmatrix} \sigma_v^2 & \\ 0 & \sigma_v^2 \end{bmatrix}
\tag{6.5}
$$

The initial process vector $\hat{x}_o^-$ can be either taken as the mean of

process (zero) or the prefault values. The latter was considered as it

gave more accurate results, especially for the unfaulted phases. The

measurement noise v_k was assumed to be a white sequence with a variance

given by equation (5.11). The initial covariance matrix P_o^- is diagonal,

and the diagonal entries are equal to the mean square of the change of the sending end voltage of the faulted phase, assuming equal probability for the fault location.

The initial process vector $\hat{x}_o^-$ is computed using a two sample sinusoidal curve fit of the prefault data which is assumed to be purely sinusoidal. Using equation (6.2), considering $t = 0$ to be the instant of fault occurrence and processing the measurements at samples $-j$ and $-m$, then

$$
\begin{bmatrix} z_{-j} \\ z_{-m} \end{bmatrix} = \begin{bmatrix} \cos (\omega_o j \Delta t) & \sin (\omega_o j \Delta t) \\ \cos (\omega_o m \Delta t) & \sin (\omega_o m \Delta t) \end{bmatrix} \begin{bmatrix} \hat{x1}_o \\ \hat{x2}_o \end{bmatrix}
\tag{6.6}
$$

Solving equations (6.6) yields

$$
\begin{bmatrix} \hat{x1}_o \\ \hat{x2}_o \end{bmatrix} = \frac{1}{\sin (\omega_o (m-j) \Delta t)} \begin{bmatrix} \sin (\omega_o m \Delta t) & -\sin (\omega_o j \Delta t) \\ -\cos (\omega_o m \Delta t) & \cos (\omega_o j \Delta t) \end{bmatrix} \begin{bmatrix} z_{-j} \\ z_{-m} \end{bmatrix}
\tag{6.7}
$$

The values of j and m can be arbitrarily chosen, but to reduce the computation effort, j and m are chosen so that

$$
\omega_o m \Delta t = 2 \omega_o j \Delta t = \pi/2 \text{ radians}
$$

Therefore,

$$
\begin{bmatrix} \hat{x1}_o^- \\ \hat{x2}_o^- \end{bmatrix} = \begin{bmatrix} \sqrt{2} & -1 \\ 0 & 1 \end{bmatrix} \begin{bmatrix} z_{-j} \\ z_{-m} \end{bmatrix}
\tag{6.8}
$$

As shown from equation (6.8), with the above choice of j and m, the computation of the initial process vector $\hat{x}_o^-$ requires only one multiplication, and one subtraction.

C. Three-State Kalman Filter for Current Model

A three-state Kalman filter is considered for the current model. The third state is the exponential process in the current noise signal, described by equation (5.15). The model can be explained as follows:

1. State equations:

$$
\begin{bmatrix} x1_{k+1} \\ x2_{k+1} \\ x3_{k+1} \end{bmatrix} = \begin{bmatrix} 1 & 0 & 0 \\ 0 & 1 & 0 \\ 0 & 0 & e^{-\beta \Delta t} \end{bmatrix} \begin{bmatrix} x1_k \\ x2_k \\ x3_k \end{bmatrix} + \begin{bmatrix} 0 \\ 0 \\ w_k \end{bmatrix}
\tag{6.9}
$$

2. Measurement equation:

$$
z_k = [\cos \omega_o k\Delta t \quad -\sin \omega_o k\Delta t \quad 1] \begin{bmatrix} x1_k \\ x2_k \\ x3_k \end{bmatrix} + v_k
\tag{6.10}
$$

3. The initial covariance matrix:

$$
\begin{bmatrix} \sigma_i^2 & 0 & 0 \\ 0 & \sigma_i^2 & 0 \\ 0 & 0 & \sigma_i^2 \end{bmatrix}
\tag{6.11}
$$

The initial process vector $\hat{x}_o^-$ is the same as in the two-state model

for x1 and x2. So $\hat{x1}_o^-$ and $\hat{x2}_o^-$ are obtained by equation (5.8) using

current prefault data. The inital estimate of x3 is considered zero as

the process has zero mean. The measurement error v_k is assumed to be a

white noise sequence with a variance given by equations (5.16) and

(5.17). A third state noise w_k is assumed to be white with a variance

(Q_k) of .01. Again, the initial covariance matrix is diagonal, and the

diagonal entries are equal to the mean square of the fault current at

the relay location.

D. Testing the Kalman Filter Models

The two-state and the three-state Kalman filter models described in

the previous sections were tested using waveforms obtained from the

power system model described in Chapter 4. Then the estimated states of

the current and voltage were compared with the exact values of the post-

fault transient-free current and voltage states.

The actual error and predicted estimation error were computed as

follows (in per unit):

$$(\text{Actual error})_k = \frac{\left| \left| \hat{x}_1 + j\,\hat{x}_2 \right|_k - \text{exact value} \right|}{\text{exact value}} \quad \text{p.u.} \qquad (6.12)$$

where

$\hat{x}_1$ and $\hat{x}_2$ are the estimated states at step k for the current or

voltage phasor. The error predicted by the Kalman filter was

computed as

$$(\text{Predicted estimation error})_k = \frac{(P_{11} + P_{22})_k^{\frac{1}{2}}}{\text{exact value}} \quad \text{p.u.} \qquad (6.13)$$

where P_{11} and P_{22} are the predicted estimation variances of the estimated states at step k for the current or voltage phasors.

The models were tested for all kinds of faults: single line to ground, line to line, double line to ground, and three-phase faults at different locations. Some of these results will be shown here. More results will be shown in the next two chapters.

Figure 6.1 shows the estimation process of the two states of the voltage waveform of the faulted phase for a fault of 90 miles. Along with estimates are shown the post-fault exact states. Figure 6.2 shows the actual error and the predicted estimation error in the magnitude of the same voltage. Figures 6.3 and 6.4 show similar results for the unfaulted phase voltage.

It can be seen from the shown results that the actual error in the voltage magnitude is less than 2 percent for the faulted phase and less than 5 percent for the unfaulted phase after half a cycle. (A half cycle at 60 Hz is approximately 8 ms.) Figures 6.5 and 6.6 show the estimation process of the current states in the faulted phase, the actual errors, and predicted estimation error. Figures 6.7 and 6.8 show similar quantities for the current in the unfaulted phase.

Also, it can be seen that the actual error in the magnitude of the current in the faulted phase is less than 1 percent after half a cycle. Moreover the predicted estimation error was always higher than the actual error, which can be used to indicate the degree of confidence of the estimated values.
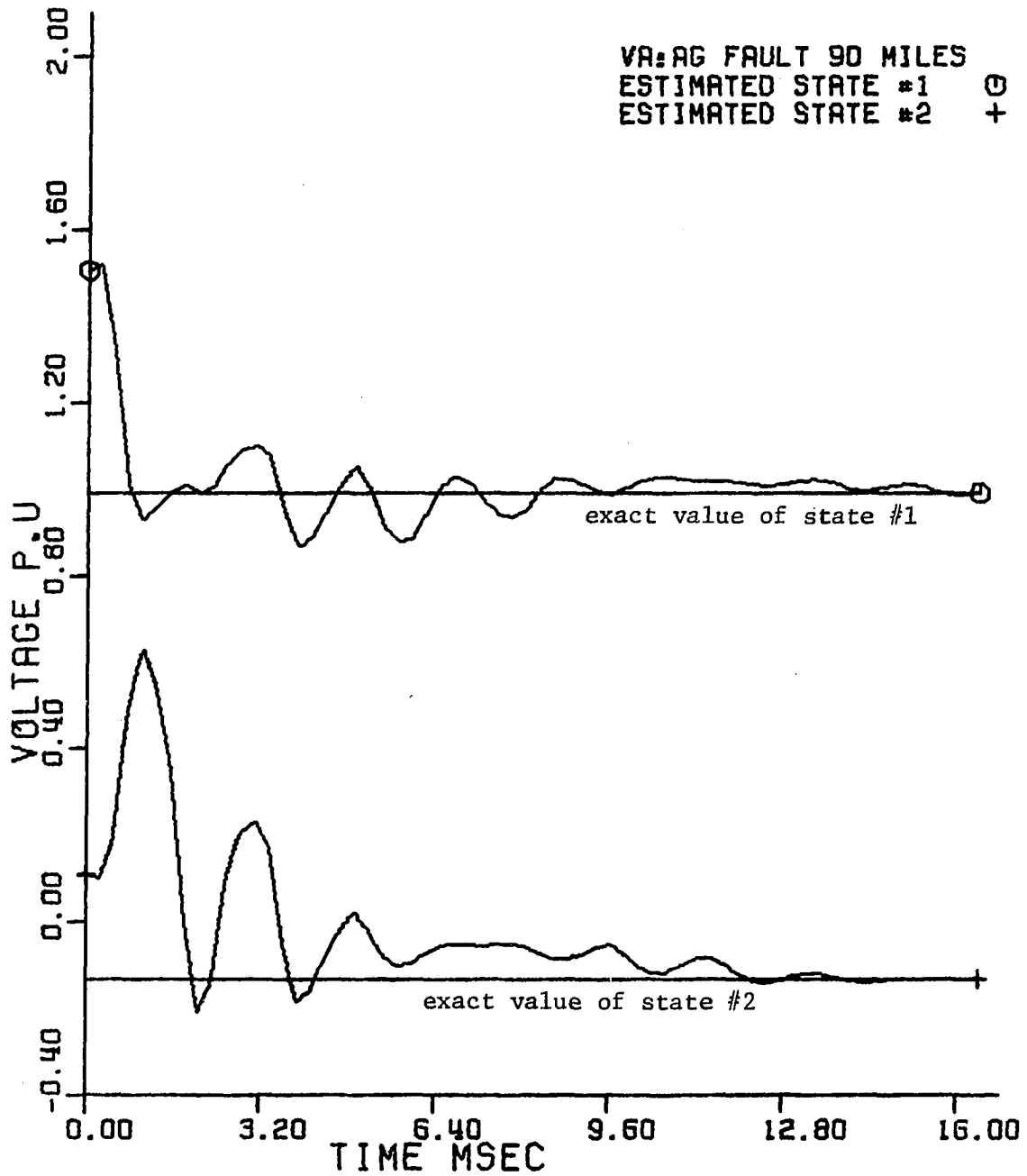
Figure 6.1. Estimated and exact states of the voltage
of the faulted phase
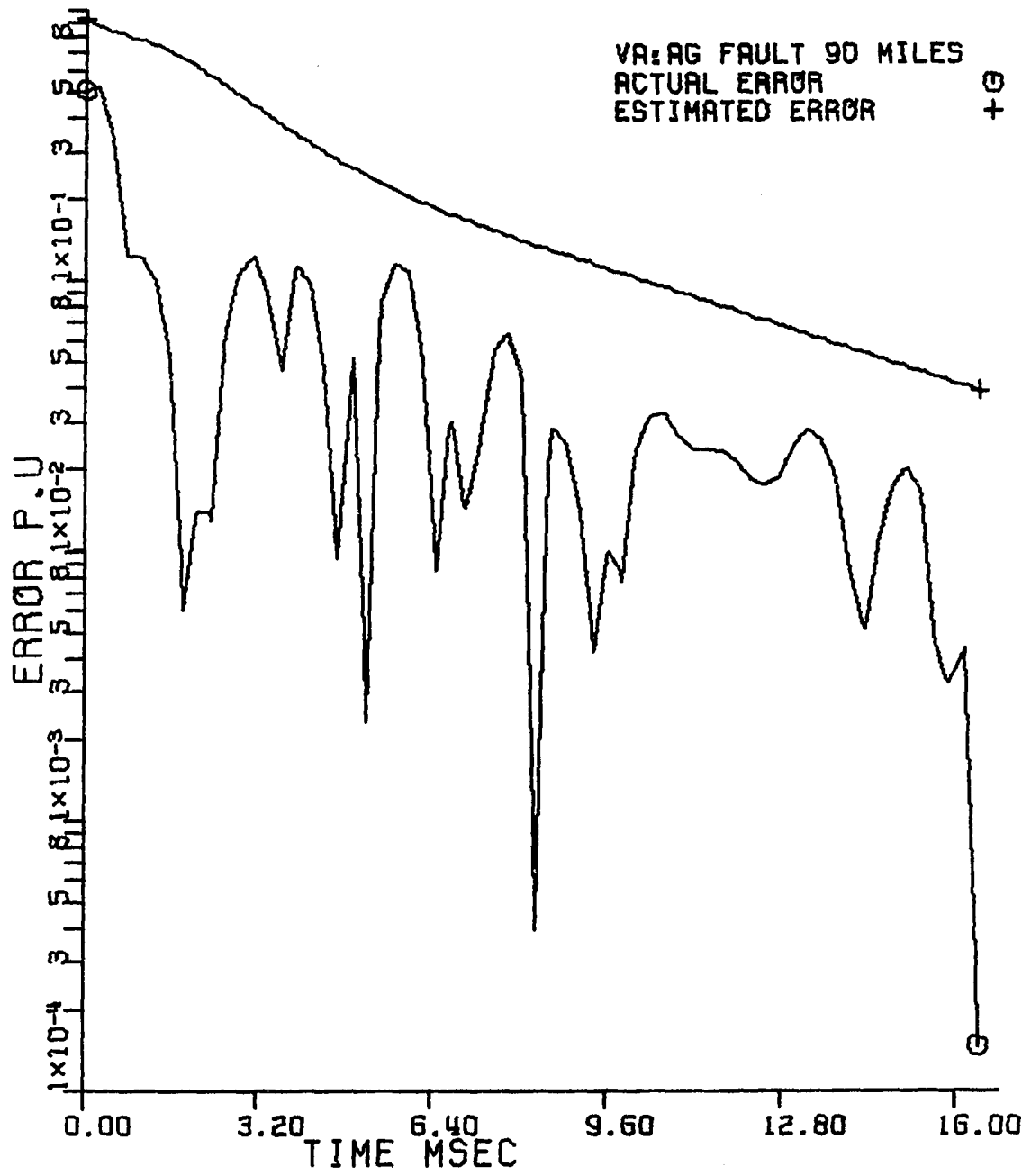
Figure 6.2. Actual and predicted estimation error in the
voltage magnitude of the faulted phase

VB:AG FAULT 90 MILES
ESTIMATED STATE #1   ⊙
ESTIMATED STATE #2   +

exact value of state #1

exact value of state #2

VOLTAGE P.U

TIME MSEC
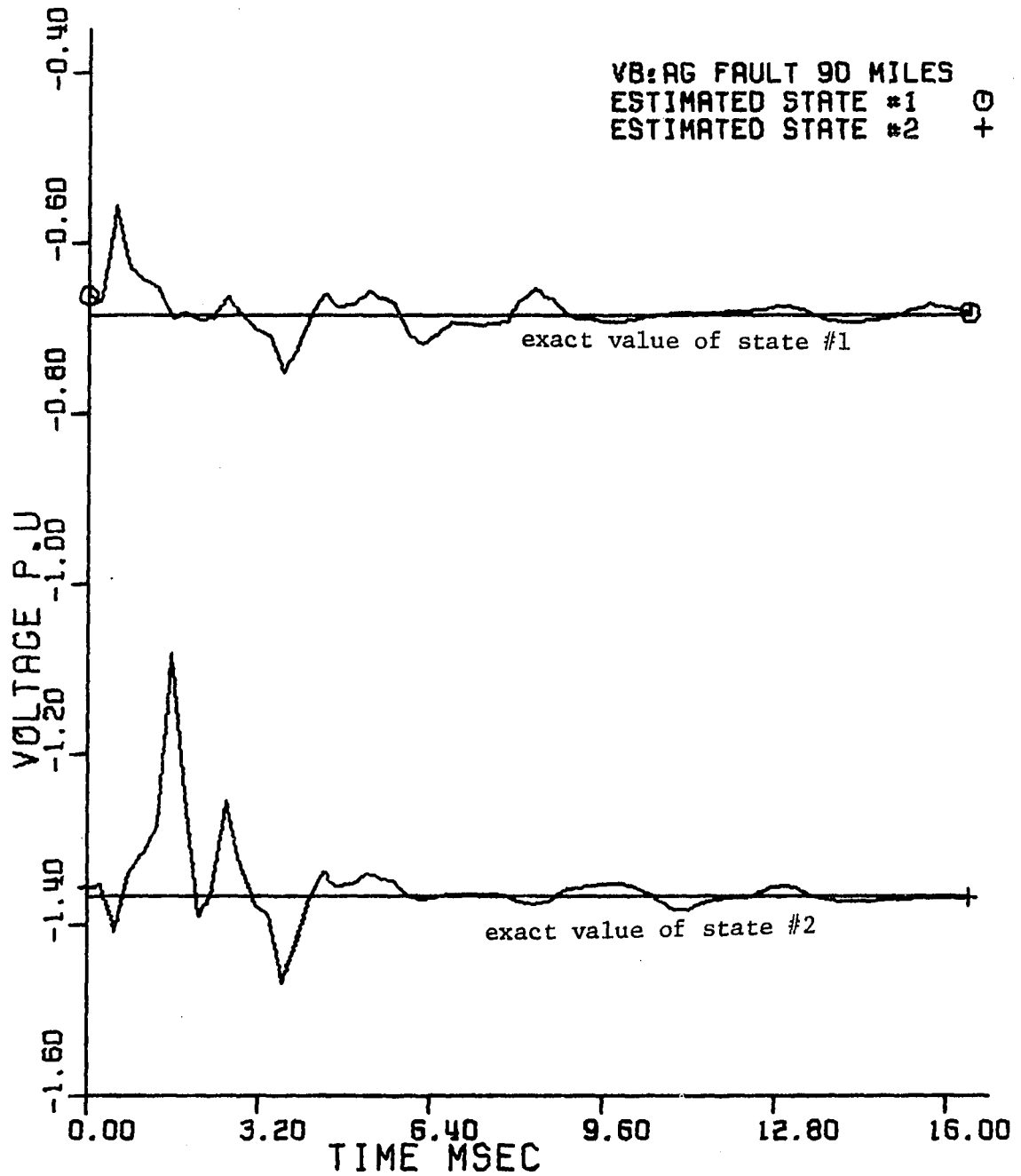
Figure 6.3. Estimated and exact states of the
voltage of the unfaulted phase
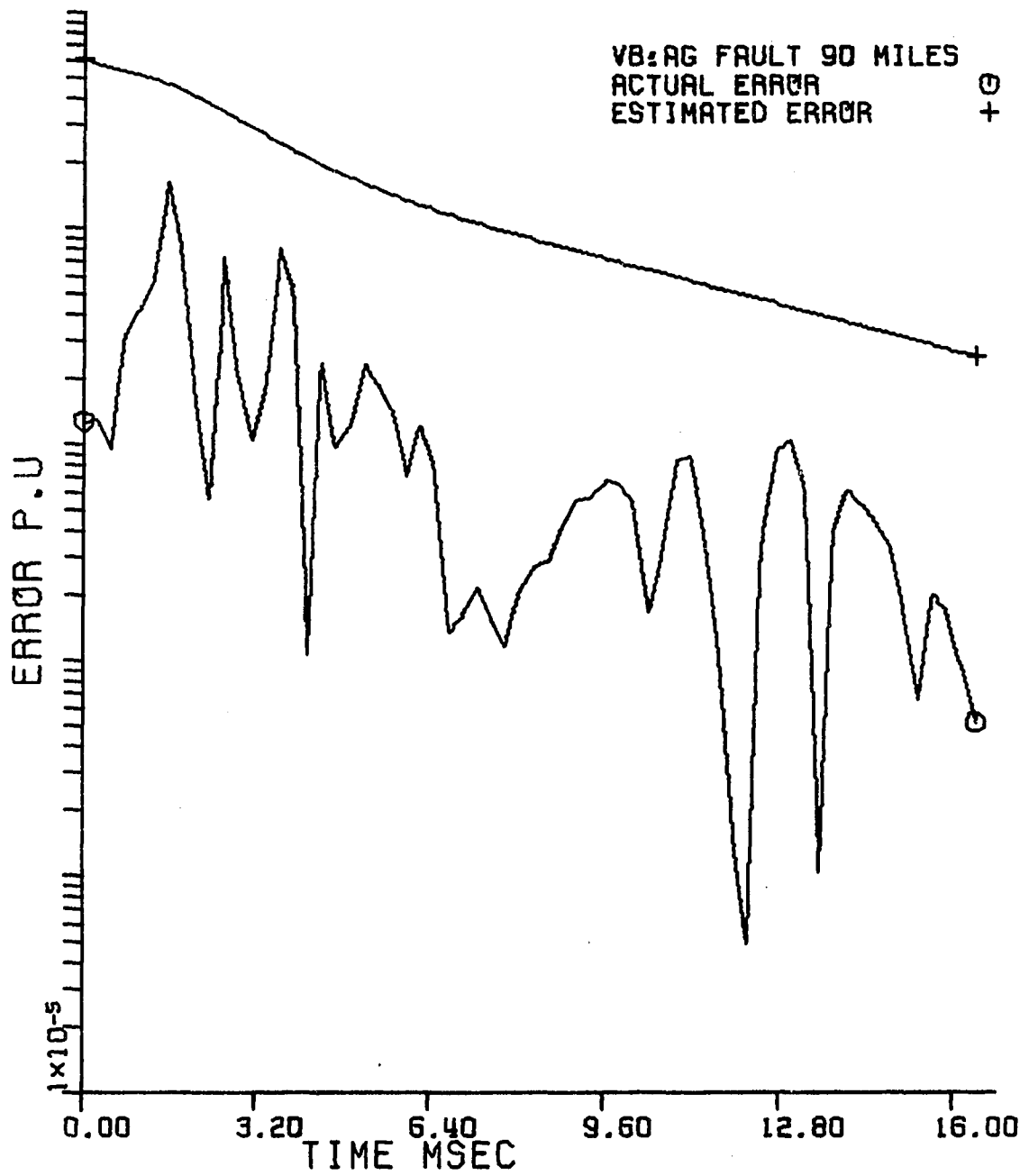
Figure 6.4. Actual and preducted estimation error in the voltage magnitude of the unfaulted phase
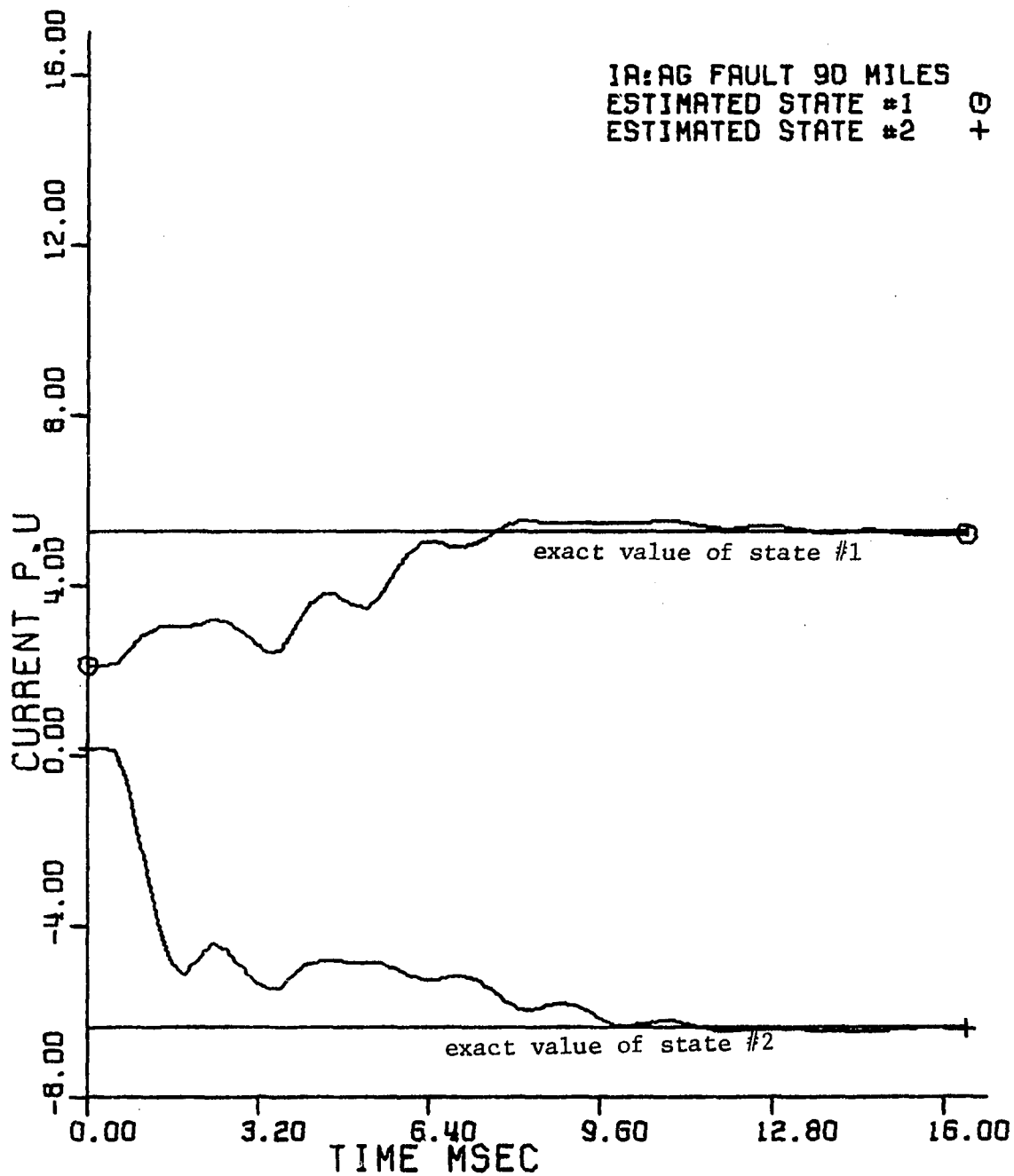
Figure 6.5. Estimated and exact states of the
current in the faulted phase
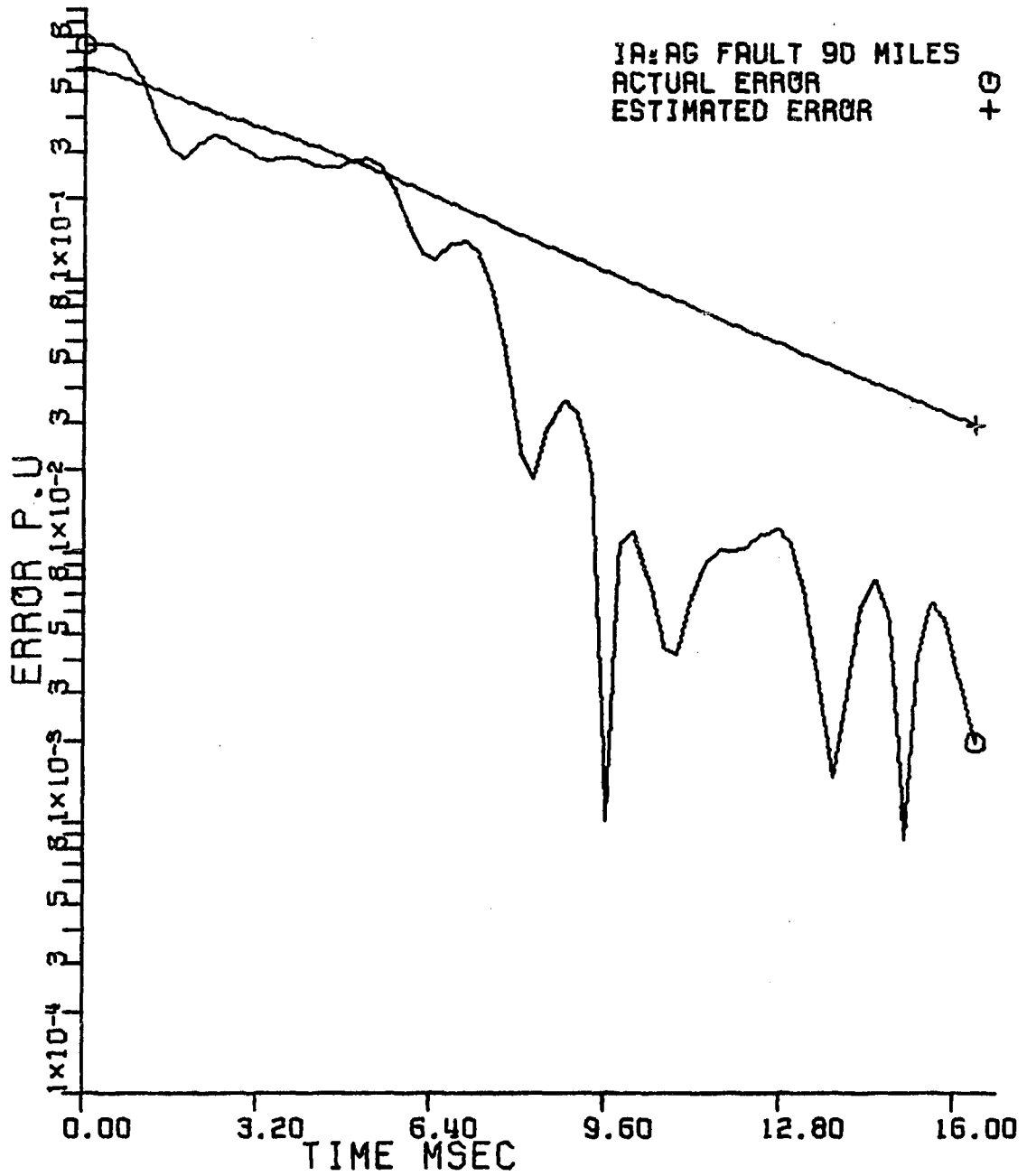
Figure 6.6. Actual and predicted estimation error in the current magnitude in the faulted phase
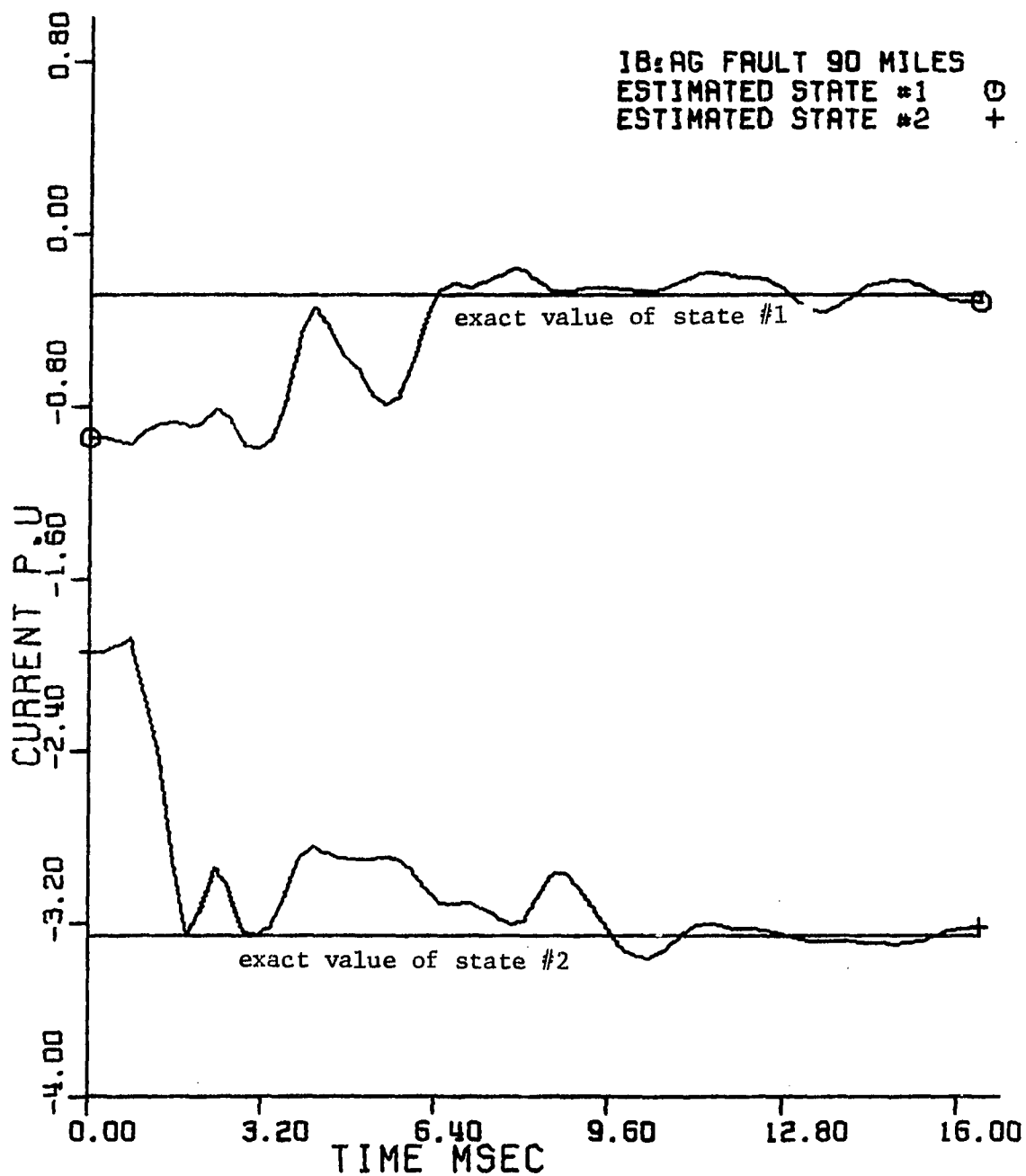
Figure 6.7. Estimated and exact states of the
current in the unfaulted phase
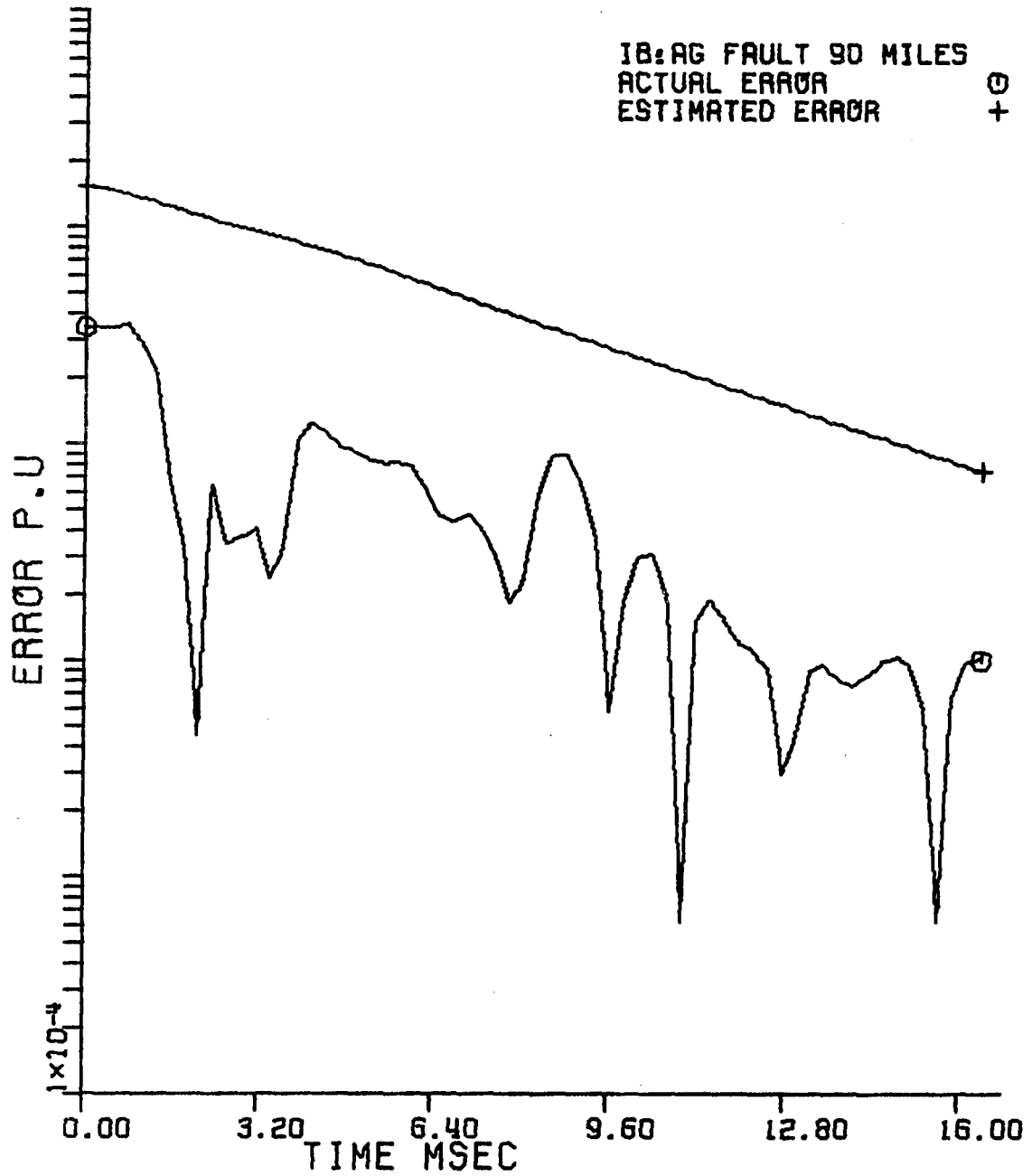
Figure 6.8. Actual and predicted estimation error of the
current magnitude in the unfaulted phase

E.   Sensitivity to Changes in the Model Parameters

To study the sensitivity of the Kalman filter models to changes in the parameters, the two-state and the three-state Kalman filter models were tested for changes in the initial covariance, noise variance parameters, and the sampling rate.

Figure 6.9 shows the estimation process of the voltage magnitude for an initial value of the voltage noise variance of 0.6, 0.3, and 0.9 $(p.u.)^2$. As can be seen from the results, changing KV by ±50 percent did not change the estimated values after half a cycle. Even before half a cycle, the differences are not essential. The same conclusion applies for changes in the rate of decreasing of the noise variance as shown in Figure 6.10. Similarly, changing the diagonal entries of the initial covariance matrix from 0.57 to 0.9 and then to 0.3 $p.u.^2$ did not essentially change the estimation process as shown in Figure 6.11. Changing the sampling rate from 64 to 32 samples per cycle did not change the estimated values appreciably. However, a change was noticed at a sampling rate of 16 samples per cycle. This change increased further at a sampling rate of 8 samples per cycle as shown in Figure 6.12.

Also the three-state Kalman filter model was tested for its sensitivity to changes in parameters. As can be seen from Figure 6.13, 6.14, and 6.15, the three-state Kalman filter model is not sensitive to ±50 percent changes in the noise variance parameters, or, ±50 percent change in the initial covariance matrix. The test results showed large sensitivity to a change in Q (the third-state steady state noise variance) as can be seen from Figure 6.16. The effect of changing the sampling

rate is shown in Figure 6.17. From the shown test results, a sampling rate of 32-64 samples per cycle is recommended.

Deleting the third state in the Kalman filter for the current reduced the rate of convergence and increased the steady state error as shown in Figure 6.18. Therefore, a three-state Kalman filter model should be used for the current.

Finally, increasing the parameter β by a factor of 2 introduced error less than 2 percent after half a cycle. Decreasing the parameter β by a factor of 4 introduced error less than 2 percent after half a cycle. However, a value of $1/T_1$ for β was considered to be adequate as it gave the minimum error after half a cycle. These results are shown in Figure 6.19.
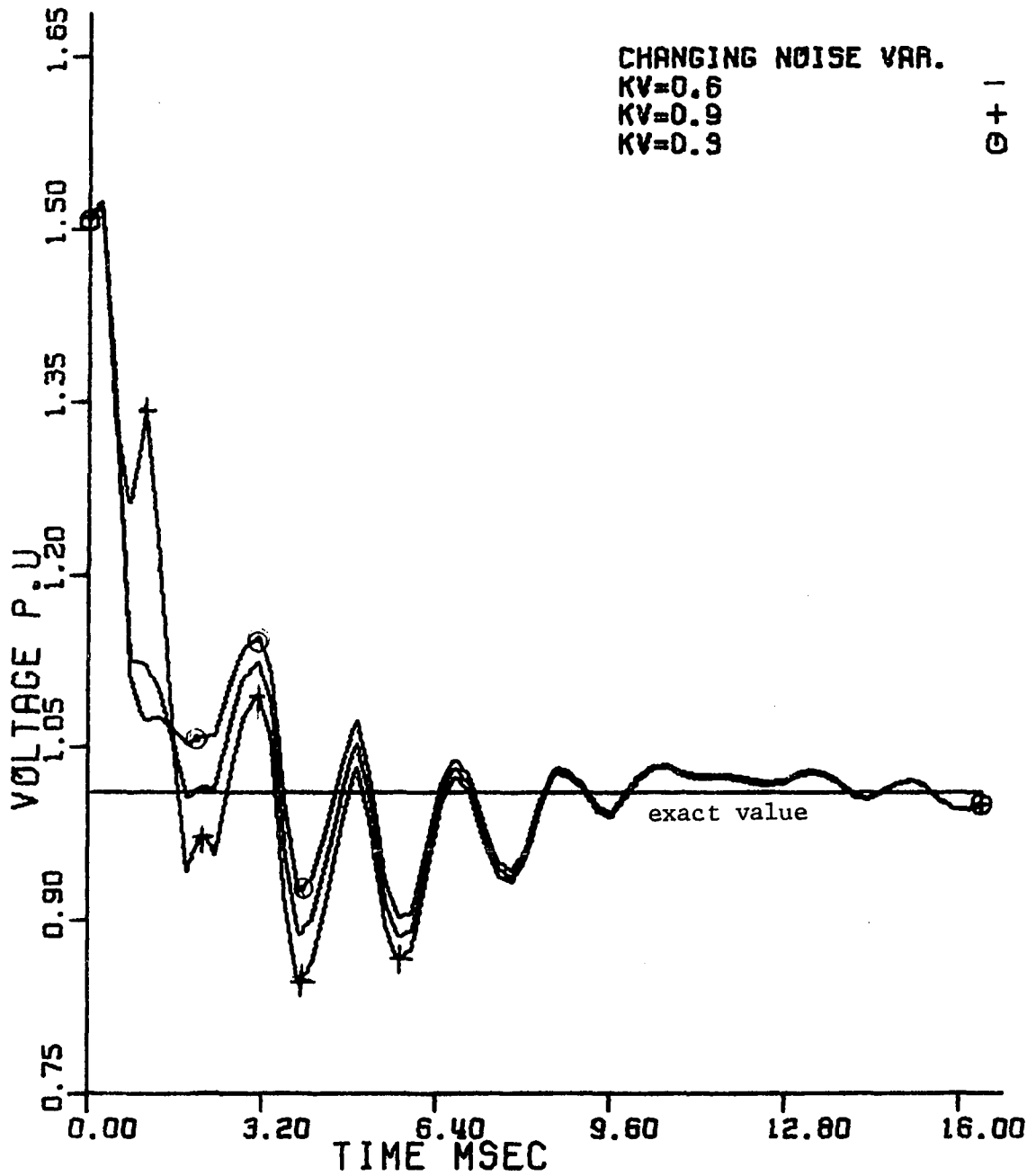
Figure 6.9. Effect of changing the initial variance of the voltage
noise in estimating the magnitude of the voltage
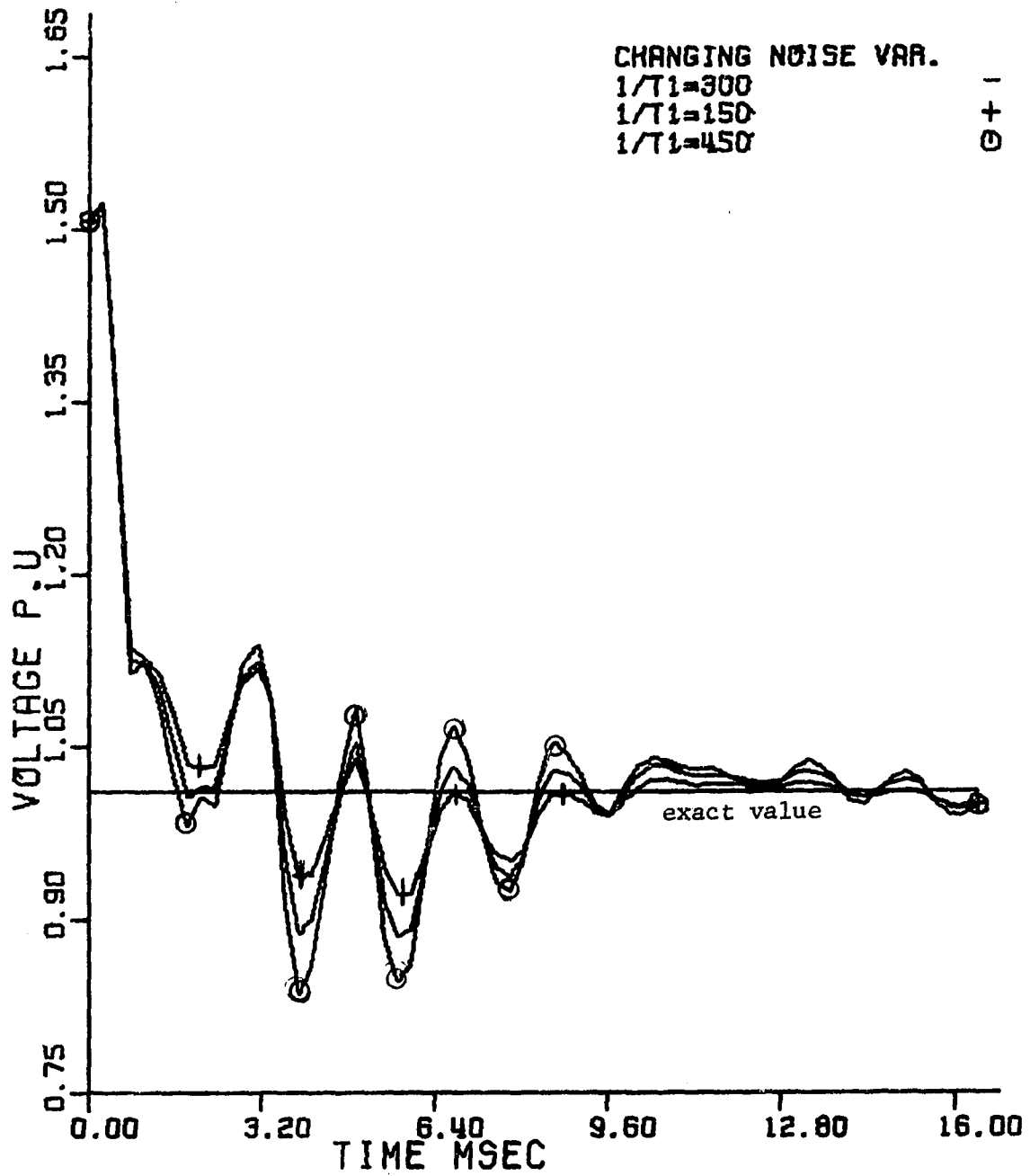
Figure 6.10. Effect of changing the rate of decrease of the voltage
noise variance in estimating the magnitude of the voltage
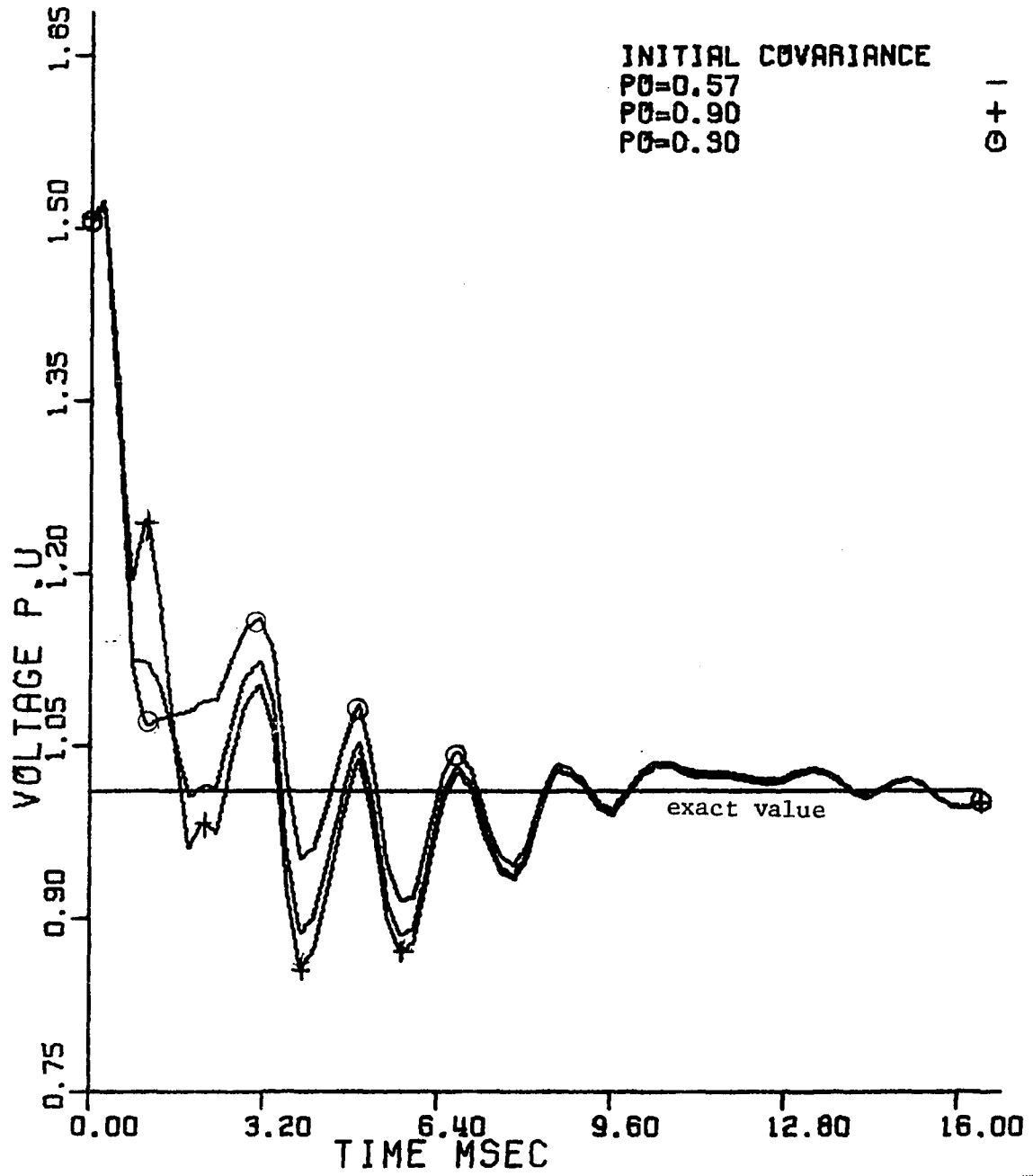
Figure 6.11. Effect of changing the initial covariance matrix
in estimating the magnitude of the voltage
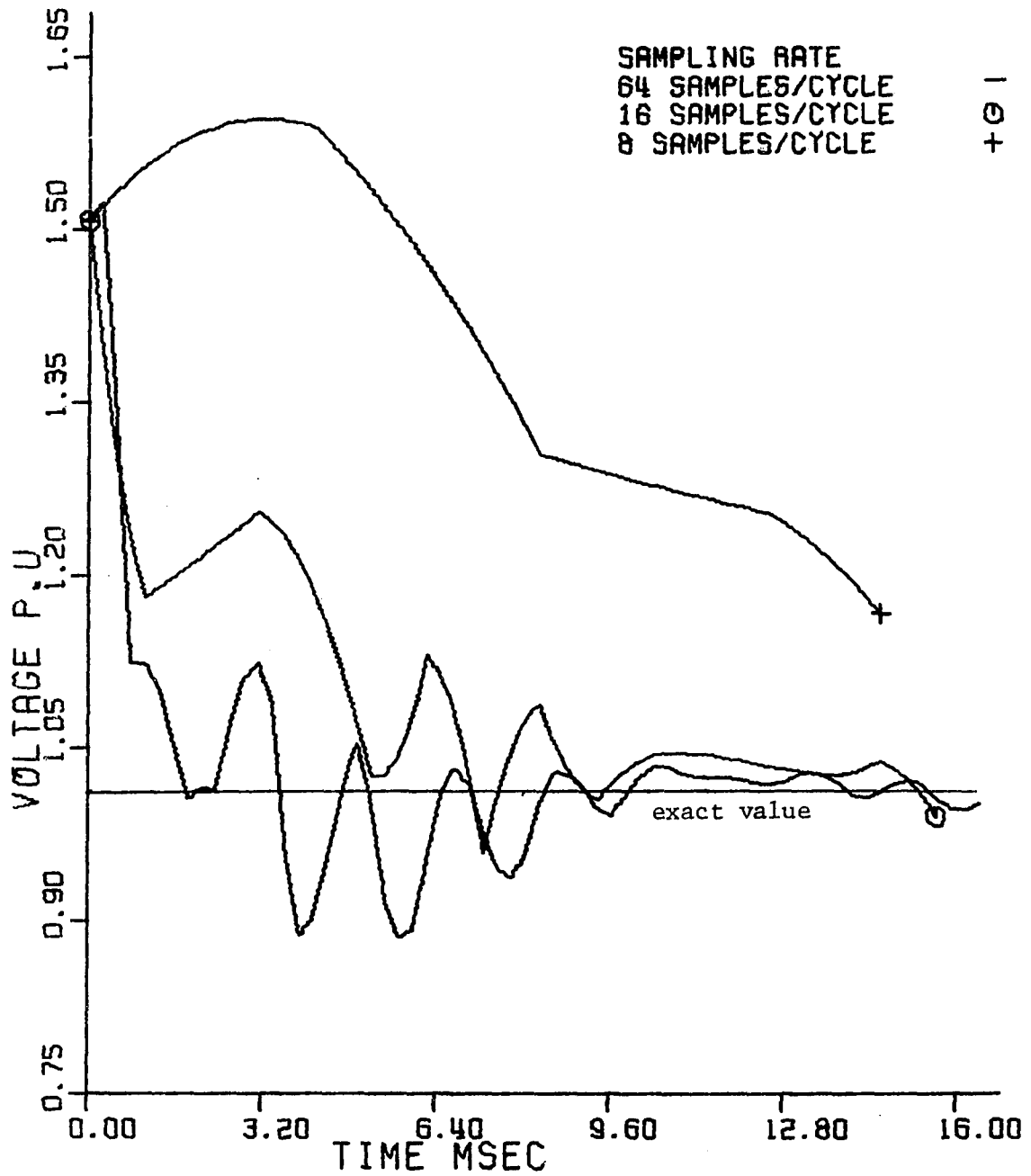
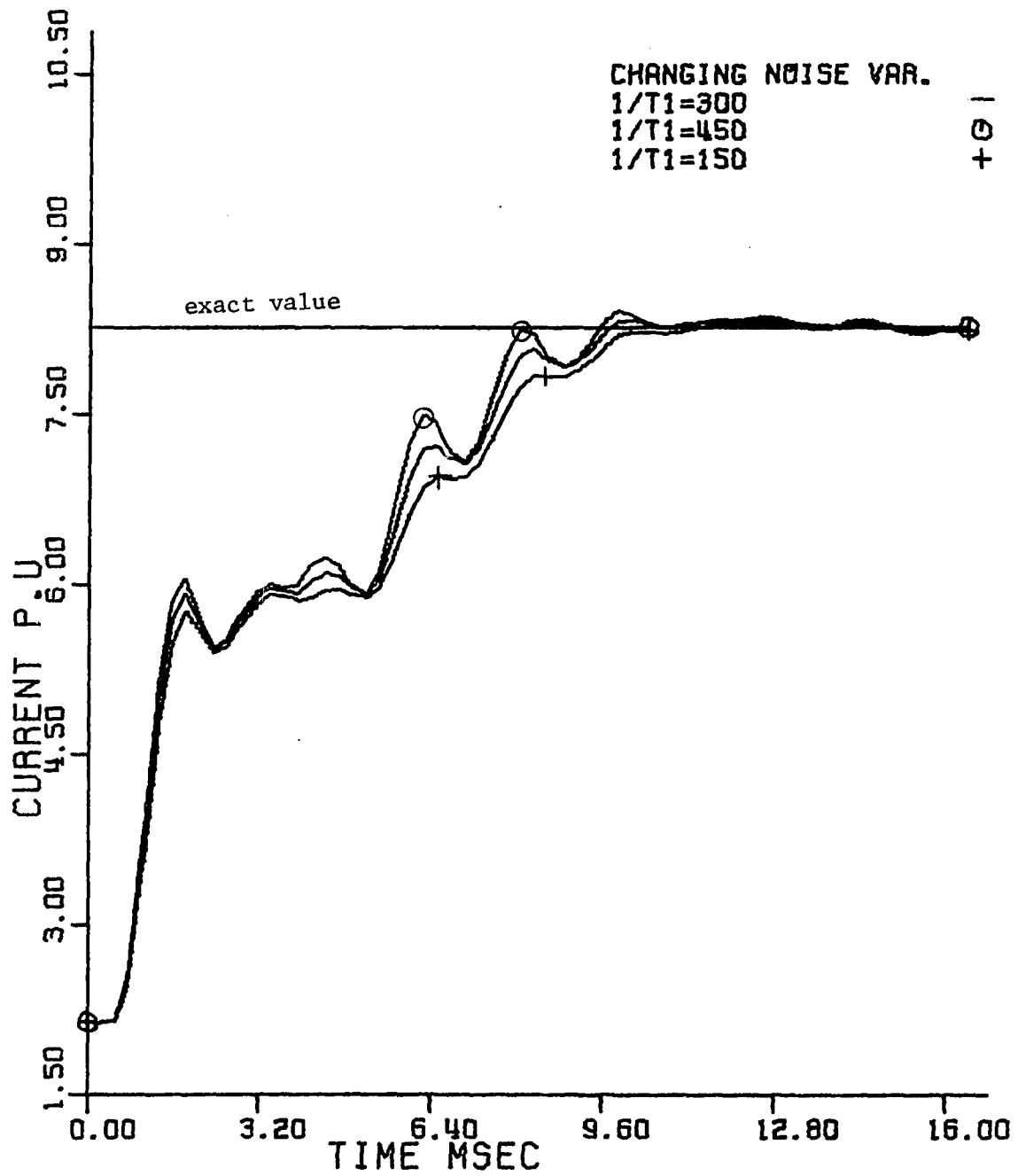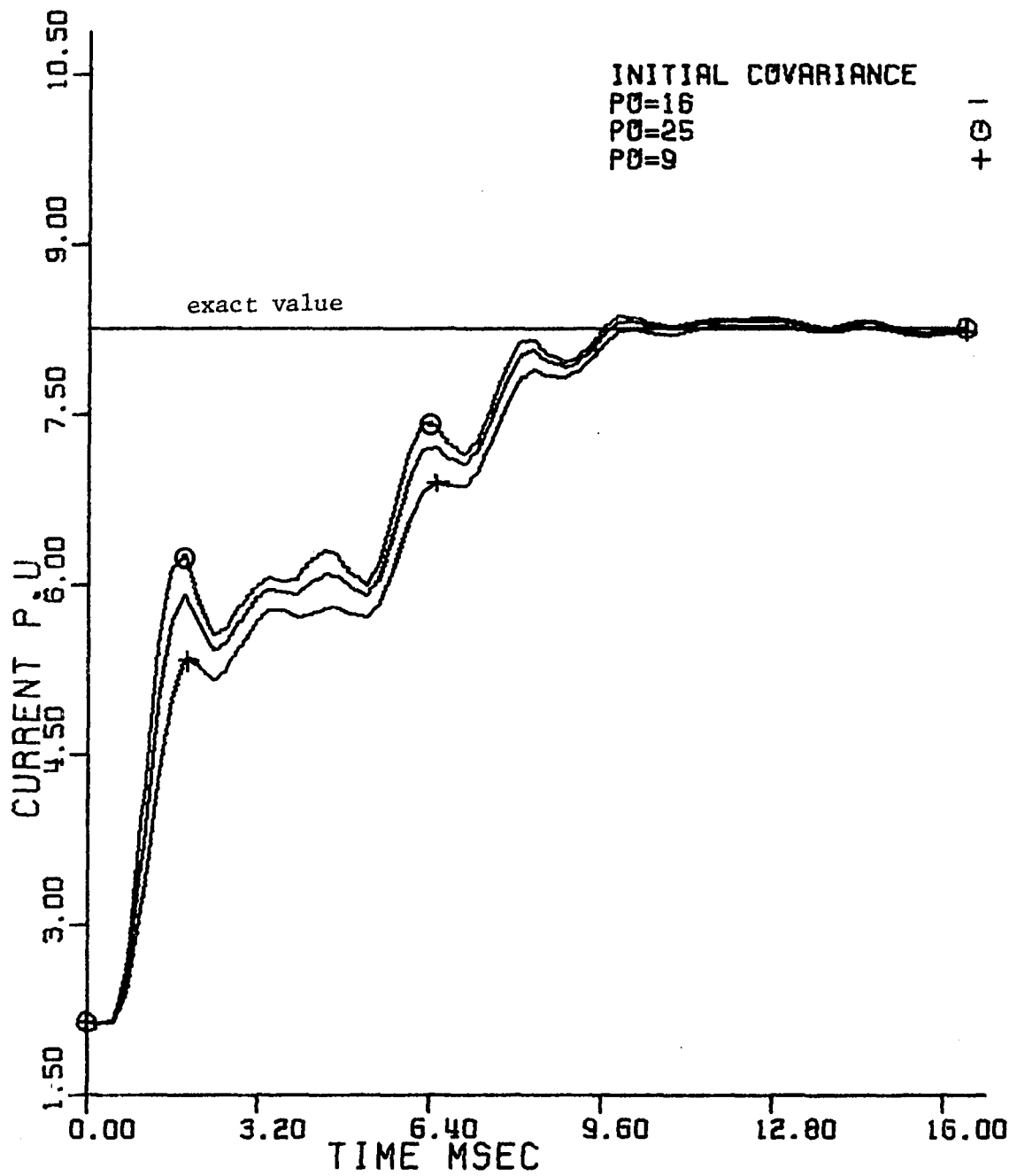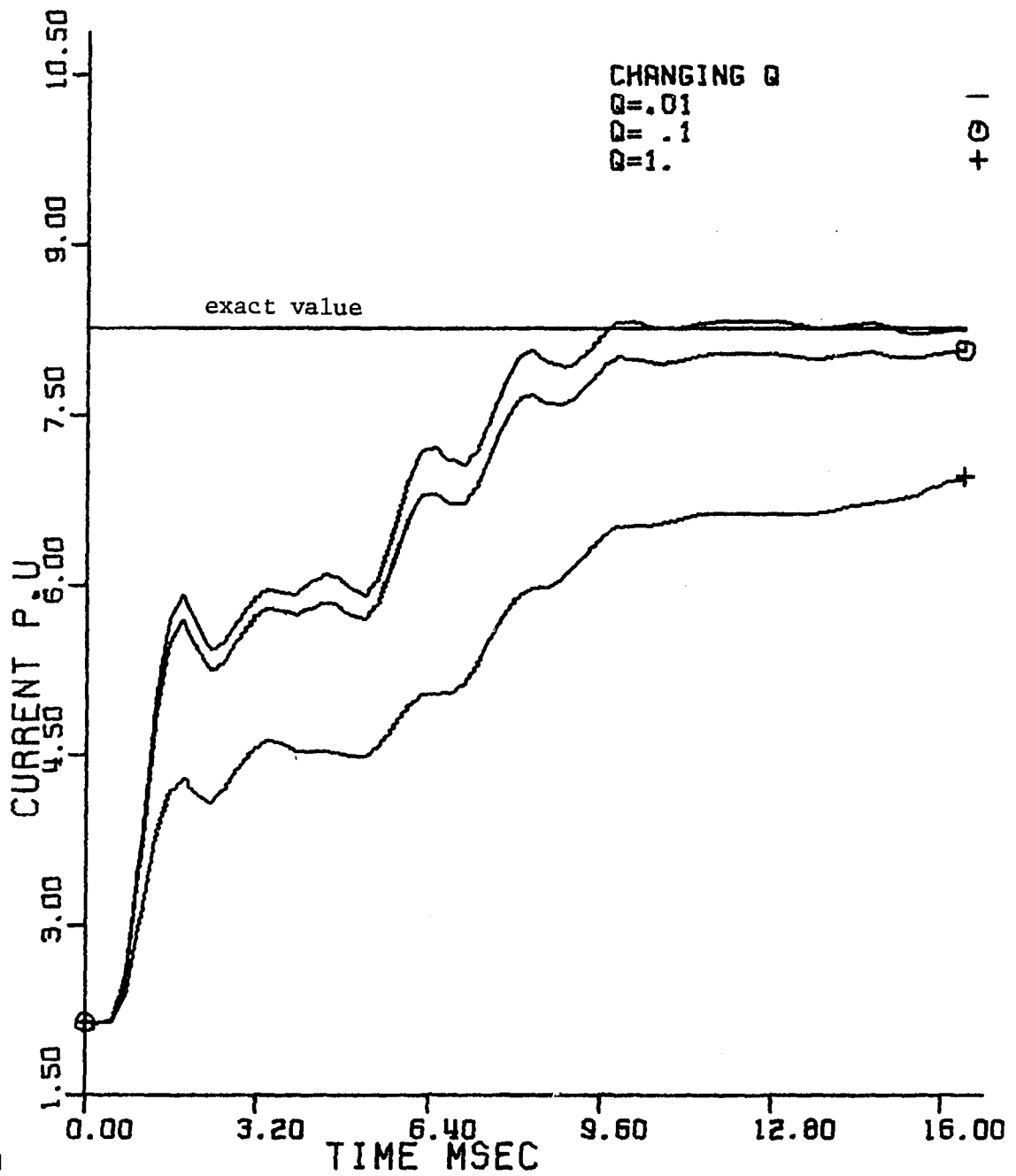Figure 6.12. Effect of changing the sampling rate in
estimating the magnitude of the voltage
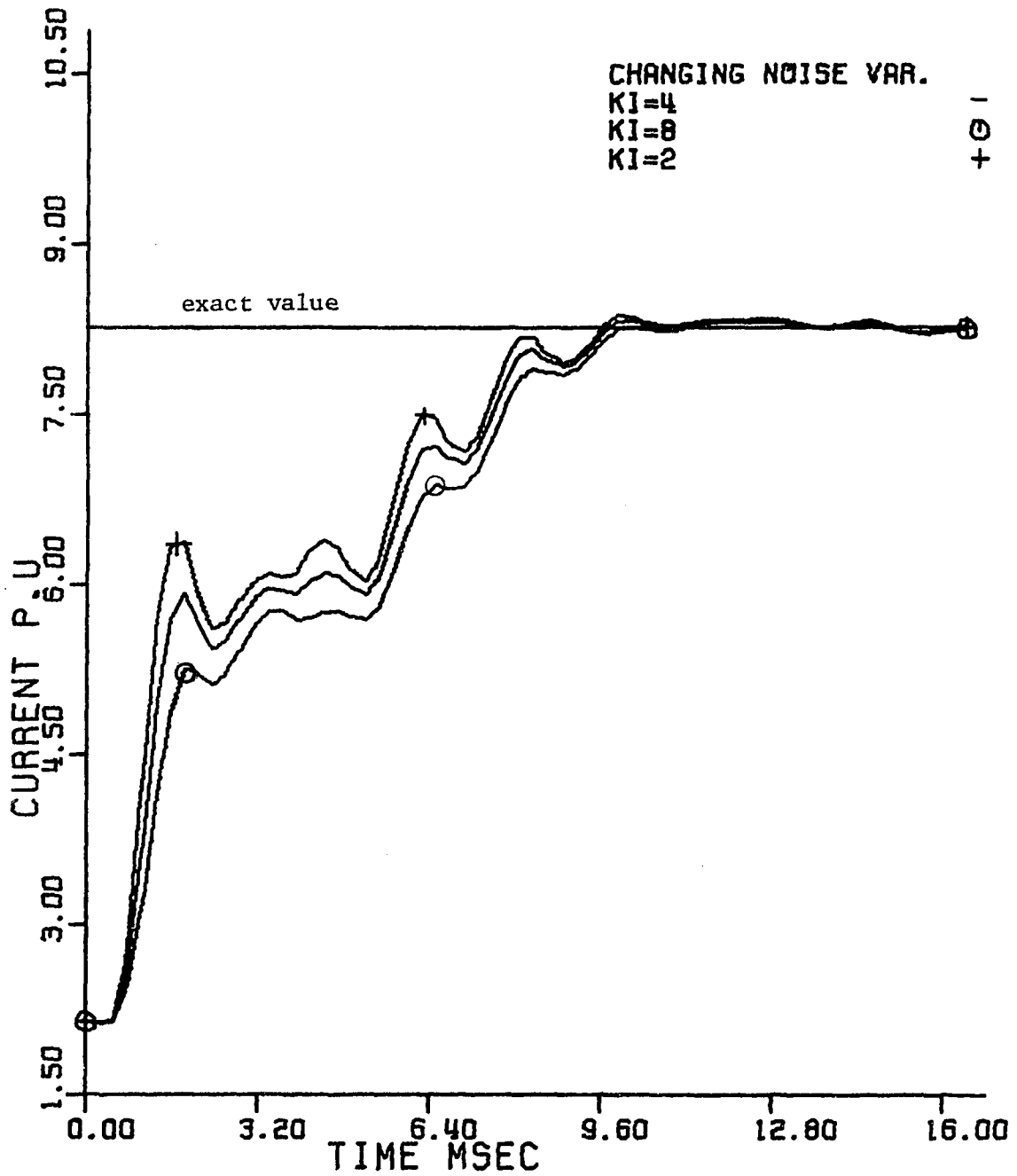
Figure 6.13. Effect of changing the initial variance of the current
noise in estimating the magnitude of the current

Figure 6.14. Effect of changing the rate of decrease of the current
noise variance in estimating the magnitude of the current

6.15. Effect of changing the initial covariance matrix in estimating the magnitude of the current

Figure 6.16. Effect of changing Q in estimating the
magnitude of the current
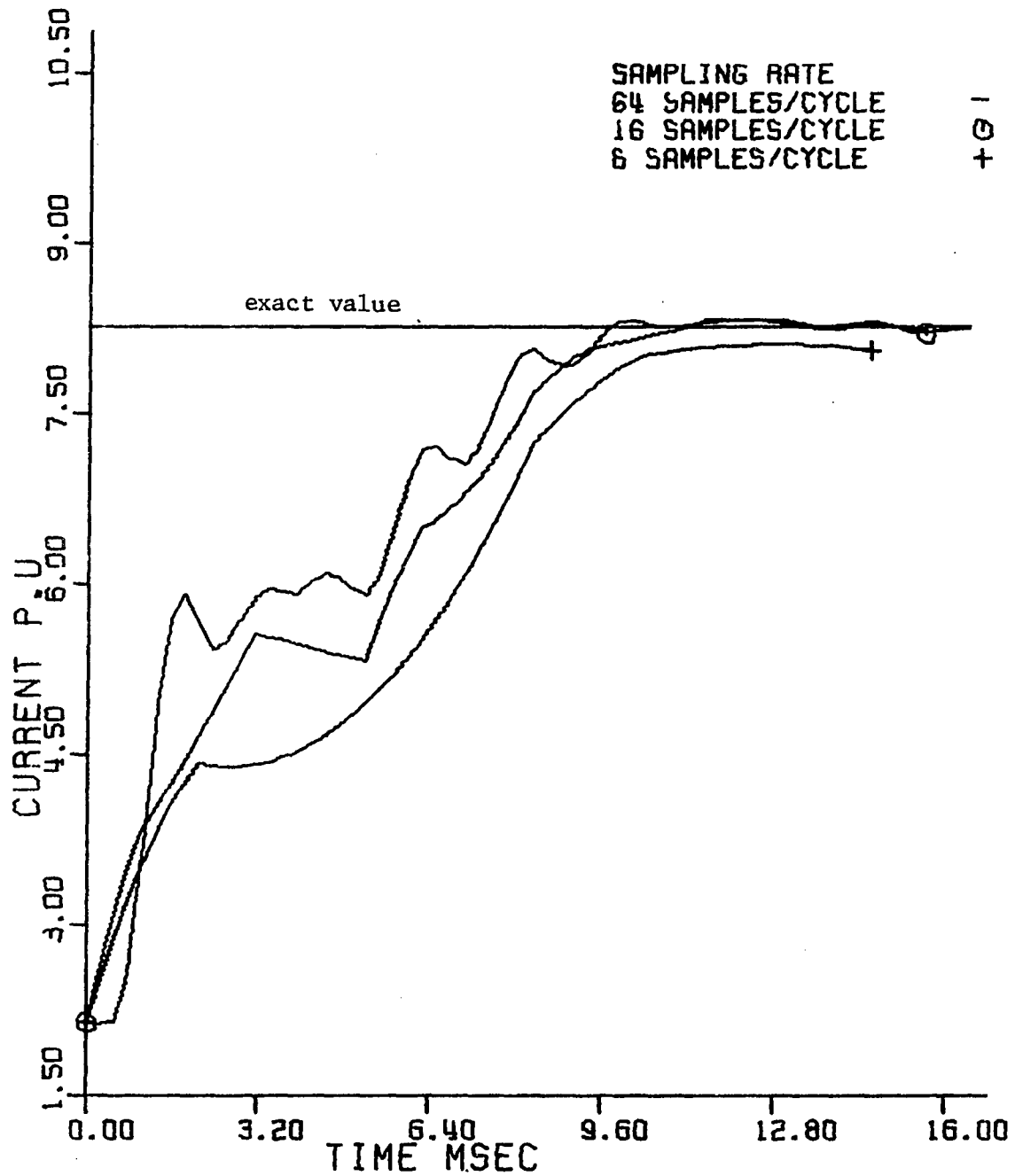
Figure 6.17. Effect of changing the sampling in
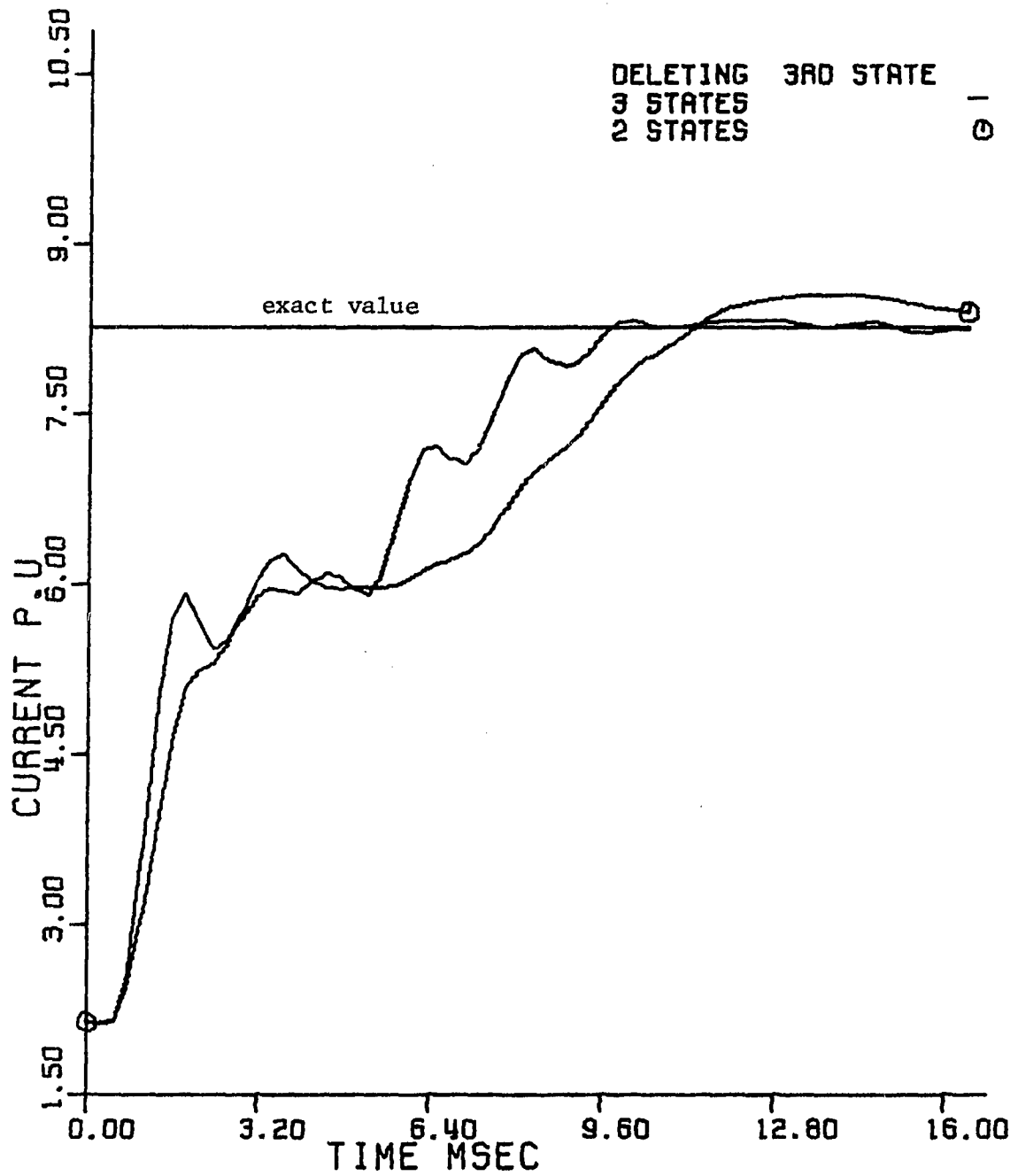estimating the magnitude of the current

Figure 6.18. Effect of deleting the third state in estimating the magnitude of the current
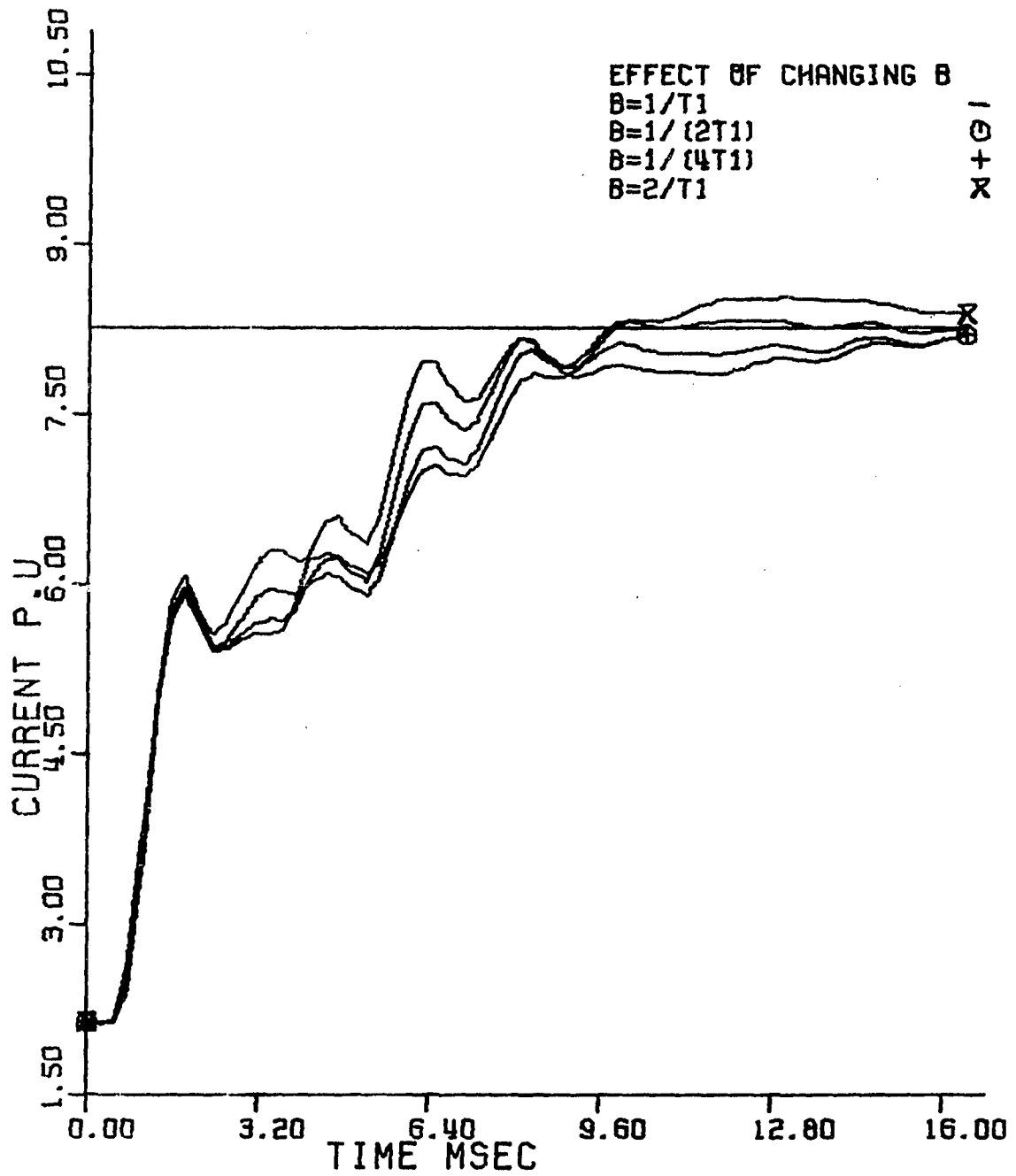
Figure 6.19. Effect of changing the value of β in
estimating the magnitude of the current

VII. A KALMAN FILTERING-BASED DIGITAL DISTANCE PROTECTION SCHEME

A digital distance relaying scheme is the heart of transmission line protection and also the most challenging problem due to the complexity and the importance of the scheme. A digital distance relaying scheme must securely answer the following questions:

(i) Is there a fault in the system?

(ii) What is the type of fault and in which zone is it located?

(iii) What is the exact location of the fault?

The answers to these questions are the general requirements of a distance relaying scheme. If the answer to the first question is yes, then the relay decides if the fault is within the protected zone or not. If the fault is within the relay first zone, then a tripping signal should be issued to the appropriate circuit breaker. In the meantime, the algorithm computes the exact location of the fault, if it is possible. These three requirements are implemented in three stages, namely, fault detection, fault classification, zone and fault location computation.

A. Fault Detection

In the scheme considered here the three line currents and the three line to neutral voltages are sampled at either 64 or 32 samples per cycle. The samples of the six quantities for two cycles are stored in the memory. When a new sample comes, it is compared with the corresponding sample one cycle earlier. If the change is .05 pu between the new sample and the corresponding sample one cycle before, in any of

the three line currents a fault will be detected. Upon detecting a
fault, four three-state Kalman filter models start to estimate the
states of the three line currents and the zero sequence current. Also
three two-state Kalman filter models start to estimate the three line to
neutral voltages. As soon as the estimates of the currents become avail-
able, the fault classification routine will be initiated.

B. Fault Classification

The method adopted in the design consists of calculating the peak
value of the three line currents (I_{af}, I_{bf}, I_{cf}) and the zero sequence
current (I_{of}) from the estimated states of the Kalman filters. The
computed currents are used for fault classification and later in zone and
fault location calculations. In large interconnected power systems, the
load currents might be comparable to the magnitude of the fault current.
Load currents are, therefore, subtracted from the post fault currents
before applying the criteria of fault classification shown in Table 7.1.

The value of K, which denotes the ratio of the current in the
unfaulted phase to the current in the faulted phase, depends mainly on
the system to be protected. Usually the highest value of K corresponds
to single line to ground fault. For the power system example used in
this work, K was found to be 0.2. To avoid any misclassification, a
value of 0.4 was chosen for this application. Also for secure classi-
fication of the fault, the fault has to be classified as the same type
for three consecutive computational steps.

Table 7.1. Fault classification criteria

Criterion No.	I_F	Then class of fault is
1	$I_{bf} < K I_{af}$ and $I_{cf} < K I_{af}$	Phase A to ground fault
2	$I_{af} < K I_{bf}$ and $I_{cf} < K I_b$	Phase B to ground fault
3	$I_{af} < K I_{cf}$ and $I_{bf} < K I_{cf}$	Phase C to ground fault
4	$I_{af} \simeq I_{bf} \simeq I_{cf}$ and $I_{af} > I_{min}$	Three-phase fault
5	$I_{cf} < K I_{af}$ and $I_{bf} \simeq I_{af}$	Phase A to phase B or Phase A to phase B to ground
6	$I_{af} < K I_{bf}$ and $I_{cf} \simeq I_{bf}$	Phase B to phase C or Phase B to phase C to ground
7	$I_{bf} < K I_{af}$ and $I_{af} \simeq I_{cf}$	Phase A to phase C or Phase A to phase C to ground

C. Zone Computation and Fault Location Calculation

After the fault type has been determined, the appropriate voltage and current pairs are selected to compute the apparent resistance and apparent reactance seen by the relay. In conventional distance relaying schemes, the distributed nature of the line parameters, capacitive current, and fault resistance are sources of inaccuracy. These sources of inaccuracy introduce significant errors in long transmission lines (69) (350 miles and above). There is no doubt that some of these factors may be included in computer relaying schemes, if it is necessary. In this work, the distributed nature of the line parameters were considered first. As the power system example used to test the technique has a 160-mile transmission line, the equations were modified with reasonable assumptions to simplify the computation procedure. The fault resistance was first ignored to find the suitable voltage and current pairs for the calculation of the apparent resistance and the apparent reactance seen by the relay. Then, the fault resistance was considered in the relay zone characteristic and the fault location computation.

In the following sections, the computation of the apparent resistance, the apparent reactance, and the fault location for the different types of faults are explained.

1. Single line to ground fault

Assuming a fault on phase A to ground, referring to Figures 4.1 and 4.2, and using the transmission line equations for the phasor quantities of voltages and currents we then have

$$v_{f_1} = D_1 v_{s_1} - V_1 i_{s_1} \tag{7.1}$$

$$v_{f_2} = D_1 v_{s_2} - B_1 i_{s_2} \tag{7.2}$$

$$v_{f_o} = D_o v_{s_o} - B_o i_{s_o} \tag{7.3}$$

For a complete short circuit on phase A to ground

$$v_{f_1} + v_{f_2} + v_{f_o} = V_{F_A} = 0$$

Therefore

$$(v_{s_1} + v_{s_2} + v_{s_o}) + \frac{D_o - D_1}{D_1} v_{s_o}$$

$$= \frac{B_1}{D_1} (i_{s_1} + i_{s_2} + i_{s_o}) + \frac{B_o - B_1}{B_1} i_{s_o} \tag{7.4}$$

Then

$$VA_s + \frac{D_o - D_1}{D_1} v_{s_o} = \frac{B_1}{D_1} IA_s + \frac{B_o - B_1}{B_1} i_{s_o} \tag{7.5}$$

For a transmission line of 160 miles or less

$$\frac{D_o - D_1}{D_1} < .02 \; ; \quad \frac{B_o - B_1}{B_1} \simeq \frac{Z_o - Z_1}{Z_1} \; ; \quad \frac{B_1}{D_1} \simeq Z_1 X$$

where

Z_1 = the positive sequence impedance per unit length

Z_o = the zero sequence impedance per unit length

X = the distance to the fault

For an extremely long transmission line, the above assumptions will not be valid. Some investigators (70) suggested iterative techniques using the Newton-Raphson method to solve for the unknown parameters. These techniques represent a heavy computer burden. Thus it was suggested that these techniques could be used off line for fault location computation, not for relaying purposes.

However, in extremely long transmission lines, information from both ends of the line are used for protection.

Proceeding with equation (7.5), we then have

$$Z_{app} = \frac{VA_s}{IA_s + \dfrac{Z_o - Z_1}{Z_1} \, i_{s_o}} \qquad (7.6)$$

for phase A to ground fault.

Similar expressions are used for phase B to ground and phase C to ground faults.

2. Compensating for the fault arc resistance

Neglecting the phase difference between the currents fed into the fault resistance, the apparent impedance seen by the relay is in the form (71)

$$Z_{app} = Z_1 X + \frac{R_F \, i_{s_o} \, K}{IA_s + \dfrac{Z_o - Z_1}{Z_o} \, i_{s_o}} \qquad (7.7)$$

Equation 7.7 may be used to calculate the fault location. The detailed analysis of inaccuracy due to fault resistance is discussed in reference

(71). It should be noted that it is not intended in this work to study all the sources of inaccuracy in distance relaying. However, these sources are studied in detail in many references (64,69,71), but with particular reference to electromechanical and solid-state relays.

3. Line to line or double line to ground fault

Proceeding in a similar way to the single line to ground fault, then for a line to line fault between phases b and c, the apparent impedance will be (64)

$$Z_{app} = \frac{VB_s - VC_s}{IB_s - IC_s} \tag{7.8}$$

To correct for the fault resistance, the apparent impedance is

$$Z_{app} = Z_1 X + \frac{I_{bsf} - I_{csf}}{IB_s - IC_s} KR_F \tag{7.9}$$

Similar expressions to equations (7.8) and (7.9) are also used for faults between other phases.

4. Three-phase fault

If a three-phase fault occurs, it is usually due to an accident and any of the above expressions could be used to compute the apparent impedance and the fault location.

A computer program was written in Fortran to simulate and test the stages of the complete scheme mentioned above. The data obtained from the transient program were fed into the algorithm for different types of faults at different locations.

D. Testing the Proposed Scheme

1. Test results of fault detection

Figures 7.1 and 7.2 show the samples of the current in the faulted phase and unfaulted phase for a single line to ground fault at 30 miles along with the prefault currents one cycle prior to the fault. The fault was detected after one sample (64 samples/cycle). A fault at 90 miles was detected after three samples and a fault at 150 miles was detected after 5 samples. These are shown in Figure 7.3 to 7.6. It was also noticed that the fault detection was independent of the type of fault. Therefore, in the worst conditions, the Kalman filters were initiated after the fault occurrence by 5 samples (64 s/c) for a 150-mile zone.

2. Test results of fault classification

The fault classification subroutine was able to classify the type of fault properly in a maximum of one-eighth of a cycle. The single line to ground fault was classified properly in one-sixteenth of a cycle. The reason is that the current in the faulted phase changes much faster than the current in the unfaulted phase. Moreover, the initial estimate of the current in the unfaulted phase is much closer to the exact value. The recursive estimation of the change in current in the faulted and un-faulted phases for a single line to ground fault at 30 miles, 90 miles, and 150 miles are shown in Figures 7.7 to 7.9.

Faults involving two phases were classified in one-eighth of a cycle. The recursive estimation of the change in the currents for a
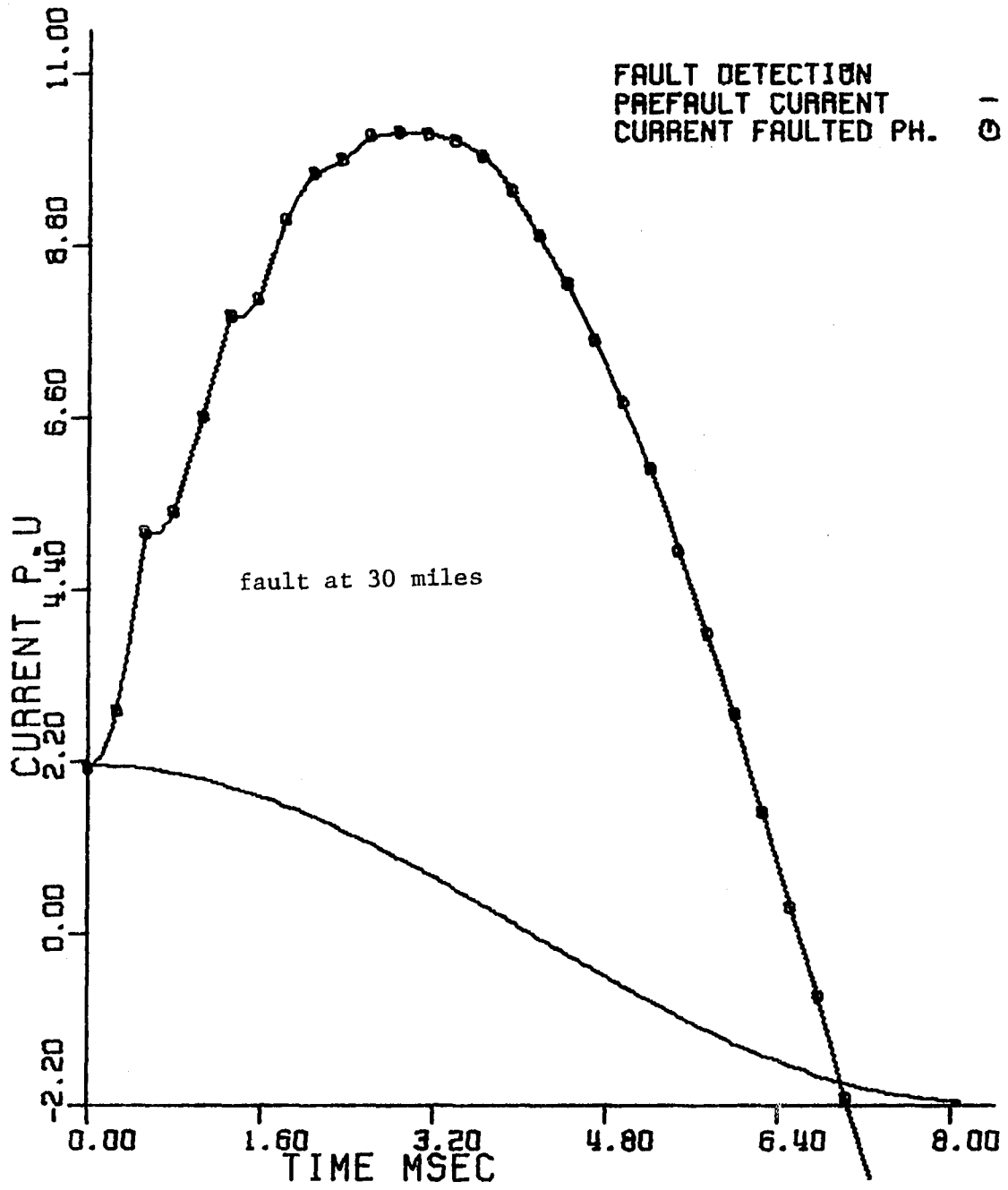
Figure 7.1. Samples of the current in the faulted phase and the
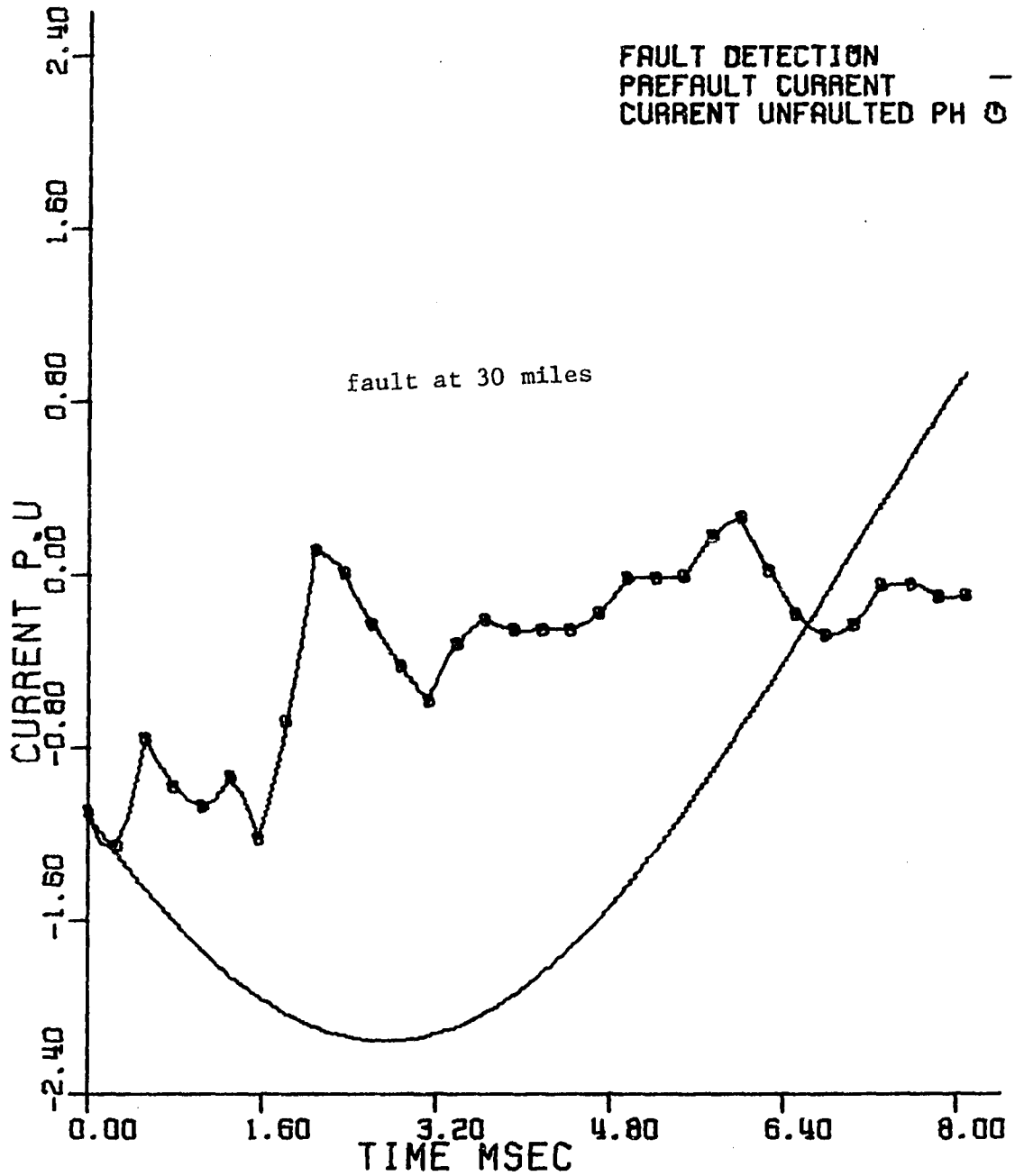prefault current one cycle prior to the fault occurrence

Figure 7.2. Samples of the current in the unfaulted phase and the prefault current one cycle prior to the fault occurrence
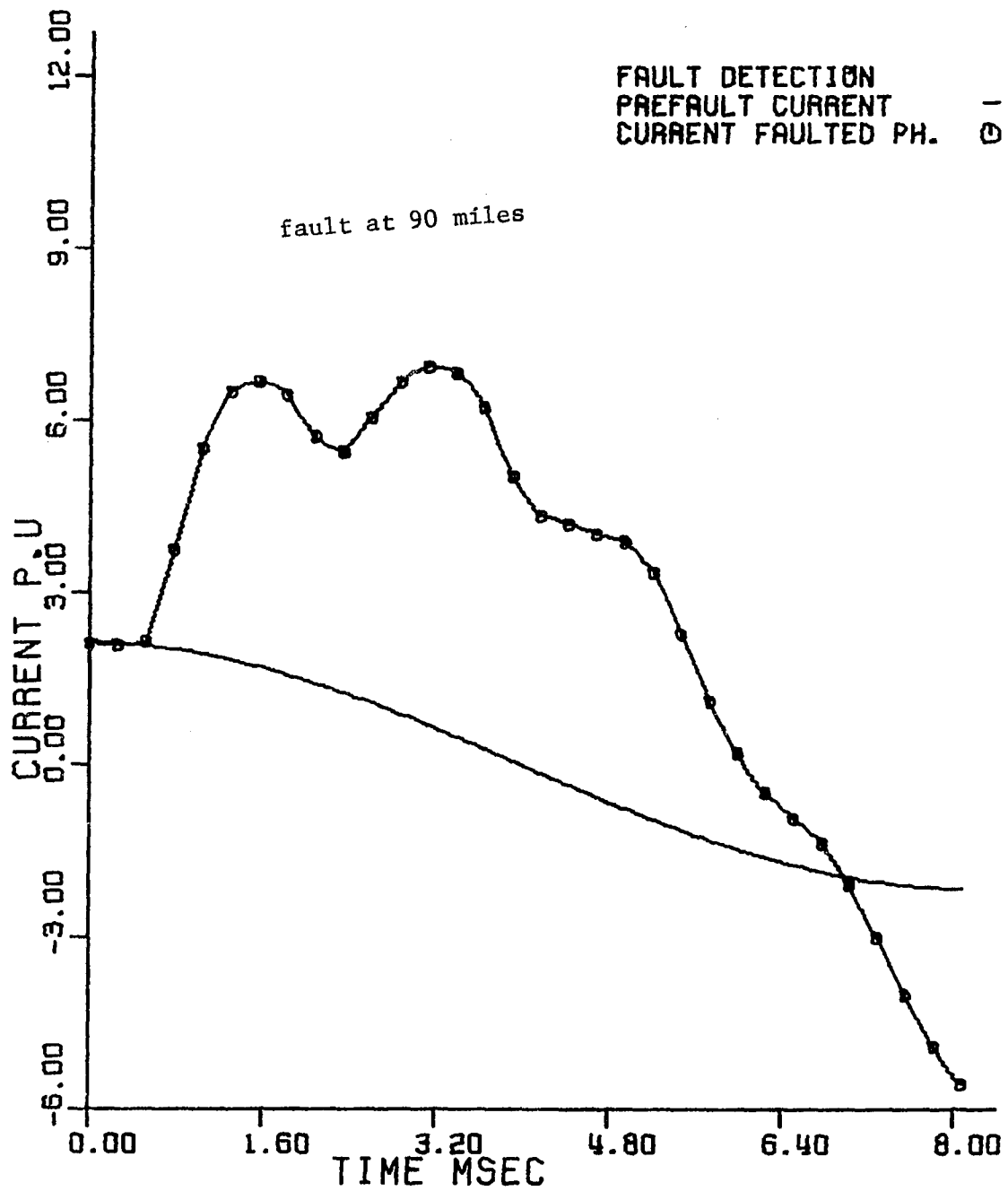
Figure 7.3. Samples of the current in the faulted phase and the prefault current one cycle prior to the fault occurrence
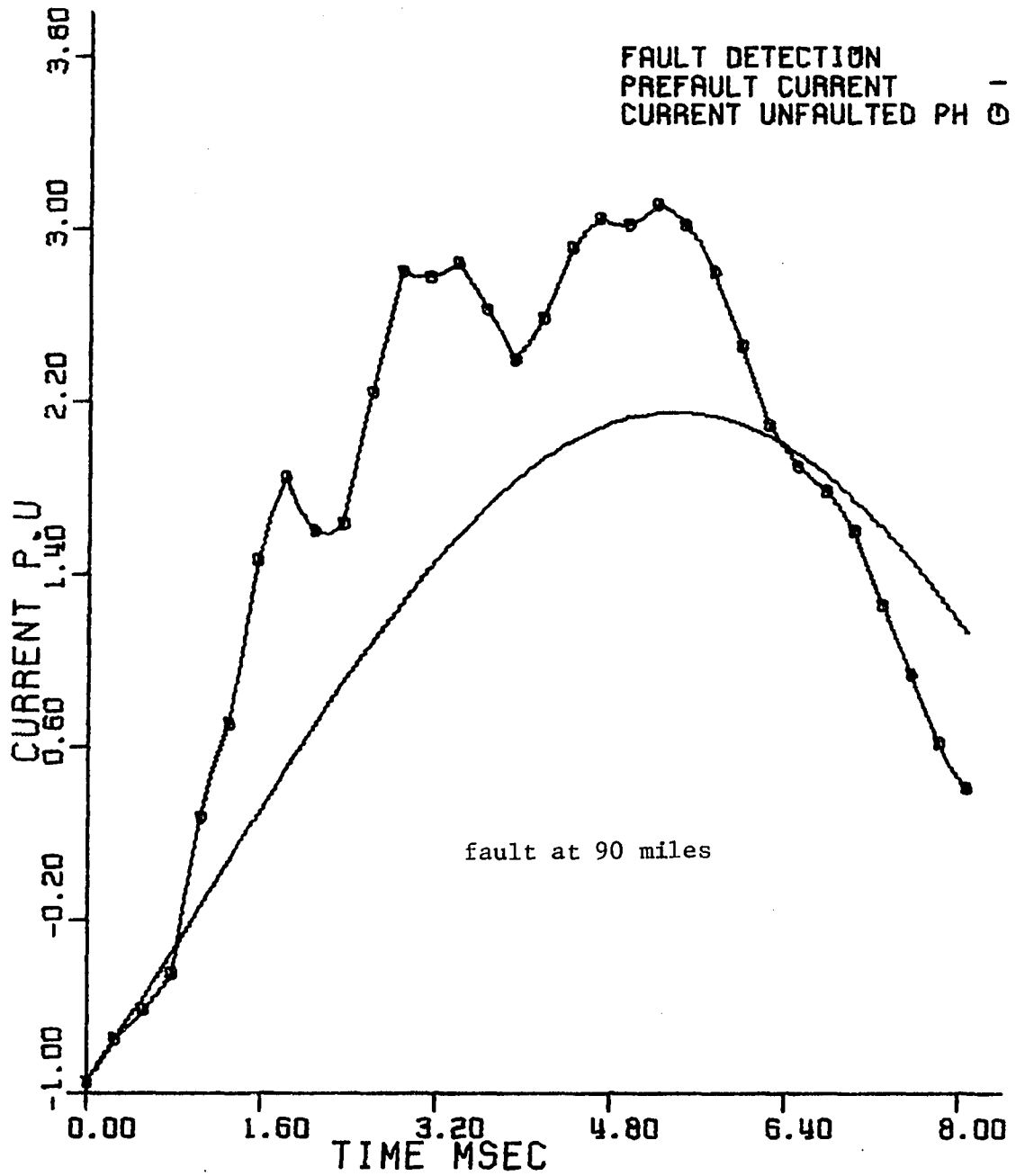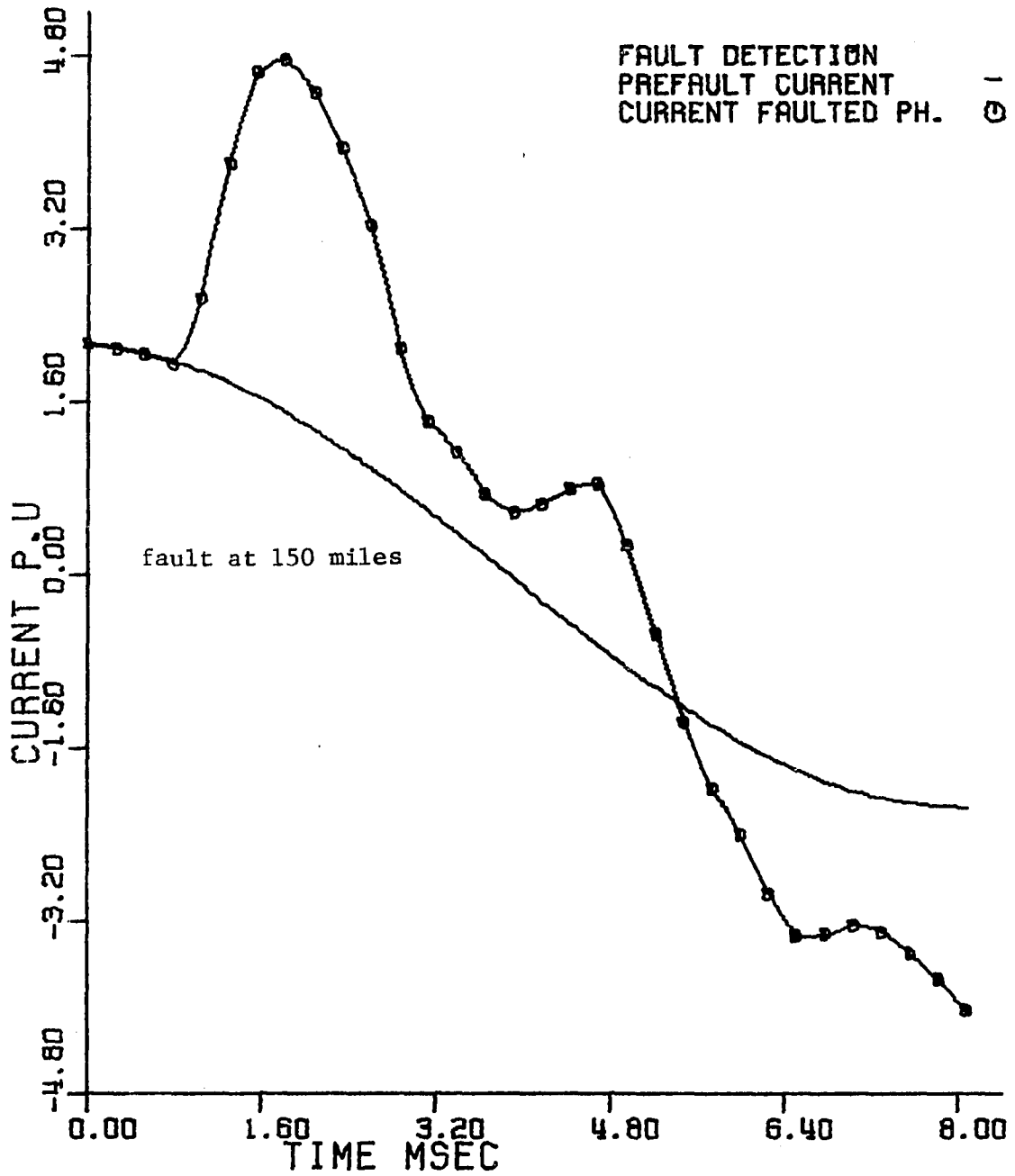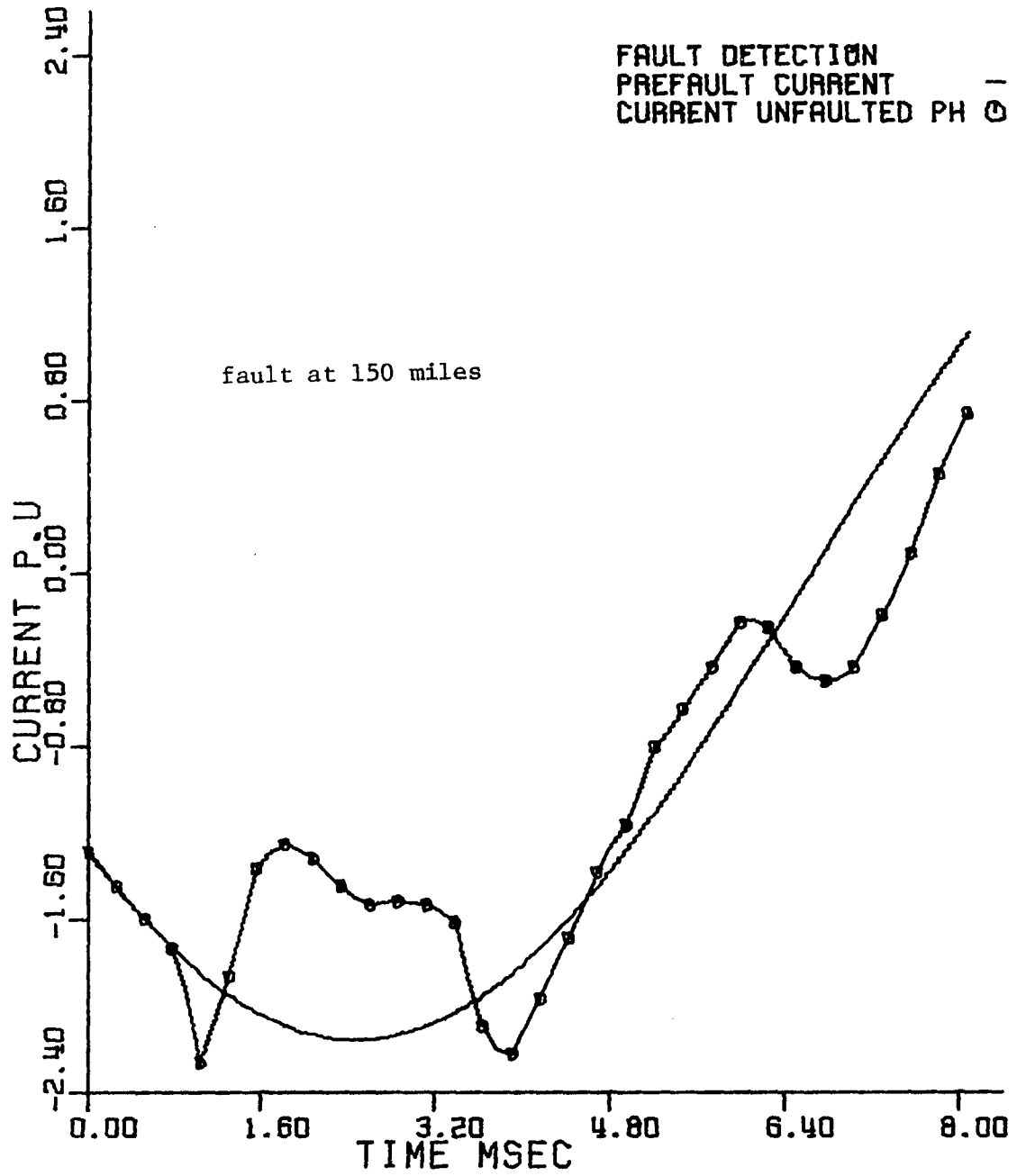
Figure 7.4. Samples of the current in the unfaulted phase and the
prefault current one cycle prior to the fault occurrence

FAULT DETECTION
PREFAULT CURRENT —
CURRENT FAULTED PH. ⊙

fault at 150 miles

Figure 7.5. Samples of the current in the faulted phase and the
prefault current one cycle prior to the fault occurrence

Figure 7.6. Samples of the current in the unfaulted phase and the
prefault current one cycle prior to the fault occurrence
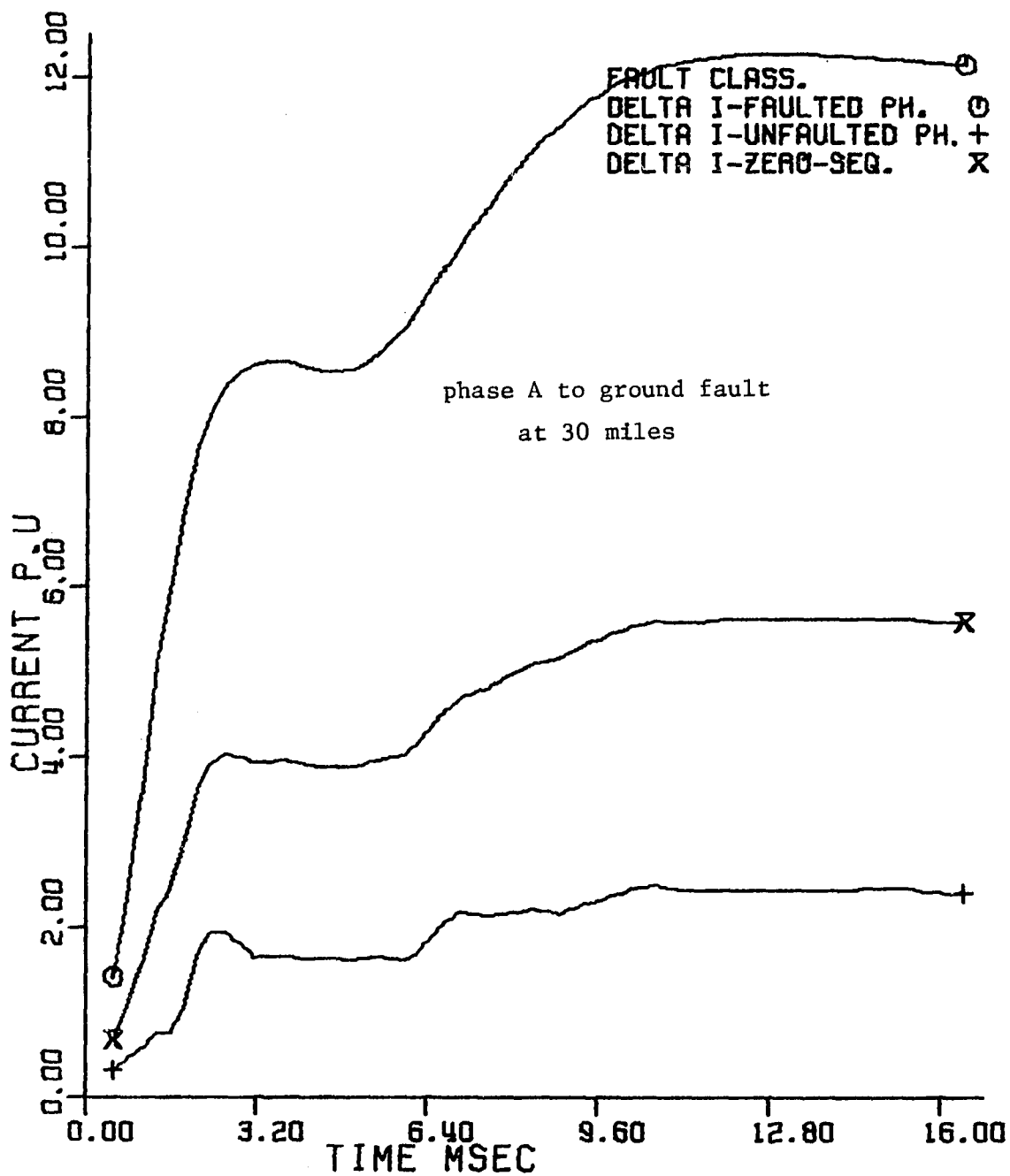
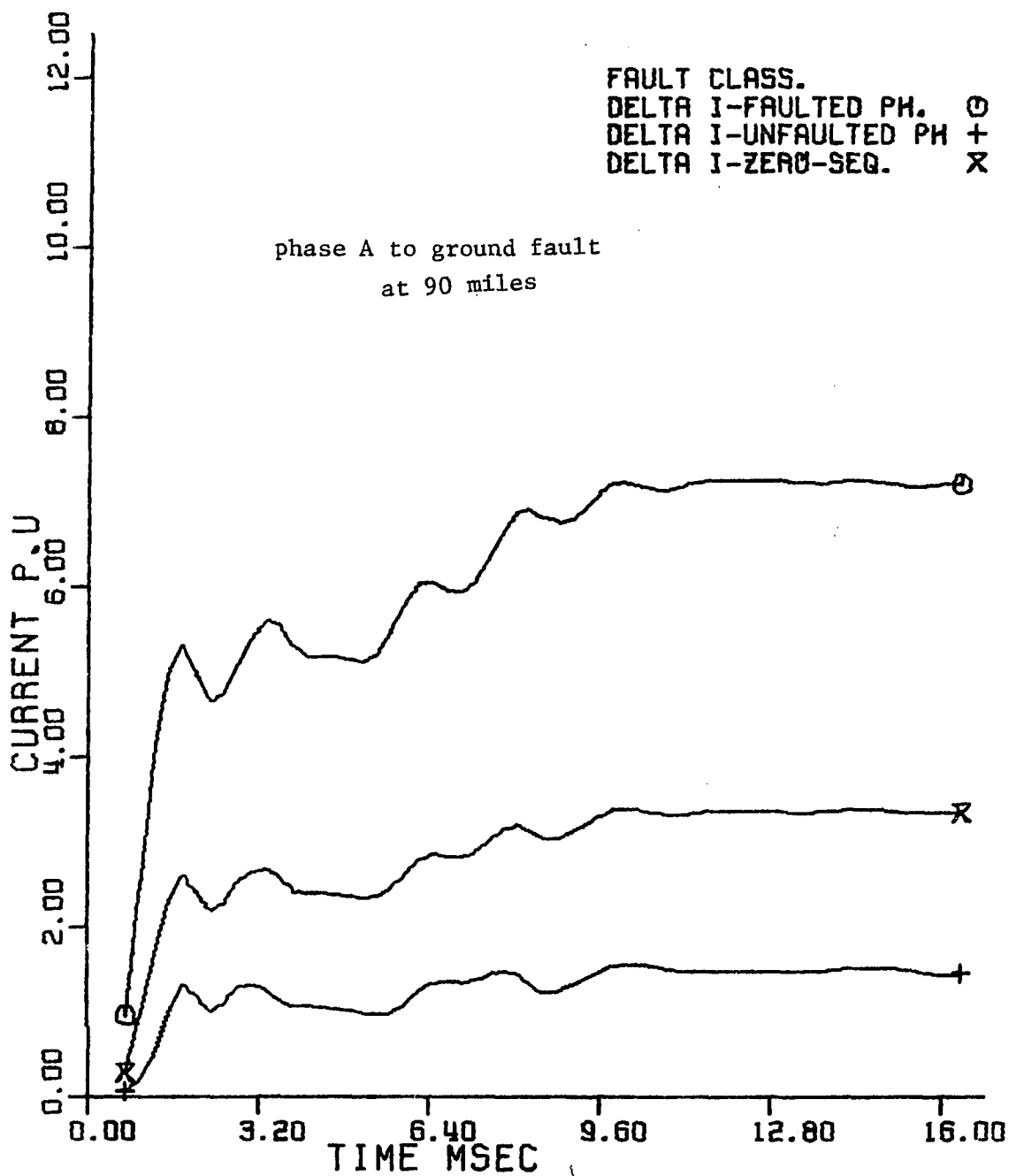Figure 7.7. Recursive estimation of the change in the currents

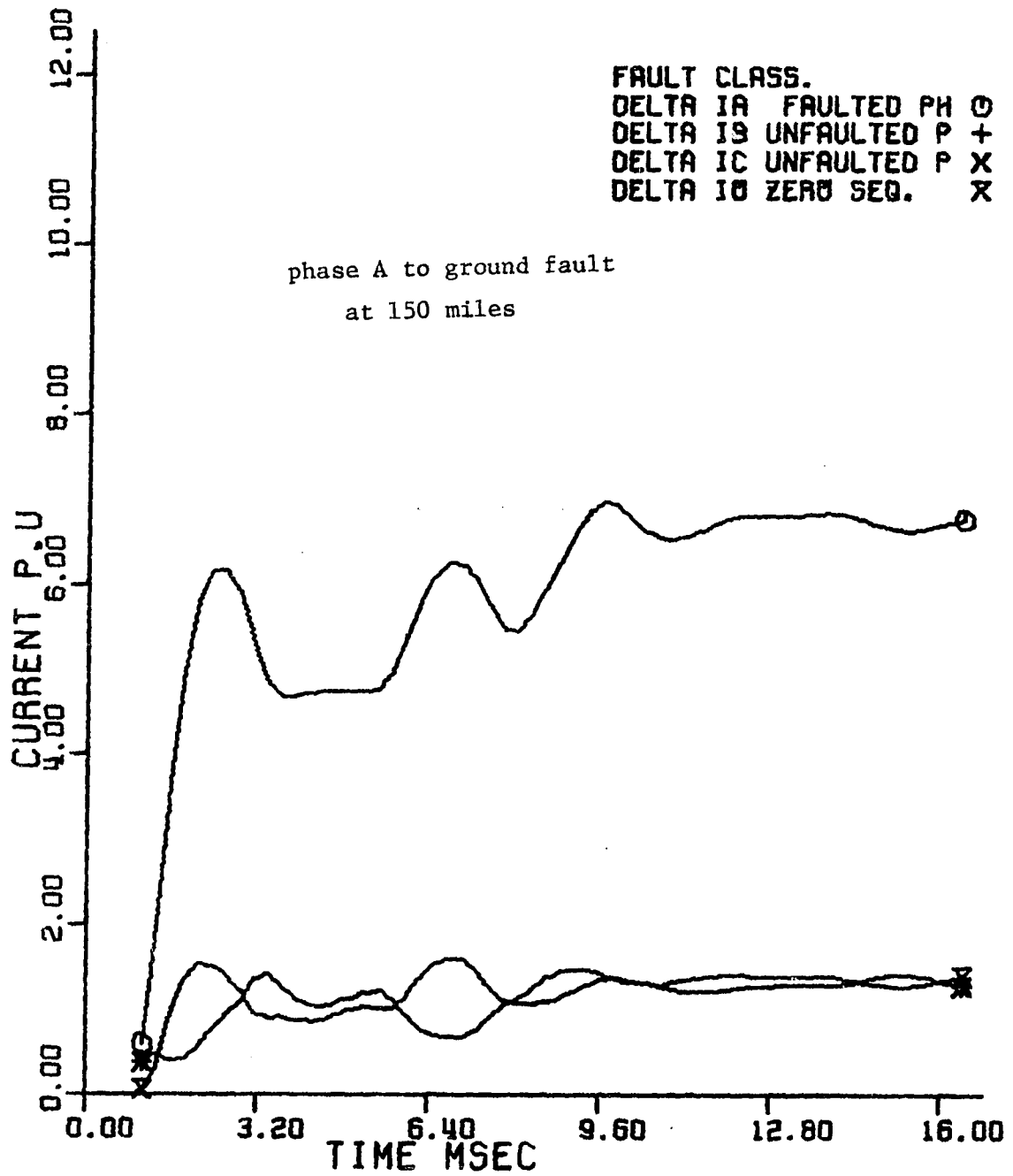Figure 7.8. Recursive estimation of the change in the currents

Figure 7.9. Recursive estimation of the change in the currents

double line to ground fault at 90 miles is shown in Figure 7.10.
When the scheme was tested on a three-phase fault, the fault was
classified as a line to line fault in one-eighth of a cycle. The reason
for this misclassification was the initial slow change in the current of
one of the phases. However, this misclassification of the three-phase
fault does not affect the calculation of the apparent impedance or the
fault location computation. As the three-phase fault is extremely rare,
it was decided not to delay the decision of the fault classification
subroutine, but if the fault is classified as a line to line fault, the
program will proceed to the next step and continue checking the type of
fault for another one-eighth of a cycle. The recursive estimation of the
change in the currents in the three phases for a three-phase fault at
90 miles is shown in Figure 7.11.

E. Testing the Calculation of the Apparent Impedance

After the fault was classified, the appropriate voltages and cur-
rents, along with the appropriate subroutine, were used to compute the ap-
parent impedance seen by the relay. Also, the covariance matrices of the
estimated voltages and currents may be used to predict the estimation
error in the computed apparent impedance. If the apparent resistance is
less than the relay zone resistance setting and the apparent reactance is
less than the relay reactance setting, a tripping signal will be issued
to the circuit breaker to trip the line. During the operating time of
the circuit breaker, the algorithm continues to compute the fault
location. For simplicity, the relay is considered to have one zone up
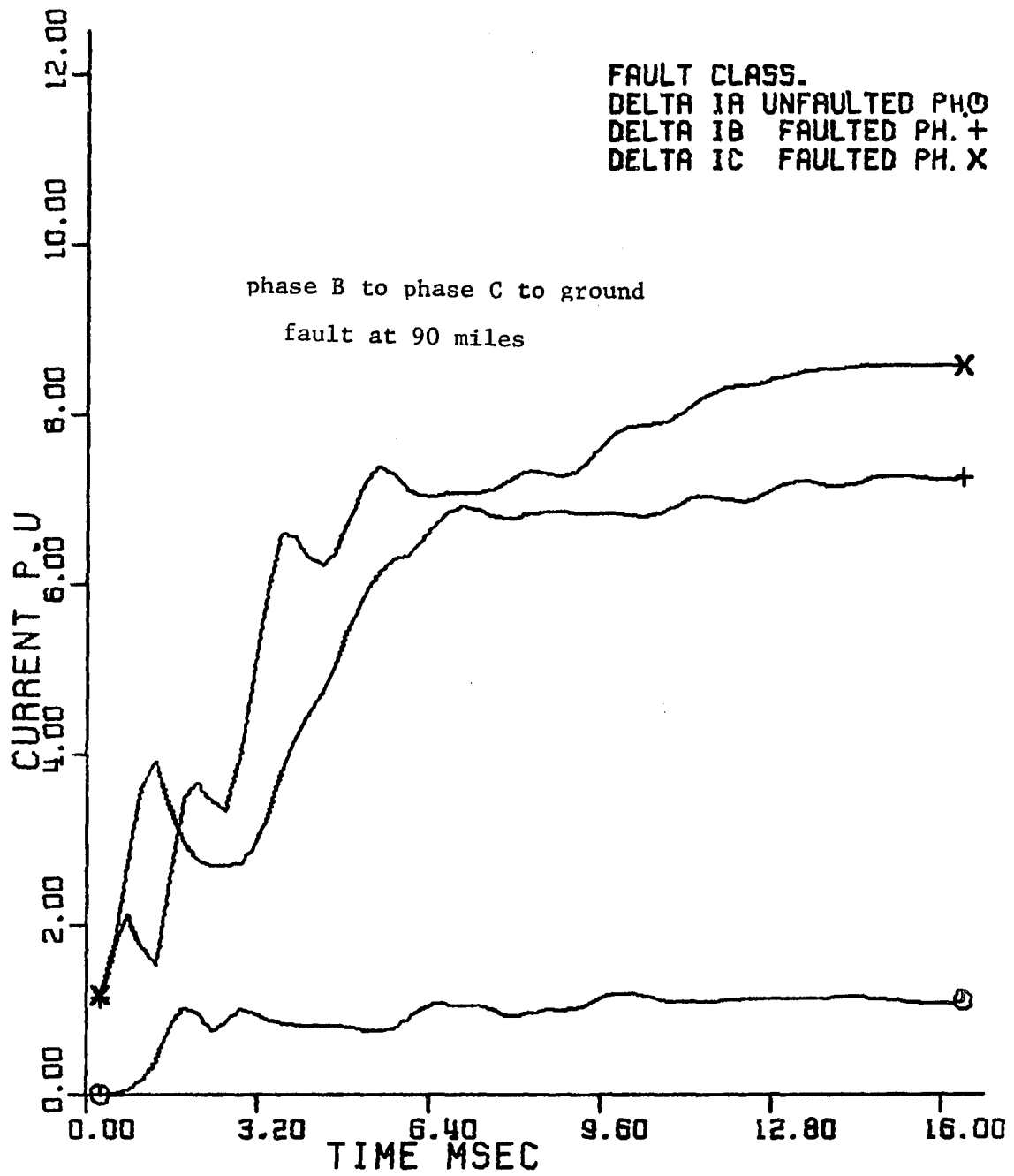to 150 miles. Therefore, the relay reactance setting is 0.08 p.u. and

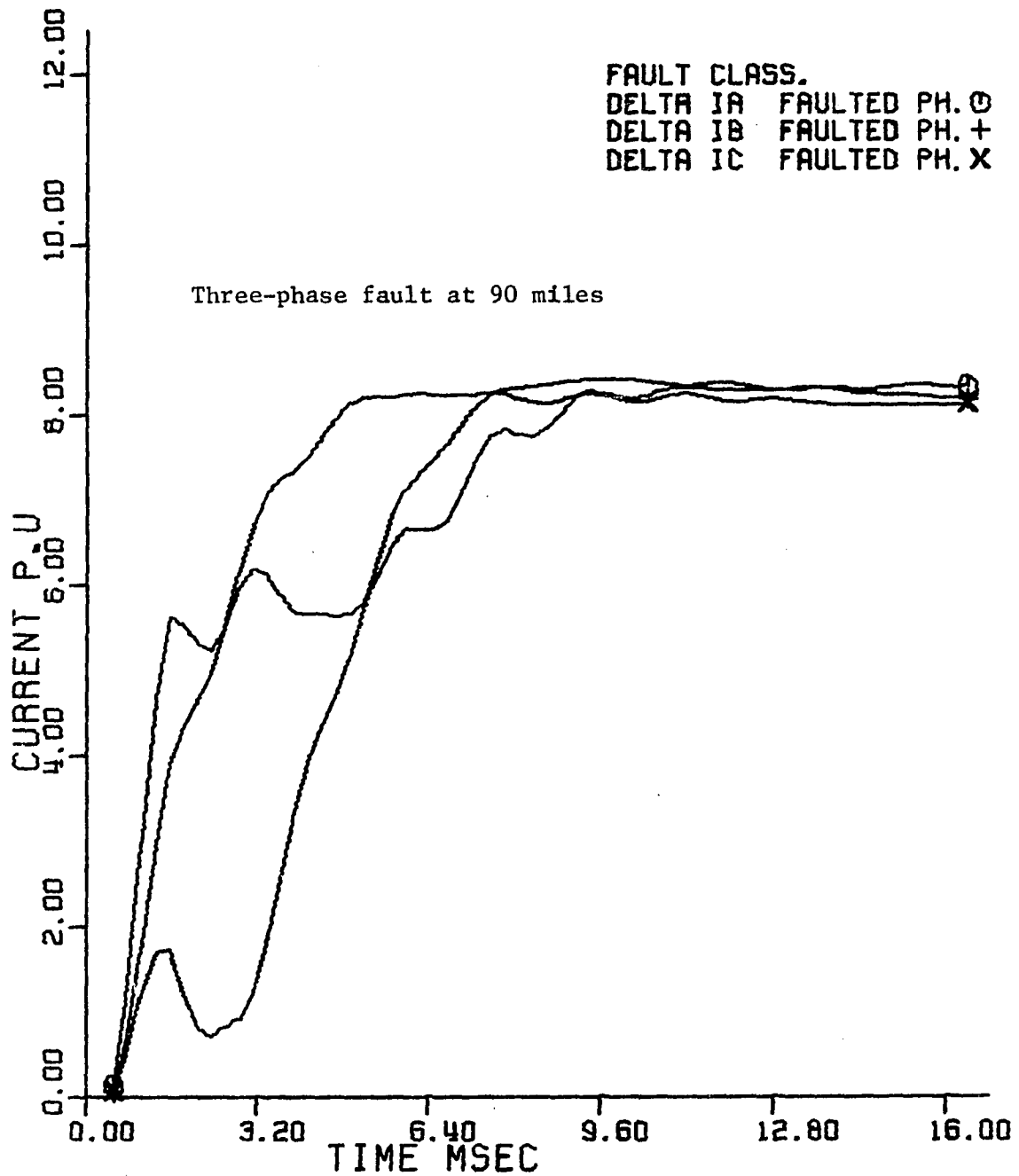Figure 7.10. Recursive estimation of the change in the currents

Figure 7.11. Recursive estimation of the change in the currents

the resistance setting is 0.08 p.u. to include the maximum fault resistance. Figures 7.12 and 7.13 show the computation of the apparent impedance and its trajectory for a single line to ground fault at 30 miles. It can be concluded from 7.12 that the relay operates in less than one-fourth of a cycle. The computation of the fault location is shown in Figure 7.14, and it is highly accurate in less than one-half cycle.

Figures 7.15 and 7.16 show the recursive computation of the apparent resistance, apparent reactance, and impedance trajectory seen by the relay for a single line to ground fault at 90 miles. It is clear from these figures that the relay operates in less than 6 msec. The computation of the fault location is shown in Figure 7.17, which indicates an accurate value after half a cycle. Figures 7.18 to 7.20 show the test results of a single line to ground fault at 150 miles. These results indicate a relay operating time less than 10 msec.

The scheme was also tested for double line to ground and three-phase faults. The results of these tests are shown in Figures 7.21 to 7.26. As a conclusion of the test results, the mean operating time of the relay is less than one-half of a cycle (8 msec). An under-reach of 10 percent occurred in double line to ground faults and three-phase faults. This under-reach is due to the phase angle between the actual current in the fault resistance and the current at the relay location. Reported test results on other schemes (26) show an over- or under-reach of more than 10 percent due to inaccuracy of the algorithm with operating time of more than 23 msec (3).
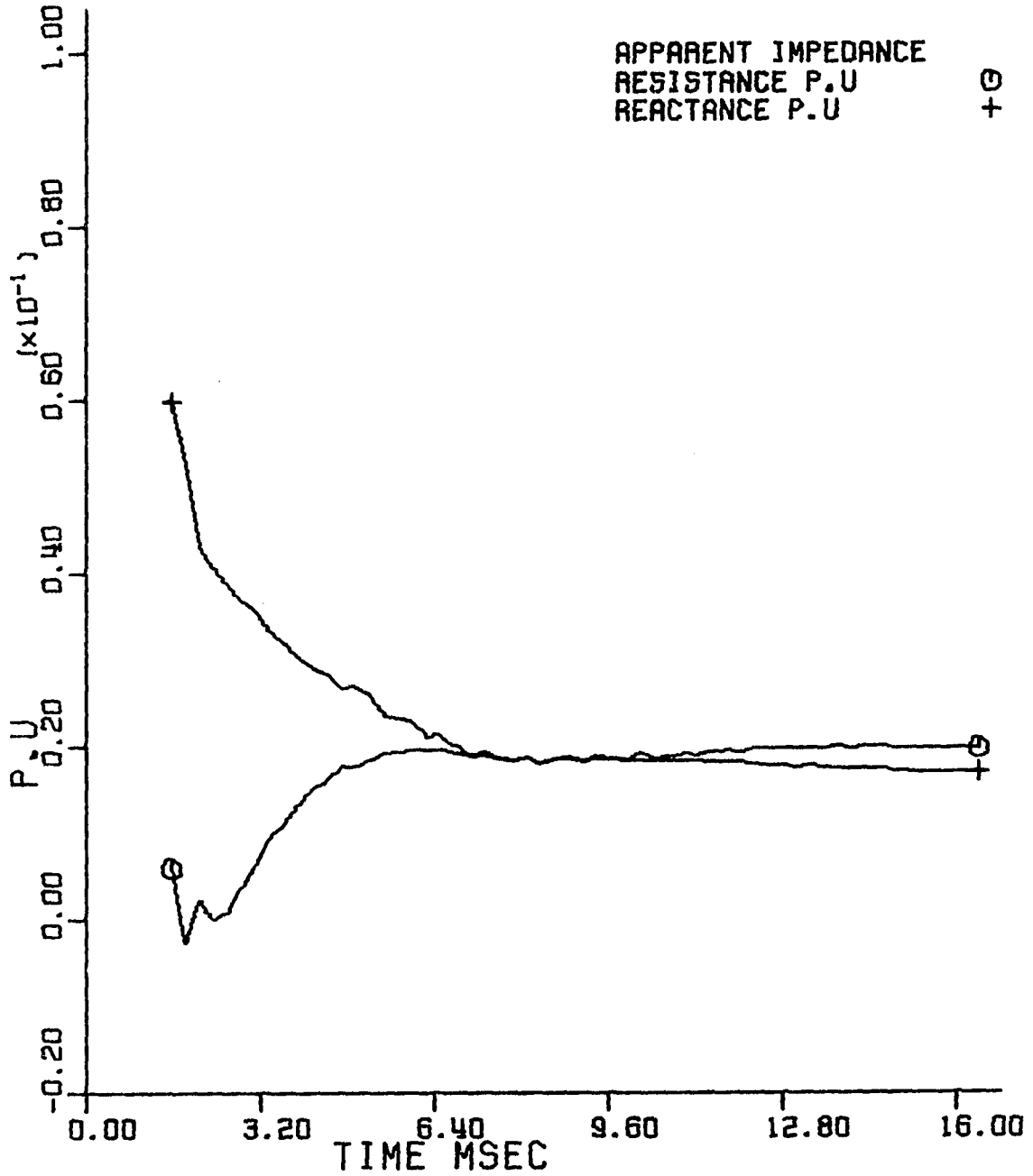
Figure 7.12. Apparent resistance and apparent reactance seen
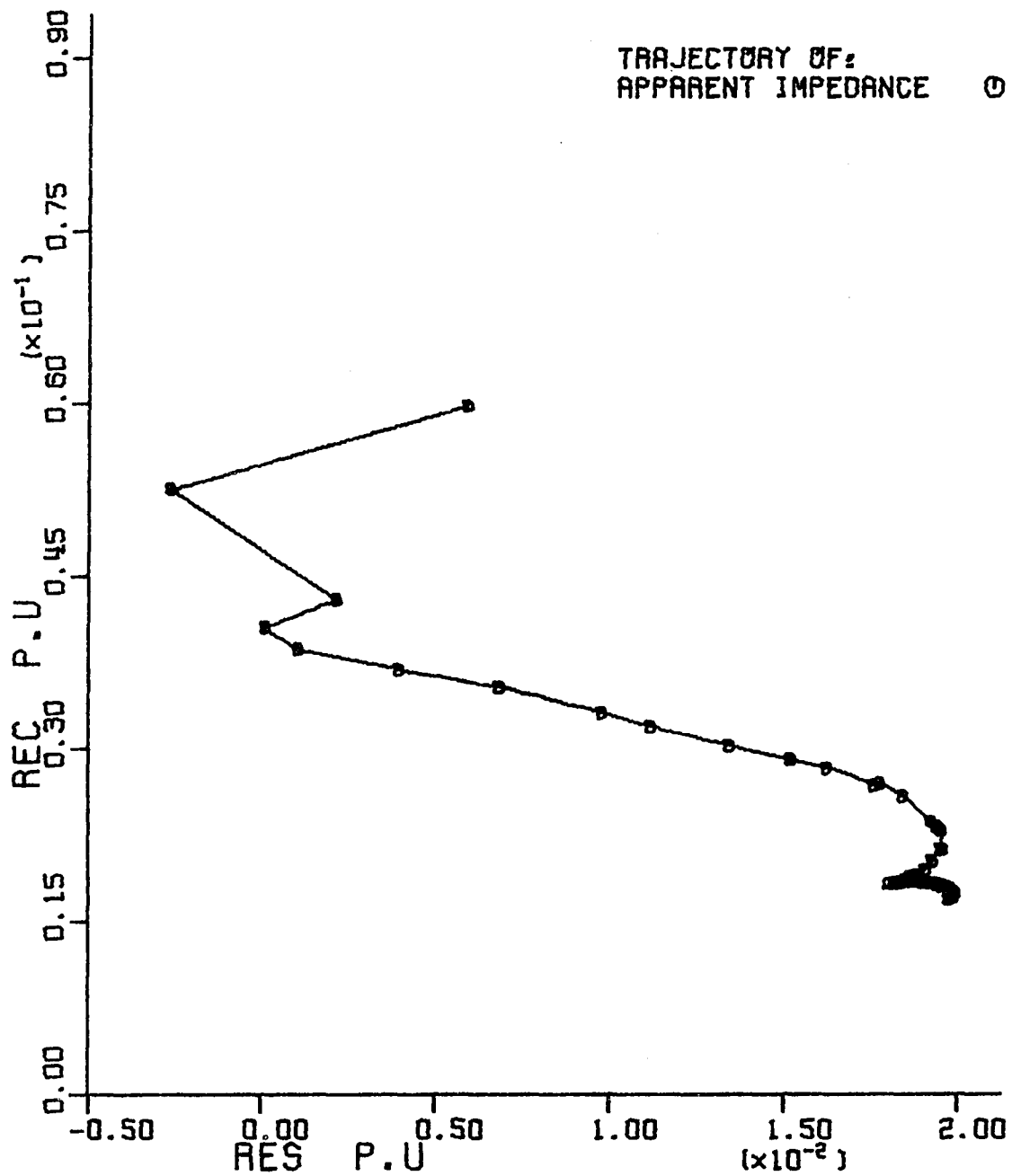by the relay for A-G fault at 30 miles

Figure 7.13. Trajectory of apparent impedance seen by
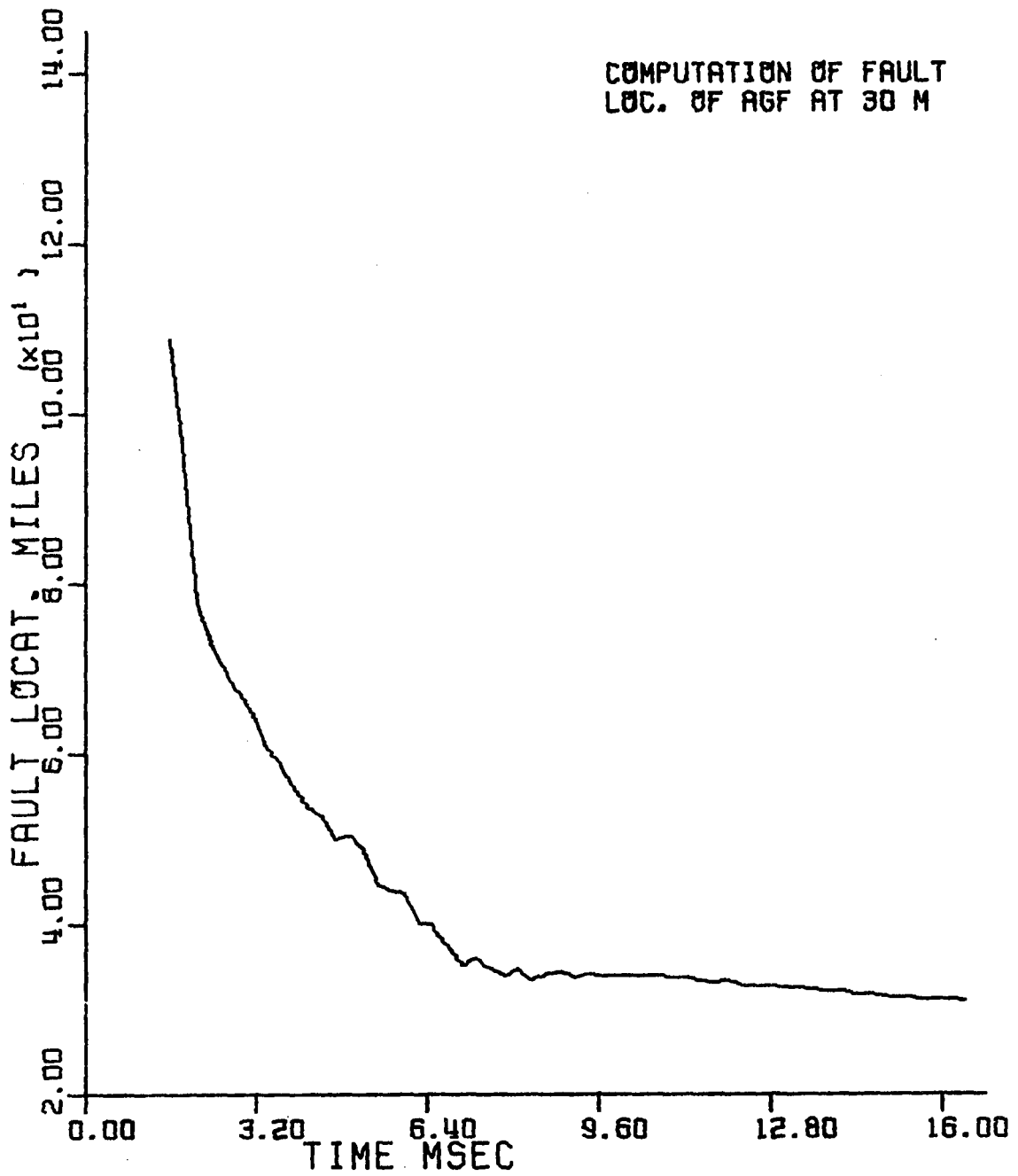the relay for A-G fault at 30 miles

Figure 7.14. Computation of fault location for A-G fault at 30 miles

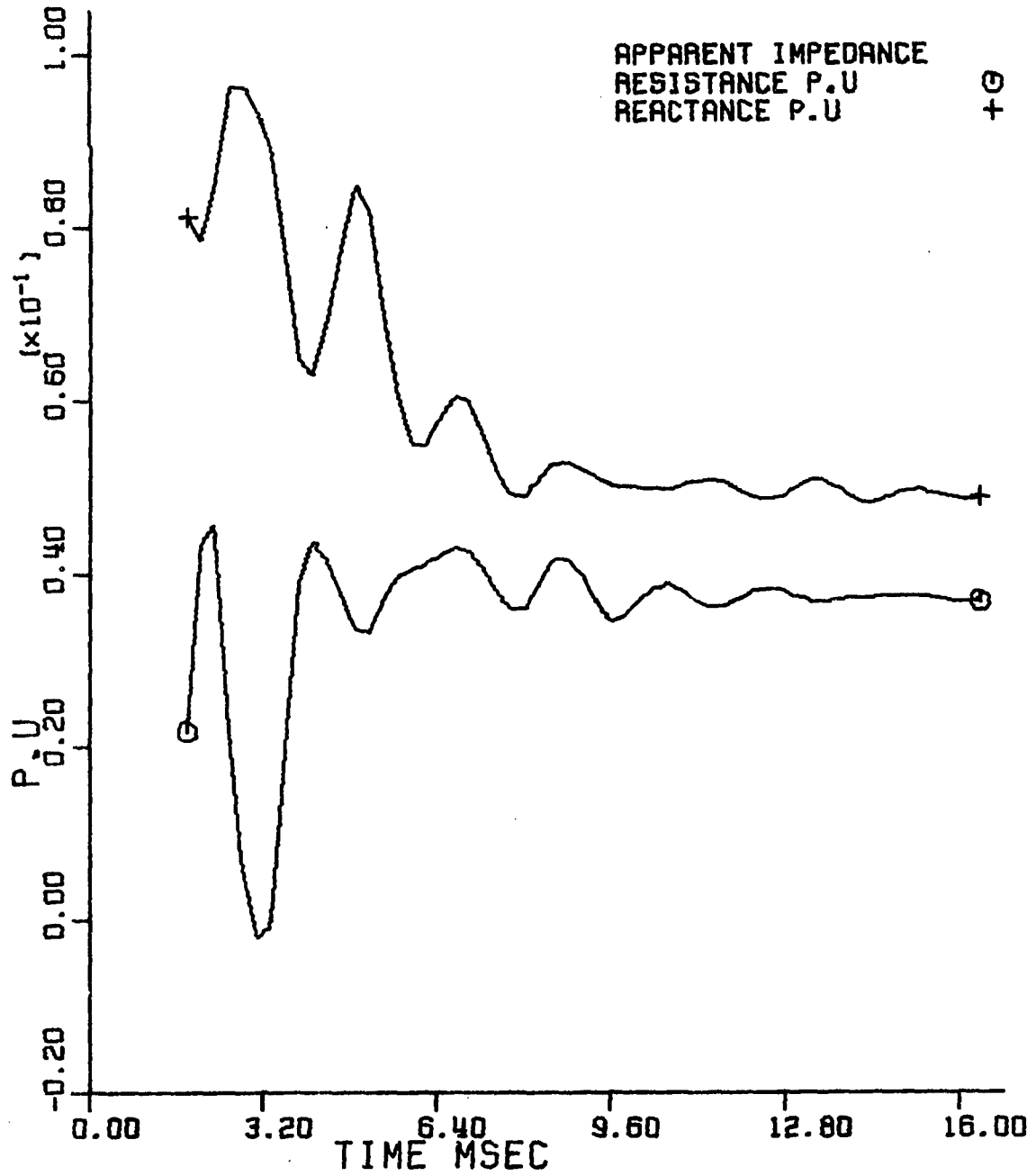Figure 7.15. Apparent resistance and apparent reactance
seen by the relay for A-G fault at 90 miles

Figure 7.16. Trajectory of apparent impedance
for A-G fault at 90 miles

Figure 7.17. Computation of fault location for
A-G fault at 90 miles

Figure 7.18. Apparent resistance and apparent
reactance for A-G fault at 150 miles

Figure 7.19. Trajectory of apparent impedance
for A-G fault at 150 miles

Figure 7.20. Computation of fault location
for A-G fault at 150 miles

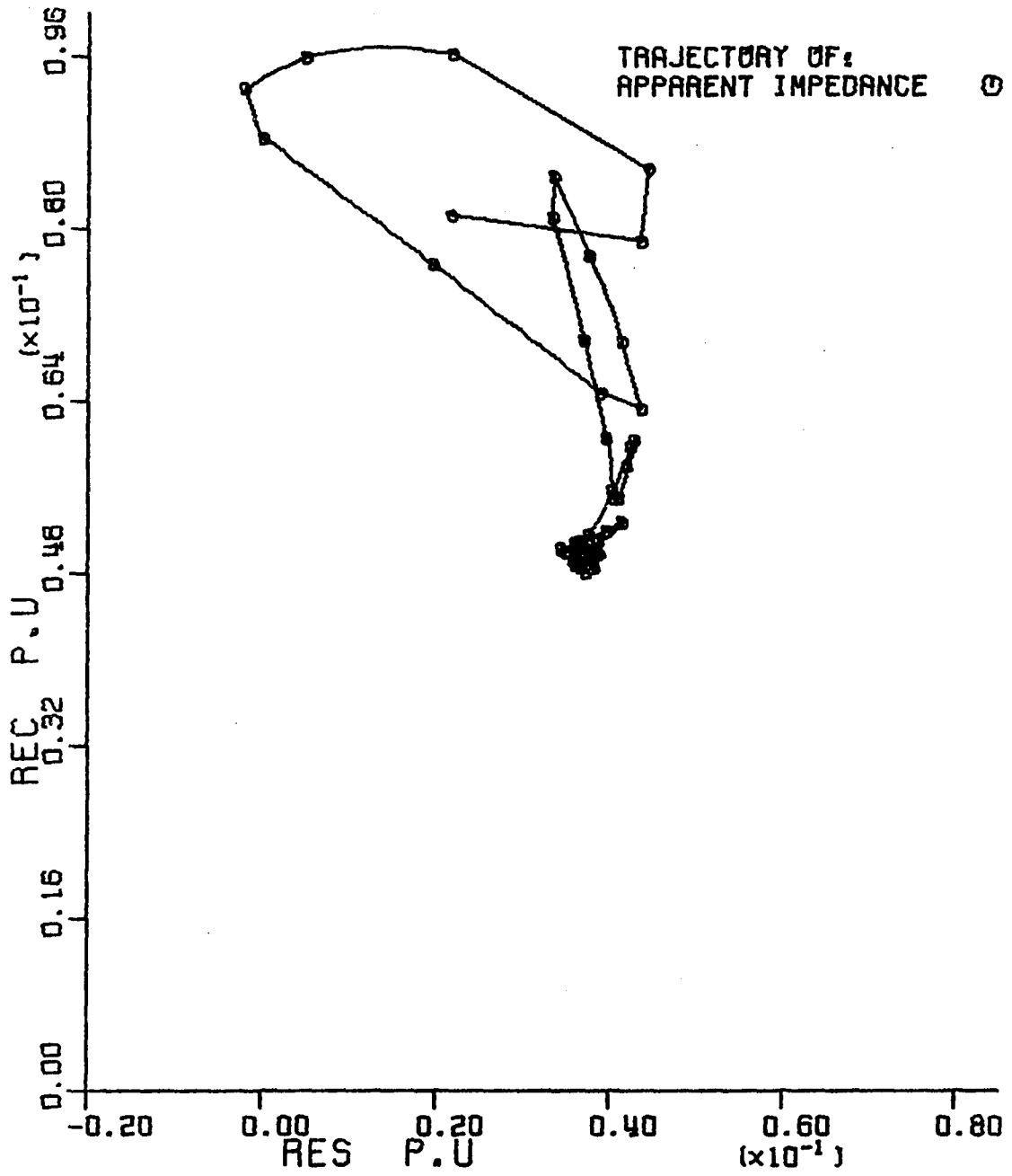Figure 7.21. Apparent resistance and apparent reactance
for BCG fault at 90 miles

Figure 7.22. Trajectory of apparent impedance
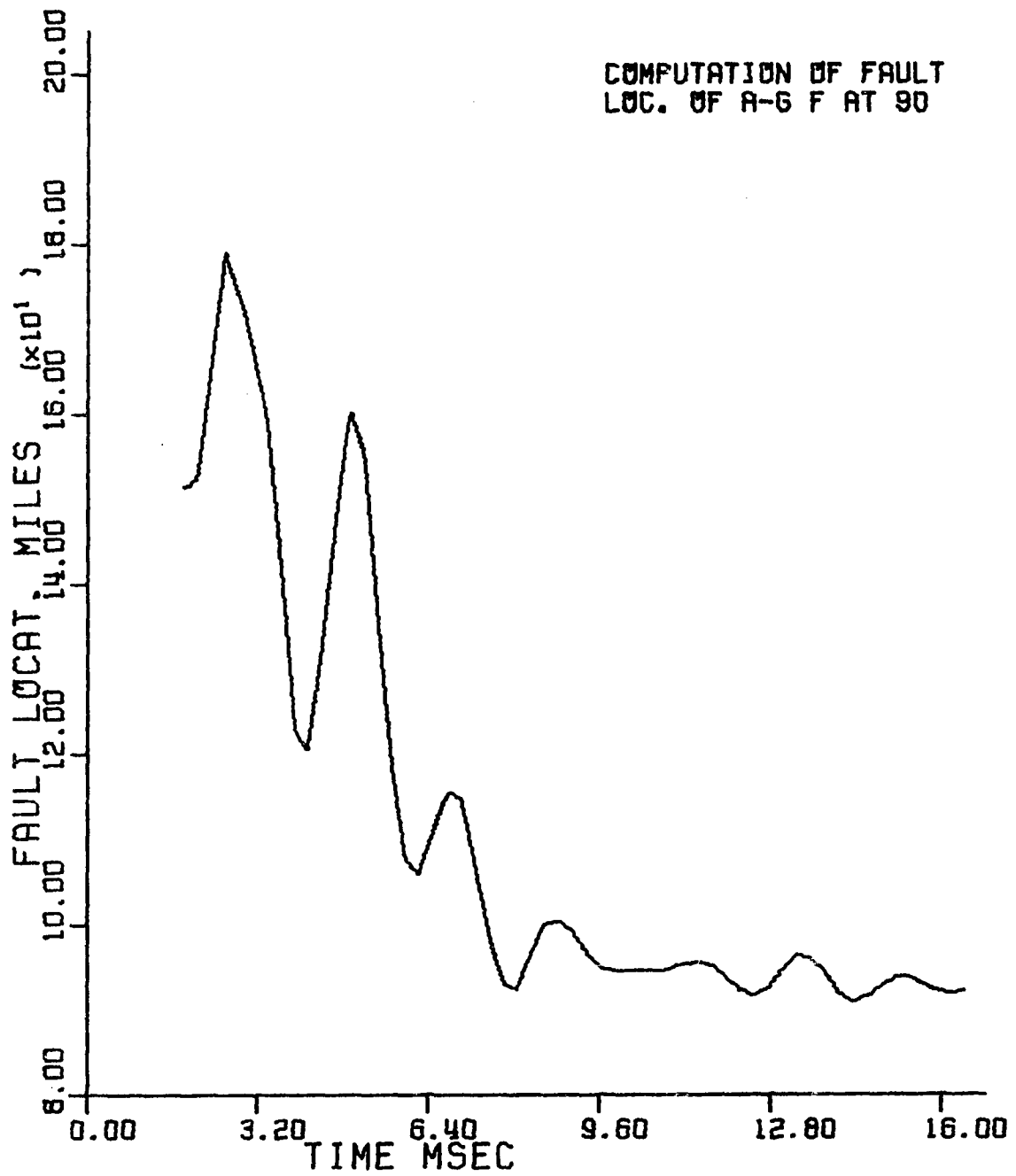for BCG fault at 90 miles

Figure 7.23. Computation of fault location
for BCG fault at 90 miles

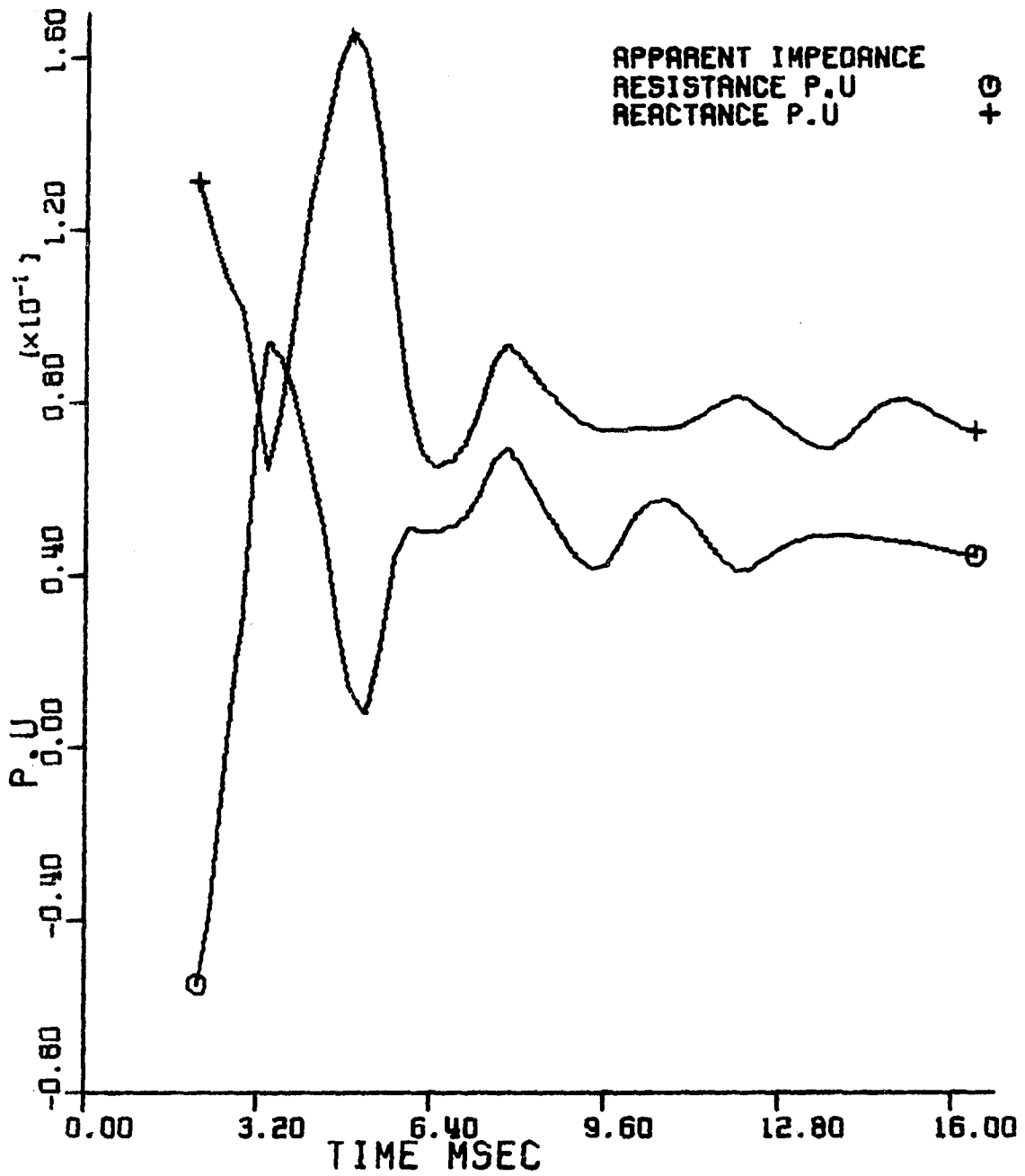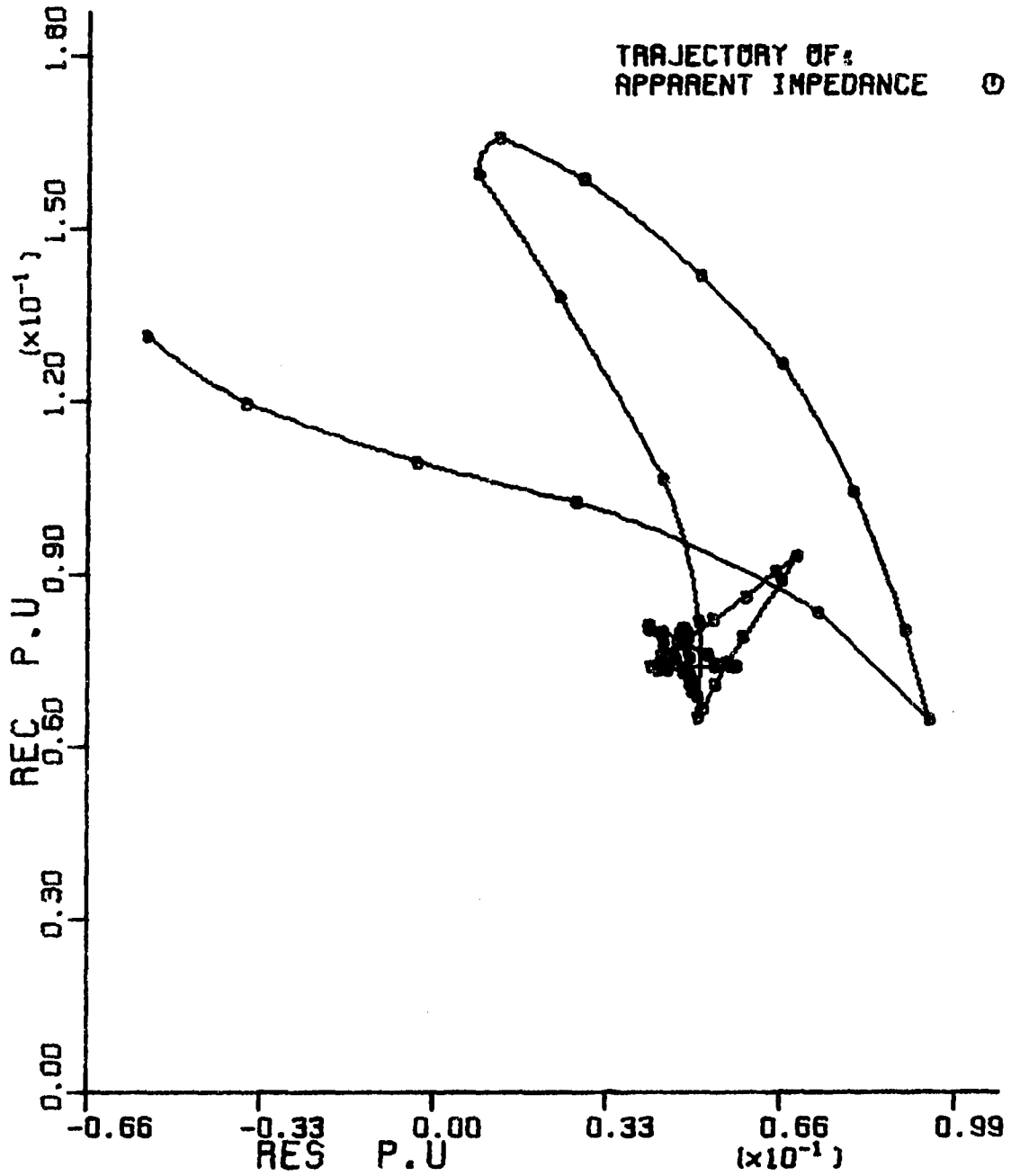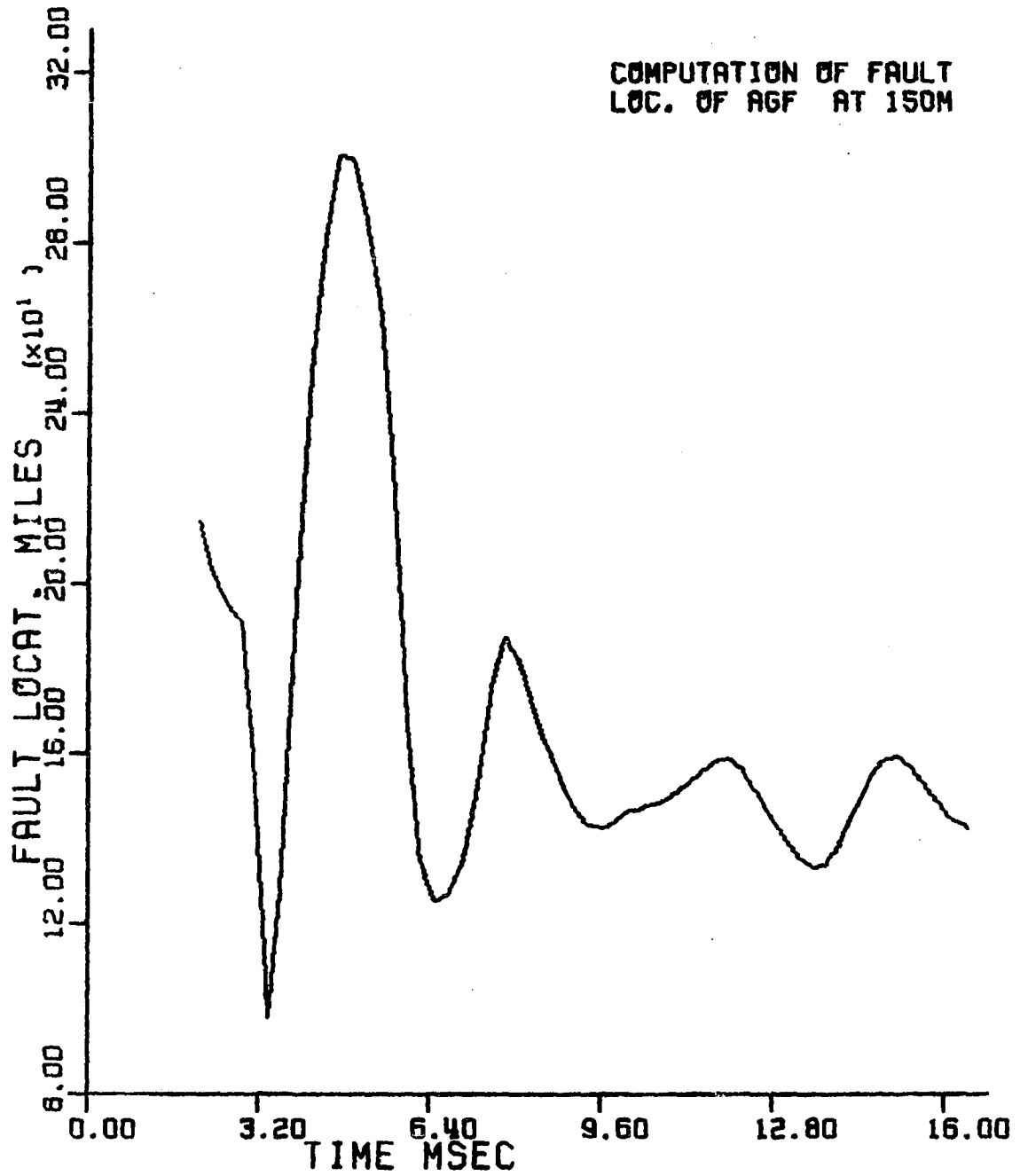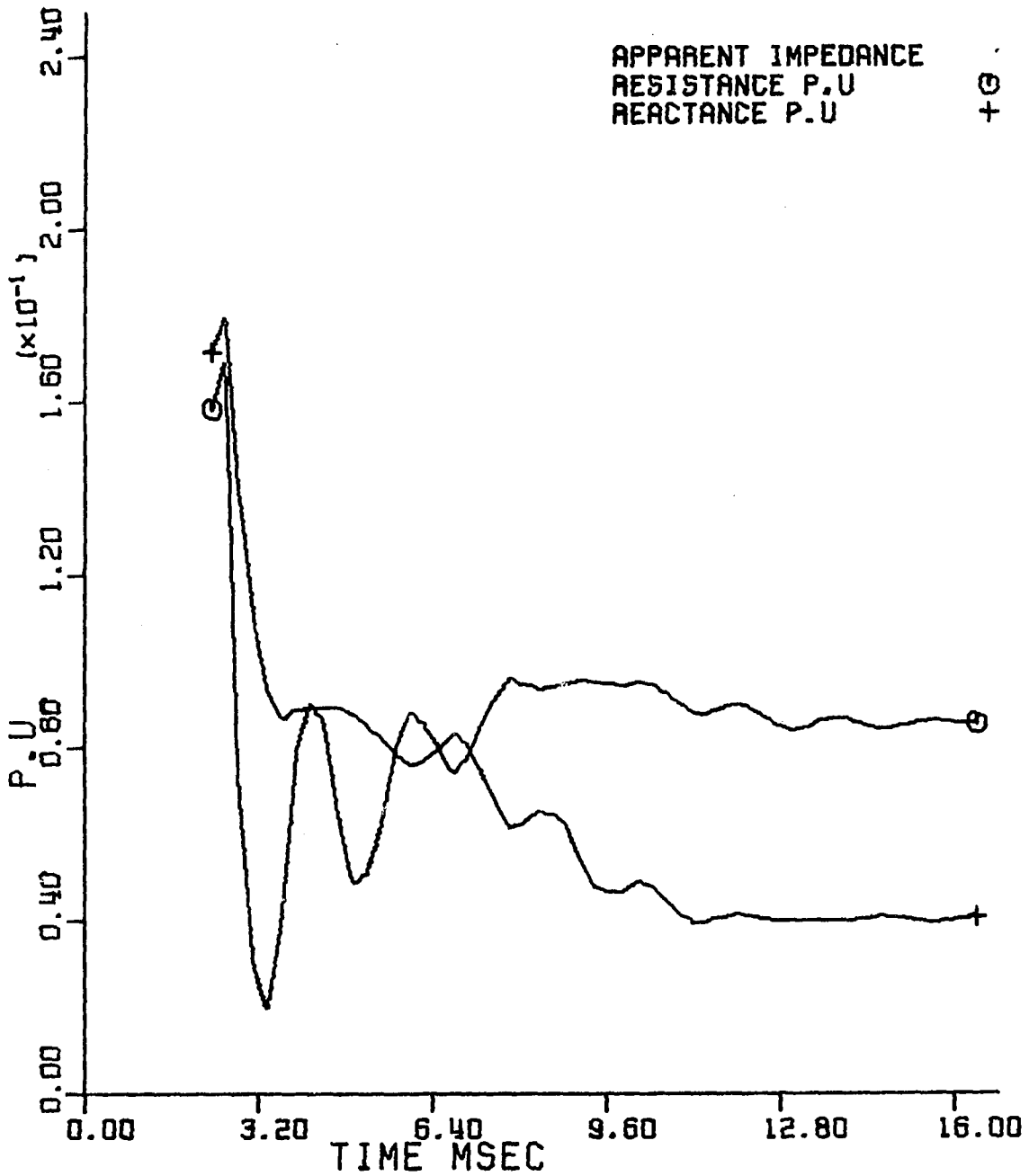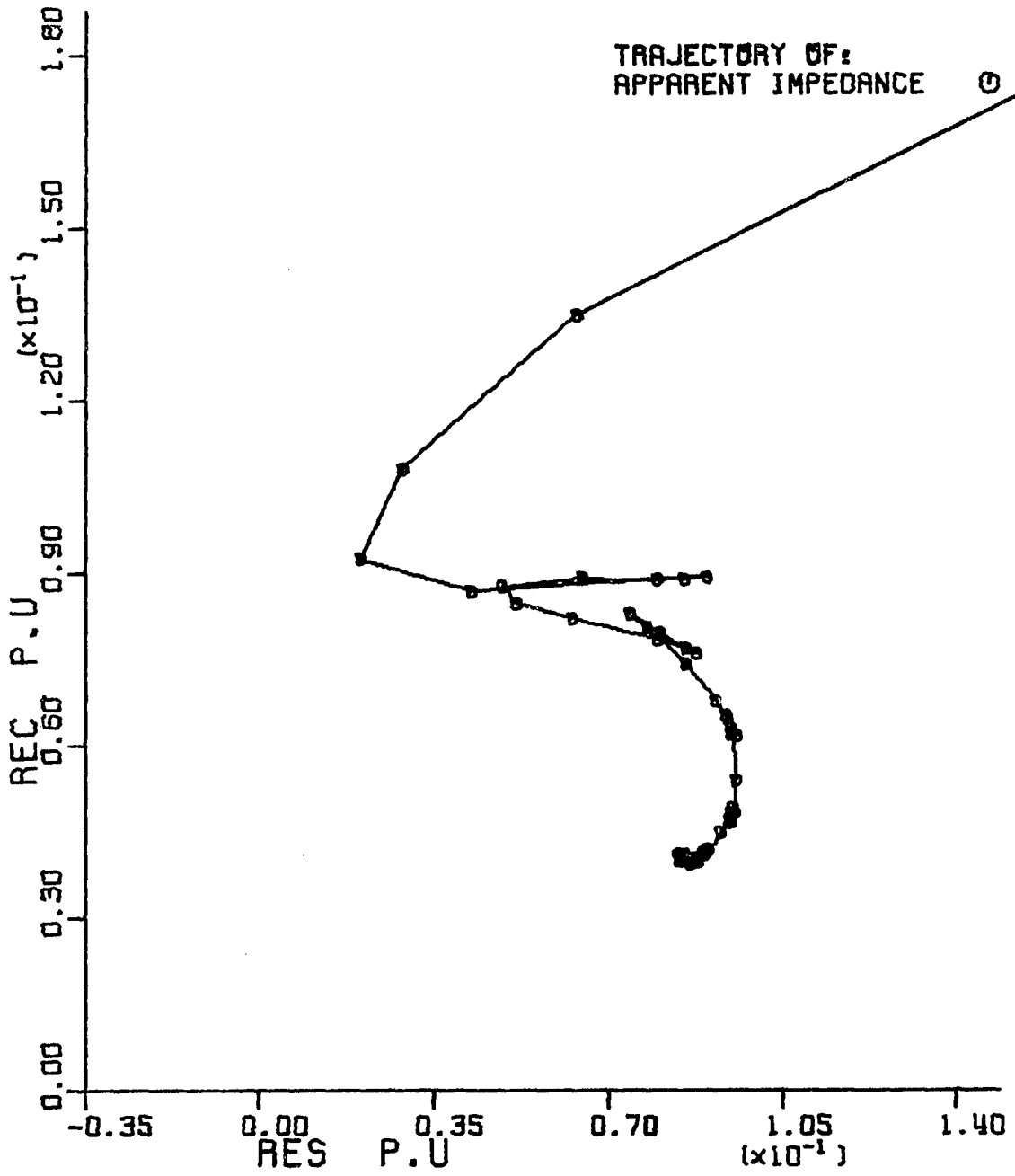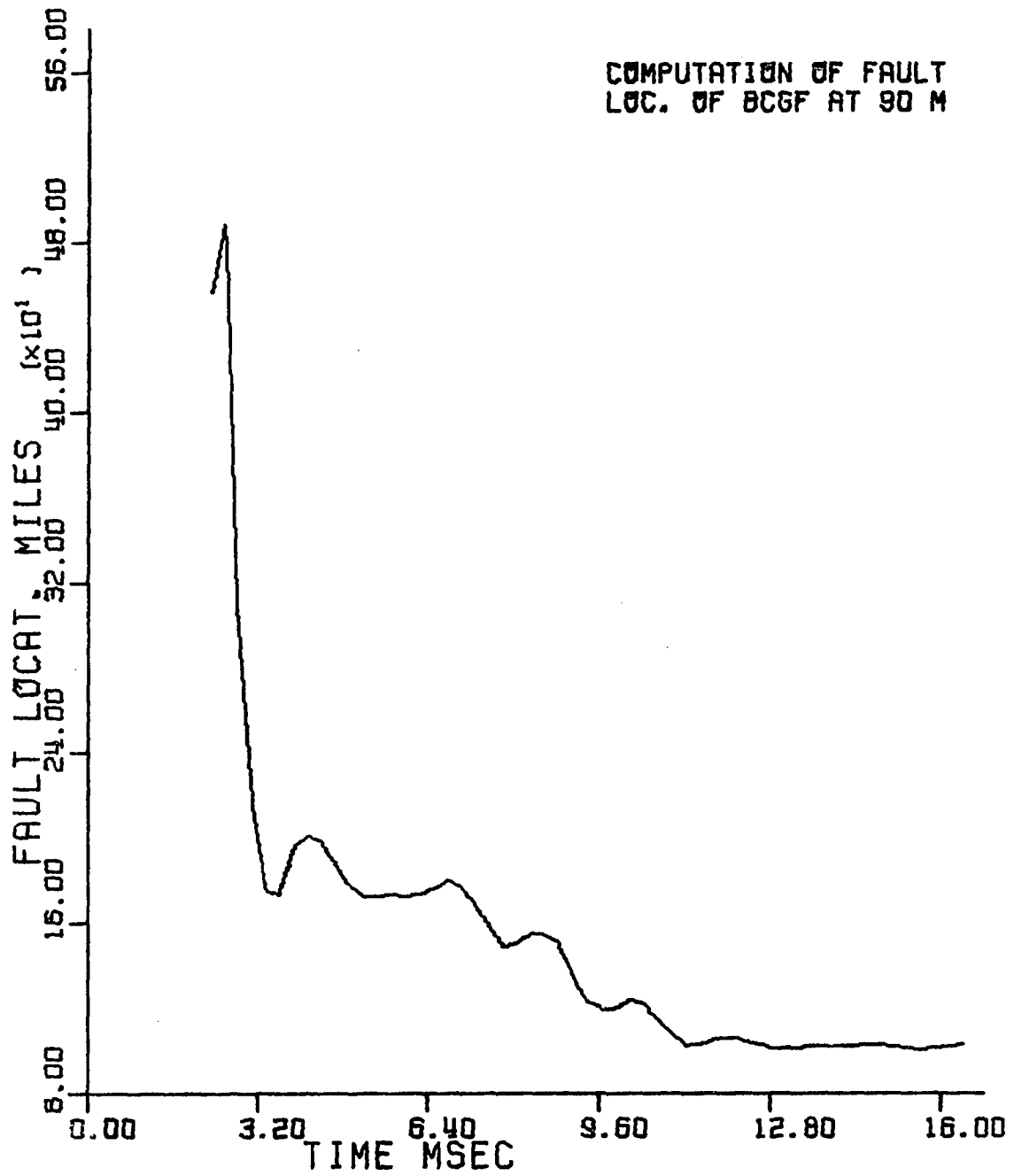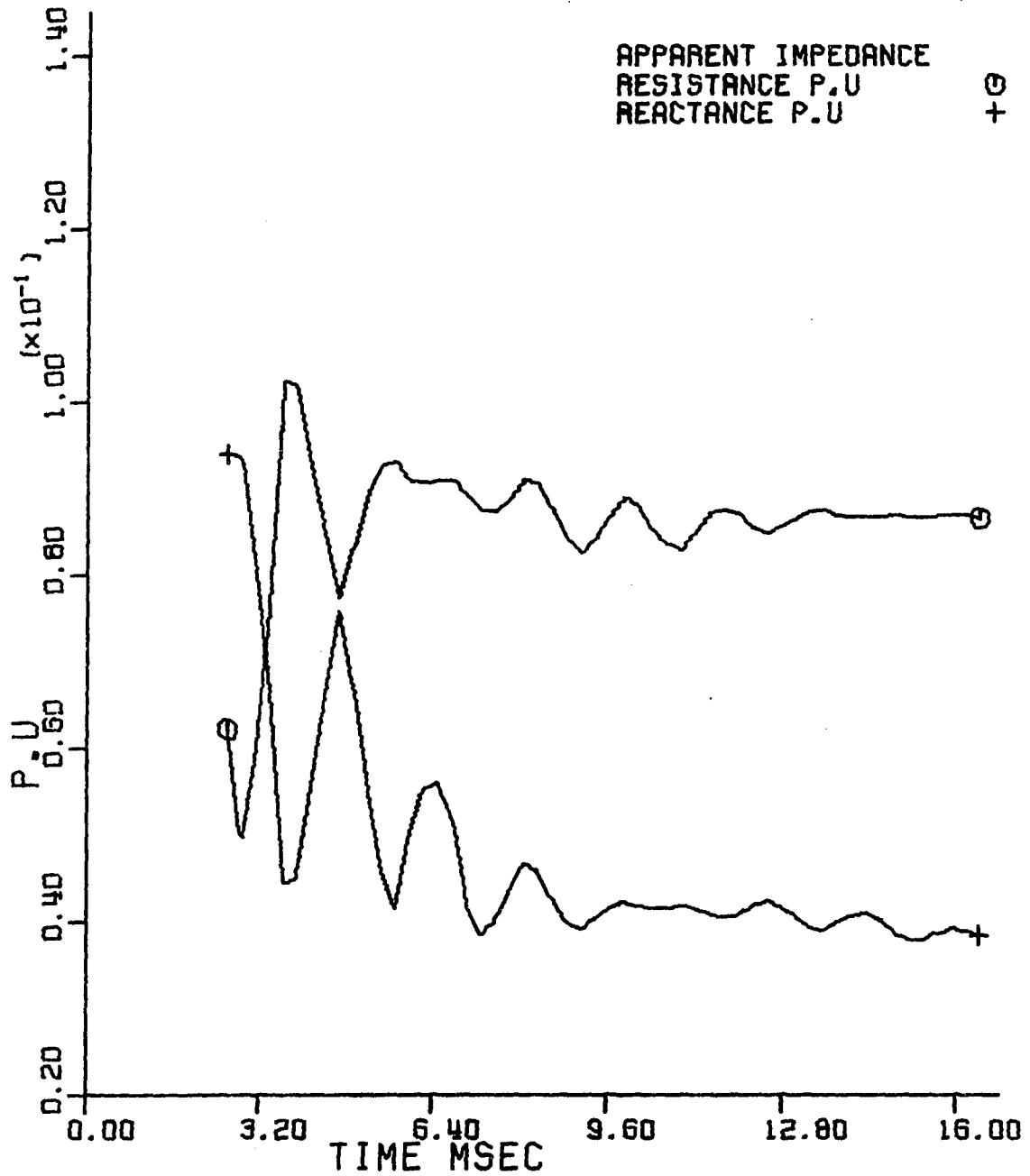Figure 7.24. Apparent resistance and apparent reactance
for three-phase fault at 90 miles
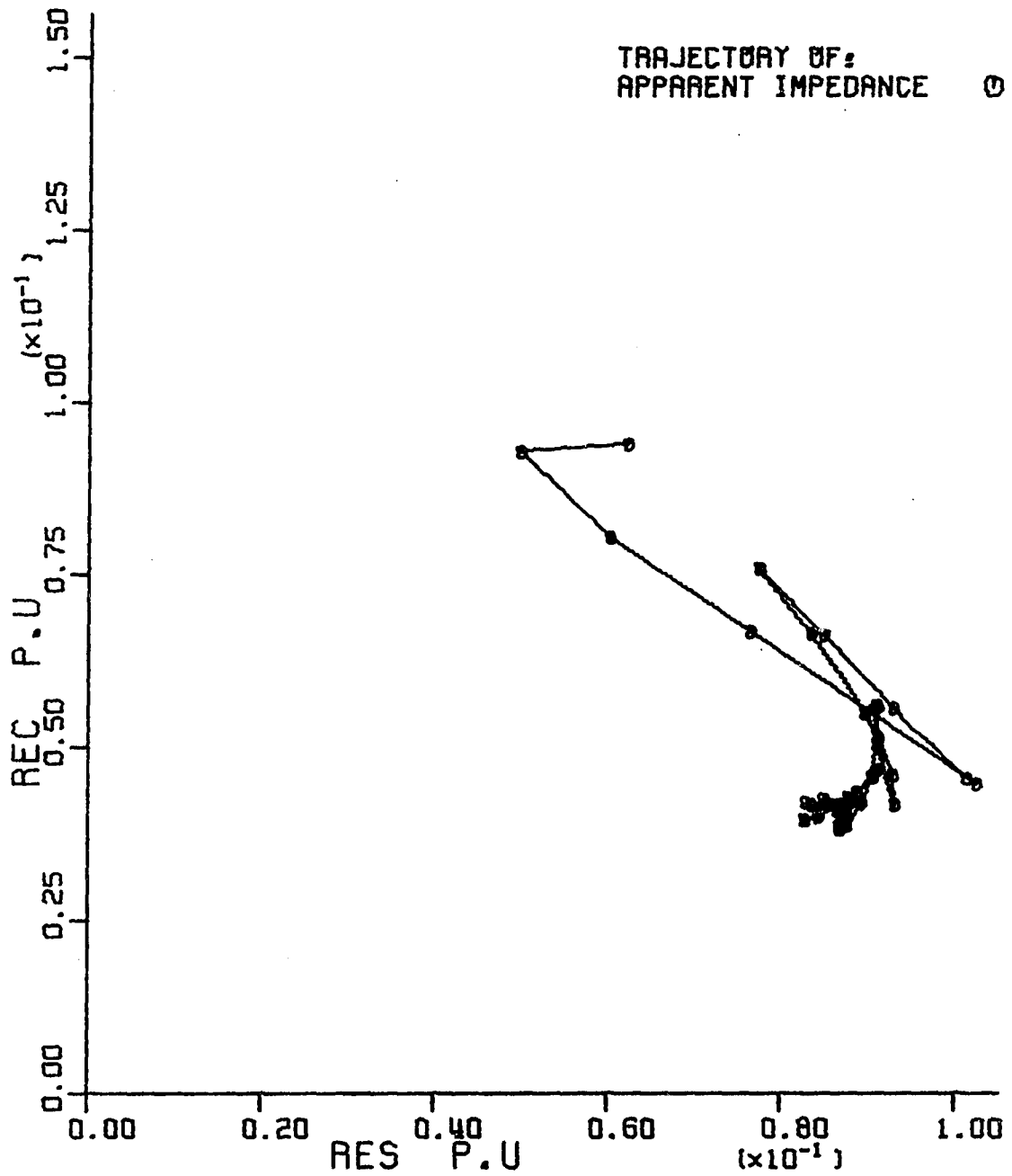
Figure 7.25. Trajectory of apparent impedance
for three-phase fault at 90 miles
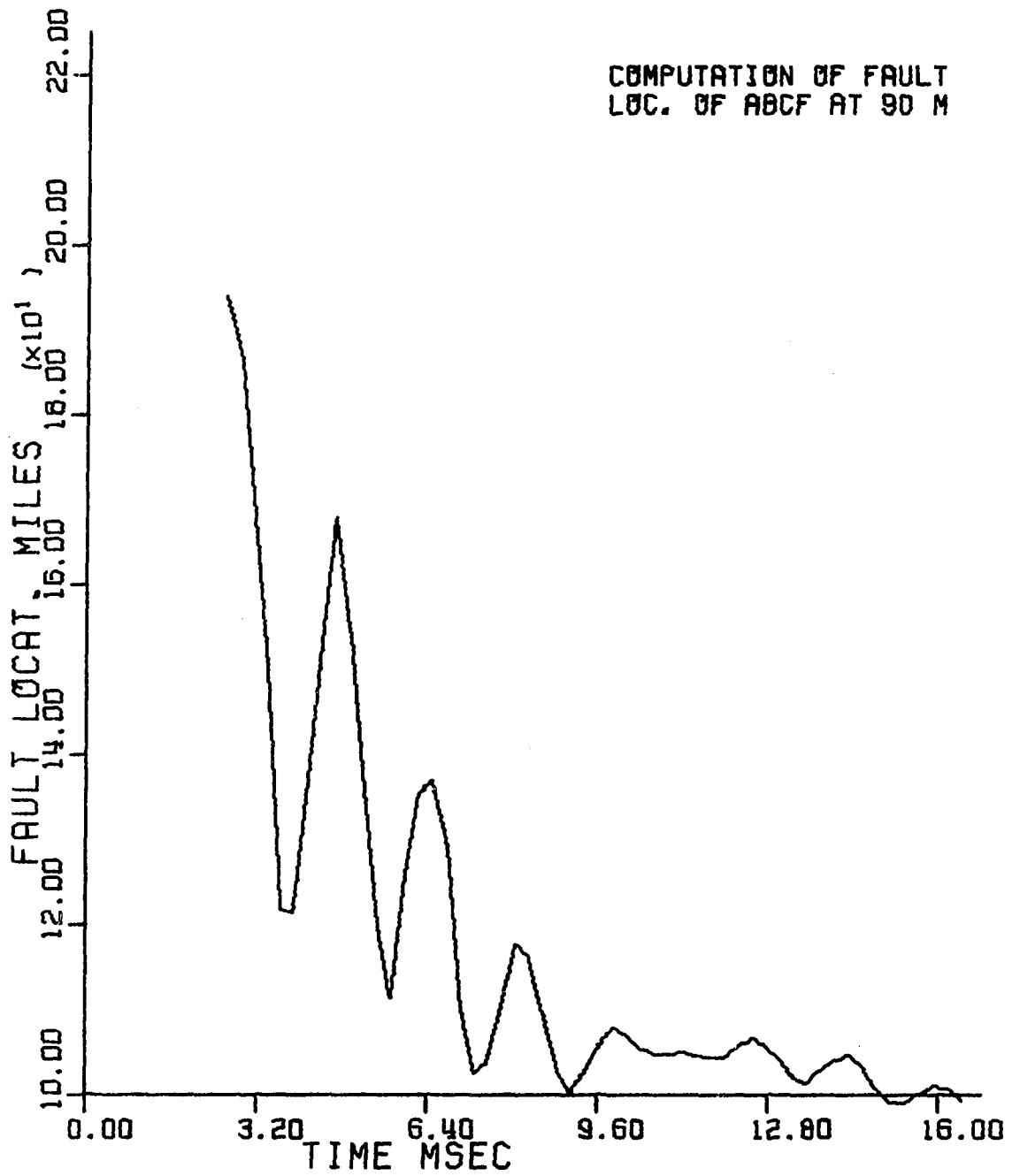
Figure 7.26. Computation of fault location for three-phase fault at 90 miles

VIII. COMPARISON OF KALMAN FILTERING-BASED SCHEME WITH OTHER TECHNIQUES AND DISCUSSIONS

As previously mentioned in Chapter II, the topics of digital computer relaying in general and digital transmission line relaying in particular have been the subject of a large number of papers over the last ten years. Four algorithms were selected to be compared with the technique presented in this work. Three of these algorithms have received national acceptance and were implemented in computer relaying projects by large industrial firms in the United States. The fourth algorithm was recently published. These algorithms are discussed in detail in Chapter II and will be briefly mentioned here.

The first algorithm was implemented by Gilcrest, Rockefeller, and Udren (19). The algorithm was used by Westinghouse in its joint project with Pacific Gas and Electric and is designated as "PRODAR 70." The project has been in research, evaluation, and test since 1971. Equations (2.6, 2.7, and 2.8) indicate how the phasor quantities are computed.

The second algorithm is based on the solution of the line differential equation (equation 2.14). The algorithm was implemented by General Electric Co. - Philadelphia computer relaying joint project (26,27). The derivation of the algorithm is shown in Appendix C.

These two algorithms are highly sensitive to the high frequency components; thus, they require prefiltering of the data.

The third algorithm uses the discrete Fourier transform to extract the fundamental components of the current and voltage. This

algorithm was implemented by American Electric Power Co. in their computer relaying project (62).

The fourth algorithm was recently published and it suggests representing the line by a single PI section (28). Using the current and voltage samples of the faulted phase(s), assuming that the type of fault is known to the relay, the algorithm computes R and L of the line up to the fault. The model equation is given in (2.23); the derivation of the algorithm is explained in Appendix C.

A digital filter was designed to prefilter the data used with the first two algorithms. The digital filter is a nonrecursive FIR digital filter that uses a trapezoidal window truncated by a Hanning window. The advantage of the nonrecursive FIR digital filter is that coefficient truncation cannot cause instability as it might with the recursive filter since the latter involves feedback. A combination of a trapezoidal window and a Hanning window was used to reduce the sidelobes in the frequency domain and to achieve a reasonable time response.

For more details of design of digital filters see Childers and Durling (72). The impulse response and the frequency response are shown in Figures 8.1 and 8.2. Identical digital filters were used to filter all the currents and all the voltages. Figures 8.3 through 8.5 show the filtered and unfiltered waveform of the voltage of the faulted phase and currents in the faulted phase and unfaulted phase respectively.

A. Test Results of the Comparison

The first (PRODAR 70) and the third (DFT) algorithms estimate first the phasor quantities of the currents and voltages, then use the selected

Figure 8.1. Impulse response of the FIR digital filter
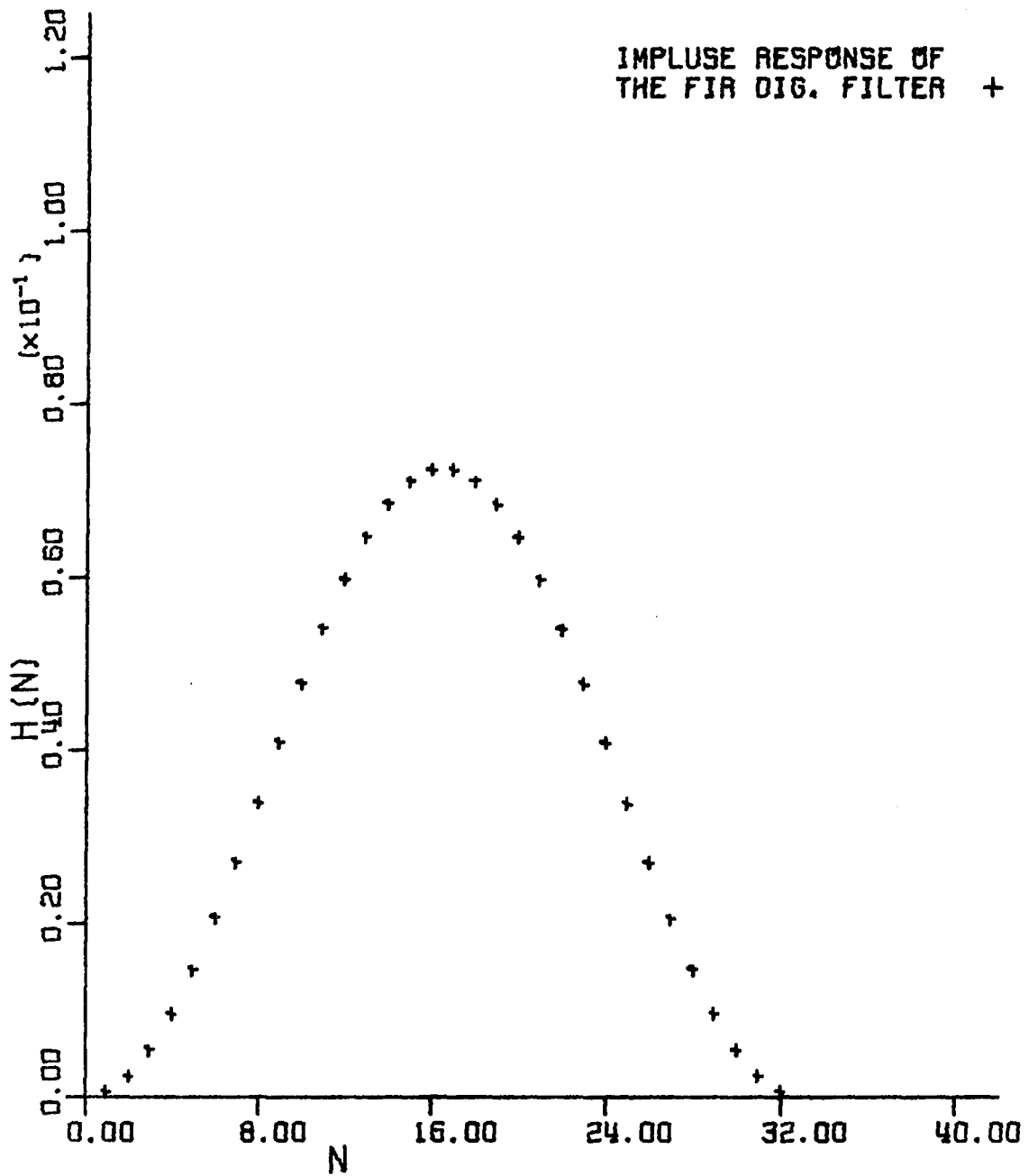used with PRODAR 70 and G.E. algorithms
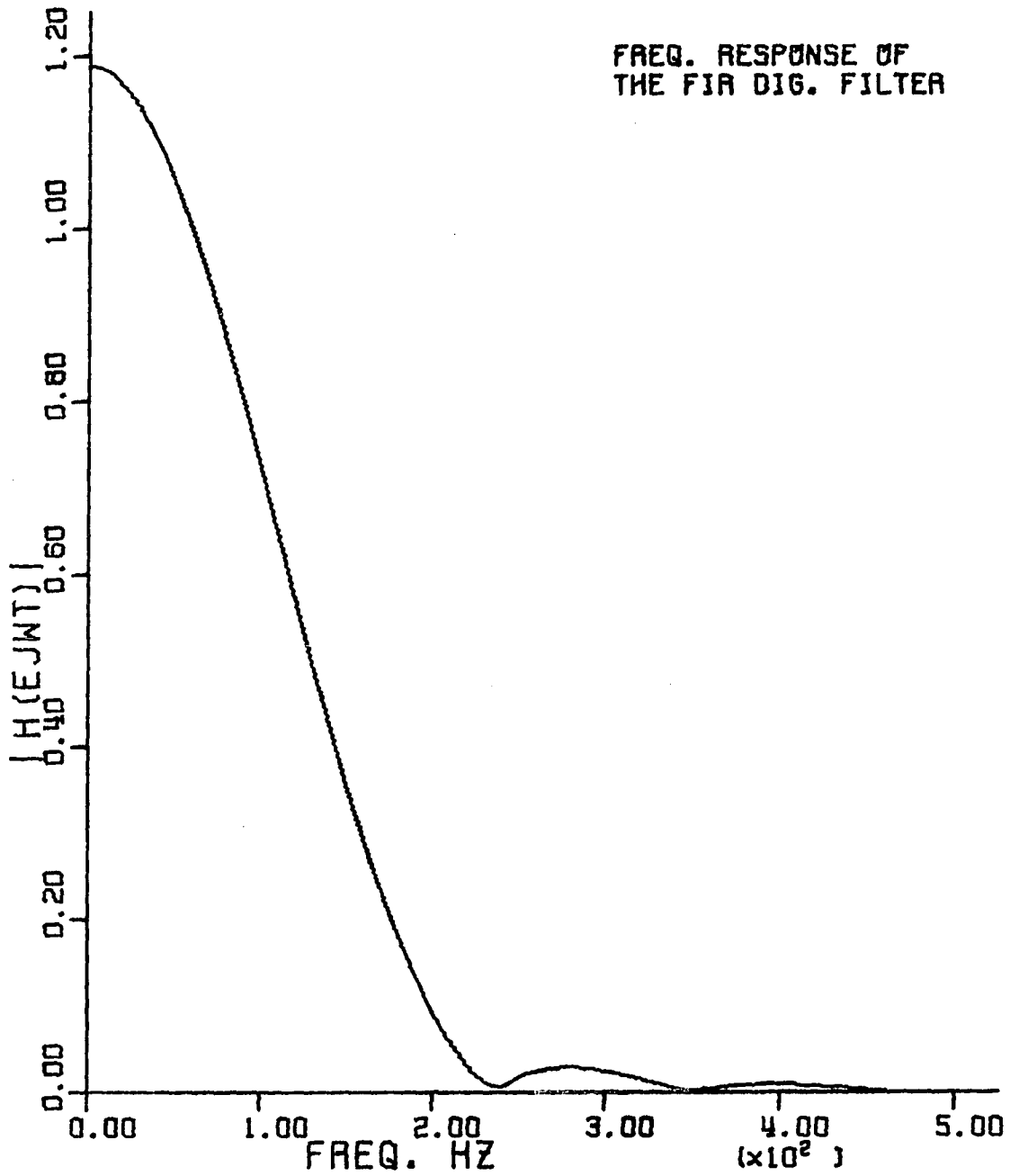
Figure 8.2. Frequency response of the FIR digital filter
used with PRODAR 70 and G.E. algorithms
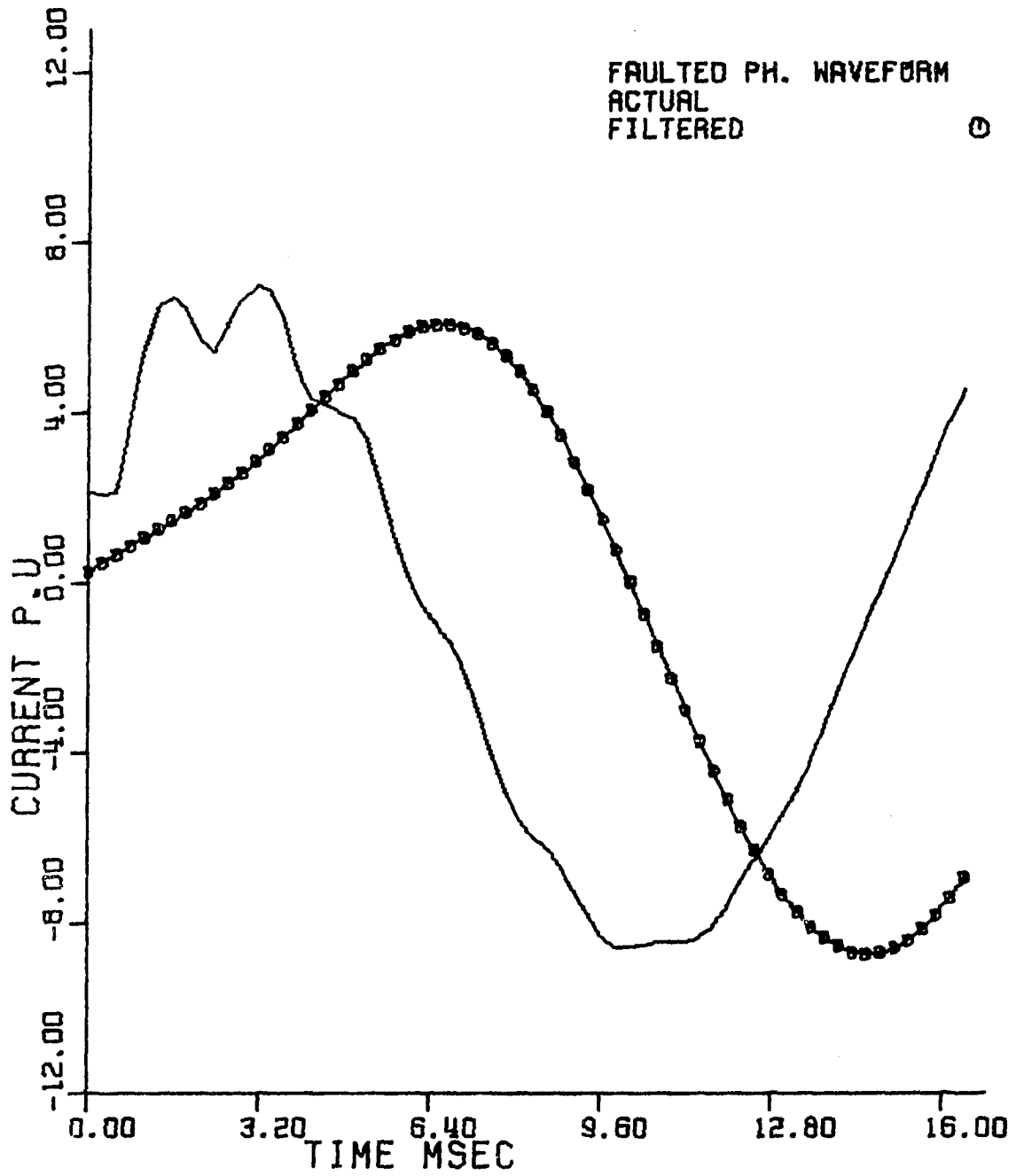
Figure 8.3. Actual and filtered current of Phase A
for AG fault at 90 miles
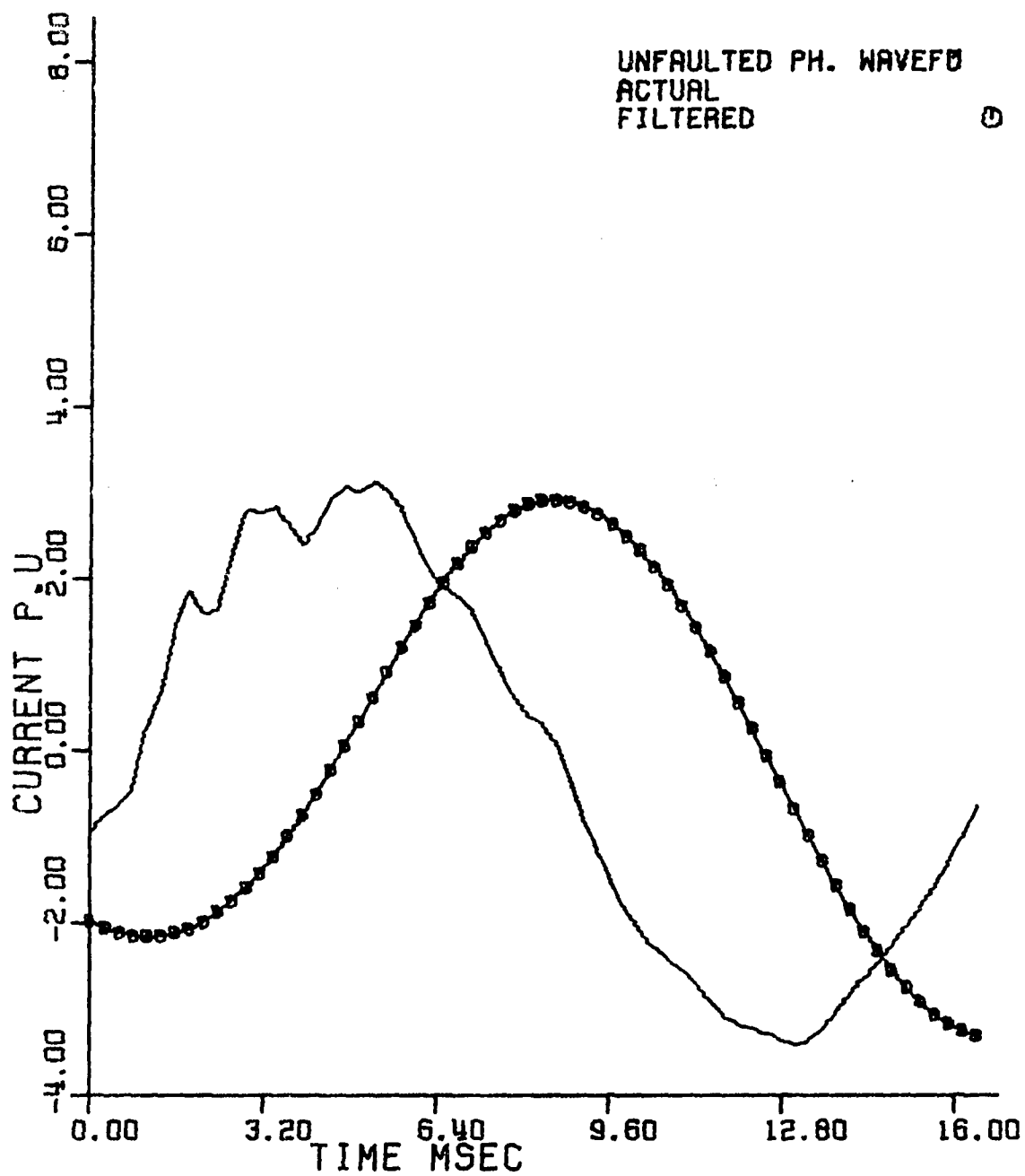
Figure 8.4. Actual and filtered current of Phase B
for AG fault at 90 miles
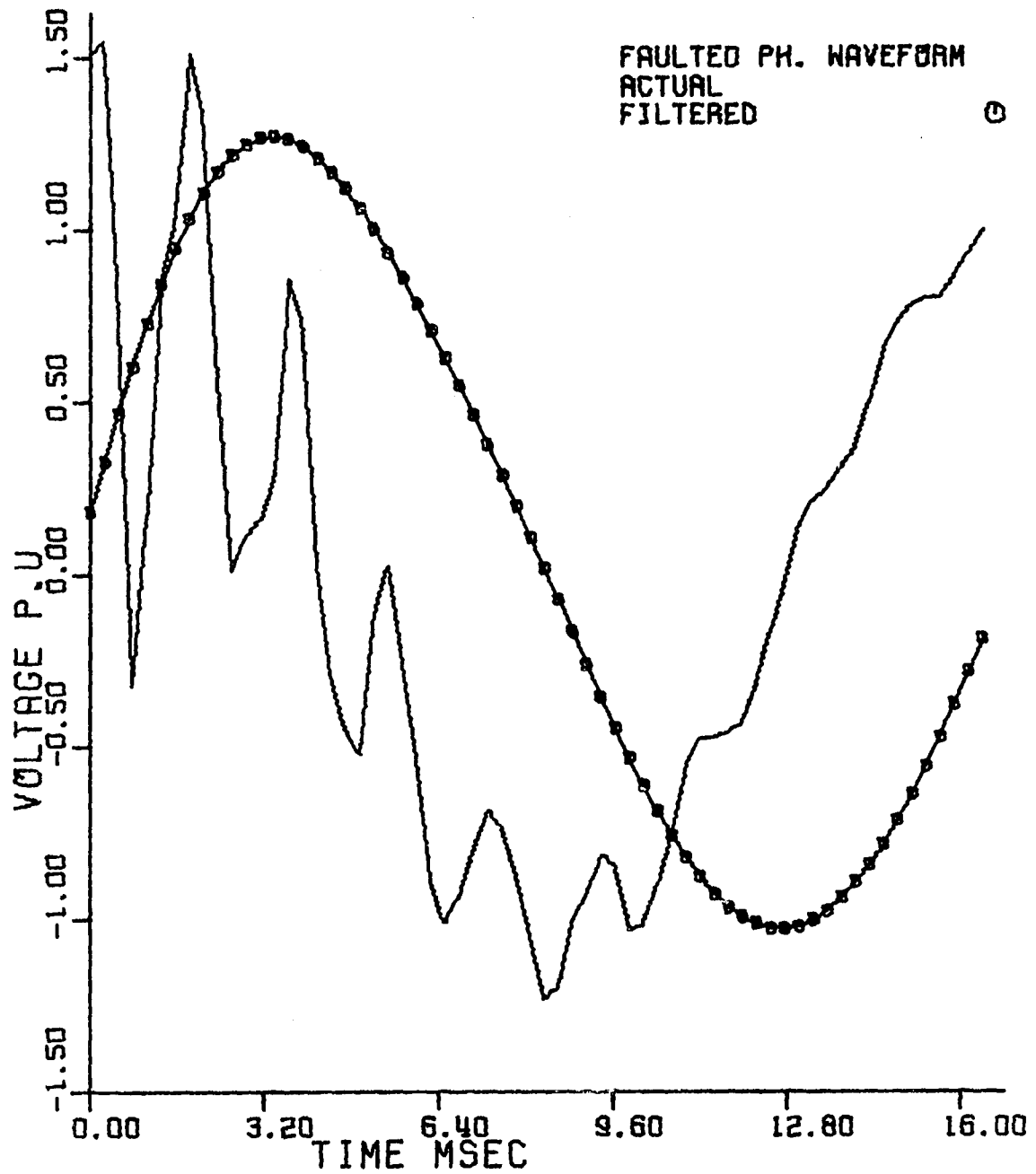
Figure 8.5. Actual and filtered voltage of Phase A
for AG fault at 90 miles

pair of voltage and current to compute the apparent impedance and fault location. The second (G.E.) and the fourth (PI model) algorithms use the samples of the selected voltage and current pair to compute the apparent impedance and the fault location.

The four reference algorithms and the Kalman filter algorithm were programmed by the author, and the magnitude of the estimated voltage of the faulted phase and the currents of the faulted phase, unfaulted phase, and the zero sequence were obtained for the first and third algorithms and compared with those obtained using the Kalman filter algorithm. Then the apparent resistance, apparent reactance, and fault location were computed using the four algorithms, and these were compared with the results of the Kalman-filtering-based algorithm. These results are shown in Figures 8.6 and 8.38 for faults at 30 miles, 90 miles, and 150 miles respectively.

The shown results indicate that the Kalman-filtering-based algorithm converges faster than the discrete Fourier transform and the PRODAR 70 algorithm in estimating the phasor quantities of voltage and current in the faulted or unfaulted phases for all fault locations. This faster convergence is due to the realistic modelling of the voltage and current noise signals and the states to be estimated in the Kalman-filtering-based algorithm. Moreover, the Kalman-filtering-based algorithm converges to the exact post-fault values with steady state error of about 1 percent after half a cycle and less than 0.2 percent after a complete cycle. The discrete Fourier transform showed an error of about 5 percent after a complete cycle.

This error in the half-cycle discrete Fourier transform algorithm is due to the assumption that any non-60 Hz component is an odd harmonic. The PRODAR 70 algorithm gave results less accurate than the discrete Fourier transform algorithm in the first three quarters of a cycle, but it was comparable with the discrete Fourier transform after 12 msec for faults less than 100 miles. The fluctuations in the estimated current or voltage were too high in the PRODAR 70 algorithm for a fault at 150 miles. This is due to the high sensitivity of the PRODAR 70 algorithm to high frequency components because of the double differentiation in the algorithm.

Although a low pass filter was accurately designed for the PRODAR 70 algorithm, all the high-frequency components (300 Hz or less) would not be completely rejected. In an evaluation of this algorithm, it was reported (73) that a 5 percent fifth harmonic (300 Hz) would introduce more than 200 percent error in the estimated phasors. The investigators who implemented the PRODAR 70 algorithm suggested post-calculation smoothing for more than one cycle to avoid false decisions.

The second (GE) and the fourth (PI model) algorithms assume that the fault type has been correctly classified and the appropriate current and voltage pair are used to compute the apparent resistance, apparent reactance, and fault location.

Examining the computed values of the apparent resistance, apparent reactance, and fault location using the mentioned four algorithms and the Kalman-filtering-based algorithm, the following remarks are in order:

1. For a fault at 30 miles, the computed values of the apparent
    resistance, apparent reactance, and fault location using the
    PRODAR 70 algorithm were relatively accurate after 12 msec.
    This in turn is due to the relatively pure sinusoidal waveform
    (filtered) used in the algorithm. The G.E. algorithm computed
    the reactance with 10 percent error which may be considered an
    over-reach of 10 percent in the relay zone.

    The results obtained using the PI model algorithm fluctuate
    widely in the first half cycle after the fault occurrence. The
    fluctuations seem to decrease exponentially. This is because
    the high frequency components decrease exponentially. These
    fluctuations were extremely high when a sampling rate of 64
    samples per cycle was used. Therefore, it was decided to use a
    sampling rate of 32 samples per cycle in the PI model algorithm
    to have comparable results. Also, the DFT algorithm gave a
    smaller reactance by more than 10 percent and consequently a
    fault location shorter, by about 10 percent, than the exact
    fault location.

2. For a fault at 90 miles, the fluctuations increased in the G.E.
    algorithm, the PRODAR 70 algorithm, and the PI model algorithm.
    The PRODAR 70 algorithm has higher fluctuations than the G.E.
    algorithm. This again is due to the double differentiation
    process in the PRODAR 70 algorithm. The PI model algorithm
    introduced the highest fluctuations in the computed values.
    This is not only due to the double differentiation in the PI

model algorithm, but also due to the high frequency components in the current and voltage waveforms. The computed fault location using the DFT algorithm was 12 percent lower than the exact value. It should be noted here that the computed fault location using the Kalman-filtering-based algorithm was fluctuating between 98 and 102 of the exact value after half a cycle.

3. For a fault at 150 miles, the fluctuations in the computed values increased in all the algorithms including the Kalman-filtering-based algorithm. However, the Kalman-filtering-based algorithm has the least fluctuations and the least steady state error. The G.E. algorithm had the largest steady state error, and the PRODAR 70 had the highest fluctuations excluding the PI model algorithm which gave errors more than 500 percent and even a non-discriminating characteristic (negative value for the fault location).

The advantage of the Kalman-filtering-based algorithm is not only the expeditious rate of convergence of the estimated states to the exact values, but also the low computer burden of the computations involved. The three-state Kalman filter requires only seven multiplications and divisions plus six additions and subtractions to compute the two states of the current, provided that the covariance is computed off line and stored in the memory. As a comparison with the computer burden of the other techniques, the half-cycle DFT algorithm requires N multiplications and N additions to compute the required states. Considering the lowest sampling rate used in computer relaying (12 samples/cycle), the

DFT algorithm requires 12 multiplications and 12 additions. The G.E. algorithm requires 9 multiplications and divisions plus 7 additions and subtractions (26) not including the digital filter computer burden. Moreover, it has been shown that the G.E. algorithm may be ill-conditioned, especially with full offset in the fault current. It was proven that the denominator of equations (14.1) and (14.2) (Appendix C) may tend to be zero (25). Finally, the PI model algorithm, which is the most recent technique, requires 54 multiplications and divisions plus 44 additions, subtractions, and shifting operations. It was reported (28) that the latter does not require analog or digital filtering, but it is evident from the shown test results that the algorithm also requires filtering.

In summary, it would be nice if the comparison of the four reference algorithms with the Kalman filter algorithm could be condensed to a table listing figures of merit for each algorithm. This does not appear to be possible in this case because of the time-varying behavior of the errors. One can simply conclude that on the average, from viewing the various simulations analyzed, the Kalman filter appears to be superior to the others, both in terms of speed of response and accuracy at any given time after the fault.

A listing of the Kalman filter program used to obtain these comparative results is shown in Appendix D.

Figure 8.6.   Recursive estimation of the voltage
magnitude of Phase A using the Kalman
filter, DFT, and PRODAR 70 algorithms

Figure 8.7. Recursive estimation of the current magnitude
in Phase A using Kalman filter, DFT, and
PRODAR 70 algorithms

Figure 8.8. Recursive estimation of the current magnitude
in Phase B using Kalman filter, DFT, and
PRODAR 70 algorithms

Figure 8.9. Recursive estimation of the current magnitude
in Phase C using Kalman filter, DFT, and
PRODAR 70 algorithms

Figure 8.10. Recursive estimation of the zero sequence current magnitude using Kalman filter, DFT, and PRODAR 70 algorithms

Figure 8.11. Computed apparent resistance using
Kalman filter, DFT, and PI model
algorithms

Figure 8.12. Computed apparent resistance using Kalman
filter, PRODAR 70, and G.E. algorithms

Figure 8.13. Computed apparent reactance using Kalman
filter, DFT, and PI model algorithms

Fiture 8.14.   Computed apparent reactance using Kalman
filter, PRODAR 70, and G.E. algorithms

Figure 8.15. Computed fault location using Kalman
filter, DFT, and PI model algorithms

Figure 8.16. Computed fault location using Kalman
filter, PRODAR 70 and G.E. algorithms
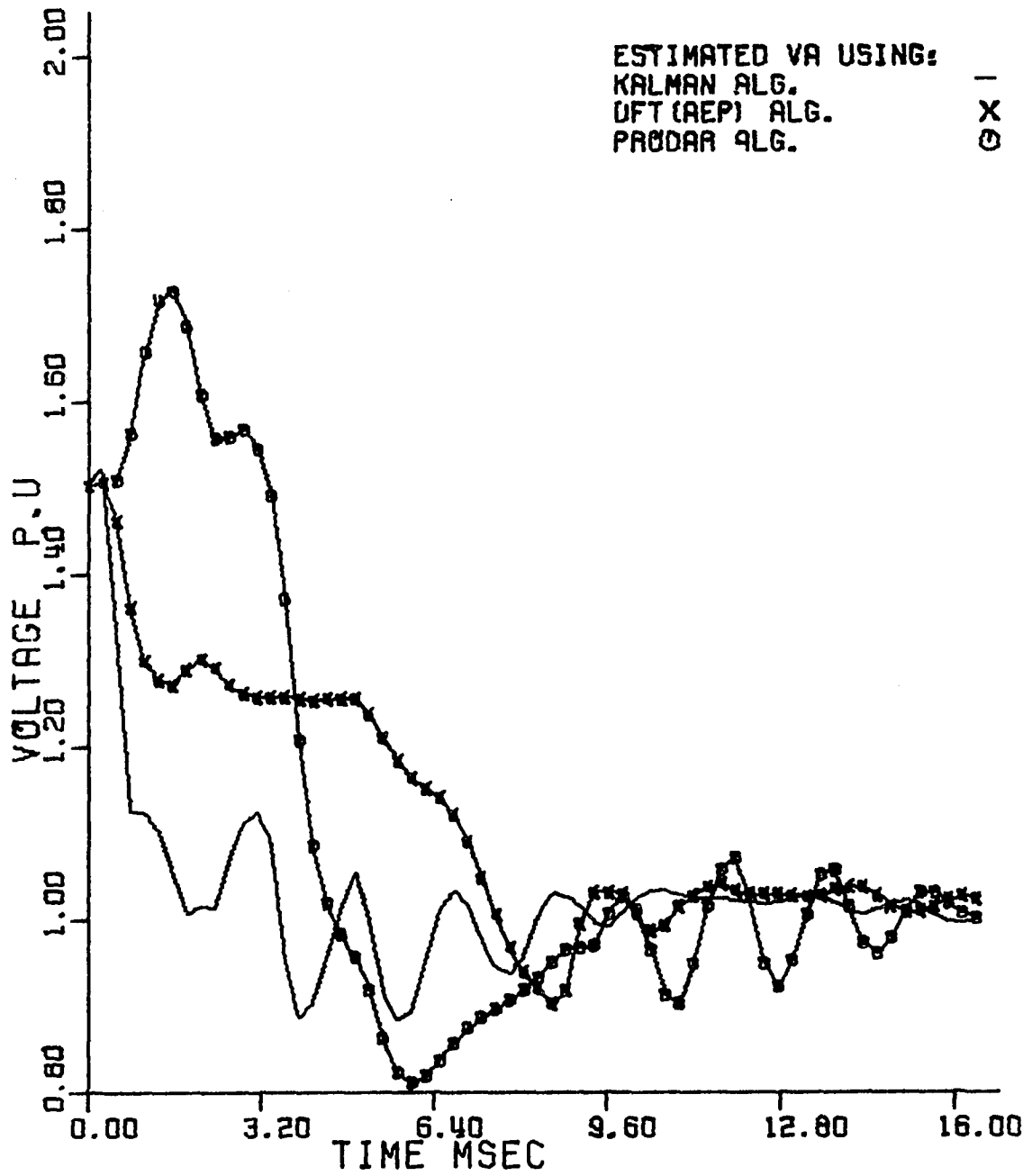
Figure 8.17. Recursive estimation of the voltage magnitude
of Phase A using Kalman filter, DFT, and
PRODAR 70 algorithms
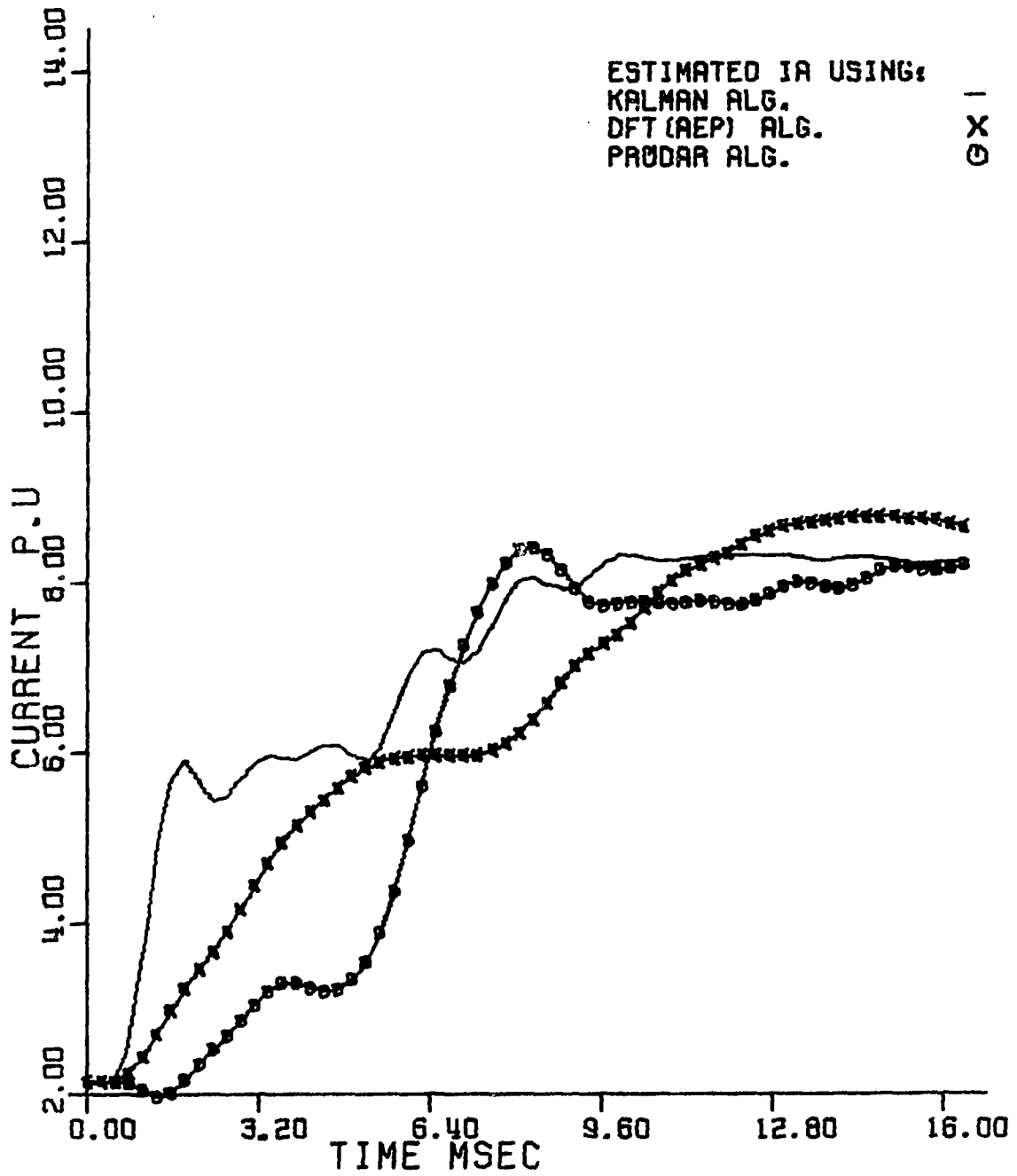
Figure 8.18. Recursive estimation of the current magnitude
in Phase A using Kalman filter, DFT, and
PRODAR 70 algorithms
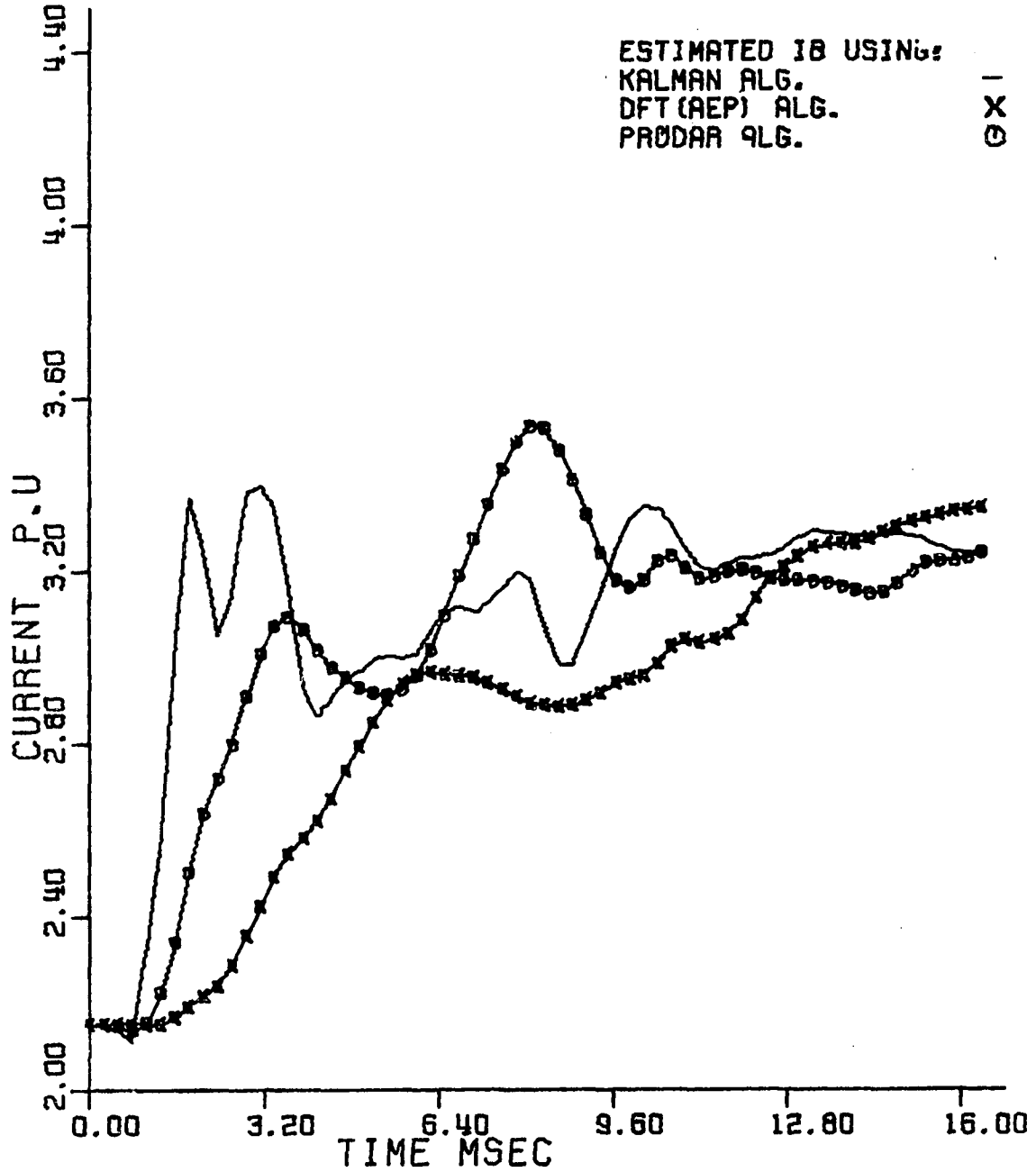
Figure 8.19. Recursive estimation of the current magnitude
in Phase B using Kalman filter, DFT, and
PRODAR 70 algorithms
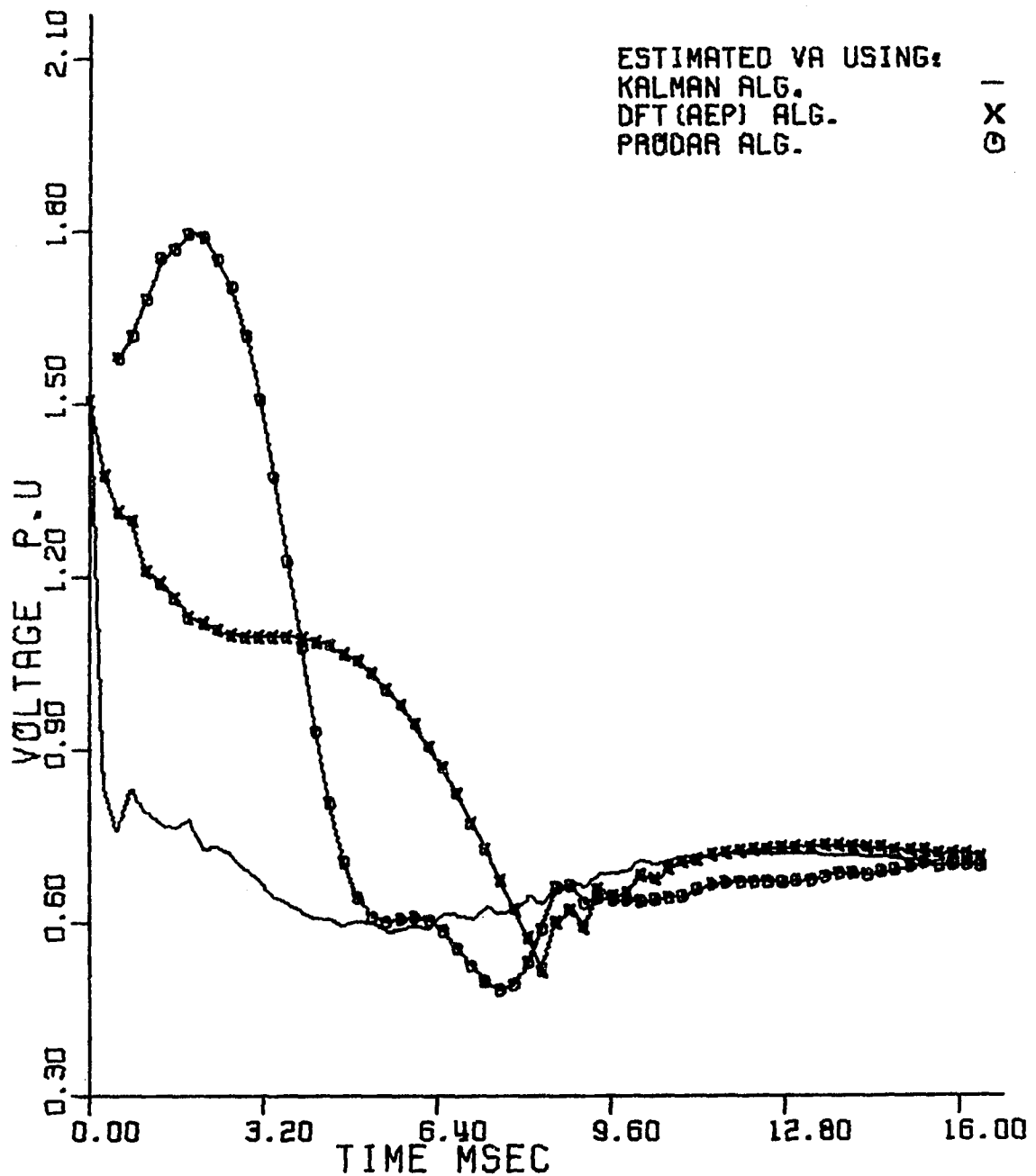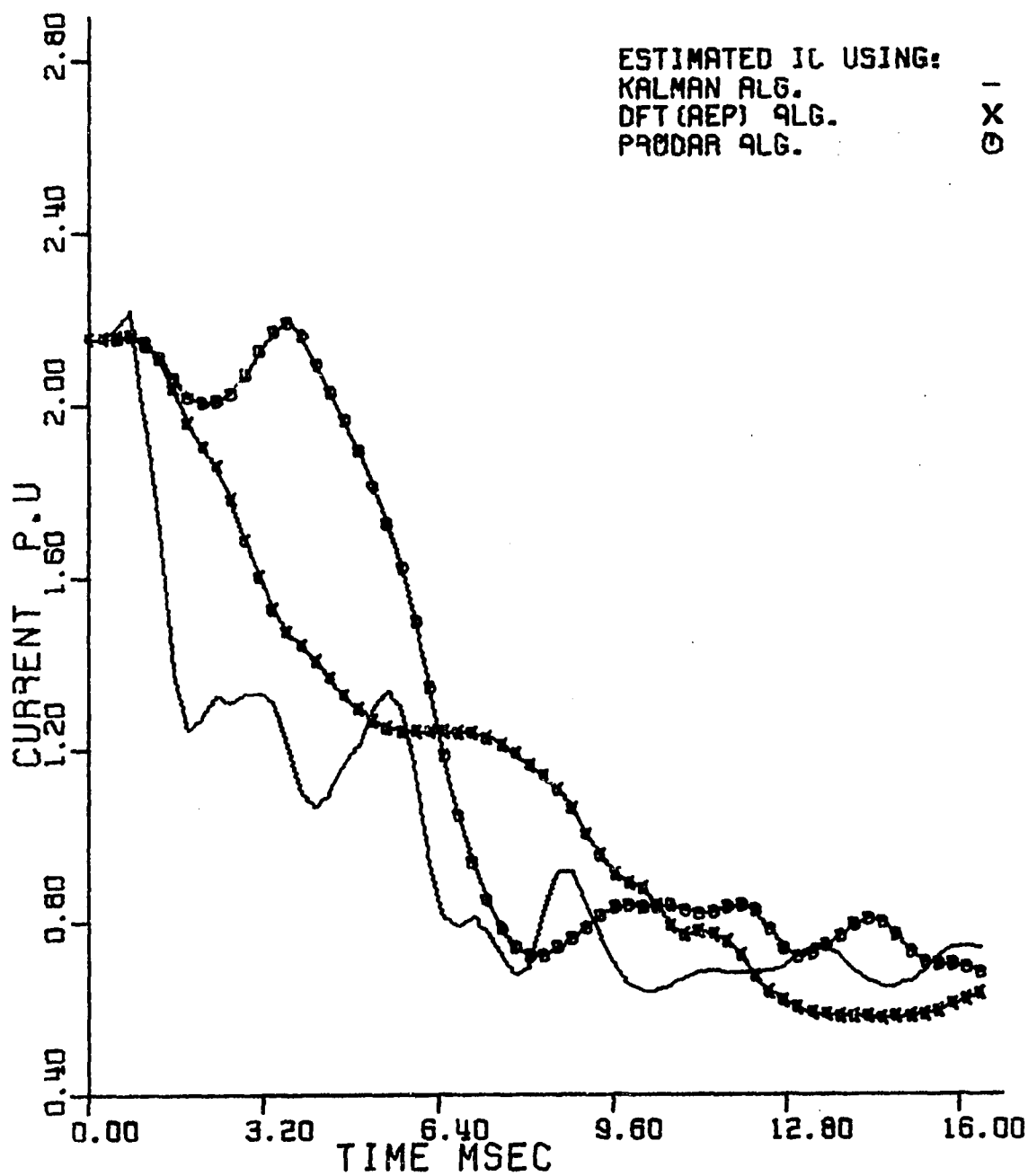
Figure 8.20. Recursive estimation of the current magnitude
in Phase C using Kalman filter, DFT, and
PRODAR 70 algorithms
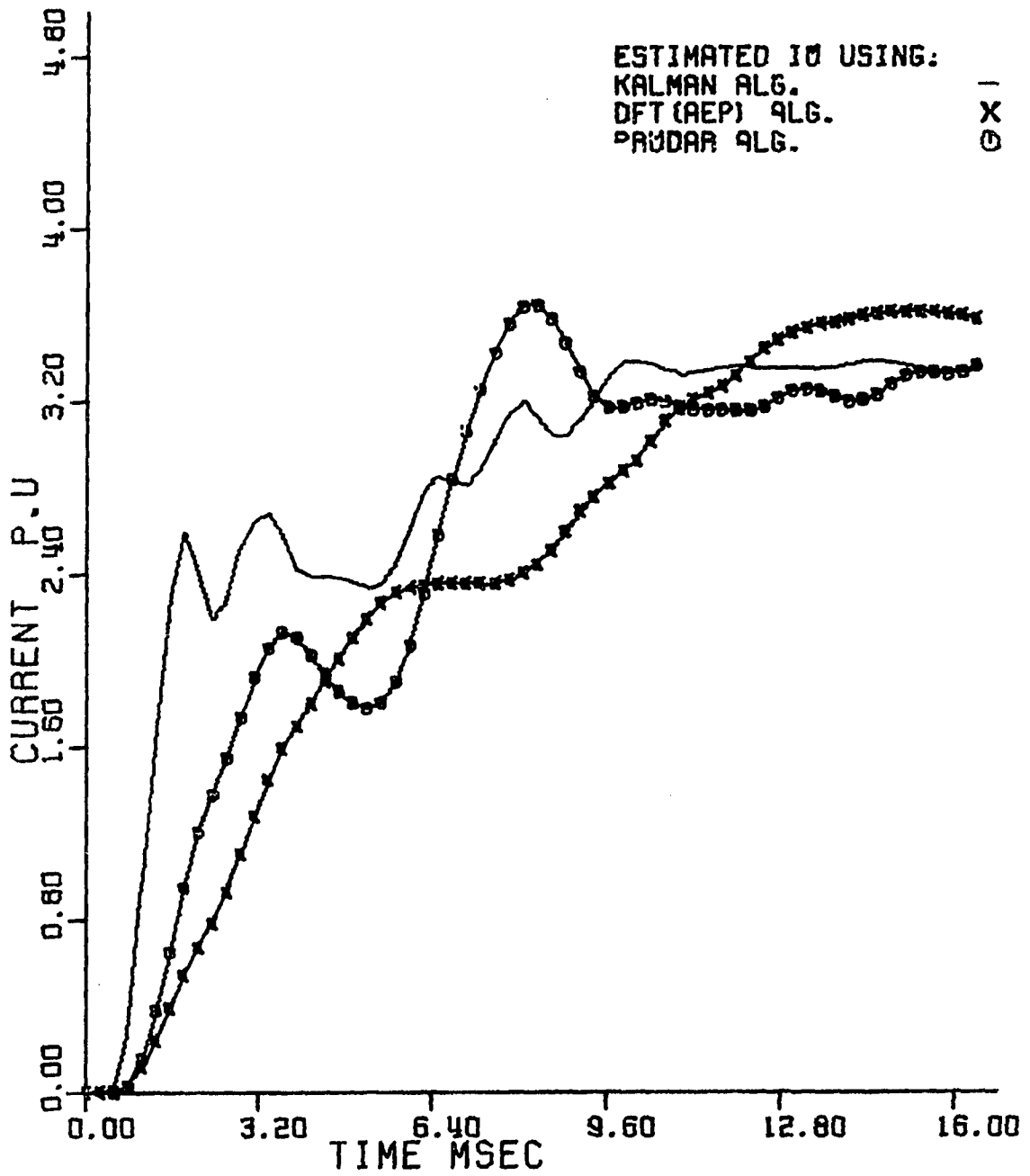
Figure 8.21. Recursive estimation of the zero sequence
current magnitude using Kalman filter,
DFT, and PRODAR 70 algorithms
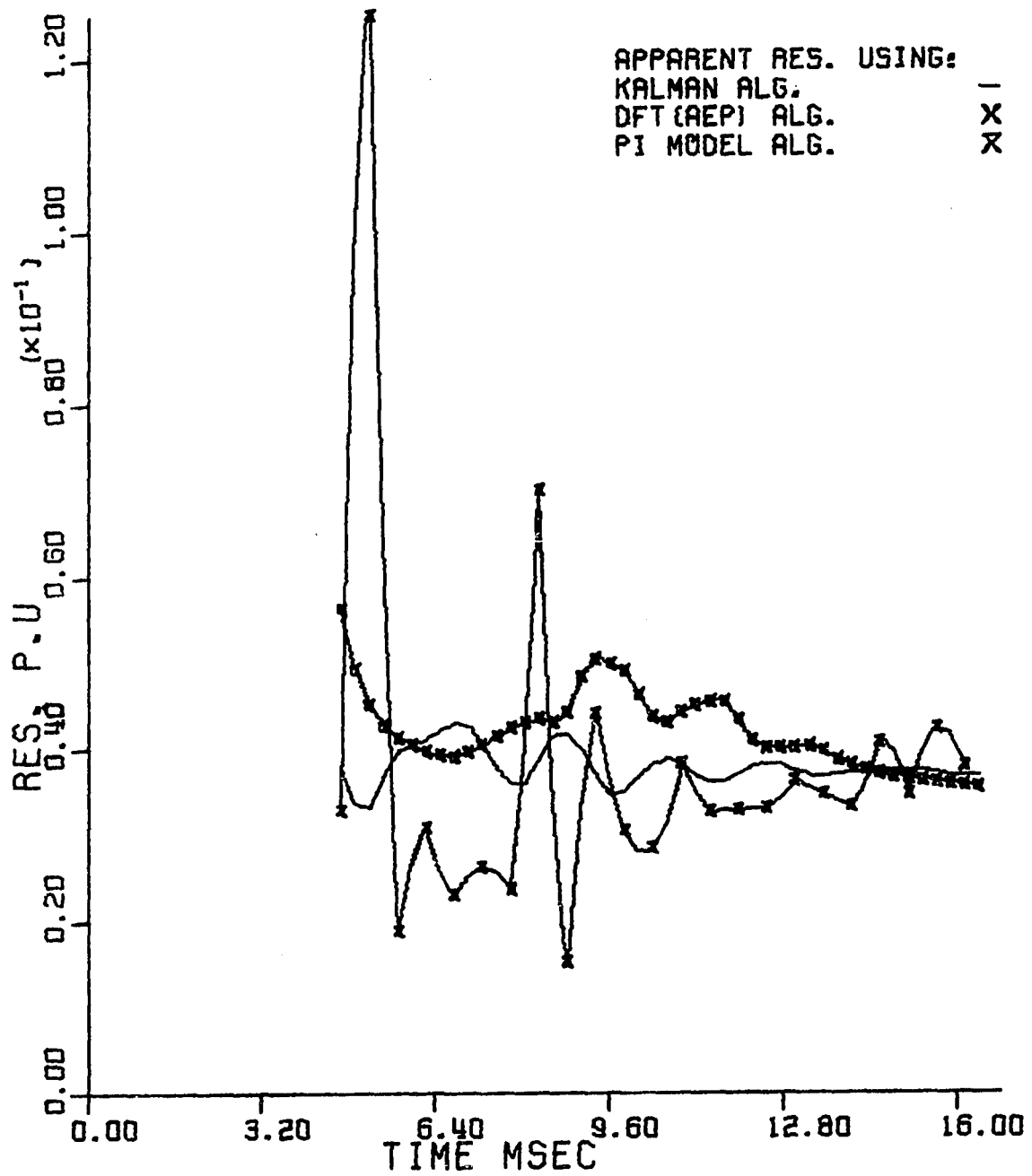
Figure 8.22. Computed apparent resistance using Kalman
filter, DFT, and PI model algorithms
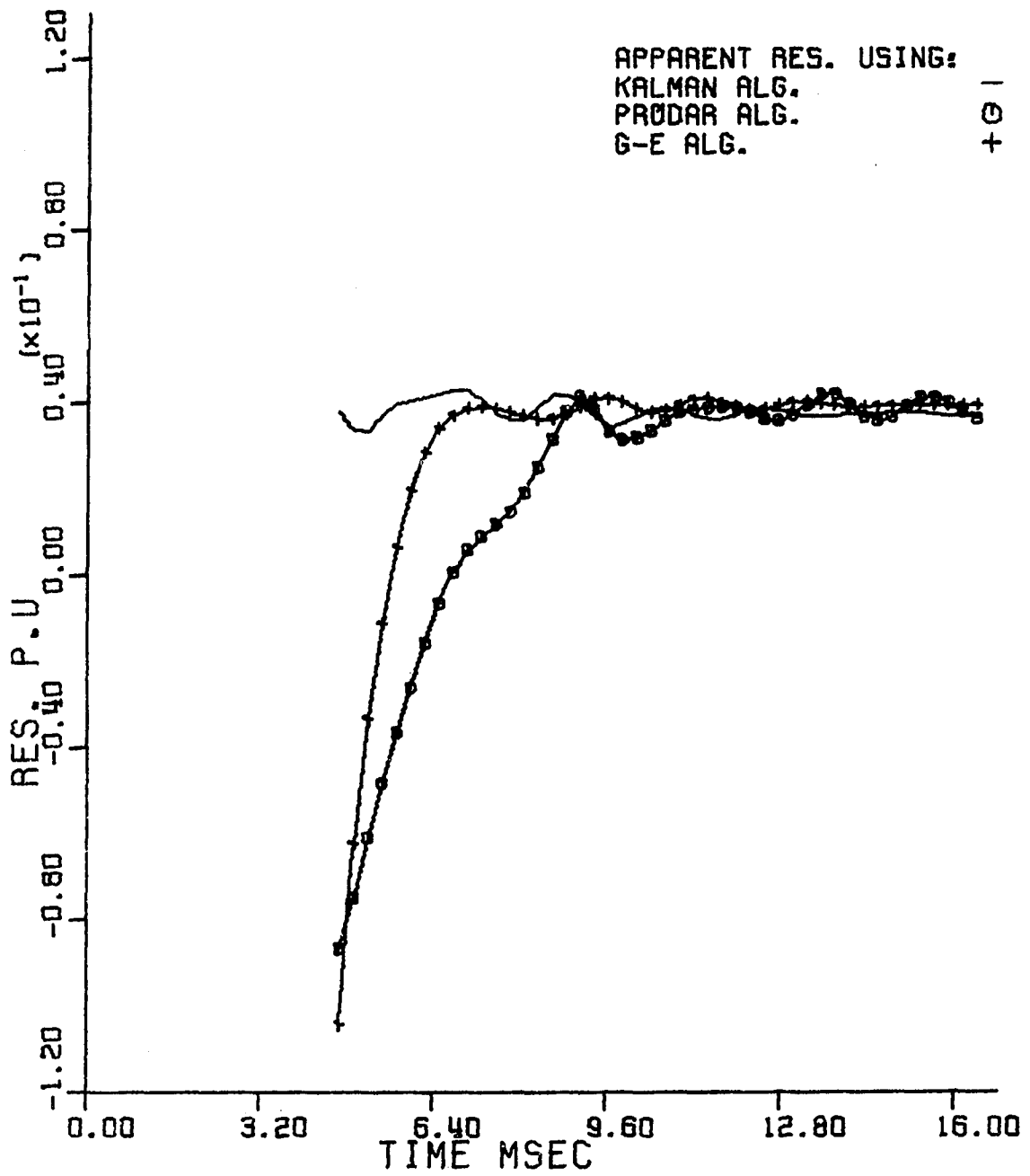
Figure 8.23. Computed apparent resistance using Kalman
filter, PRODAR 70, and G.E. algorithms
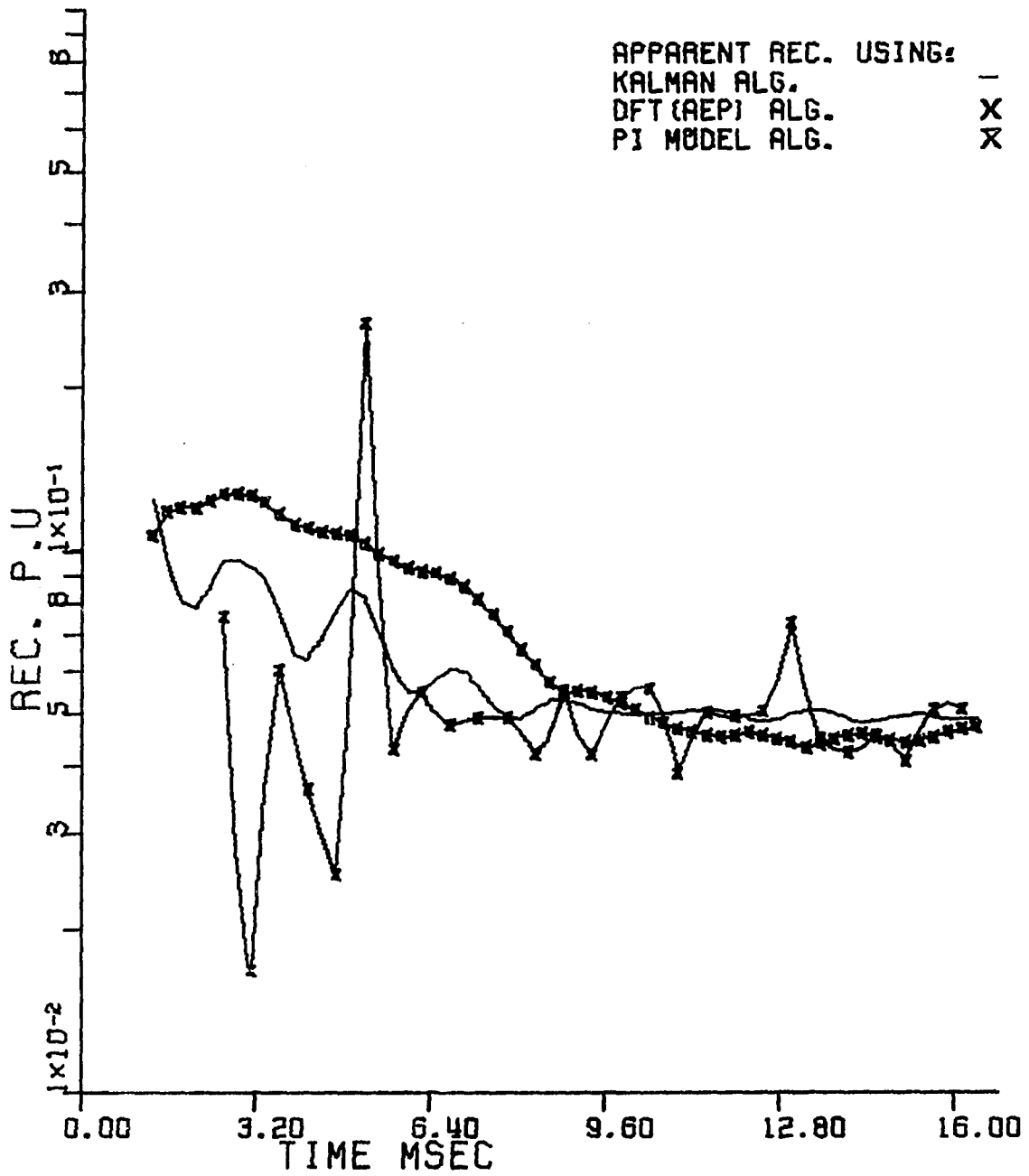
Figure 8.24. Computed apparent reactance using Kalman
filter, DFT, and PI model algorithms
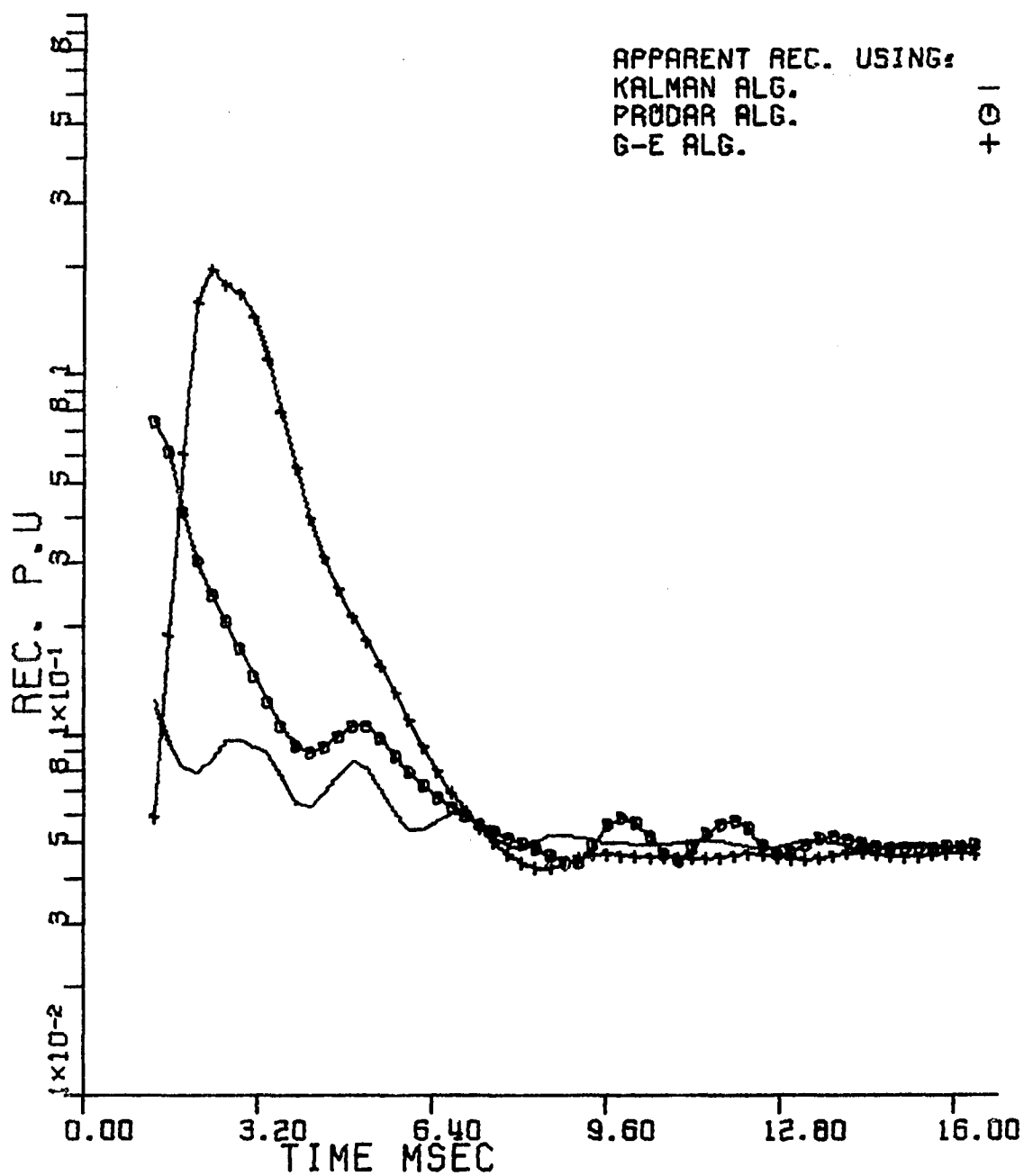
Figure 8.25. Computed apparent reactance using Kalman
filter, PRODAR 70, and G.E. algorithms
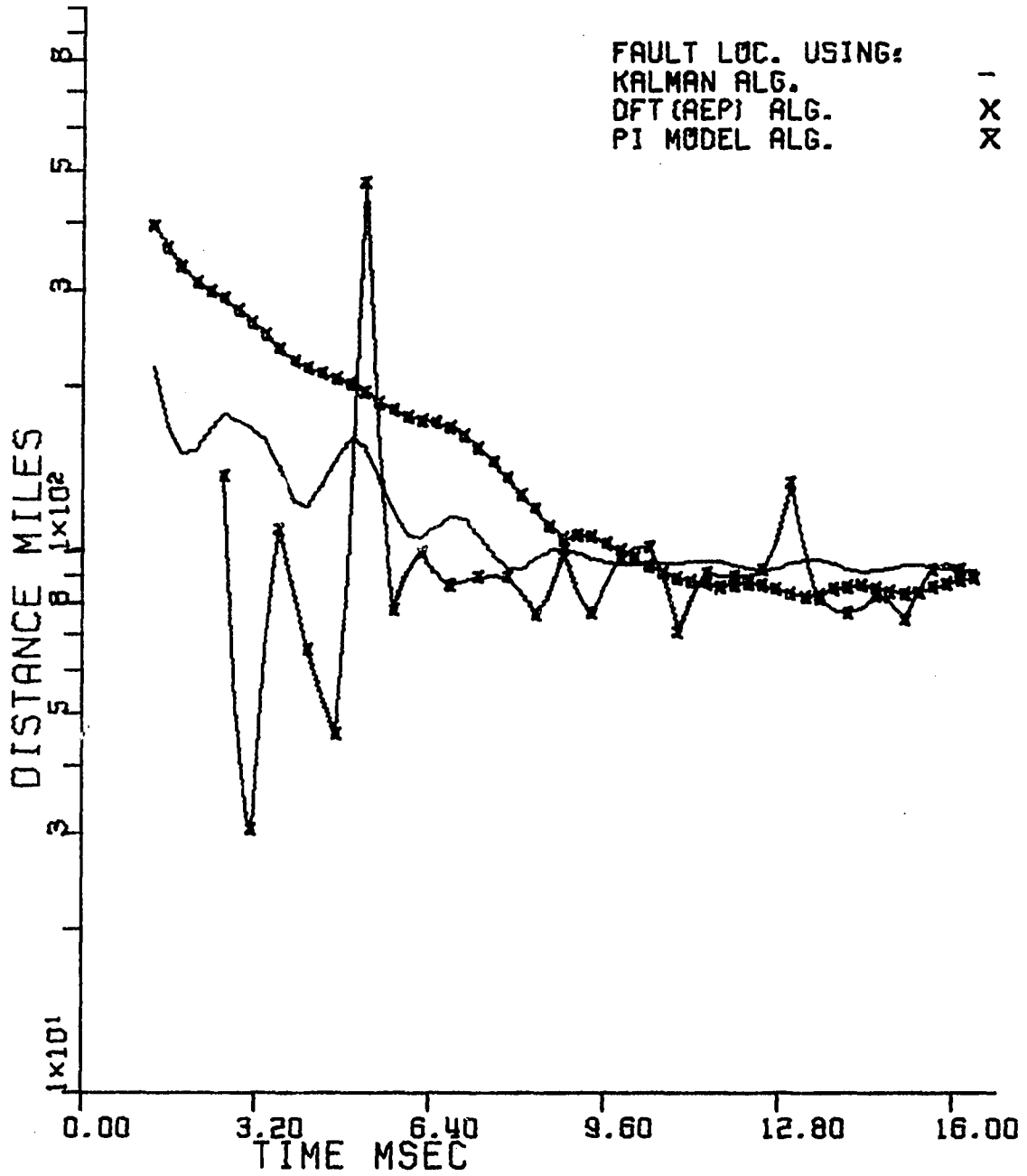
Figure 8.26. Computed fault location using Kalman
filter, DFT, and PI model algorithms
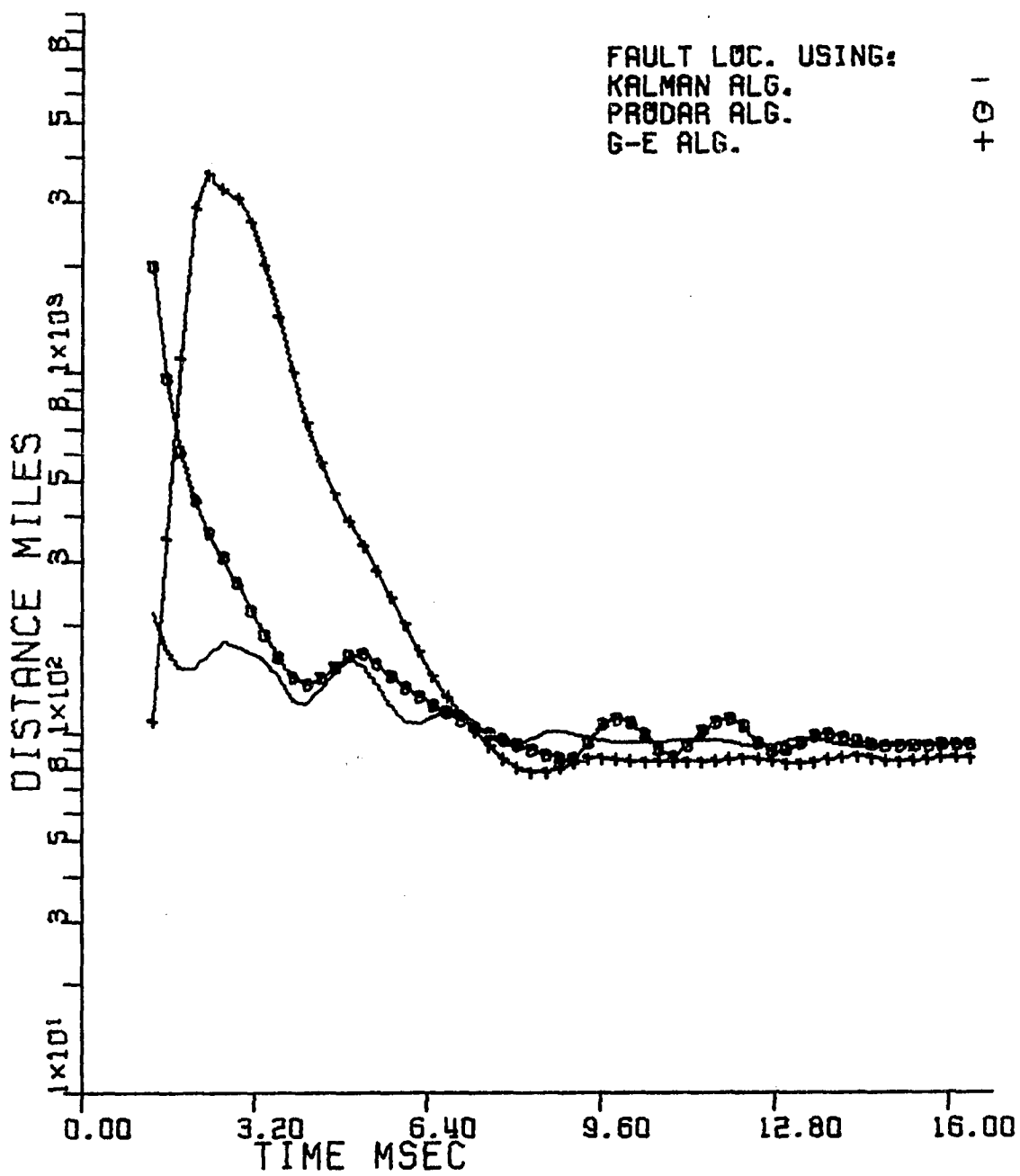
Figure 8.27. Computed fault location using Kalman
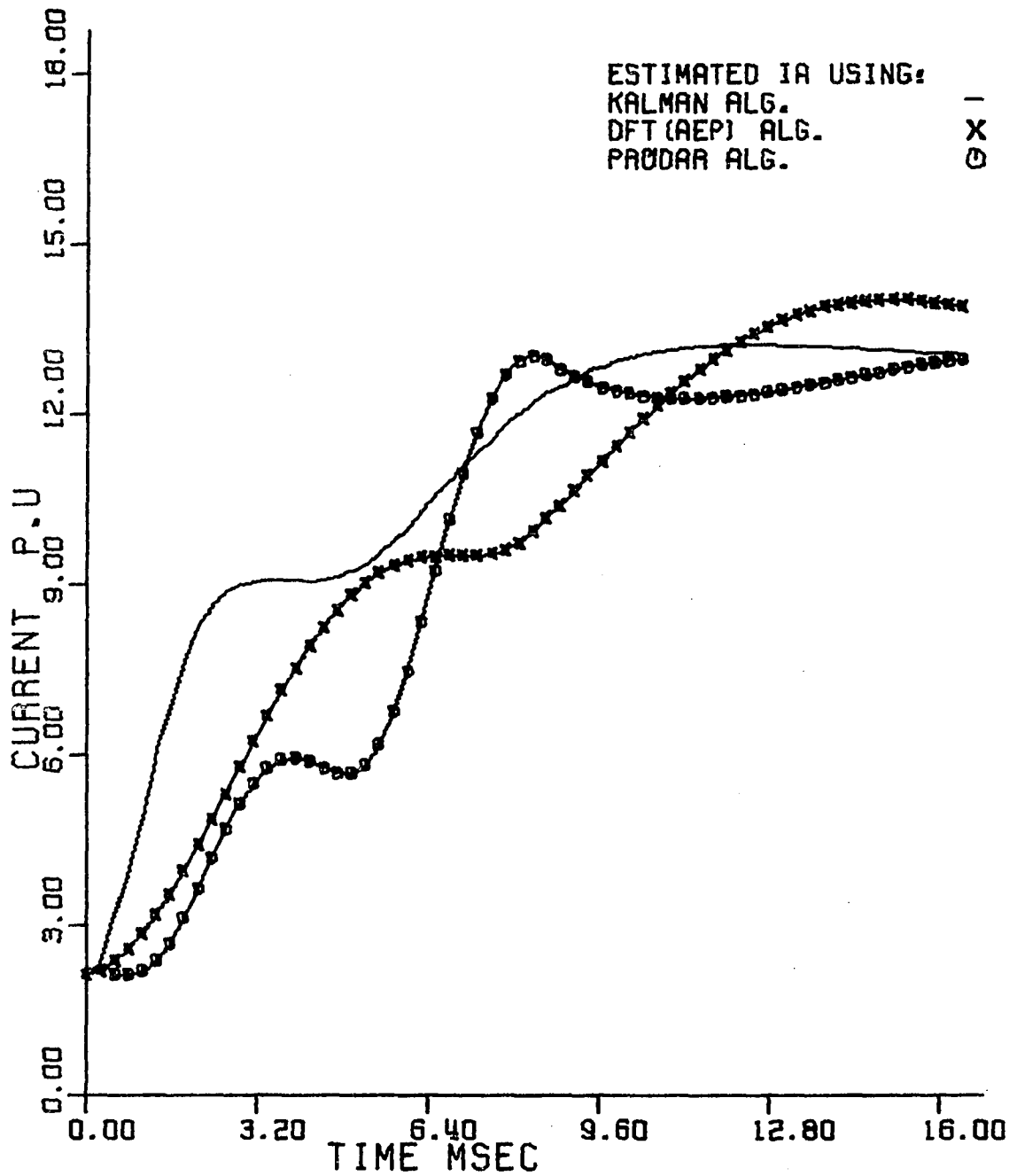filter, PRODAR 70, and G.E. algorithms
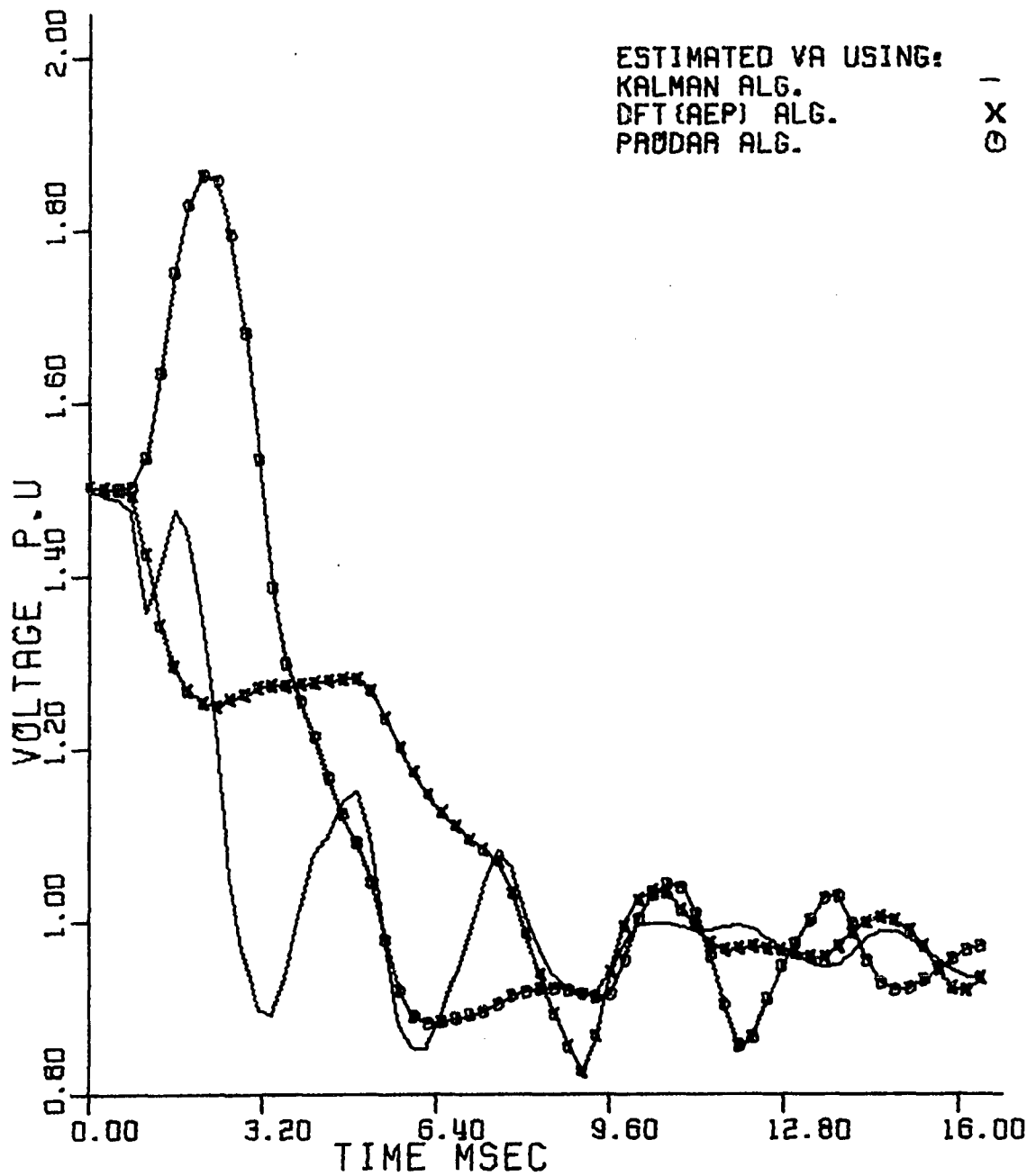
Figure 8.28. Recursive estimation of the voltage magnitude of Phase A using Kalman filter, DFT, and PRODAR 70 algorithms
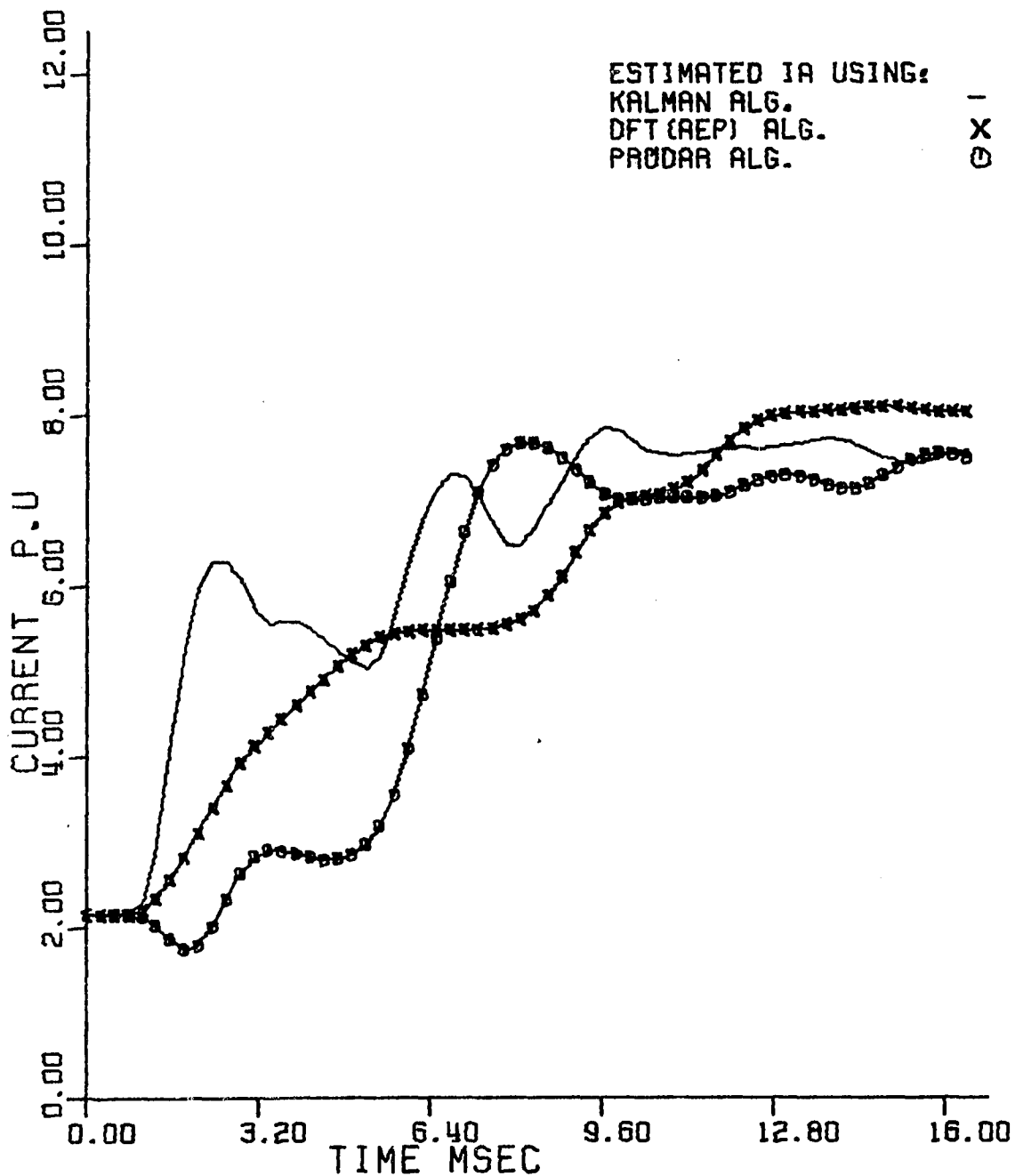
Figure 8.29. Recursive estimation of the current magnitude
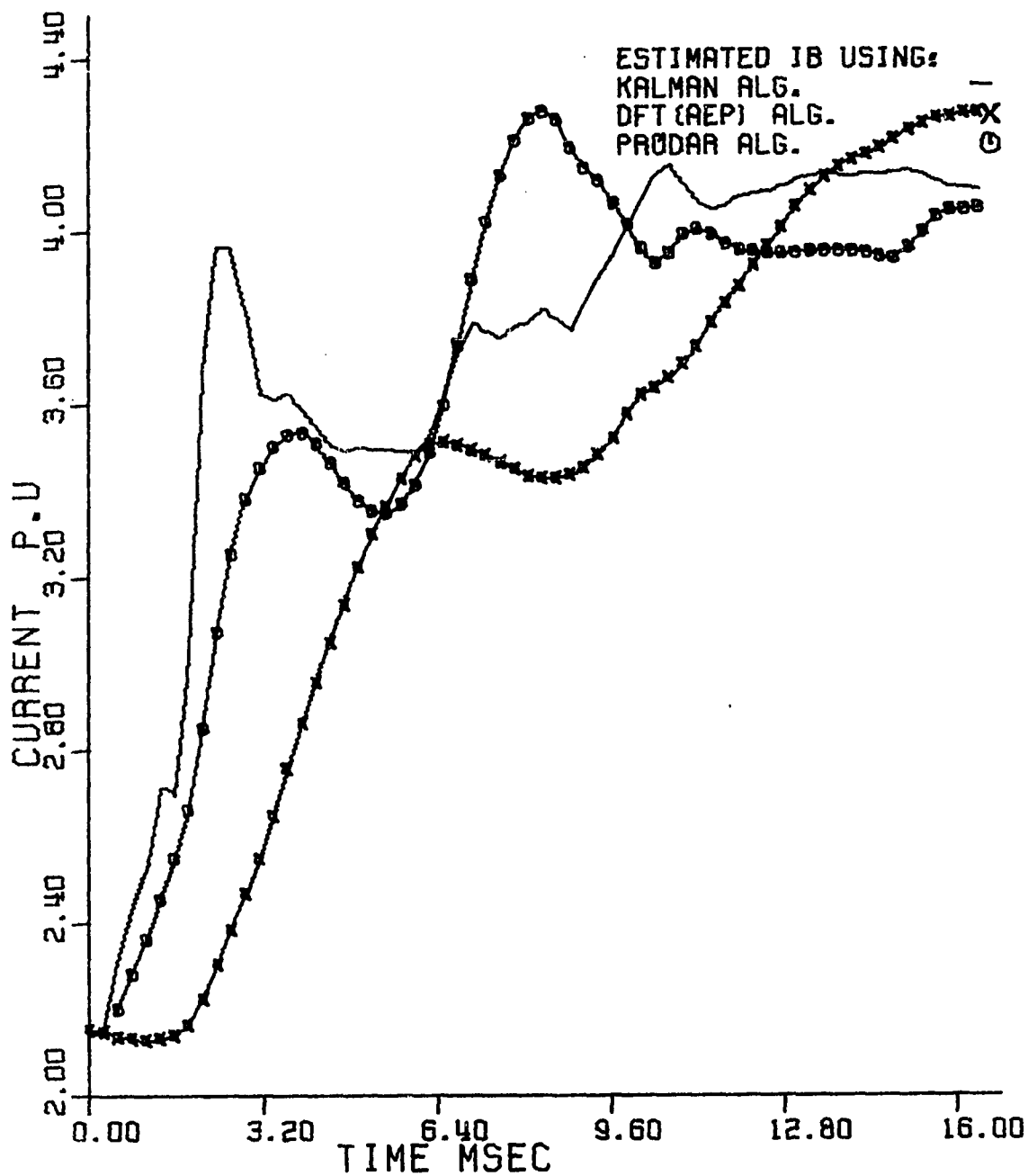in Phase A using Kalman filter, DFT, and
PRODAR 70 algorithms
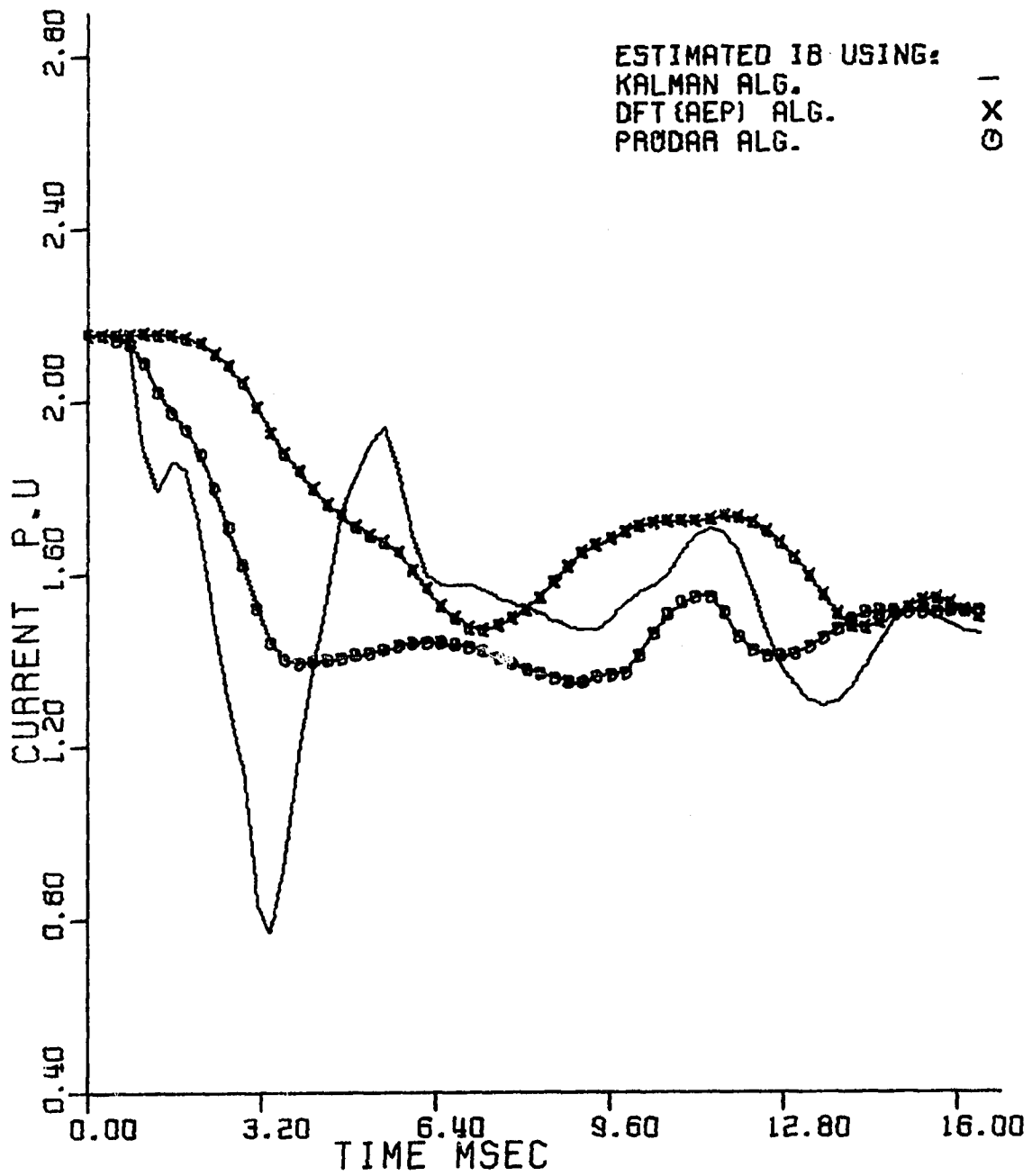
Figure 8.30. Recursive estimation of the current magnitude
in Phase B using Kalman filter, DFT, and
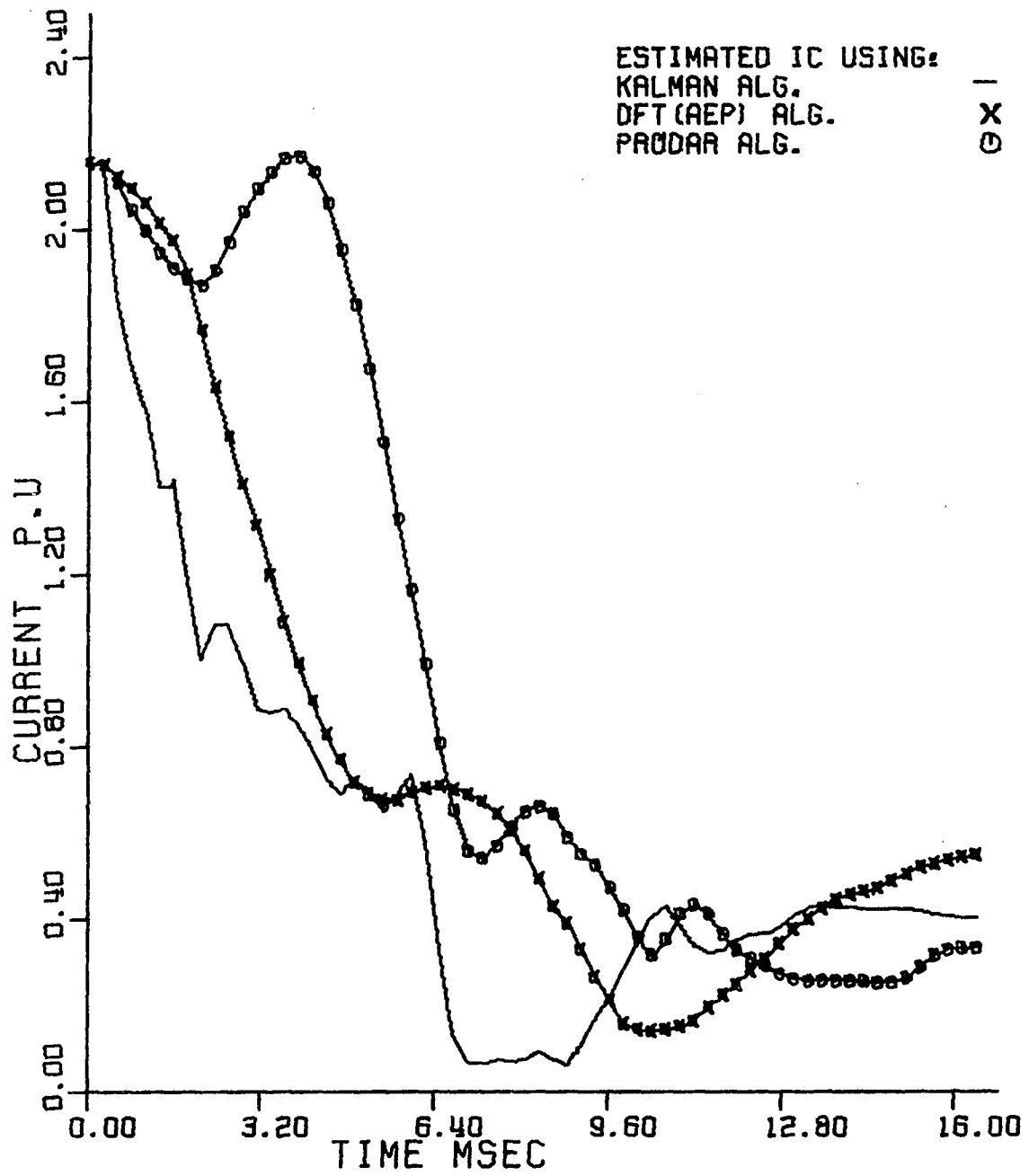PRODAR 70 algorithms
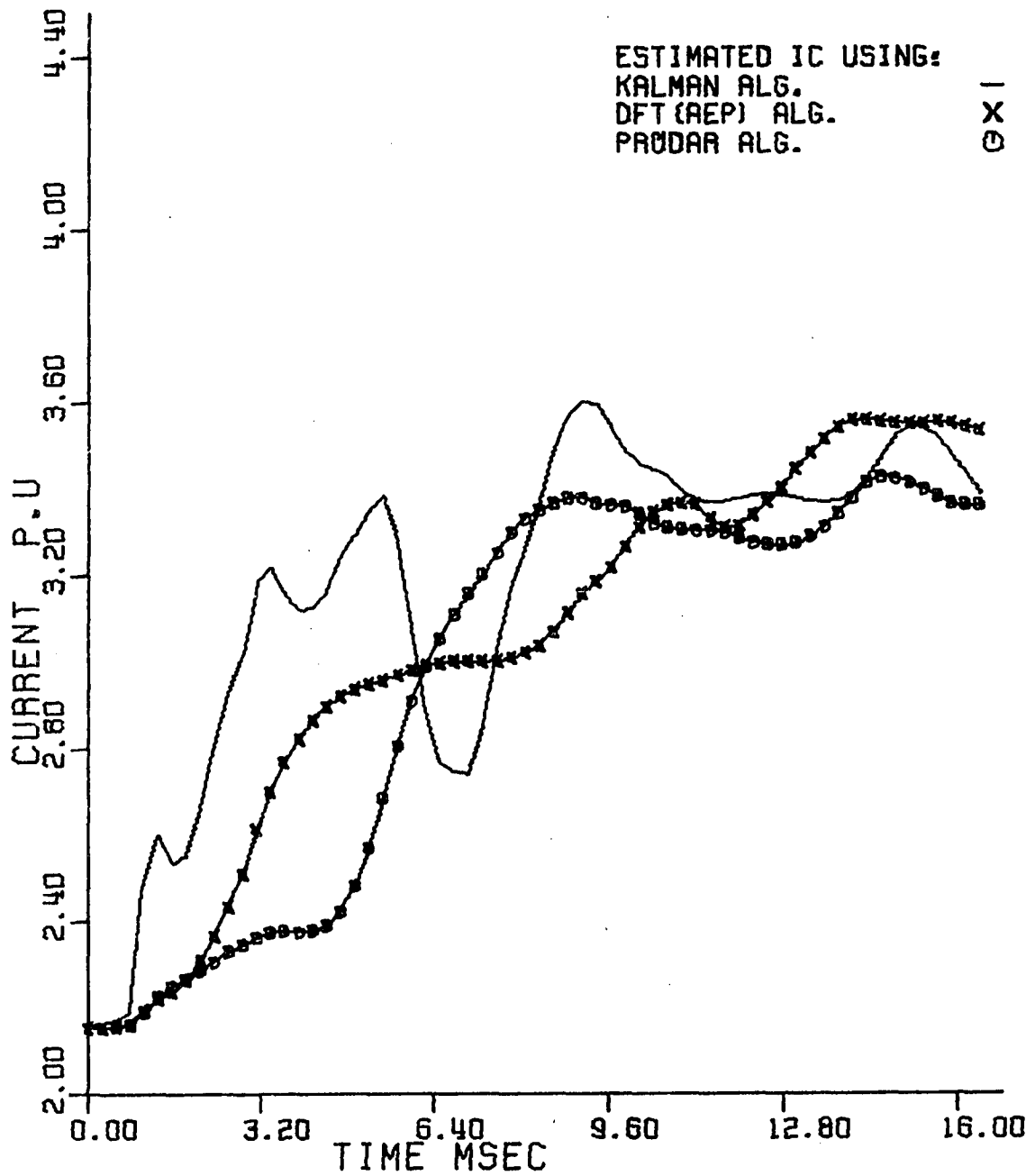
Figure 8.31. Recursive estimation of the current magnitude
in Phase C using Kalman filter, DFT, and
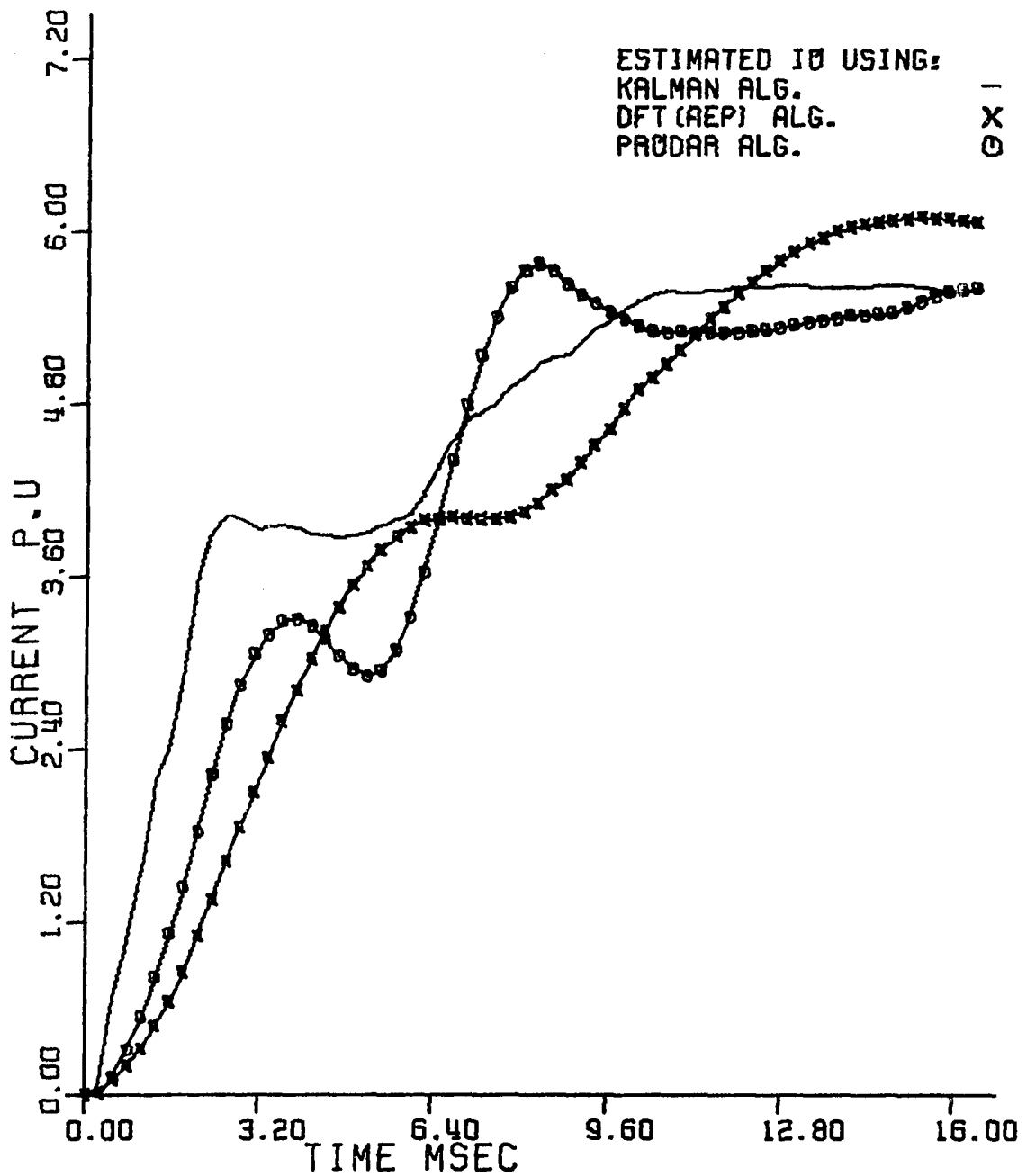PRODAR 70 algorithms
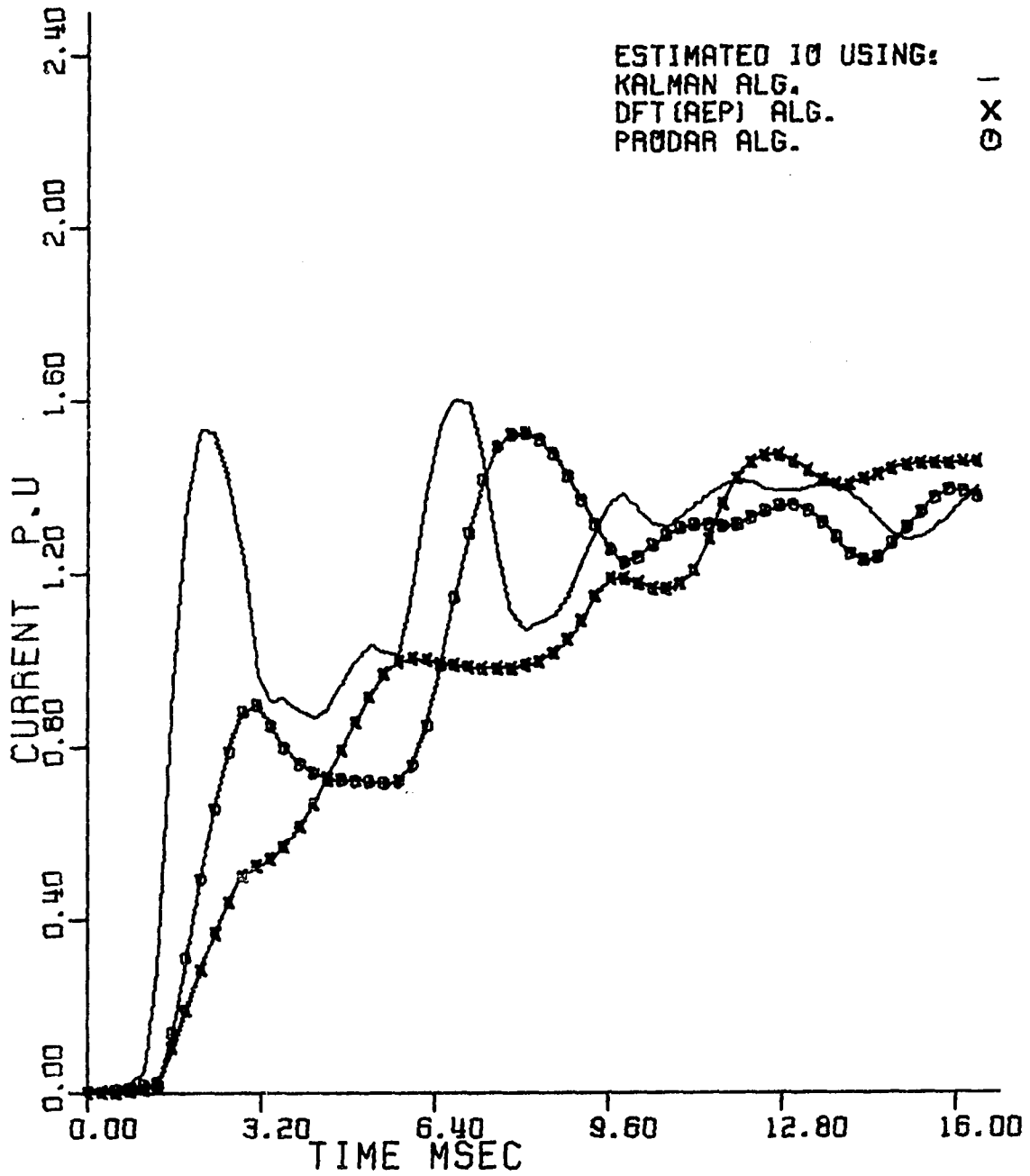
Figure 8.32. Recursive estimation of the zero sequence
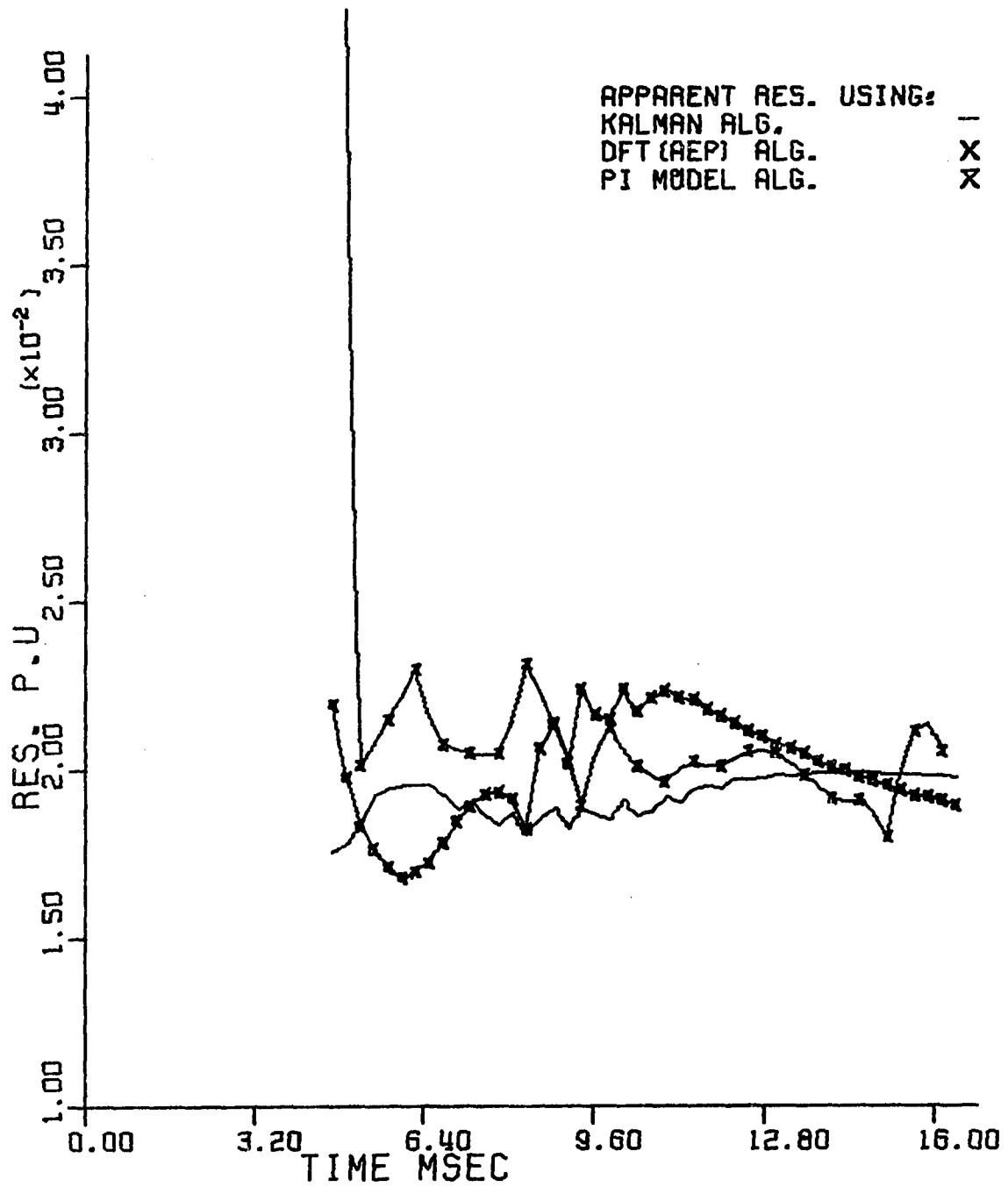using Kalman filter, DFT, and PRODAR 70
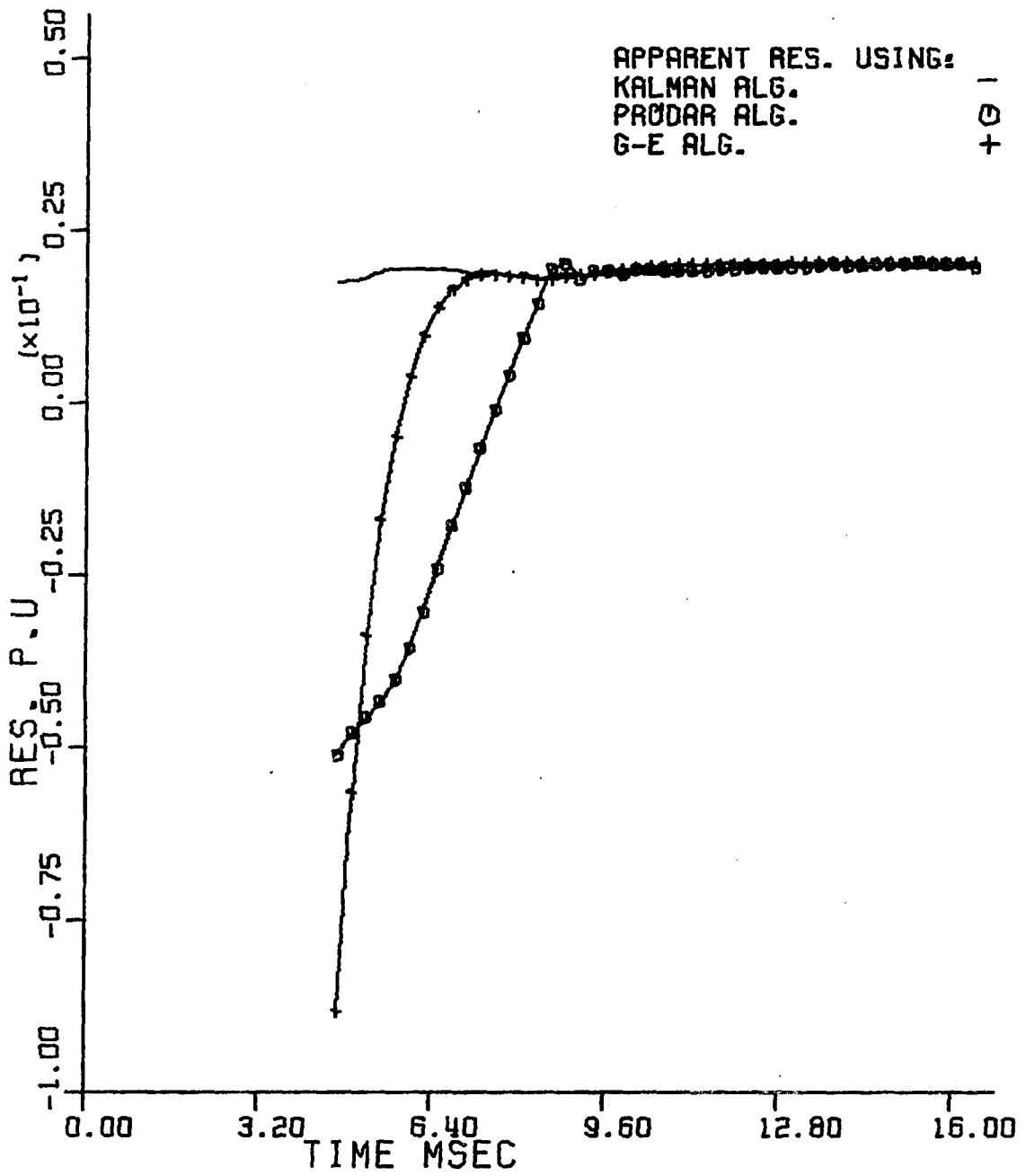algorithms
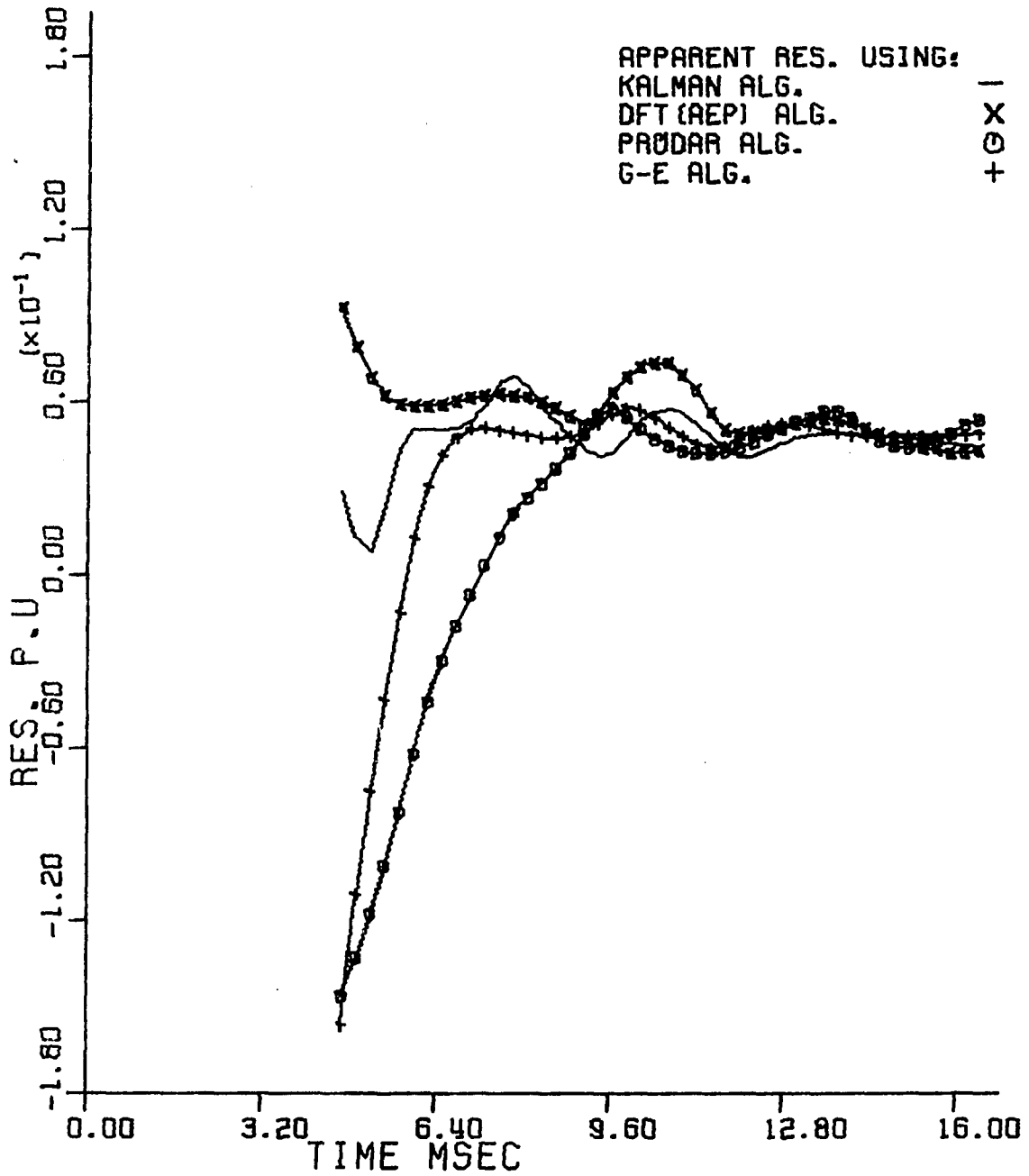
Figure 8.33. Computed apparent resistance using Kalman
filter, DFT, PRODAR 70, and G.E. algorithms
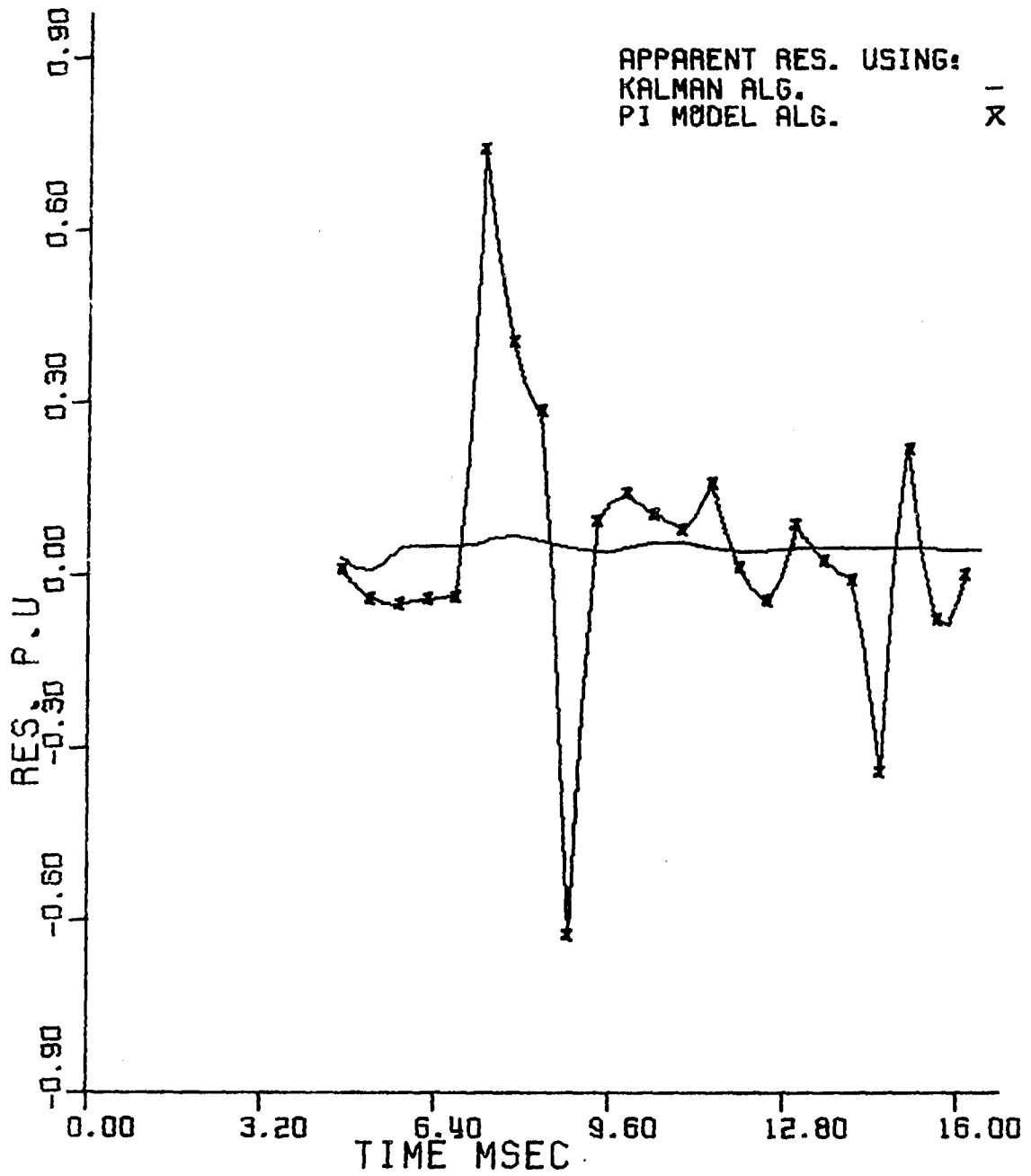
Figure 8.34. Computed apparent resistance using Kalman
filter and PI model algorithms
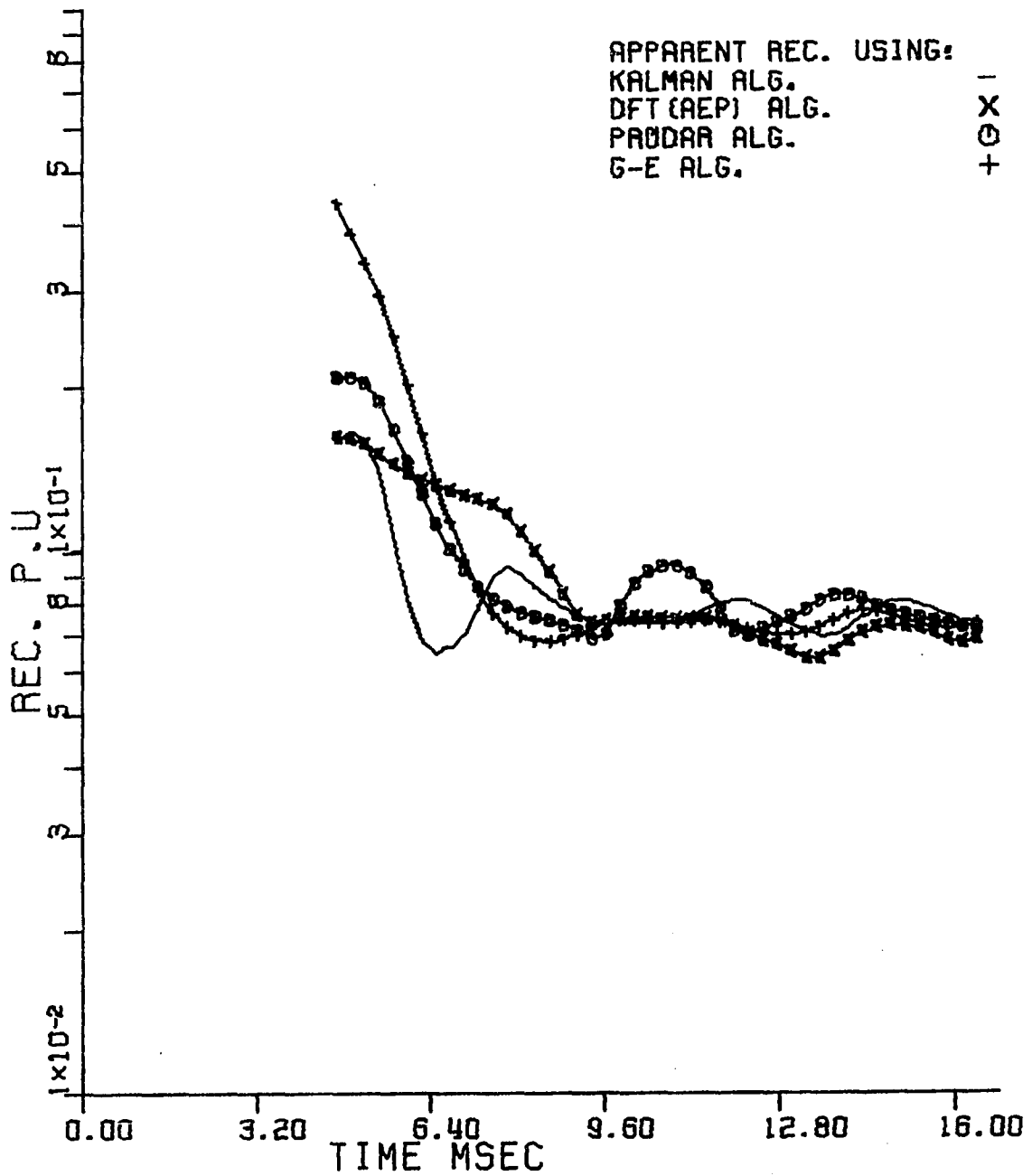
Figure 8.35. Recursive estimation of the apparent
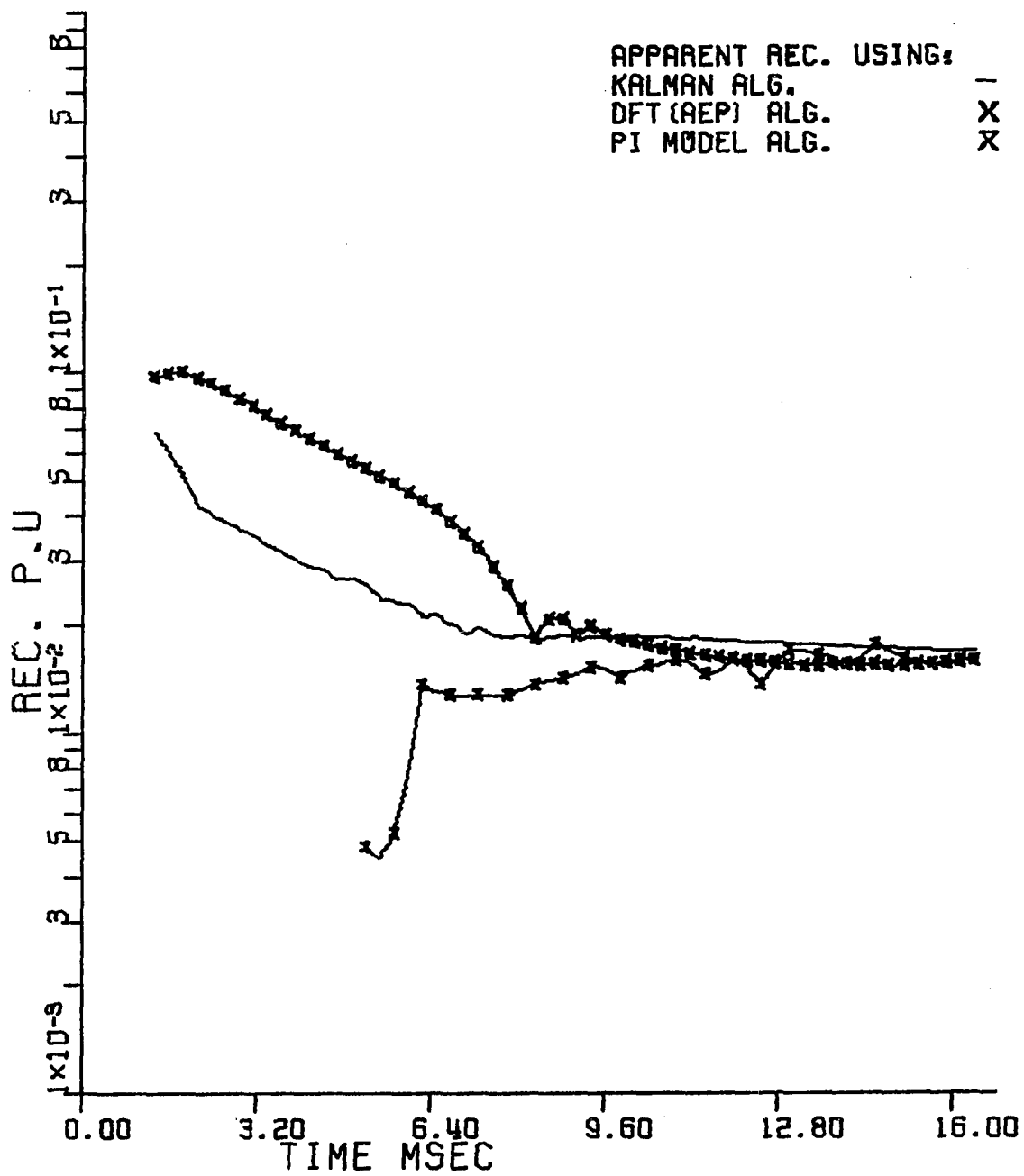reactance using Kalman filter, DFT,
PRODAR 70, and G.E. algorithms
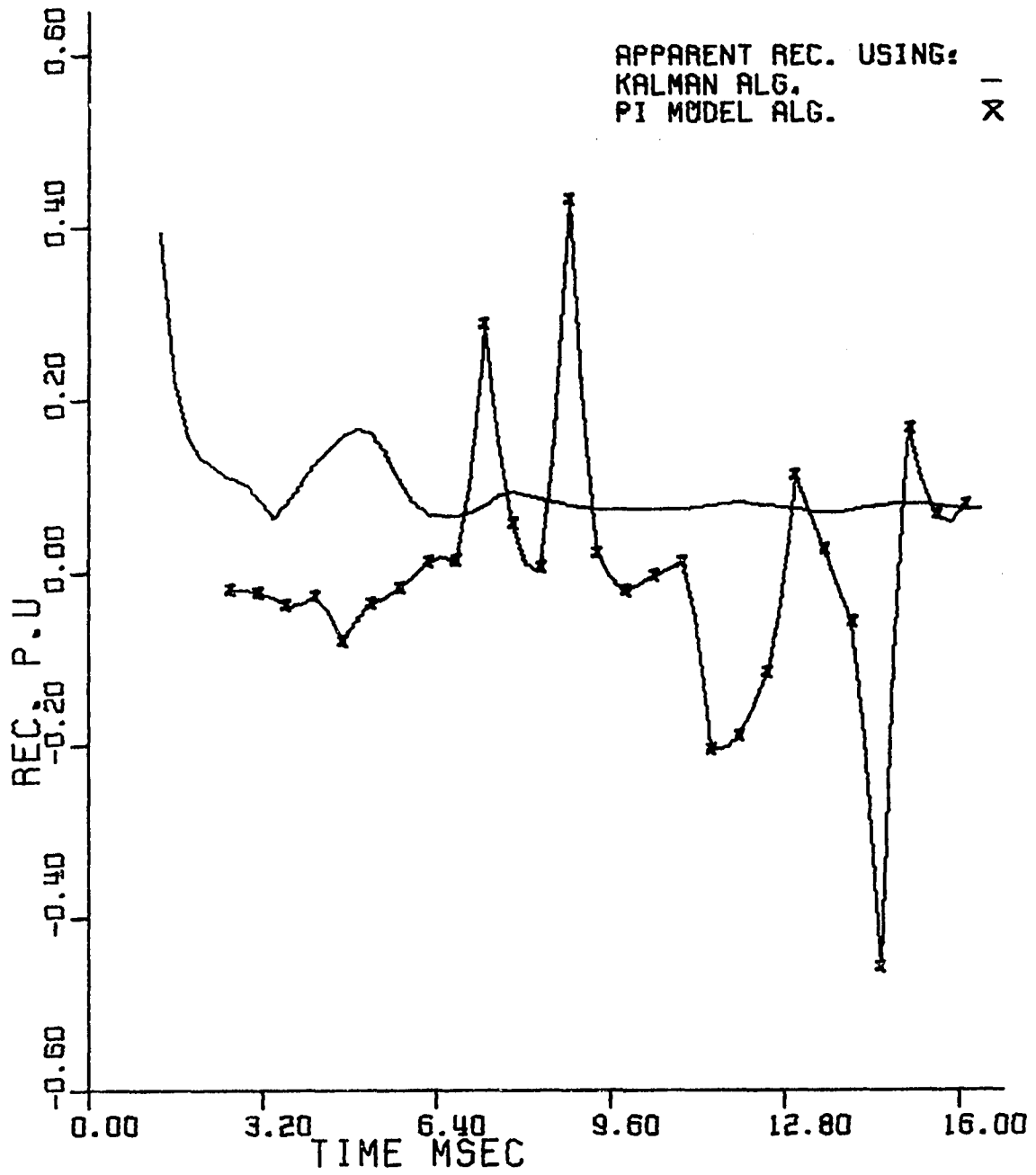
Figure 8.36. Computed apparent reactance using
Kalman filter and PI model algorithms
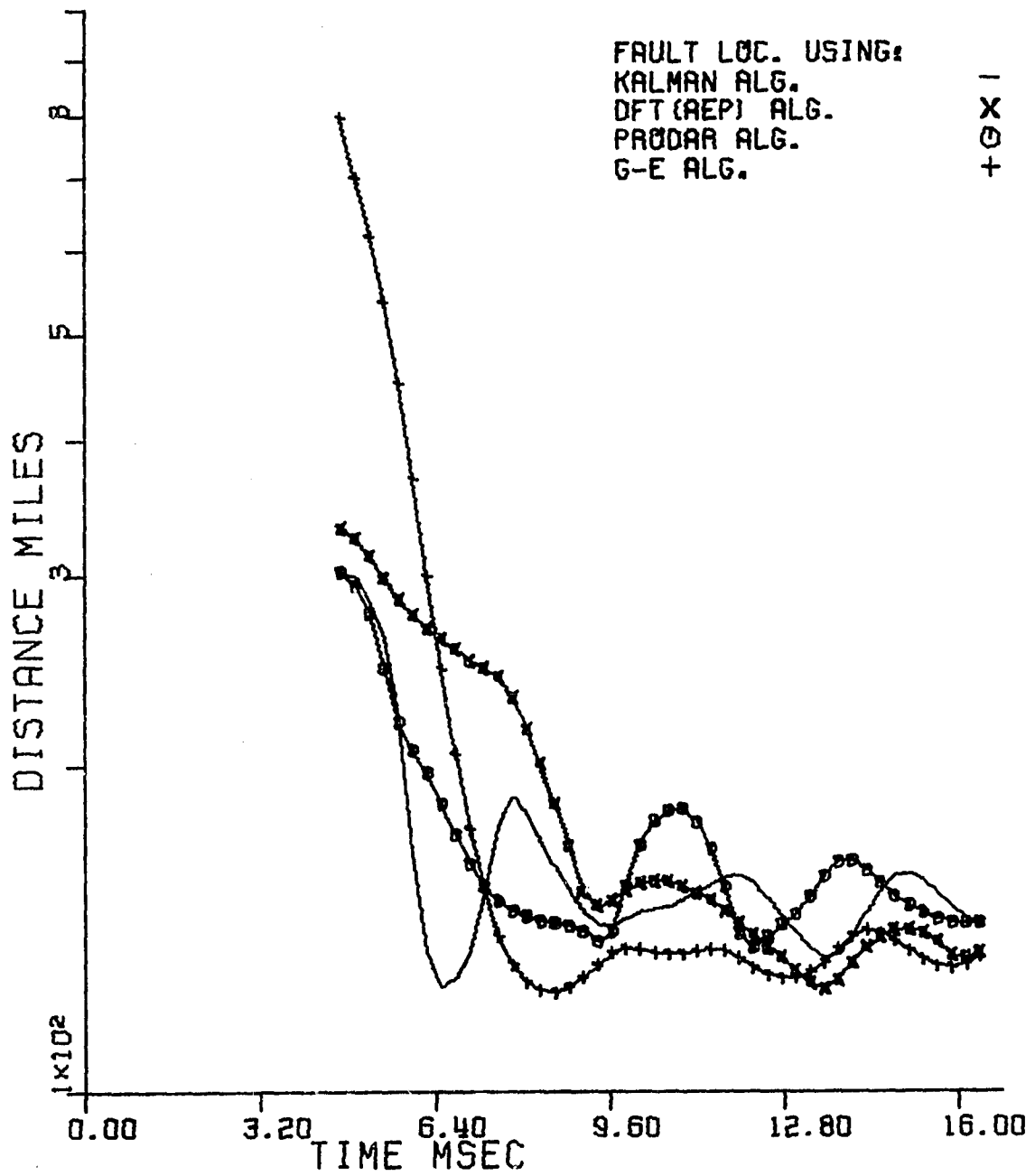
FAULT LOC. USING:
KALMAN ALG.   —
DFT(REP) ALG.   X
PRODAR ALG.   ⊕
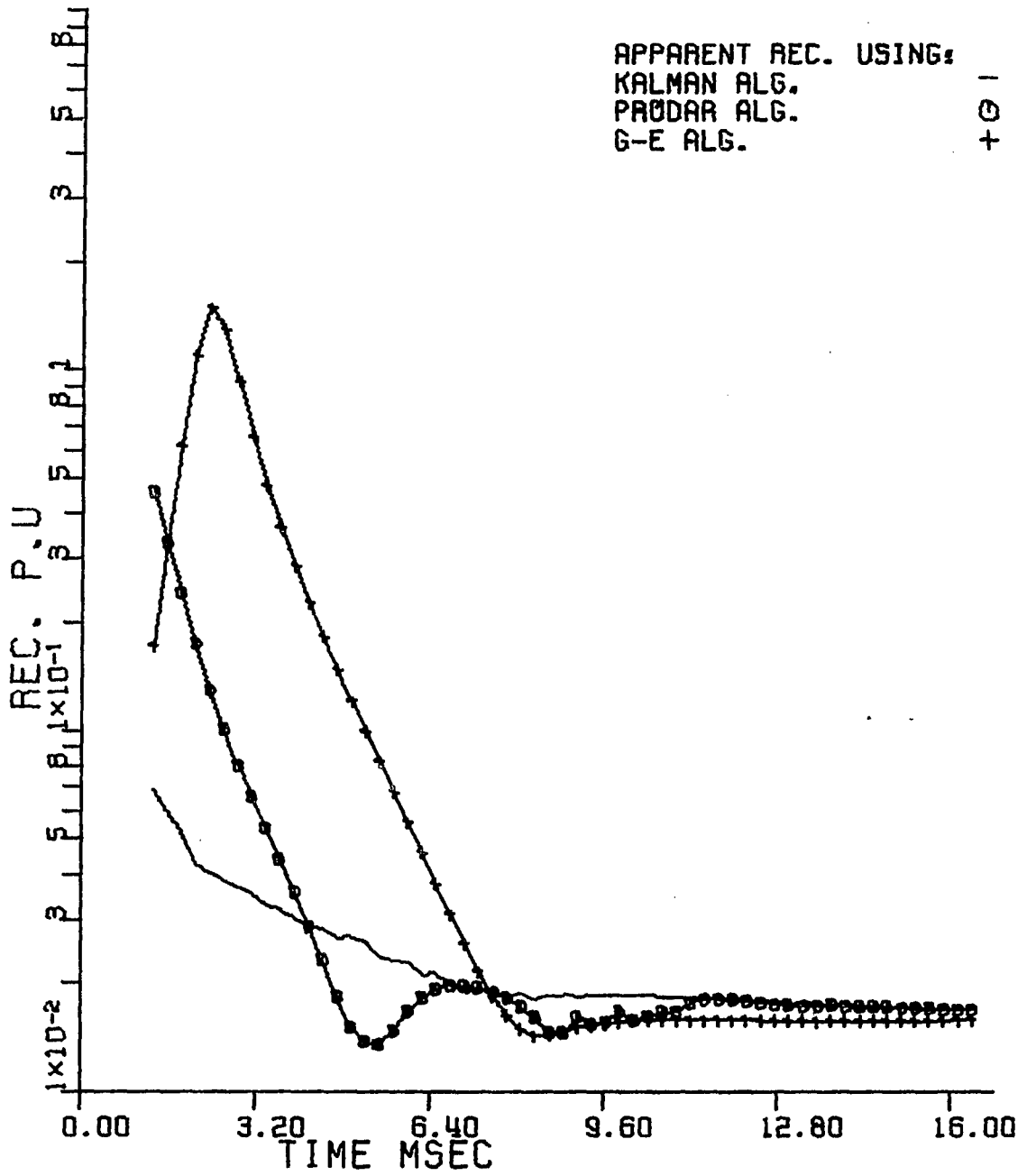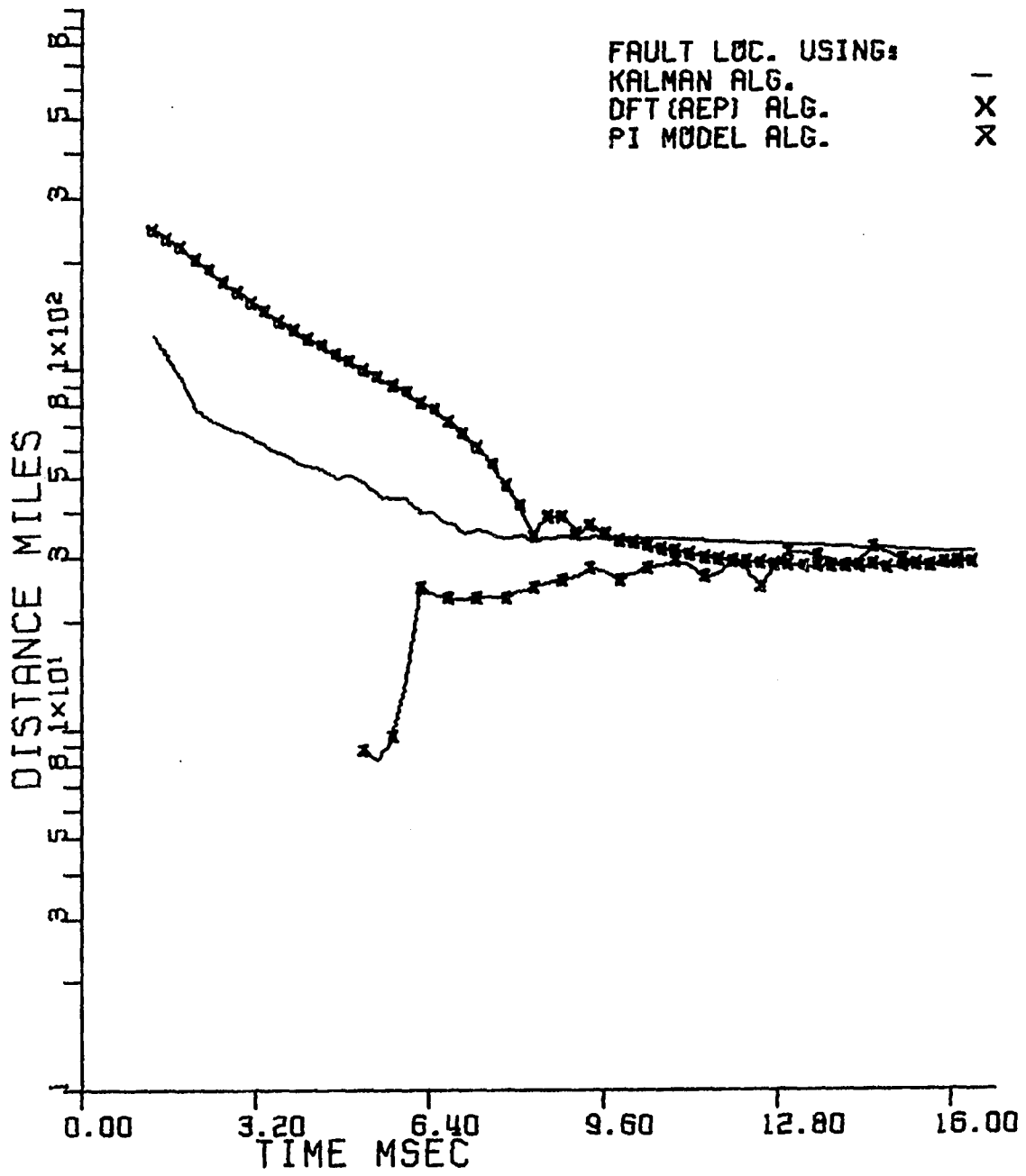G-E ALG.   +

Figure 8.17. Computed fault location using Kalman
filter, DFT, PRODAR 70, and G.E.
algorithms

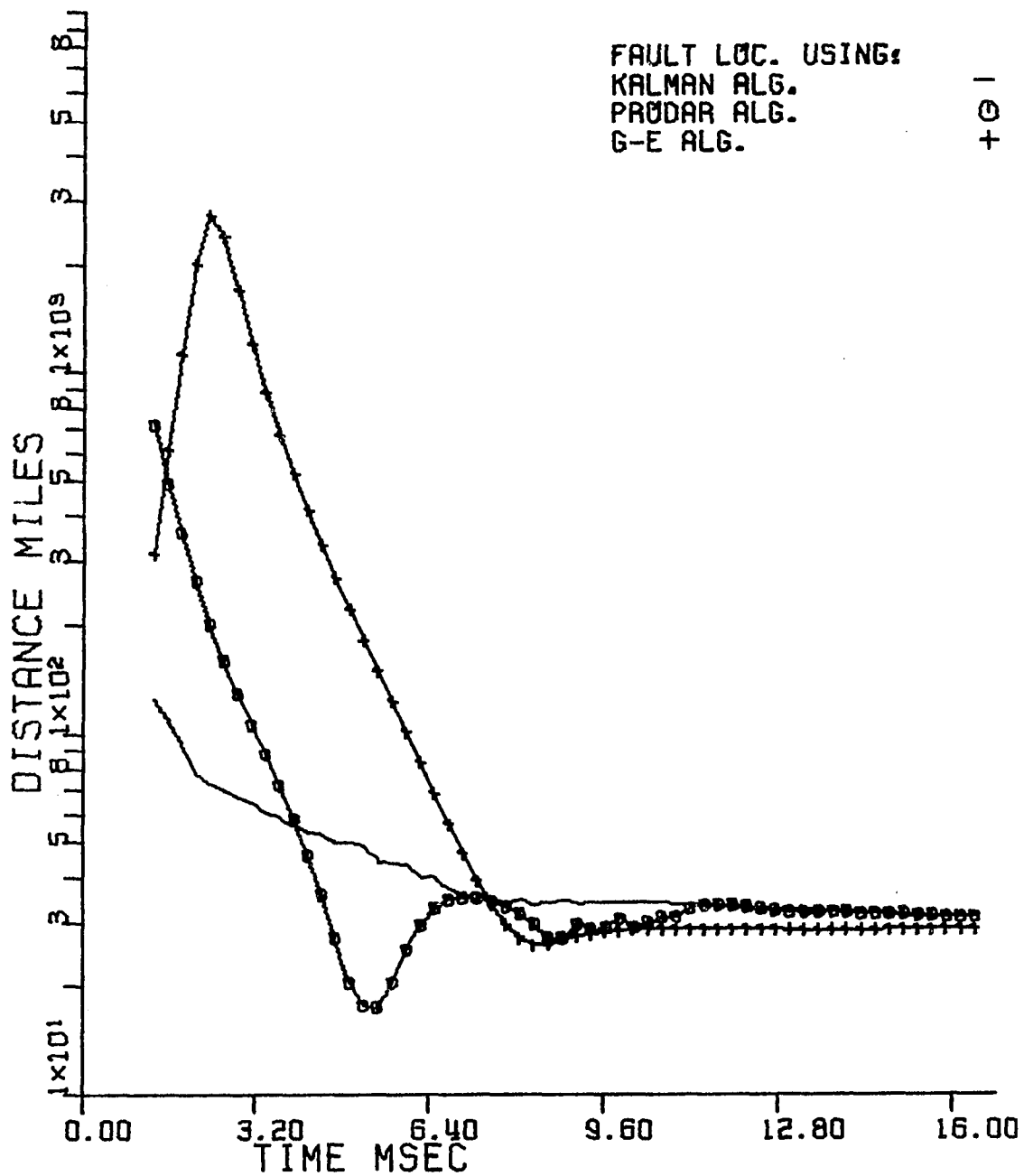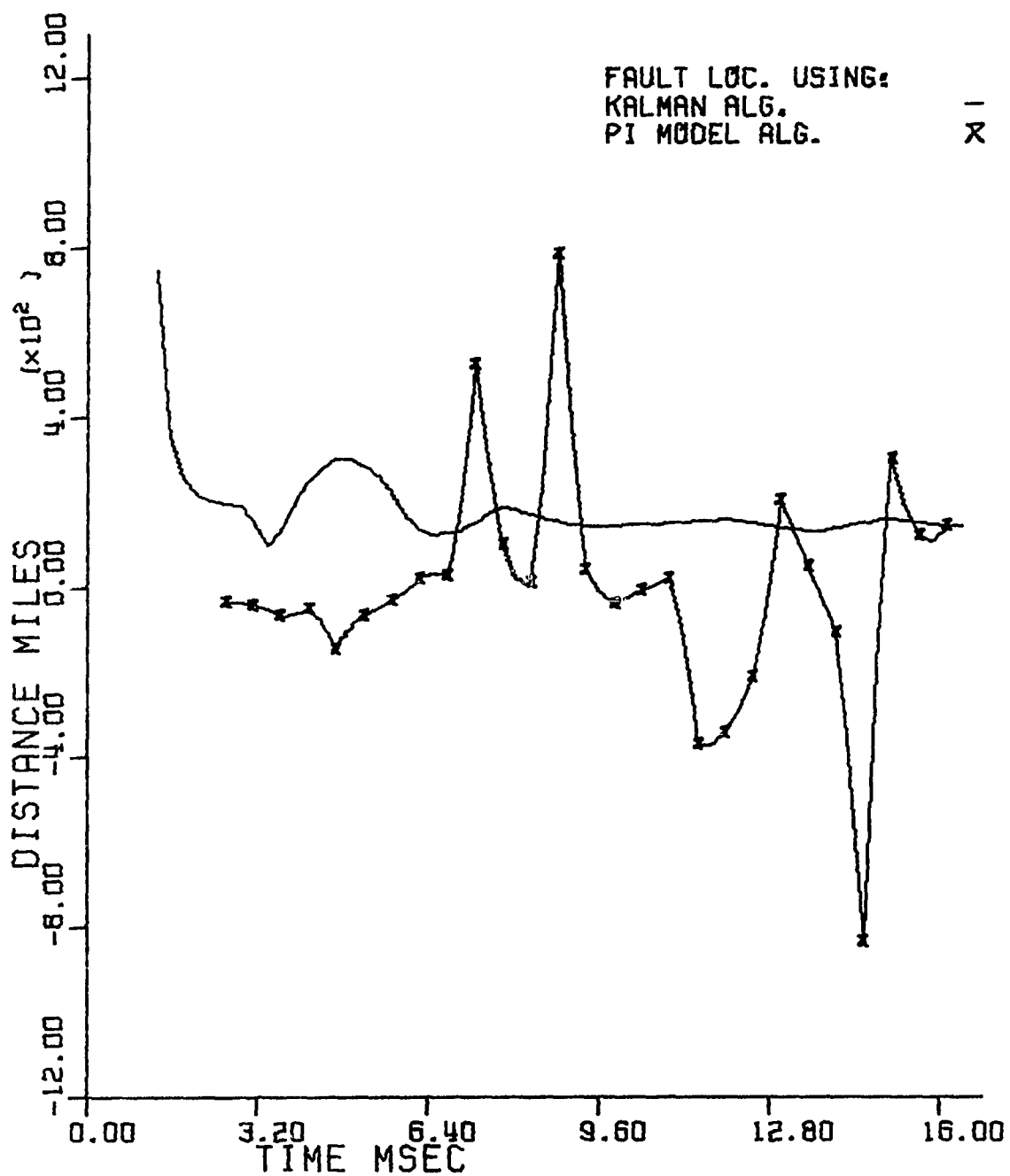Figure 8.38. Computed fault location using Kalman filter and PI model algorithms

IX. CONCLUSIONS

The characterization of the voltage and current noise signals due to a fault in a power system is required for the development of computer relaying algorithms based on statistical approaches or estimation techniques. The empirical formulas derived here for the variance of the current and voltage noise signals, along with the autocorrelation functions and the frequency spectra, offer a simple way to apply new techniques in computer relaying.

A two-state Kalman filter was shown to be sufficient for the estimation of voltage states. A three-state Kalman filter was used for the current, because it was necessary to include the exponentially decaying component of the current. The relative insensitivity of the Kalman filters to changes in the model parameters of ± 50 percent allows the use of standard Kalman filter algorithms in groups of transmission line protection. Because of the low computer burden of the technique, it appears that any of the modern 16-bit microprocessors with parallel processing structure can be used to implement a Kalman-filtering-based digital distance relaying scheme.

The fault detection algorithm implemented in the proposed Kalman filtering-based digital distance relay would be continuously monitoring the power system status. Therefore, no misoperation would occur due to a change in the operating condition of the system.

The adaptive capability of the digital distance relaying scheme allows an ultra high speed operation (less than 4 ms) for close in faults (within 40 percent of the protected line). This in turn would

improve the stability of the system, if it were used with a high speed circuit breaker.

The comparison with four other algorithms demonstrated with confidence that the Kalman-filtering-based digital distance relay is not only a new technique for computer relaying but also a highly accurate solution for computer relaying problems.

X. REFERENCES

1. Rockefeller, G. D. "What Are the Prospects for Substation-Computer Relaying?" Westinghouse Engineer 32 (September 1972):152-156.

2. Baird, T. C. "Computer Relaying: A Report on the State of the Art by a Propsective User." M.S. Report, Iowa State University, Fall 1975.

3. IEEE Tutorial Course. "Computer Relaying." Publication No. 79EH0148-7 PWR.(February 1979).

4. Morrison, I. E. "Prospects of On-Line Computer Control in Transmission Systems and Substations." Inst. Engineers, Australia, Elec. Eng. Transactions, EE3 (September 1967):234-236.

5. Grimes, J. D. "A Computer-Centered Relaying Scheme for the Protection of Bulk Power Transmission Lines." M.S. Thesis, Iowa State University, 1968.

6. Rockefeller, G. D. "Fault Protection with a Digital Computer." IEEE Transactions on Power Apparatus and Systems, PAS 88, No. 4 (April 1969):438-461.

7. Mantey, P. E. "Computer Requirements for Event Recording, Digital Relaying and Substation Monitoring." Sixth IEEE PICA Conf. Record 6 (May 1969):262-272.

8. Walker, L. N., Ogden, A. D., Ott, G. E., and Tudor, J. R. "Special Purpose Digital Computer Requirements for Power System Substation Needs." Paper No. 70 CP 142-PWR, IEEE Winter Power Meeting, New York, January 1970.

9. Hope, G. S. "Techniques Using Sequential Logic for Power System Protection." IEE Conference 1, 1970, pp. 167-175.

10. Hope, G. S., Bell, D. H., and Jura, S. J. "Development of a Computer Interface for Transmission Protection." Seventh PICA Conference Proceedings, Boston, Mass., 1971.

11. Mann, B. J. and Morrison, I. F. "Digital Calculation of Impedance for Transmission Line Protection." IEEE Transactions on Power Apparatus and Systems, PAS 90, No. 1 (January/ February 1971):270-279.

12. Mann, B. J. and Morrison, I. F. "Relaying a Three Phase Transmission Line with a Digital Computer." IEEE Transactions on Power Apparatus and Systems, PAS 90, No. 2 (March/ April 1971):742-750.

13. Poncelet, R. "The Use of Digital Computers for Network Protection." CIGRE Paper No. 32-08, 1972.

14. Edgley, R. K., Poon, S. K. L., and Lau, W. "Design Aspects of a Computer System for Back Up Protection and Post Fault Control." IEE International Conference on Developments in Power System Protection 1, London, March 1975, pp. 261-267.

15. Edgley, R. K. "A Central Computer for Power System Back Up Protection." Electrical Review 14 (March 1975):321-324.

16. Cheetham, W. J. "Computerized Protection or Not? - Remote Back Up Protection." IEE International Conference on Developments in Power System Protection 1, London, March 1975, pp. 297-302.

17. Mann, B. J. "Real Time Computer Calculation of the Impedance of a Faulted Single Phase Line." Elec. Eng. Trans. Inst. Engineers, EE4, Australia (March 1969):26-28.

18. Durbeck, R. C. and Mantey, P. E. "Power System Protection Relaying by Time Coordinated Sampling and Calculation." U.S. Patent 3569785, 1971.

19. Gilcrest, G. B., Rockefeller, G. D., and Udren, E. A. "High Speed Distance Relaying Using a Digital Computer, 1-System Description." IEEE Transactions on Power Apparatus and Systems, PAS 91, No. 3 (May/June 1975):872-883.

20. Rockefeller, G. D. and Udren, E. A. "High Speed Distance Relaying Using a Digital Computer, II Test Results." IEEE Transactions on Power Apparatus and Systems, PAS 91, No. 3 (May/June 1972):1244-1258.

21. Gilbert, J. G. and Shovlin, R. J. "High Speed Transmission Line Fault Impedance Calculation Using a Dedicated Minicomputer." IEEE Transactions on Power Apparatus and Systems, PAS-94, No. 3 (May/June 1975):872-883.

22. Makino, J. and Miki, Y. "Study of Operating Principles and Digital Filters for Protective Relays with Digital Computers." IEEE Publication No. 75 CH0990-2 PWR, Paper No. C75-197-9, IEEE PES Winter Power Meeting, New York, January 1975.

23. McInnes, A. D. and Morrison, I. F. "Real Time Calculation of Resistance and Reactance for Transmission Line Protection by Digital Computer." Elec. Eng. Trans. Inst. Engineers Australia, EE 7, No. 1 (January 1971):16-23.

24. Ranjbar, A. and Cory, B. J. "An Improved Method for the Digital Protection of High Voltage Transmission Lines." IEEE Transactions on Power Apparatus and Systems, PAS 94, No. 2 (March/April 1975):579-590.

25. Sanderson, J. V. H. and Wright, A. "Protective Scheme for Series Compensated Transmission Lines." Proceedings of IEE 121, No. 11 (November 1974):1377-1384.

26. Breingan, W. D., Chen, M. M., Gallan, T. F. "Laboratory Investigation of a Digital System for the Protection of Transmission Lines." IEEE Transactions on Power Apparatus and Systems, PAS 98, No. 2 (March/April 1979):350-368.

27. Gallen, T. F., Chen, M. M., and Breingan, W. D. "A Digital System for Directional Comparison Relaying." IEEE Transactions on Power Apparatus and Systems, PAS 98, No. 3 (May/June 1979):948-956.

28. Smolinski, W. J. "An Algorithm for Digital Impedance Calculation Using a Single PI Section Transmission Line." IEEE Transactions on Power Apparatus and Systems, PAS 98, No. 5 (September/October 1979):1546-1551.

29. Suda, N. and Furuse, M. "High Speed Protection for a Transmission Line in the Time Domain." Paper No. A80 065-3, IEEE PES Winter Power Meeting, New York, February 1980, pp. 1-9.

30. Laycock, G. K. and McLaren, P. G. "Programming Techniques for the Derivation of Impedance Loci." IEE Conference, 1970, pp. 148-166.

31. Laycock, G. K., McLaren, P. G., and Redfern, M. A. "Signal Processing Techniques for Power System Protection Applications." IEE International Conference in Power System Protection 1, London, March 1975, pp. 284-290.

32. Hope, G. S., Malik, O. P., and Dash, P. K. "A New Algorithm for Impedance Protection of Transmission Lines." Paper No. A79 413-6, IEEE PES Summer Power Meeting, Vancouver, British Columbia, Canada, July 1979.

33. Malik, O. P., Hope, G. S., and Dash, P. K. "A Unified Approach to Differential and Impedance Protection." Paper No. A79 547-1, IEEE PES Summer Power Meeting, July 1979.

34. Ramamoorty, M. "Application of Digital Compters to Power System Protection." Journal of Inst. Eng. (India), 52, No. 10 (June 1972):235-238.

35. Phadke, A. G., Hlibka, T., and Ibrahim, M. "A Digital Computer
    System for EHV Substations: Analysis and Field Tests."
    IEEE Transactions on Power Apparatus and Systems, PAS 95,
    No. 1 (January/February 1976):291-301.

36. Horton, J. W. "The Use of Walsh Functions for High Speed Digital
    Relaying." IEEE Publication No. 75 CH1034-8 PWR, Paper No.
    A75 5827, IEEE PES Summer Power Meeting, San Francisco,
    July 1975, pp. 1-9.

37. Luckett, R. G., Munday, P. J., and Murray, B. E. "A Substation-
    Based Computer for Control and Protection." IEE Conference
    Publication No. 125, London, March 1975, pp. 291-296.

38. Sachdev, M. S. and Baribeau, M. A. "A New Algorithm for Digital
    Impedance Relays." IEEE Transactions on Power Apparatus and
    Systems, PAS 98, No. 6 (November/December 1979):2232-2240.

39. Dommel, H. W. and Michels, J. M. "High Speed Relaying Using
    Travelling Wave Transient Analysis." IEEE Publication No.
    78 CH1295-5 PWR, Paper No. A78-114-1, IEEE PES Winter Power
    Meeting, New York, January/February 1978, pp. 1-7.

40. Takagi, T., Baba, J., Uemura, K., and Sakoguchi, T. "Fault Protec-
    tion Based on Travelling Wave Theory-Part I: Theory."
    IEEE Publication No. 77 CH1193-2 PWR, Paper No. A77 750-3,
    IEEE PES Summer Meeting, Mexico City, July 1977, pp. 1-7.

41. Takagi, T., Baba, J., Uemura, K, and Sakaguchi, T. "Fault Protec-
    tion Based on Travelling Wave Theory-Part II: Sensitivity
    Analysis and Laboratory Tests." IEEE Publication No.
    78 CH1295-5 PWR, Paper No. A78 220-6, IEEE Winter Meeting,
    New York, January/February 1978, pp. 1-7.

42. Takagi, T., Miki, T., Makino, J., and Matori, I. M. "Feasibility
    Study for a Current Differential Carrier Relay System Based
    on Travelling Wave Theory." IEEE Publication No. 78 CH1295-5
    PWR, Paper No. A78 132-3, IEEE PES Winter Meeting, New York,
    January/February 1978, pp. 1-5.

43. Takagi, T. et al. "Digital Differential Relaying System for Trans-
    Mission Line Primary Protection Using Travelling Wave Theory-
    Its Theory and Field Experience." IEEE Publication No.
    79 CH1417-5 PWR, Paper No. A79 096-9, IEEE PES Winter
    Meeting, New York, February 1979, pp. 1-9.

44. Vitins, V. "A Fundamental Concept for High Speed Relaying." Paper
    No. F80 232-9, IEEE PES Winter Meeting, New York, February
    1980.

45. Brown, R. G. A Primer on Optimal Filtering. Unpublished Notes, Iowa State University of Science and Technology, Electrical Engineering Department, 1979 (Mimeographed).

46. Gelb, A. Applied Optimal Estimation. Cambridge, Mass.: MIT Press, 1974.

47. Day, S. J., Mullineax, N., and Reed, R. J. "Developments in Obtaining Transient Response Using Fourier Transform-Part 1: Gibbs Phenomena and Fourier Integrals." Int. J. Elect. Engrg. Educ. 3 (1965):501-506.

48. Day, S. J., Mullineax, N., Reed, R. J. "Developments in Obtaining Transient Response Using Fourier Transform-Part 2: Use of the Modified Fourier Transform." Int. J. Elect. Engrg. Educ. 4 (1966):31-40.

49. Day, S. J., Mullineax, N., Reed, R. J. "Developments in Obtaining Transient Response Using Fourier Transform-Part 3: Global Response." Int. J. Elect. Engrg. Educ. 6 (1968):259-265.

50. Mullineax, N. and Reed, R. J. "Developments in Obtaining Transient Response Using Fourier Transform-Part 4: Survey of the Theory." Int. J. Elect. Engrg. Educ. 10 (1974):256-267.

51. Ametani, A. "The Application of the Fast Fourier Transform to Electrical Transient Phenomena." Int. J. Elect. Engrg. Educ. 10 (1973):277-287.

52. Johns, A. T., and Aggarwal, R. K. "Digital Simulation of Faulted E.H.V. Transmission Lines with Particular Reference to Very High Speed Protection." Proc. IEE 123, No. 4 (April 1976): 353-359.

53. Johns, A. T. an El-Kateb, M. M. T. "Developments in Techniques for Simulating Faults in E.H.V. Transmission Systems." Proc. IEE 125, No. 3 (March 1978):221-229.

54. Berkebile, L. E., Nilson, S. and Sun, Shan. "Digital EHV Current Transducer." Paper No. 80 SM647-8, IEEE PES Summer Meeting, 1980.

55. Swift, G. W. "The Spectra of Fault-Induced Transient." IEEE Transactions on Power Apparatus and Systems, PAS 98, No. 2 (May/June 1979):940-947.

56. Thorp, J. S., Phadke, A. G., Horowitz, S. H., and Bechler, J. E. "Limits to Impedance Relaying." Transactions on Power Apparatus and Systems, PAS 98, No. 1 (January/February 1979):246-260.

57. Bickford, J. P., Mullineax, N., and Reed, J. R. Computation of Power System Transients. IEE Monograph Series 18, Peter Peregrinus Ld, 1976.

58. Chen, M. and Dillon, W. E. "Power System Modeling." Proceedings of IEEE 62, No. 7 (July 1974):901-915.

59. Wedepohl, L. M. "Application of Matrix Methods to the Solution of Travelling-Wave Phenomena in Polyphase Systems." Proc. IEE 110, No. 12 (December 1962):2200-2212.

60. Laughton, M. A. "Analysis of Unbalanced Polyphase Networks by the Method of Phase Coordinates, Part 1: System Representation in Phase Frame of Reference." Proc. IEE 115, No. 8 (1968):1163-1172.

61. Oppenheim, A. V. and Schafer, R. W. Digital Signal Processing. Englewood Cliffs, New Jersey: Prentice Hall, Inc., 1975.

62. Girgis, A. A. and Ham, F. "A Quantitative Study of Pitfalls in the FFT." IEEE Transactions on Aerospace and Electronic Systems, AES-16, No. 4 (July 1980):434-439.

63. Anderson, P. M. Analysis of Faulted Power Systems. Ames, Iowa: Iowa State University Press, 1973.

64. Warrington, Van C. Protective Relays: Their Theory and Practice. New York: John Wiley and Sons, Inc., 1969.

65. Van Zee, W. H. and Felton, R. J. "500-KV System Relaying Design and Operating Experience." Paper No. 34-07, CIGRE, Paris, 1978.

66. Liew, A. C. "Computer Methods for the Design and Assessment of the Lightning Performance of Transmission Lines." IFAC Symposium on Automatic Control and Protection of Power Systems, 1977, pp. 229-236.

67. Beckmann, Peter. Probability in Communication Engineering. New York: Harcourt, Brace and World, Inc., USA, 1967.

68. Whalen, A. D. Detection of Signals in Noise. New York: Academic Press, 1971.

69. Wright, A. "Limitations of Distance-Type Protective Equipment When Applied to Long Extremely-High-Voltage Power Lines." IEE Monograph No. 421S, December 1960, pp. 271-280.

70. Westin, S. E. and Bubenko, J. A. "Newton-Raphson Technique Applied
        to the Fault Location Problem." Paper No. A76-334-3, IEEE PES
        Summer Meeting, July 1976, pp. 1-6.

71. Davison, E. B. and Wright, A. "Some Factors Affecting the Accuracy
        of Distance-Type Protective Equipment Under Earth Fault
        Conditions." Proc. IEE 110, No. 9 (September 1963):
        1678-1688.

72. Childers, D. and Durling, A. Digital Filtering and Signal
        Processing. New York: West Publishing Company, 1975.

73. Gilbert, J. G., Udren, E. A. and Sackin, M. "Evaluation of
        Algorithms for Computer Relaying." IEEE Publication No.
        77 CH1193-2 PWR, Paper No. A77-520-0, IEEE PES Summer Meeting,
        Mexico City, July 1977, pp. 1-8.

XI. ACKNOWLEDGEMENTS

The author wishes to express his appreciation to all the members of his committee, Dr. R. G. Brown, Dr. K. C. Kruempel, Dr. R. J. Lambert, Dr. A. A. Mahmoud, and Dr. A. Pohm. A special thanks is given to his major professor Dr. R. G. Brown for his invaluable guidance, suggestions, intensive discussions, constructive criticism, and encouragement.

The author expresses his deepest gratitude to Assiut University, Egypt, and the Egyptian Cultural and Educational Bureau in the United States for their financial support. Also the author expresses his gratitude to the Electrical Engineering Department of Iowa State University for the help and the financial support of this project.

Thanks are also given to Jeanne Gehm for her patience and excellent typing.

Last but not least, the author wishes to thank his wife and his son for their love, understanding, and sacrifice.

180

XII. APPENDIX A: DATA OF THE POWER SYSTEM MODEL

A. Transmission Line Data

The configuration of the transmission line used is as shown in Figure A.1.

Conductors: 26/7 ACSR, 0.795 MCM.

Ground wires: 3/8", 6Ω/mile

Ground resistivity: 100 (medium)

The following are the parameters of the line at 60 Hz

$$L_1 = 1.734 \text{ mH/mile} \quad , \quad L_o = 5.9944 \text{ mH/mile}$$

$$R_1 = .0614 \text{ }\Omega\text{/mile} \quad , \quad R_o = 0.461 \text{ }\Omega\text{/mile}$$

$$C_1 = 18.56 \text{ nf/mile} \quad , \quad C_o = 15 \text{ nf/mile}$$
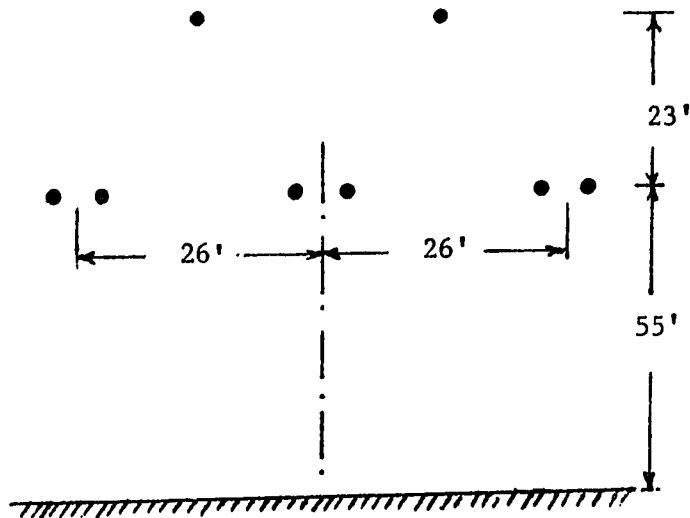
Figure 12.1. Configuration of the 160-mile, 345 KV transmission line used

B. Generator Data

Ratings:

400 MVA, 15 KV, wye grounded.

The following are the parameters of the generator in p.u. based on 100 MVA base:

$$X_1 = X_2 = .06770796$$

$$X_o = 0.034375$$

$$r_a = 0.36458 \times 10^{-3}$$

$$X_D = 0.468229$$

C. Transformer Data

Rating:

400 MVA, 15 KV/345, Wye grounded – wye grounded

Parameters in p.u. based on 100 MVA base are:

$$X_T = .020417$$

$$R_T = .1042 \times 10^{-2}$$

XIII. APPENDIX B: BOUNDARY CONDITIONS OF DIFFERENT TYPES OF FAULTS

A. Single Line to Ground Fault

For a single line to ground fault on phase A, the following relations exist:

$$IFB(s) = IFC(s) = 0 \qquad (13.1)$$

The superimposed voltage on phase A is $-VFA(s)$, where $VFA(s)$ is the Laplace transform of the prefault voltage on phase A.
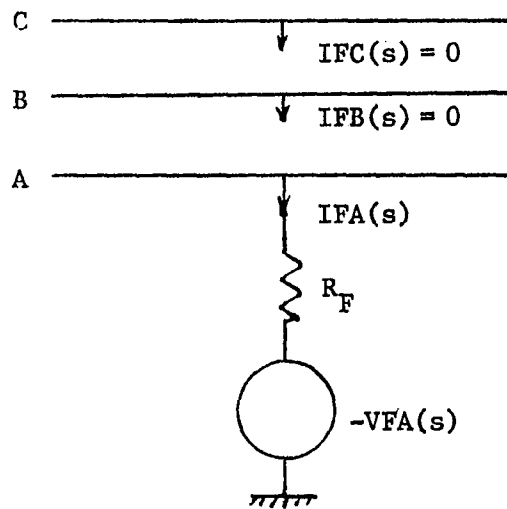
Figure 13.1. Single line to ground fault on phase A

Using equation (13.1) and the symmetrical component concept, then:

$$IF_0(s) = IF_1(s) = IF_2(s) \qquad (13.2)$$

Also

$$vff_0(s) + vff_1(s) + vff_2(s) = -VFA(s) \qquad (13.3)$$

Then using equations (4.20) to (4.23) and (13.2) and (13.3):

$$IF_1(s) = IF_2(s) = IF_0(s) = \frac{VFA(s)}{TV_1(s) + TV_2(s) + TV_0(s) + 3R_F} \qquad (13.4)$$

Then

$$VF_j(s) = -TV_j(s) \; IF_j(s) - -TV_j(s) \; \frac{VFA(s)}{TV_1(s) + TV_2(s) + TV_0(s) + 3R_F} \qquad (13.5)$$

where $j = 0,1,2$ for zero, positive, and negative sequences, respectively.

Using the transmission line equations (4.10), then

$$VS_j(s) = (A1_j(s) - TE1_j(s) \; B1_j(s)) \; VF_j(s) \qquad (13.6)$$

$$IS_j(s) = (C1_j(s) - TE1_j(s) \; A1_j(s)) \; VF_j(s) \qquad (13.7)$$

where $j = 0,1,2$ for zero, positive, and negative sequence components respectively.

B. Line to Line Fault

For a line to line fault between phases B and C through an arc resistance R_F, the following relations exist:

$$IFA(s) = 0 \qquad (13.8)$$

$$IFB(s) + IFC(s) = 0 \qquad (13.9)$$

Therefore,

$$IF_0(s) = 0 \qquad (13.10)$$

$$IF_2(s) = -IF_1(s) \qquad (13.11)$$

Applying the superimposed voltage as a line to line voltage between phases B and C as shown in Figure 13.2, then

$$VFB(s) - VFC(s) = R_F IFB(s) - VFBC(s) \qquad (13.12)$$
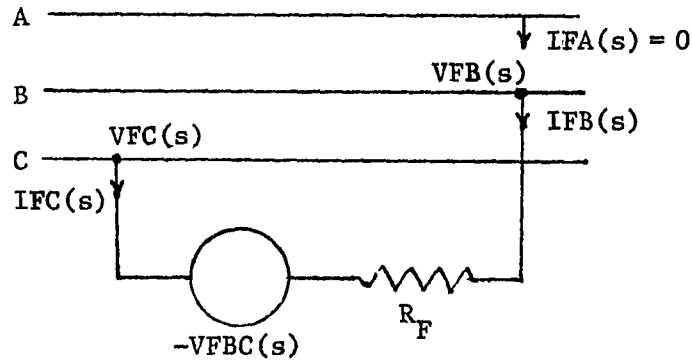
Figure 13.2. Line to line fault between phase B and C

Applying the symmetrical component concept, then

$$(a^2 - a) \, (VF_1(s) - VF_2(s)) = (a^2 - a) \, R_F \, (IF_1(s) - IF_2(s)) - VFBC(s) \qquad (13.13)$$

Using equations (4.20-4.23) and (13.13) then

$$IF_1(s) = \frac{VF(s)}{TV_1(s) + TV_2(s) + 2R_F} \qquad (13.14)$$

where

$$VF(s) = VFBC(s) \; e^{j\pi/2}/\sqrt{3} \qquad (13.15)$$

VFBC(s) = the Laplace transform of the prefault line to line

voltage between phases B and C.

Therefore,

$$VF_j(s) = \frac{TV_j(s) \; VF(s)}{TV_1(s) + TV_2(s) + 2R_F} \qquad (13.16)$$

where j = 1,2 for positive and negative sequence components

$$VF_0(s) = 0 \qquad (13.17)$$

Then equations (13.6) and (13.7) are applicable too.

C. Double Line to Ground Fault

Assuming each of lines B and C are grounded through an arc resistance (R_F), then the following relations exist:

$$IFA(s) = 0 \tag{13.18}$$

So

$$IF_0(s) + IF_1(s) + IF_2(s) = 0 \tag{13.19}$$

Also

$$VB(s) = IFB(s)\ R_F \tag{13.20}$$

$$VC(s) = IFC(s)\ R_F \tag{13.21}$$
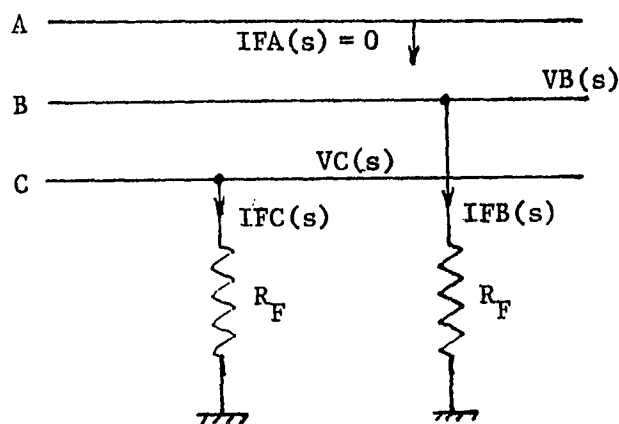
Figure 13.3. B-C to ground fault

Applying the symmetrical component concept to equations (13.20) and (13.21), subtracting, and then adding

$$VF_1(s) - IF_1(s)\ R_F = VF_2(s) - IF_2(s)\ R_F \tag{13.22}$$

$$VF_0(s) - IF_0(s)\ R_F = VF_2(s) - IF_2(s)\ R_F \tag{13.23}$$

Using equations (4.20-4.23), (13.22), and (13.23), then

$$IF_0(s) = IF_2(s) \frac{TV_2(s) + R_F}{TV_2(s) + R_F} \tag{13.24}$$

From (13.19) and (13.24)

$$IF_0(s) = -IF_1(s) \frac{TV_2(s) + R_F}{TV_0(s) + TV_2(s) + 2R_F} \tag{13.25}$$

$$IF_2(s) = -IF_1(s) \frac{TV_0(s) + R_F}{TV_2(s) + TV_0(s) + 2R_F} \tag{13.26}$$

Applying the superimposed voltage principles, and from Figure 13.4

$$VBF(s) = IFB(s) \, R_F - VFB(s) \tag{13.27}$$

$$VCF(s) = IFC(s) \, R_F - VFC(s) \tag{13.28}$$

Applying the symmetrical component concept to equations (13.27) and (13.28) and adding leads to

$$-2 \, IF_0(s) \, (TV_0(s) + R_F) + IF_1(s) \, (TV_1(s) + R_F)$$

$$+ \, IF_2(s) \, (TV_2(s) + R_F) = -VFB(s) - VFC(s) \tag{13.29}$$

Using equations (13.25), (13.26), and (13.29), then

$$IF_1(s) = \frac{-VFB(s) - VFC(s)}{TV_1(s) + R_F + \dfrac{2 \, (TV_2(s) + RF) \, (TV_0(s) + R_F)}{(TV_2(s) + TV_0(s) + 2R_F)}} \tag{13.30}$$

and

$$VF_j(s) = -TV_j(s) \, IF_j(s) \tag{13.31}$$

where $j = 0,1,2$ for zero, positive, and negative sequence components.
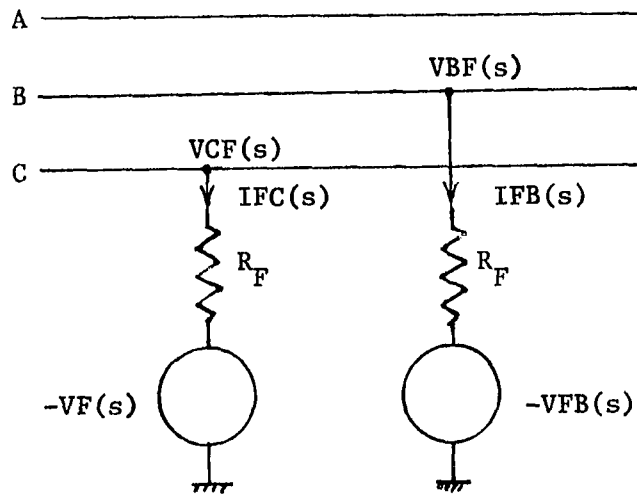
Figure 13.4. B-C to ground fault with the
superimposed phase to ground voltages

VFB(s) is the Laplace transform of prefault voltage on

phase B

VFC(s) is the Laplace transform of prefault voltage on

phase C.

Finally, equations (13.6) and (13.7) can again be applied to find the

sending end sequence voltages and currents in the complex frequency

domain.

D. Three-Phase Fault

For this type of fault the sending end voltages and currents can

be directly obtained for the three phases in the complex frequency domain

as

$$V_j(s) = -(A1_1(s) - B1_1(s) \, TE1_1(s)) \cdot \frac{TV_1(s)}{TV_1(s) + R_F} \, VF_j(s) \qquad (13.32)$$

$$I_j(s) = -(Cl_1(s) - Al_1(s) \ TEl_1(s)) \cdot \frac{TV_1(s)}{TV_1(s) + R_F} \ VF_j(s) \qquad (13.33)$$

where j stands for A,B,C to indicate the three phase quantities
respectively.

XIV. APPENDIX C: DERIVATION OF OTHER ALGORITHMS

The derivation of two of the four algorithms used to test the relative accuracy of the Kalman filter-based algorithm will be shown here. The other two are adequately discussed in the text. No attempts were made to improve the accuracy of these algorithms, and the following derivation are based entirely on the material in the cited references.

A. Derivation of G.E. Algorithm

This algorithm (26) is based on the numerical solution of the line differential equation. The numerical conditions are that samples are taken at a fixed rate, at times t_0, t_1, and t_2. Thus there are two sample periods, the first from t_0 to t_1 is labeled A; the second from t_1 to t_2 is labeled B. The average values during these periods are as follows:

$$i_A = \frac{i_0 + i_1}{2} \quad ; \quad i_B = \frac{i_1 + i_2}{2}$$

$$v_A = \frac{v_0 + v_1}{2} \quad ; \quad v_B = \frac{v_1 + v_2}{2}$$

$$\frac{di_A}{dt} = \frac{i_1 - i_0}{t_1 - t_0} \qquad \frac{di_B}{dt} = \frac{i_2 - i_1}{t_2 - t_1}$$

Now for these two periods the following differential equation is assumed to hold

$$VA = Ri_A + L \frac{di_A}{dt}$$

$$VB = Ri_B + L \frac{di_B}{dt}$$

With this set of equations, and by using substitution, two algebraic equations with the two unknowns, R and L, will remain. These can be easily solved to give equations for R and L. However, for a calculation algorithm, the following definitions were made:

$$CA = i_0 + i_1 \qquad CB = i_1 + i_2$$

$$VA = V_0 + V_1 \qquad VB = V_1 + V_2$$

$$DA = i_1 - i_0 \qquad DB = i_2 - i_1$$

Then

$$L = \frac{DT}{2} \frac{VA - (VB * CA)/CB}{DA - (DB * CA)/CB} \qquad (14.1)$$

$$R = \frac{(DA * VB)/CB - (DB * VA)/CB}{DA - (DB * CA)/CB} \qquad (14.2)$$

These are the equations which were programmed to determine R and L from the sampled values of current and voltage.

B. Derivation of PI Model Algorithm

This algorithm is based on the single PI section transmission line model depicted in Figure 14.1. During the post-fault conditions, this single equivalent PI section model is described by equations (14.3) and (14.4).

$$V = R(i - i_c) + L \frac{d(i - i_c)}{dt} \quad ; \quad i_c = c \frac{dv}{dt} \qquad (14.3)$$

or

$$V = Ri + L \frac{di}{dt} - RC \frac{dv}{dt} - LC \frac{d^2v}{dt^2} \qquad (14.4)$$
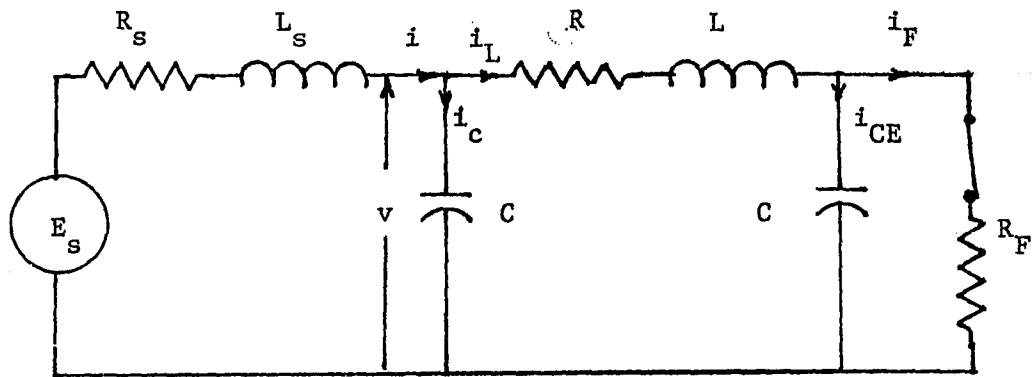
Figure 14.1. A single PI section model of a faulted trans-
mission line as seen by a relay

By selecting four successive sets of voltage and current samples

and replacing the derivatives in equation (14.4) by corresponding finite

differences, equations (14.5) are obtained for four sample sets.

$$
\begin{bmatrix}
i_{k-4} & \dfrac{i_{k-3} - i_{k-5}}{2\Delta t} & -\dfrac{v_{k-3} - v_{k-5}}{2\Delta t} & -\dfrac{v_{k-3} - 2v_{k-4} + v_{k-5}}{(\Delta t)^2} \\[2ex]
i_{k-3} & \dfrac{i_{k-2} - i_{k-4}}{2\Delta t} & -\dfrac{v_{k-2} - v_{k-4}}{2\Delta t} & -\dfrac{v_{k-2} - 2v_{k-3} + v_{k-4}}{(\Delta t)^2} \\[2ex]
i_{k-2} & \dfrac{i_{k-1} - i_{k-3}}{2\Delta t} & -\dfrac{v_{k-1} - v_{k-3}}{2\Delta t} & -\dfrac{v_{k-1} - 2v_{k-2} + v_{k-3}}{(\Delta t)^2} \\[2ex]
i_{k-1} & \dfrac{i_{k} - i_{k-2}}{2\Delta t} & -\dfrac{v_{k} - v_{k-2}}{2\Delta t} & -\dfrac{v_{k} - 2v_{k-1} + v_{k-2}}{(\Delta t)^2}
\end{bmatrix}
\begin{bmatrix}
R \\[2ex]
L \\[2ex]
CR \\[2ex]
CL
\end{bmatrix}
=
\begin{bmatrix}
v_{k-4} \\[2ex]
v_{k-3} \\[2ex]
v_{k-2} \\[2ex]
v_{k-1}
\end{bmatrix}
\qquad (14.5)
$$

Matrix equation (14.5) can also be expressed in partitioned form as shown in equation (14.6)

$$\begin{bmatrix} \underline{A} & \underline{B} \\ \underline{C} & \underline{D} \end{bmatrix} \begin{bmatrix} \underline{P} \\ \underline{CP} \end{bmatrix} = \begin{bmatrix} \underline{V}_1 \\ \underline{V}_2 \end{bmatrix} \qquad (14.6)$$

where

$$\underline{P} = [R \quad L]^t \; ; \; \underline{V}_1 = [V_{k-4} \quad V_{k-3}]^t , \; \underline{V}_2 = [V_{k-2} \quad V_{k-1}]^t$$

and $\underline{A}$, $\underline{B}$, $\underline{C}$, and $\underline{D}$ are 2×2 submatrices of the 4×4 coefficient matrix in equations (14.5).

Since vectors $\underline{P} = [R \quad L]^t$ and $\underline{CP} = [CR \quad CL]^t$ in equation (14.6) are linearly related, equations (14.6) reduce to equation (14.7) or (14.8) by matrix reduction, and the unknown line capacitance C can be eliminated in the process as well.

$$[\underline{A} - \underline{B} \; \underline{D}^{-1} \; \underline{C}] \; \underline{P} = [\underline{V}_1 - \underline{B} \; \underline{D}^{-1} \; \underline{V}_2] \qquad (14.7)$$

or

$$\underline{A1} \cdot \underline{P} = \underline{V}^1 \qquad (14.8)$$

where

$$\underline{A}_1 = [\underline{A} - \underline{B} \; \underline{D}^{-1} \; \underline{C}] \; , \; V^1 = [\underline{V}_1 - \underline{B} \; \underline{D}^{-1} \; \underline{V}_2] \text{ and}$$

$$P = \begin{bmatrix} R \\ L \end{bmatrix} \qquad (14.9)$$

These are the equations that were programmed in the PI model algorithm to compute the resistance and the inductance of the faulted section of the line.

XV. APPENDIX D: A PROGRAM LISTING FOR THE KALMAN-
FILTERING-BASED DIGITAL DISTANCE PROTECTION SCHEME

```
C     ***************************************************************
C     *     A KALMAN - FILTERING - BASED DIGITAL DISTANCE PROTECTION    *
C     *     SCHEME                                                      *
C     ***************************************************************
C     ***************************************************************
C     *     THIS SCHEME CONSISTS OF:                                    *
C     *         (1)   A FAULT DETECTION SUBROUTINE   DETECTS ANY        *
C     *         UBNORMALITIES IN THE CURRENT WAVEFORMS IN ANY OF        *
C     *         THE THREE PHASES                                        *
C     *         (2) KALMAN FILTERS TO OPTIMALLY ESTIMATE THE PHASOR     *
C     *         QUANITITIES OF THE CURRENTS AND VOLTAGES UPON THE       *
C     *         FAULT DETECTION                                         *
C     *         (3) A FAULT CLASSIFICATION SUBROUTINE   CLASSIFIES THE  *
C     *         TYPE OF THE FAULT USING THE ESTIMATES OF THE KALMAN     *
C     *         FILTERS AND THE PREFAULT CURRENTS                       *
C     *         (4)TWO DISTANCE RELAY SUBROUTINES THAT COMPUTE THE      *
C     *         APPPARENT IMPEDANCE SEEN BY THE RELAY IN CASE OF        *
C     *         (I)   EARTH FAULT                                       *
C     *         (II) INTERPHASE FAULT OR THREE-PHASE FAULT              *
C     *         IF THE FAULT IS WITHIN THE RELAY ZONE THE ALGORITHM     *
C     *         COMPUTES THE EXACT FAULT LOCATION                       *
C     ***************************************************************
      COMPLEX ZO,Z1,CK
      DIMENSION VA(128),VB(128),VC(128),CA(128),CB(128),CC(128),TIME(128
     *),XVA1(128),XVA2(128),PVA1(128),PVA2(128),CRO(128),RI(128)
      DIMENSION XNVC(2),XVC1(128),XVC2(128),PVC1(128),PVC2(128)
      DIMENSION RIO(128),RV(128),XIA1(128),XIA2(128),PIA1(128),PIA2(128)
     *,XO1(128),XO2(128),PO1(128),PO2(128),RES(128),REC(128),PNVA(2,2)
      DIMENSION XNVA(2),PNIA(3,3),XNIA(3),PNO(3,3),XNO(3)
      DIMENSION VRO(128),RVO(128),XIA(128),XIB(128),XIC(128),XIO(128)
      DIMENSION XIB1(128),XIB2(128),PIB1(128),PIB2(128),XIC1(128)
      DIMENSION XIC2(128),PIC1(128),PIC2(128),XVO1(128),XVO2(128)
      DIMENSION PVO1(128),PVO2(128),XNIB(3),XNIC(3),PNVO(2,2)
      DIMENSION PNVB(2,2),PNIB(3,3),PNIC(3,3),PNVC(2,2),XNVB(2)
      DIMENSION X1(96),X2(96),X3(96),X4(96),X5(96)
```

194

```
      DIMENSION XA1(96),XC1(96),XC2(96),XC3(96),XCD(96),CR(96)
      DIMENSION XAR(64),XAI(64),XAP(64),CAR(64),CAI(64),CAP(64)
      DIMENSION CBR(64),CBI(64),CBP(64),CCR(64),CCI(64),CCP(64)
      DIMENSION COR(64),COI(64),COP(64)
      DIMENSION XIK(96),XLFK(96),RESD(64),RECD(64),XLFD(64)
      DIMENSION RESP(64),RECP(64),XLFP(64),RGL(96),XGL(96),XLFG(96)
      DIMENSION VA1(96),VA2(96),VAP(96),CA1(96),CA2(96),CB1(96),CB2(96)
      DIMENSION CC1(96),CC2(96),CRD1(96),CRD2(96)
      DIMENSION YAP(96),YBP(96),YCP(96),CROP(96),TIME1(96)
      DIMENSION VDF(96),ADF(96),BDF(96),CDF(96),ODF(96),RDF(96),TIM1E(9
     *6)
      DIMENSION XVB1(128),XVB2(128),PVB1(128),PVB2(128)
      DIMENSION A1(32),F(32),H(32),XFLTR(32)
      DIMENSION XLFE(96)
      DIMENSION TIMP(96),TA(96),TB(96),TC(96)
      DT=1.0/(64.0*50.0)
      XFAULT=90.0
        PI=3.141592651
      N=64
      NN=N-4
      N2=N/2
      M=N2-1
      N3=M+N
        NV=2
      NC=3
      R1=.515858E-04
      XF1M=.549214E-03
        ZO=(.3343404E-03,.1900599E-02)
        Z1=(0.515858E-04,0.549214E-03)
      CK=(ZO-Z1)/Z1
        RK=REAL(CK)
        XK=AIMAG(CK)
50    FORMAT(6E13.6)
      DO 20 I=1,N
      READ(5,50) VA(I),VB(I),VC(I),CA(I),CB(I),CC(I)
```

```
        CRO(I)=(CA(I)+CB(I)+CC(1))/3.0
        TIME(I)=FLOAT(I-1)*DT
        RV(I)=0.6*EXP(-300.0*TIME(I))
        RI(I)=4.0*EXP(-300.0*TIME(I))
       RIO(I)=1.0*EXP(-300.0*TIME(I))
        TA(I)=TIME(I)*1000.0
20      CONTINUE
         PNVA(1,1)=0.57
         PNVA(1,2)=0.0
         PNVA(2,1)=0.0
         PNVA(2,2)=0.57
        DO 51 I=1,NV
        DO 51 J=1,NV
        PNVB(I,J)=PNVA(I,J)
        PNVC(I,J)=PNVA(I,J)
51      CONTINUE
        DO 201 I=1,NC
        DO 201 J=1,NC
        PNIA(I,J)=0.0
        PNO(I,J)=0.0
        PNIA(I,I)=16.0
        PNO(I,I)=4.0
201     CONTINUE
        XX1=1.512567*SQRT(2.)
        XX2=.175485*SQRT(2.)
        XX3=-.6043089*SQRT(2.)
        XX4=-1.397662*SQRT(2.)
        XX5=-.9082557*SQRT(2.)
        XX6=1.222178*SQRT(2.)
        XNIA(1)=XX1
        XNIA(2)=XX2
        XNIA(3)=0.0
        XNIB(1)=XX3
        XNIB(2)=XX4
        XNIB(3)=0.0
```

```
      XNIC(1)=XX5
      XNIC(2)=XX6
      XNIC(3)=0.0
      XND(1)=0.0
      XND(2)=0.0
      XND(3)=0.0
      DO 200 I=1,NC
      DO 200 J=1,NC
      PNIB(I,J)=PNIA(I,J)
      PNIC(I,J)=PNIA(I,J)
200   CONTINUE
      XNVA(1)=1.06*SQRT(2.)
      XNVA(2)=.075*SQRT(2.)
      XNVB(1)=-.47*SQRT(2.)
      XNVB(2)=-.9586*SQRT(2.)
      XNVC(1)=-.60*SQRT(2.)
      XNVC(2)=.88*SQRT(2.)
      DO 103 I=1,N
      J=I-1
      AJ=FLOAT(J)
      AN2=FLOAT(N2)
      XC1(I)=XNIA(1)*COS(AJ*PI/AN2)-XNIA(2)*SIN(AJ*PI/AN2)
      XC2(I)=XNIB(1)*COS(AJ*PI/AN2)-XNIB(2)*SIN(AJ*PI/AN2)
      XC3(I)=XNIC(1)*COS(AJ*PI/AN2)-XNIC(2)*SIN(AJ*PI/AN2)
      XCO(I)=0.0
      CR(I)=XC1(I)
      TIMP(I)=DT*AJ*1000.0
103   CONTINUE
      EPSI=0.06
      CALL DETECT  (CA,CB,CC,XC1,XC2,XC3,EPSI,KDT,TDT,DT)
      CALL VKLMN(PNVA,XNVA,RV,XVA,RV,VA,XVA1,PVA1,PVA2,N,NV)
      CALL VKLMN(PNVB,XNVB,RV,VB,RV,VB,XVB1,PVB1,PVB2,N,NV)
      CALL VKLMN(PNVC,XNVC,RV,VC,XVC1,XVC2,PVC1,PVC2,N,NV)
      CALL CKLMN(PNIA,XNIA,RI,CA,XIA1,XIA2,PIA1,PIA2,N,NC)
      CALL CKLMN(PNIB,XNIB,RI,CB,XIB1,XIB2,PIB1,PIB2,N,NC)
```

```
      CALL CKLMN(PNIC,XNIC,RI,CC,XIC1,XIC2,PIC1,PIC2,N,NC)
      CALL CKLMN(PNO,XNO,RIO,CRO,XO1,XO2,PO1,PO2,N,NC)
      NP=N-KDT
      DO 104 I=1,NP
      J=I+KDT
      XI(I)=SQRT((XIA1(J)-XX1)**2+(XIA2(J)-XX2)**2)
      X2(I)=SQRT((XIB1(J)-XX3)**2+(XIB2(J)-XX4)**2)
      X3(I)=SQRT((XIC1(J)-XX5)**2+(XIC2(J)-XX6)**2)
      X4(I)=SQRT(XO1(J)*XO1(J)+XO2(J)*XO2(J))
      TB(I)=TA(J)
104   CONTINUE
      EPSC=0.3
      CALL CLASS(X1,X2,X3,KT,KCL,TCL,DT,EPSC)
      KDC=KDT+KCL
      NADC=N-KDC
      IF(KT.EQ.1) CALL DSTR(XIA1,XIA2,XO1,XO2,XVA1,XVA2,KDC,DT,RK,XK,R1
     *,XF1M,RES,REC,TC,XLFK)
      IF(KT.EQ.2) CALL DSTR(XIB1,XIB2,XO1,XO2,XVB1,XVB2,KDC,DT,RK,XK,R1
     *,XF1M,RES,REC,TC,XLFK)
      IF(KT.EQ.3) CALL DSTR(XIC1,XIC2,XO1,XO2,XVC1,XVC2,KDC,DT,RK,XK,R1
     *,XF1M,RES,REC,TC,XLFK)
      IF(KT.EQ.4)CALL DSTR2(XIA1,XIA2,XIB1,XIB2,XVA1,XVA2,XVB1,XVB2,XX1
     *,XX2,XX3,XX4,KDC,DT,R1,XF1M,RES,REC,TC,XLFK)
      IF(KT.EQ.5)CALL DSTR2(XIB1,XIB2,XIC1,XIC2,XVB1,XVB2,XVC1,XVC2,XX3
     *,XX4,XX5,XX6,KDC,DT,R1,XF1M,RES,REC,TC,XLFK)
      IF(KT.GE.6)CALL DSTR2(XIA1,XIA2,XIC1,XIC2,XVA1,XVA2,XVC1,XVC2,XX1
     *,XX2,XX5,XX6,KDC,DT,R1,XF1M,RES,REC,TC,XLFK)
      WRITE(6,500) KDT,TDT
500   FORMAT('1',10X,'FAULT IS DETECTED AFTER',5X,I2,'SAMPLES',//,10X,'
     *OR',5X,F7.5,5X,'MILLISECONDS',5X,'USING 64 SAMPLES PER CYCLE')
      WRITE(6,501) KCL,TCL ,KT
501   FORMAT('0',10X,'FAULT IS CLASSIFIED  AFTER',5X,I2,5X,'
     *COMPUTATION STEPS',//,10X,'OR',10X,F7.5,5X,'MILLISECONDS USING 64
     *   SAMPLES PER CYCLE',//,10X,'TYPE OF FAULT IS   #',2X,I1)
      WRITE(6,601)
```

```
601     FORMAT('1',10X,'TIME MSEC',10X,'IA SUPERIMPOSED',5X,'IB SPER.',10
       *X,'IC SUP.',10X,'IO SUP.')
        DO 105 I=1,NP
105     WRITE(6,602)TB(I),X1(I),X2(I),X3(I),X4(I)
602     FORMAT(5E16.6)
        WRITE(6,603)
603     FORMAT('1',10X,'TIME MSEC',5X,'RESISTANCE',5X,'RECTANCE',5X,'DIST
       *ANCE MILES')
        DO 106 I=1,NADC
106     WRITE(6,604) TC(I),RES(I),REC(I),XLFK(I)
604     FORMAT(4E16.6)
        CALL ORIGIN(.05,0.0,5)
        CALL GRAPH(N2,TIMP,XC1,0,102,5.25,6.25,1.6,0.,1.6,-4.8,'    TIME M
       *SEC;','      CURRENT P.U;','FAULT DETECTION;','PREFAULT CURRENT;')
        CALL GRAPHS(N2,TA,CA,1,101,'CURRENT    FAULTED PH.;')
        CALL GRAPH(N2,TIMP,XC2,0,102,5.25,6.25,1.6,0.,.75,-1.5,'    TIME M
       *SEC;','      CURRENT P.U;','FAULT DETECTION;','PREFAULT CURRENT;')
        CALL GRAPHS(N2,TA,CB,1,101,'CURRENT UNFAULTED PH.;')
        CALL GRAPH(N2,TIMP,XC3,0,102,5.23,6.25,1.6,0.,0.3,-2.4,'    TIME M
       *SEC;','      CURRENT P.U;','FAULT DETECTION;','PREFAULT CURRENT;')
        CALL GRAPHS(N2,TA,CC,1,101,'CURRENT UNFAULTED PH.;')
        CALL GRAPH(NP,TB,X1,1,102,5.25,6.25,3.2,0.,0.,0.,'      TIME MSEC;
       *','      CURRENT P.U;','FAULT CLASS.;','DELTA IA  FAULTED PH.;')
        CALL GRAPHS(NP,TB,X2,3,102,'DELTA IB UNFAULTED PH.;')
        CALL GRAPHS(NP,TB,X3,4,102,'DELTA IC UNFAULTED PH.;')
        CALL GRAPHS(NP,TB,X4,7,102,'DELTA IO ZERO SEQ.;')
        CALL GRAPH(NADC,TC,RES,1,102,5.25,6.25,3.2,0.,0.,0.,'      TIME MS
       *EC;','      P.U;','APPARENT IMPEDANCE;','RESISTANCE P.U;')
        CALL GRAPHS(NADC,TC,REC,3,102,'REACTANCE P.U;')
        CALL GRAPH(NADC,TC,XLFK,0,102,5.25,6.25,3.2,0.,0.,0.,'      TIME MS
       *EC;','FAULT LOCAT. MILES;','COMPUTATION OF FAULT;','LOC. OF AGF
       *AT 150M;')
        CALL GRAPH(NADC,RES,REC,1,101,5.25,6.25,.033,-.066,.03,0.,' RES
       * P.U;','     REC P.U;','TRAJECTORY OF:;','APPARENT IMPEDANCE;')
        CALL GRAPH(N2,TIMP,XC1,0,2,4.,4.5,2.1,0.,0.,0.,'    TIME MSEC;','
```

```
*          I   P.U;',"   ;',"   ;')
   CALL GRAPHS(N2,TA,CA,1,1,'   ;')
   CALL GRAPH(N2,TIMP,XC2,0,2,4.,4.5,2.1,0.,0.,0.,'      TIME MSEC;',"
*          I   P.U;',"   ;',"   ;')
   CALL GRAPHS(N2,TA,CB,1,1,'   ;')
   CALL GRAPH(NP,TB,X1,0,2,4.,4.5,4.,0.,0.,0.,'      TIME MSEC;',"
*   I   P.U;',"   ;',"   ;')
   CALL GRAPHS(NP,TB,X2,0,2,'   ;')
   CALL GRAPHS(NP,TB,X3,0,2,'   ;')
   CALL GRAPH(NADC,TC,RES,0,2,4.,4.5,4.,0.,0.,0.,'      TIME MSEC;',"
*          P.U;',"   ;',"   ;')
   CALL GRAPHS(NADC,TC,REC,0,2,'   ;')
   CALL GRAPH(NADC,TC,XLFK,0,2,4.,4.5,4.,0.,0.,0.,'      TIME MSEC;',
*'      MILES;',"   ;',"   ;')
   CALL GRAPH(NADC,RES,REC,1,1,4.,4.5,.05,-.1,.04,0.,'          RES
*P.U;',"      REC P.U;',"   ;',"   ;')
   STOP
   END
C
C
C      ***************************************************************
C      *          SUBROUTINE DETECT(DETECT) DETECTS THE UBNORMALITIES      *
C      *          IN ANY OF THE CURRENTS IN THE THREE PHASES              *
C      ***************************************************************
C

   SUBROUTINE DETECT(CA,CB,CC,XC1,XC2,XC3,EPSI,KDET,TDET,DT)
   DIMENSION CA(96),CB(96),CC(96),XC1(96),XC2(96),XC3(96)
   I=1
5  J=I
   XD1=ABS(CA(I)-XC1(J))
   XD2=ABS(CB(I)-XC2(J))
   XD3=ABS(CC(I)-XC3(J))
   IF(XD1.GT.EPSI) GO TO 10
   IF(XD2.GT.EPSI) GO TO 10
   IF(XD3.GT.EPSI) GO TO 10
   I=I+1
```

```
      GO TO 5
10    KDET=I
      TDET=DT*FLOAT(I-1)*1000.0
      RETURN
      END
C
C     ***************************************************************
C     *       SUBROUTINE CLASS CLASSIFIES THE TYPE OF FAULT        *
C     *       THE VALUE OF JT INDICATES THE TYPE                   *
C     ***************************************************************
C
C
      SUBROUTINE CLASS(X1,X2,X3,KT,NTEST,TCL,DT,EP)
      DIMENSION X1(32),X2(32),X3(32)
      DIMENSION KTEST(32),JT(7)
      E1=.7
      I=1
5     DO 1 J=1,7
1     JT(J)=0
      XLA=X1(I)
      IF(XLA.LT.X2(I)) XLA=X2(I)
      IF(XLA.LT.X3(I)) XLA=X3(I)
      XKA=X1(I)/XLA
      XKB=X2(I)/XLA
      XKC=X3(I)/XLA
C
C     *** TEST FOR THE DIFFERENT TYPES OF FAULTS
C
      IF(XKA.GT.E1.AND.XKB.LT.EP.AND.XKC.LT.EP) JT(1)=1
C     TEST FOR B-G FAULT
C
      IF(XKB.GT.E1.AND.XKA.LT.EP.AND.XKC.LT.EP)  JT(2)=1
C
C     TEST FOR A C-G FAULT
C
```

```
      IF(XKC.GT.E1.AND.XKA.LT.EP.AND.XKB.LT.EP) JT(3)=1
C
C   TEST FOR A-B FAULT
C
      IF(XKA.GT.E1.AND.XKB.GT.E1.AND.XKC.LT.EP) JT(4)=1
C
C    TEST FOR   B-C FAULT
C
      IF(XKA.LT.EP.AND.XKB.GT.E1.AND.XKC.GT.E1) JT(5)=1
C
C   TEST FOR C-A FAULT
C
      IF(XKA.GT.E1.AND.XKB.LT.EP.AND.XKC.GT.E1) JT(6)=1
C
C    TEST FOR A 3 PHASE FAULT
C
      IF(XKA.GT.E1.AND.XKB.GT.E1.AND.XKC.GT.E1) JT(7)=1
C
CFIND THE TYPE OF FAULT
C
       K=1
  7     IF(JT(K).EQ.1) GO TO 15
      IF(K.EQ.7) KTEST(I)=0
      IF(K.EQ.7) GO TO 20
       K=K+1
       GO TO 7
  15    KTEST(I)=K
C
C     CHECK THE TYPE OF FAULT FOR THREE CONSECUTIVE COMPUTATION STEPS
C
      IF(I.LT.4) GO TO 20
        I1=I-1
      I2=I-2
      IF(KTEST(I2).LT.1) GO TO 20
      IF(KTEST(I).EQ.KTEST(I1).AND.KTEST(I1).EQ.KTEST(I2)) GO TO 21
```

```
20       I=I+1
         GO TO 5
21       KT=KTEST(I)
         NTEST=I
      TCL=DT*FLOAT(NTEST-1)*1000.0
      RETURN
      END
C
C
C
C        ****************************************************************
C        *        SUBROUTINE DSTR COMPUTES THE APPARENT IMPEDANCE SEEN BY *
C        *        THE RELAY IN CASE OF :                                 *
C        *           PHASE A TO GROUND FAULT                             *
C        *           PHASE B TO GROUND FAULT                             *
C        *           PHASE C TO GROUND FAULT                             *
C        ****************************************************************
C
C
      SUBROUTINE DSTR(Y1,Y2,Y3,Y4,Y5,Y6,KR,DT,RK,XK,R1,X1,R,X,T1,XLF)
      DIMENSION Y1(96),Y2(96),Y3(96),Y4(96),Y5(96),Y6(96),T1(96)
      DIMENSION R(96),X(96),XLF(96)
      NMM=64-KR
      DO 1 I=1,NMM
      J=I+KR
      CRR=Y1(J)+Y3(J)*RK-Y4(J)*XK
      CRI=Y2(J)+Y4(J)*RK+Y3(J)*XK
      CRM2=CRR*CRR+CRI*CRI
      AK1=Y3(J)*CRR+Y4(J)*CRI
      AK1=AK1/CRM2
      AK2=Y4(J)*CRR-Y3(J)*CRI
      AK2=AK2/CRM2
      R(I)=(Y5(J)*CRR+Y6(J)*CRI)/CRM2
      X(I)=(Y6(J)*CRR-Y5(J)*CRI)/CRM2
      XLF(I)=(X(I)*AK1-R(I)*AK2)/(AK1*X1-AK2*R1)
      T1(I)=FLOAT(J-1)*DT*1000.0
1        CONTINUE
```

```
      RETURN
      END
C
C      ****************************************************************
C      *        SUBROUTINE DSTR2 COMPUTES THE APPARENT IMPEDANCE SEEN    *
C      *        BY THE RELAY IN CASE OF:                                 *
C      *        PHASE A TO PHASE B OR PHASE A TO PHASE B TO GROUND FAULT*
C      *        PHASE B TO PHASE C OR PHASE B TO PHASE C TO GROUND FAULT*
C      *        PHASE C TO PHASE A OR PHASE C TO PHASE A TO GROUND FAULT*
C      *        OR A THREE - PHASE FAULT                                 *
C      ****************************************************************
C
C  *   DISTANCE RELAY SUBROUTINE FOR PHASE TO PHASE FAULTS
C
      SUBROUTINE DSTR2(Y1,Y2,Y3,Y4,Y5,Y6,Y7,Y8,XY1,XY2,XY3,XY4,KR,DT,R1
     *,X1,R,X,T1,XLF)
      DIMENSION Y1(96),Y2(96),Y3(96),Y4(96),Y5(96),Y6(96),Y7(96)
      DIMENSION Y8(96),T1(96),R(96),X(96),XLF(96)
      NMM=64-KR
      DO 1 I=1,NMM
      J=I+KR
      CRR=Y1(J)-Y3(J)
      CRI=Y2(J)-Y4(J)
      CRM2=CRR*CRR+CRI*CRI
      VRR=Y5(J)-Y7(J)
      VRI=Y6(J)-Y8(J)
      R(I)=VRR*CRR+VRI*CRI
      R(I)=R(I)/CRM2
      X(I)=VRI*CRR-VRR*CRI
      X(I)=X(I)/CRM2
      A1=CRR-XY1+XY3
      A2=CRI-XY2+XY4
      AK1=A1*CRR+A2*CRI
      AK1=AK1/CRM2
      AK2=A2*CRR-A1*CRI
```

```
              AK2=AK2/CRM2
              XLF(I)=(X(I)*AK1-R(I)*AK2)/(AK1*X1-AK2*R1)
              T1(I)=FLOAT(J-1)*DT*1000.0
     1        CONTINUE
              RETURN
              END
C
C
C        ****************************************************************
C        *        SUBROUTINE VKLMN IS A TWO STATE KALMAN FILTER FILER FOR *
C        *        THE ESTIMATION OF THE VOLTAGE COMPONENTS                *
C        ****************************************************************
C
              SUBROUTINE VKLMN(PN,XN,R,Z,X1,X2,P11,P22,N,N1)
              DIMENSION PN(2,2),XN(2),PP(2,2),XP(2),AH(2),AK(2),AIAK(2,2)
              DIMENSION AKAH(2,2)
              DIMENSION Z(128),X1(128),X2(128),P11(128),P22(128),R(128)
              PI=3.141592651
              WO=120.0*PI
              DT=1.0/(60.*64.)
              DO 1 KI=1,N
              J=KI-1
              AJ=FLOAT(J)
              WOT=WO*DT*AJ
              AH(1)=COS(WOT)
              AH(2)=-SIN(WOT)
              AHR=0.0
                  DO 2 II=1,N1
                  DO 2 JJ=1,N1
                  AHR=AHR+PN(II,JJ)*AH(II)*AH(JJ)
     2            CONTINUE
              AHR=R(KI)+AHR
              DO 3 IJ=1,N1
              AK(IJ)=0.0
              DO 4 JJ=1,N1
              AK(IJ)=AK(IJ)+PN(IJ,JJ)*AH(JJ)
```

```
4          CONTINUE
           AK(IJ)=AK(IJ)/AHR
3          CONTINUE
C
C     UP DATE THE VECTOR X
C
           AHXN=0.0
           DO 5 I=1,N1
5          AHXN=AHXN+AH(I)*XN(I)
           DO 6 I=1,N1
6          XP(I)=XN(I)+AK(I)*(Z(KI)-AHXN)
      X1(KI)=XP(1)
      X2(KI)=XP(2)
           DO 71 I=1,N1
           DO 71 IJ=1,N1
71         AKAH(I,IJ)=0.0
           DO 72 I=1,N1
           DO 72 IJ=1,N1
72         AKAH(I,IJ)=AKAH(I,IJ)+AK(I)*AH(IJ)
           DO 7 I=1,N1
           DO 7 IJ=1,N1
           IF(I.EQ.IJ) GO TO 8
           AIAK(I,IJ)=-AKAH(I,IJ)
           GO TO 7
8          AIAK(I,IJ)=1.0-AKAH(I,IJ)
7          CONTINUE
           DO 10 I=1,N1
10         XN(I)=XP(I)
           DO 11 I=1,N1
           DO 11 IJ=1,N1
           PP(I,IJ)=0.0
           DO 11 IK=1,N1
           PP(I,IJ)=PP(I,IJ)+AIAK(I,IK)*PN(IK,IJ)
11         CONTINUE
      P11(KI)=PP(1,1)
```

```
      P22(KI)=PP(2,2)
          DO 12 I=1,N1
          DO 12 IJ=1,N1
          PN(I,IJ)=PP(I,IJ)
   12     CONTINUE
   1  CONTINUE
      RETURN
      END
C
C
C     ***************************************************************
C     *         SUBROUTINE CKLMN IS A THREE STATE KALMAN FILTER       *
C     *         THE FIRST TWO STATES ARE THE COMPONENTS OF THE 60     *
C     *         HZ CURRENT WAVEFORM                                   *
C     ***************************************************************
C
      SUBROUTINE CKLMN(PN,XN,R,Z,X1,X2,P11,P22,N,N1)
      DIMENSION P33(128),XK1(128),XK2(128),XK3(128)
      DIMENSION PN(3,3),XN(3),PP(3,3),XP(3),AH(3),AK(3),AIAK(3,3)
      DIMENSION AKAH(3,3)
      DIMENSION Z(128),X1(128),X2(128),P11(128),P22(128),R(128)
      PI=3.141592651
      WO=120.0*PI
      B=-300.0
      DT=1.0/(64.*60.)
      Q=.01
      PH3=EXP(B*DT)
      DO 1 KI=1,N
      J=KI-1
      AJ=FLOAT(J)
      WOT=WO*DT*AJ
      AH(1)=COS(WOT)
      AH(2)=-SIN(WOT)
      AH(3)=1.0
      AHR=0.0
          DO 2 II=1,N1
```

```
        DO 2 JJ=1,N1
        AHR=AHR+PN(I1,JJ)*AH(II)*AH(JJ)
2       CONTINUE
        AHR=R(KI)+AHR
        DO 3 IJ=1,N1
        AK(IJ)=0.0
        DO 4 JJ=1,N1
        AK(IJ)=AK(IJ)+PN(IJ,JJ)*AH(JJ)
4       CONTINUE
        AK(IJ)=AK(IJ)/AHR
3       CONTINUE
     XK1(KI)=AK(1)
     XK2(KI)=AK(2)
     XK3(KI)=AK(3)
C
C    UP DATE THE VECTOR X
C
        AHXN=0.0
        DO 5 I=1,N1
5       AHXN=AHXN+AH(I)*XN(I)
        DO 6 I=1,N1
6       XP(I)=XN(I)+AK(I)*(Z(KI)-AHXN)
     X1(KI)=XP(1)
     X2(KI)=XP(2)
        DO 71 I=1,N1
        DO 71 IJ=1,N1
71      AKAH(I,IJ)=0.0
        DO 72 I=1,N1
        DO 72 IJ=1,N1
72      AKAH(I,IJ)=AKAH(I,IJ)+AK(I)*AH(IJ)
        DO 7 I=1,N1
        DO 7 IJ=1,N1
        IF(I.EQ.IJ) GO TO 8
        AIAK(I,IJ)=-AKAH(I,IJ)
        GO TO 7
```

```
3          AIAK(I,IJ)=1.0-AKAH(I,IJ)
7          CONTINUE
           DO 10 I=1,N1
10         XN(I)=XP(I)
      XN(3)=XN(3)*PH3
           DO 11 I=1,N1
           DO 11 IJ=1,N1
           PP(I,IJ)=0.0
           DO 11 IK=1,N1
           PP(I,IJ)=PP(I,IJ)+AIAK(I,IK)*PN(IK,IJ)
11         CONTINUE
      P11(KI)=PP(1,1)
      P22(KI)=PP(2,2)
      P33(KI)=PP(3,3)
           DO 12 I=1,N1
           DO 12 IJ=1,N1
           PN(I,IJ)=PP(I,IJ)
12         CONTINUE
      DO 13 I=1,N1
      PN(I,N1)=PP(I,N1)*PH3
      PN(N1,I)=PP(N1,I)*PH3
13    CONTINUE
      PN(N1,N1)=PN(N1,N1)+Q
1     CONTINUE
      RETURN
      END
```